Bulletin of MTA (2013) 147: 1-17

Bulletin of the Mineral Research and Exploration

http://bulletin.mta.gov.tr

THE SEGMENT STRUCTURE OF SOUTHERN BRANCH OF THE NORTH ANATOLIAN FAULT AND PALEOSEISMOLOGICAL BEHAVIOUR OF THE GEMLİK FAULT, NW ANATOLIA

Selim ÖZALP[a,*], Ömer EMRE[b] and Ahmet DOĞAN[c]

[a] *General Directorate of Mineral Research and Exploration, Dept. of Geological Researches, 06800, Ankara, Turkey*
[b] *Fugro-Sial Geoscience Consulting and Engineering Ltd Co., Farabi Sk., No: 40/4, Çankaya, Ankara, Turkey*
[c] *General Directorate of Combating to Desertification and Erosion Control, Ankara, Turkey*

Keywords:
North Anatolian Fault-Southern Branch, Gemlik Fault, paleoseismology.

ABSTRACT

The North Anatolian Fault (NAF), which is an intra-continental transform fault, is divided into two branches as Northern and Southern branches in Marmara Region. The southern branch which separates from each other by rightward stepovers between Bandırma and Dokurcun valley is formed by three main fault segments as Geyve, İznik and Gemlik from East to West. The length of fault segments ranges between 40 and 57 km and GPS data in Southern branch propose a 5 mm/year slip rate. Two surface faulting events were observed during paleoseismological excavations which had been carried out on 40 km long Gemlik segment and these can be correlated with earthquakes that occurred in 1857 and 1419. The recurrence interval between the last two earthquakes in Gemlik Fault is 438 years. Findings indicate that Gemlik fault was also included into surface faulting of the earthquake in 1419 which its presence is known in İznik fault. At least 95 km long multi-segment surface faulting developed in this earthquake. Based on 5 mm/years slip rate, the cumulative offset amount slip rate of NAF was approximately estimated as 3 meters in 595 years in region between İznik Lake and Dokurcun Valley. Accordingly; it can be stated that the southern branch of the North Anatolian Fault has a potential to trigger a large earthquake as well as the Northern branch.

1. Introduction

The North Anatolian Fault (NAF) is 1.600 km long, right lateral strike slip, intra continental transform fault and causes Anatolian plate to move westward with respect to Eurasia (Figure 1) (Ketin, 1957; Şengör, 1979). This transform fault is divided into two branches as Northern and Southern branches in Eastern Marmara Region. NAF, in world earthquake literature, is known by large earthquakes that occurred within the last century and migrates eastward. Between the years 1939 and 1999, total of 1100 km surface faulting has developed in nine large earthquakes that had developed in NAF between Erzincan and the Sea of Marmara. Within this earthquake series, each earthquake segment has been a triggering factor of a next earthquake transferring the stress to a neighboring segment (Ambraseys, 1970; Toksöz et al., 1979; Barka and Kadinsky-Cade, 1988; Stein et al., 1996). Earthquake in 1967 ended up towards western part of Mudurnu valley where the fault is divided into two branches and the following İzmit earthquake in 1999 August 17th (Mw: 7,4) and Düzce earthquake in 1999 November 12th occurred on the Northern branch of the fault. There is a consensus that the seismic hazard has increased in northern branch of the Sea of Marmara region after the occurrence of these earthquakes (Stein et al., 1996; Parsons et al., 2000; Erdik et al., 2004).

Historical records within last 2000 years and paleoseismological data have revealed the presence

* *Corresponding author: S. ÖZALP, selim.ozalp@mta.gov.tr*

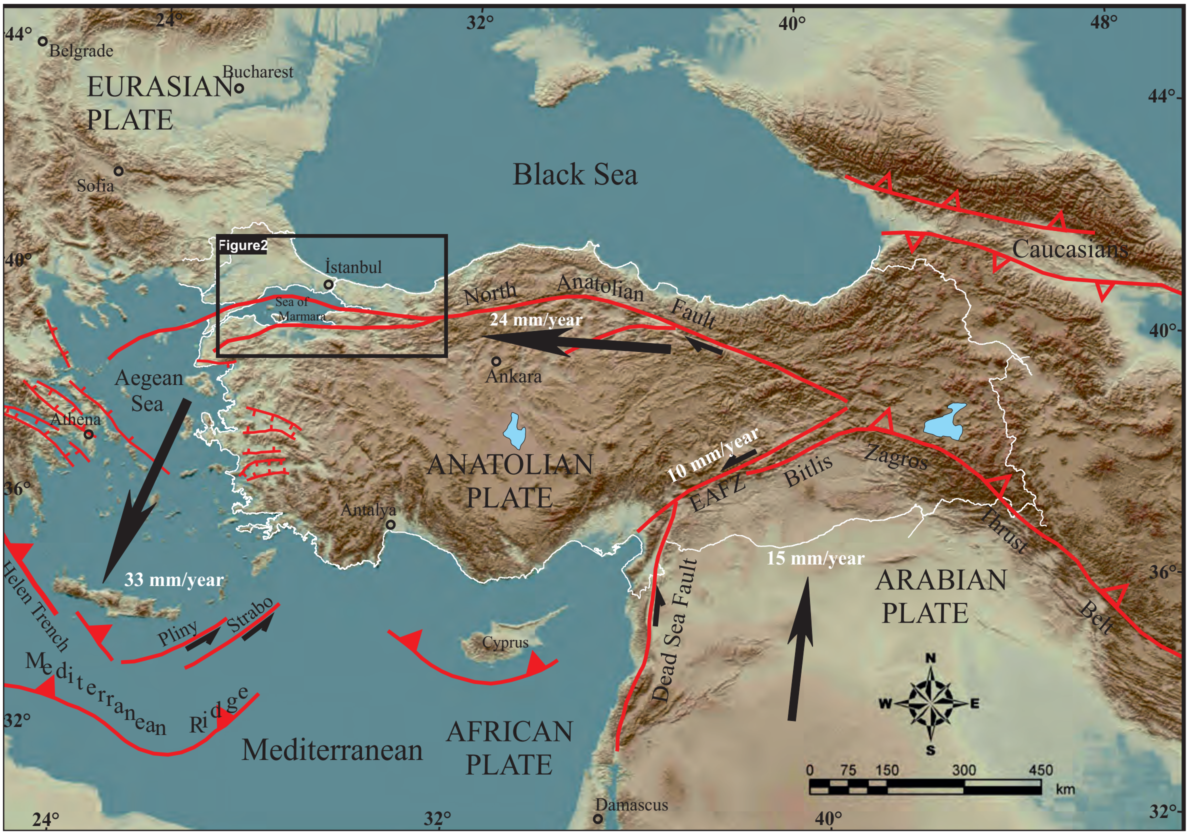

Figure 1 – Active tectonic map of Turkey. Triangles filled with red color: active subduction zones; empty triangles: active thrust belts; thick lines: strike slip faults; thin lines with small indents: normal faults. Big dark arrows and values nearby indicate the movement direction of lithospheric plates and GPS velocities according to Eurasia, respectively (modified from Okay et al., 2000; GPS velocity values were taken from Reilinger et al., 2006).

of earthquake recurrences on the Northern branch of NAF similar to the ones in the last century (Ambraseys, 1988, 2002; Ambraseys and Finkel, 1991; Guidoboni et al., 1994; Şengör et al., 2005). Despite that, data on the segment structure and paleoseismological behavior of the Southern branch are very limited. NAF which is divided into two main branches as North and South in the west of Bolu City is observed as a broad zone in Marmara Region (Figure 2). Recent GPS data indicate that plate movements in Marmara Region were basically caused by the Northern branch of NAF and these data suggest a velocity of 24±1 mm/year on this branch (McClusky et al., 2003; Reilinger et al., 2006). According to GPS data, the Southern branch which has a slip velocity of 5 mm/year causes 1/4 portion of the horizontal displacements in NAF Zone (Meade et al., 2002). Historical records and instrumental period data within the last century indicate the presence of a more intense seismicity on the Northern branch (Figure 2, Table 1) (Ambraseys, 1988, 2002; Ambraseys and Finkel, 1991; Guidoboni et al., 1994; Ambraseys and Jackson, 2000; Taymaz, 2000; Kalafat et al., 2011). Total geological offsets that have developed in NAF Zone within last 4-5 million years are compatible with GPS data and explain that the slip rate on Northern branch is 3-3.5 times higher than Southern branch (Sipahioğlu and Matsuda, 1986; Şaroğlu et al., 1987; Koçyiğit, 1988; Emre et al., 1998; Armijo et al., 2002; Meade et al., 2002; Emre and Awata, 2003; Yıldırım and Emre, 2004).

Paleoseismological studies carried out on the Northern Branch in recent years suggest that recurrence interval of large earthquakes on which surface faulting that had developed are in between 150 to 300 years (Toda et al., 2001; Emre et al., 2002; Rockwell et al., 2001, 2009; Hartleb et al., 2003, 2006; Kozacı et al., 2009, 2011; Özaksoy et al., 2010). It is known that destructive earthquakes have been occurring on the Southern branch as well during last 2000 years (Ambraseys and Finkel, 1991; Ambraseys and Jackson, 2000; Ambraseys, 2002). Large earthquakes which had formed surface faulting were defined in a limited number of paleoseismological studies. However, these data (Ikeda et al., 1989; Barka, 1992; Yoshioka and Kuşcu, 1994; Uçarkuş, 2002; Özalp et al., 2003) are not sufficient to reveal the recurrence interval and the earthquake behavior of large earthquakes on the Southern branch. In some other studies which do not have a paleoseismological basis, it is suggested that the recurrence interval of earthquakes on the Southern branch at a magnitude of M ≥ 7,0 is between 600 – 1000 years (Utkucu et al., 2011). The southern branch of NAF which is approximately 250 km long between Dokurcun and Bandırma is one of the most significant earthquake source zone of the region. After earthquakes in 1999 it is known that the earthquake hazard has greatly increased in this zone (Langridge et al., 2002). The segment structure of the Southern branch which is between Dokurcun Valley and Gemlik Bay was investigated in this study, the result of trenching carried out on Gemlik segment was presented and the earthquake hazard of the Southern branch was discussed comparing historical earthquakes with paleoseismological data.

2. Recent Tectonical Features

The study area is located in NW Anatolia which is one of the most seismically active regions of Turkey. The neotectonics of Turkey begins with continent-continent collision in Middle-Late Miocene between Arabian-African plates and Eurasian plate (McKenzie, 1972, 1978; Şengör, 1979, 1980; Jackson and McKenzie, 1984; Şengör et al., 1985). As a result of these continental collisions, North Anatolian Fault (NAF) and East Anatolian Fault (EAF), transform fault systems, which are two big recent tectonical structures of the country have revealed. NAF (Ketin, 1948) is the margin of an active plate which is approximately 1600 km long with a character of the right lateral transform strike slip (Şengör, 1979-1980) and passes across Anatolia in E-W directions. Although recent deformations are observed along a narrow zone at central and eastern parts of NAF, these deformations starting from Bolu City get a broad zonal structure towards west (Barka and Kadinsky-Cade, 1988; Barka, 1992, 1997; Armijo et al., 1999). The NAF in Eastern Marmara Region, between Bolu and the Sea of Marmara, is formed by two branches (Northern and Southern). The Southern branch of NAF, known as the Central branch in literature and separated from the main fault in Dokurcun Valley, (Barka and Kadinsky-Cade, 1988) includes into Southern Marmara region in which the bending kinematics is dominant between NAF and West Anatolian Extensional Tectonical Regime on western side (Figure 2) (Koçyiğit and Özacar, 2003; Emre et al., 2005; 2011a, b). Recent slip rate on this branch of the fault is 5 mm/year, approximately (Meade et al., 2002).

The Southern branch, which is 250 km long between Bandırma and Dokurcun valley, is formed

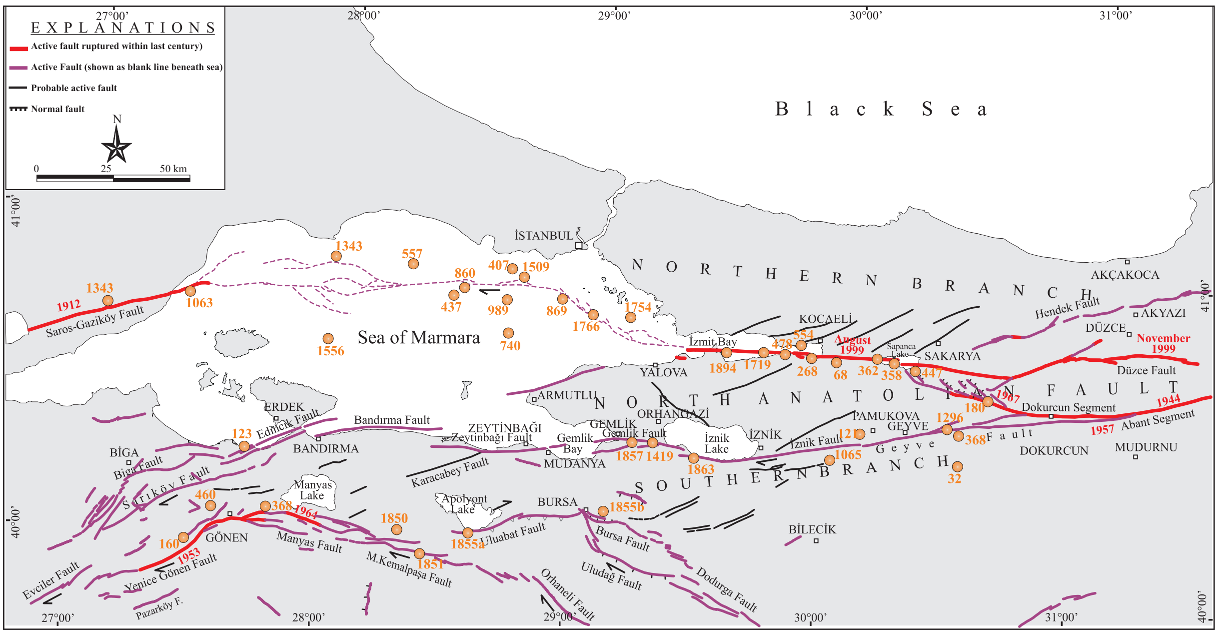

Figure 2 – Active faults of Marmara Region and the distribution map of large earthquake (Ms>6.8) epicenters that have occurred within last 2000 years. Faults that ruptured in 20th century were shown in red line (Ambraseys and Finkel, 1991; Şaroğlu et al., 1992; Emre et al., 1998; Ambraseys, 2002; Armijo et al., 2002; Tan et al., 2008).

Table 1- Large historical earthquakes along the southern Branch of the NAF

No	**Date**	**Coordinate**	**Location**	**Magnitude (Ms)**	**Intensity (I_o)**	**References**
1	??.??.29 or 24.11.29 (*e*)	40,50N – 28,90E	İznik, İzmit İznik (*e*)	?	IX $IX \leq I_o \leq XI$ (*e*)	*a, b, e*
2	??.??.32	40,50N - 30,50E	İznik	7,0 (*g*)	?	*d, g*
3	??.??.68 (*g*) or ??.??.69	40,60N – 29,90E 40,70N – 30,00E (*g*)	İznik, İzmit	7,2 (*g*)	VII $VIII \leq I_o \leq X$ (*e*)	*a, b, e, g*
4	??.??.121/122 or ??.??.120/128 (*e*)	40,60N – 29,90E	İzmit, İznik	?	VII $IX \leq I_o \leq XI$ (*e*)	*a, b, d, e*
5	03.05.170 or 03.05.181 (*e*)	40,10N – 28,00E	Bandırma, Erdek, Gemlik İzmit (*e*)	?	IX $VIII \leq I_o \leq X$ (*e*)	*a, c, e*
6	02.12.362	?	İznik	?	VIII-IX	*e*
7	11.10.368	40,40N – 29,70E (*c*) 40,50N – 29,50E (*f*) 40,50N – 30,50E (*g*)	İznik Persis (Geyve?) (*g*)	7,0<Ms<7,8 (*f*) 6,8 (g)	VII (*c*) $IX \leq I_o \leq XI$ (*e*)	*c, d, e, f, g*
8	??.??.715	40,40N – 28,90E 40,40N – 29,70E (*c*)	İznik, Gemlik	?	IX	*a, b, c*
9	26.10.740	?	İstanbul, İznik, İzmit	?	$IX \leq I_o \leq XI$	*e*
10	23.09.985	40,40N – 28,90E	İznik, Bandırma, Erdek	?	VIII	*a, c*
11	23.09.1064 or ??.09.1065 (*g*)	40,40N – 28,90E 40,40N – 30,00E (*g*)	İznik, Bandırma, Erdek	6,8 (*g*)	IX VIII (*b*)	*a, b, c, g*
12	01.06.1296	40,50N – 30,50E	Bithynia *	7,0	VIII (*c*)	*c, g*
13	15.03.1419	40,50N – 30,50E 40,40N – 29,30E (*g*)	Geyve ? Bursa (*g*)	7,0<Ms<7,8 7,2 (*g*)	?	*f, g*
14	11.04.1855	40,20N – 29,10E (*c*) 40,30N – 29,10E (*f*)	Bursa Gemlik, Mudanya (*d*)	6,6 (*f*)	X (*c*)	*c, d, f*
15	17.09.1857	?	Gemlik	?	?	*d*
16	04.06.1860	40,20N – 29,10E	Bursa	?	VII	*c*
17	06.11.1863	?	Gemlik, Umurbey, Bursa İznik (*d*)	?	IX (*c*)	*c, d*
18	16.01.1895 or 21.01.1895 (*c*)	40,44N – 29,70E 40,40N – 29,70E (*c*)	İznik	?	V	*b, c*
19	14.03.1897	40,40N – 29,10E	Gemlik	?	V	*c*

References; (a) Pınar and Lahn, 1952; (b) Ergin et al., 1967; (c) Soysal et al., 1981; (d) Ambraseys and Finkel, 1991; (e) Guidoboni et al., 1994; (f) Ambraseys and Jackson, 1998; (g) Ambraseys, 2002.

** The ancient age and after name of the geographical area of present day cities Bursa, Kocaeli, Sakarya, Bilecik, İznik, Düzce, Yalova, Bolu, Kastamonu, Bartın and Zonguldak.*

by five geometric segments namely the Geyve, İznik, Gemlik, Zeytinbağı and Bandırma faults which separate from each other by the rightward stepping structures from west to east (Figure 2). Length of segments varies between 27 and 57 km. Bandırma, Gemlik, İznik Lake and Pamukova basins have developed as transtensional structures along these segments (Barka and Kadinsky-Cade, 1988; Koçyiğit, 1988; Barka and Kuşçu, 1996; Alpar and Çizmeci, 1999; Yaltırak and Alpar, 2002; Doğan and Tüysüz, 2011). Considering geological units and the offset in Sakarya River, there is suggested a total of 17 – 26 km right lateral movement along the Southern branch (Sipahioğlu and Matsuda, 1986; Şaroğlu et al., 1987; Koçyiğit, 1988; Yıldırım and Emre, 2004; Şengör at el., 2005). Fresh fault scarps and morphological offsets indicate the presence of Holocene activity along branch (Tsukuda et al., 1988; Honkura and Işıkara, 1991; Yoshioka and Kuşçu, 1994; Barka, 1997). On the other hand, traces related to Late Quaternary activity of the fault observed on southern shelf of the Sea of Marmara on seismic profiles are quite distinctive (Alpar and Çizmeci, 1999; Yaltırak and Alpar, 2002; Okamura et al., 2003; Kurtuluş and Canbay, 2007; Kuşçu et al., 2009).

3. Seismicity

Destructive earthquakes that have occurred in Marmara Region during historical and instrumental periods are observed as dispersed on both branches of NAF (Figure 2). However, there is more intensive seismicity on the Northern branch. Although, earthquakes in the Sea of Marmara exhibit a sequential order on the Northern branch, these are observed as dispersed in Southern Marmara where the Southern branch is present. Four earthquake sequences (between 1st-2nd, 4th-6th, 11th-15th and 19th-20th centuries) can be defined within last 2000 years along Southern branch (Figure 2).

According to the historical records, destructive earthquakes occurred in AD 32, 121, 368, 1065, 1296, 1419, and 1857 along Southern branch (Figure 2) but, according to results obtained from previous paleoseismological studies, only two earthquakes have been defined which formed surface faulting along İznik and Geyve faults within last 2000 years. The last surface faulting along İznik Fault has occurred in a time between 200 and 500 years (Honkura and Işıkara, 1991). The time of occurrence of the previous large earthquake is considered that it has occurred between the years BC 250 – AD 700 and could be associated with the earthquake in AD 29 (Ambraseys and Finkel, 1991; Barka, 1997; Ambraseys, 2002). It is emphasized that recent surface faulting which is at the Eastern side of Gemlik segment occurred in 19th Century (Ikeda et al., 1991). As for the western side of the Southern branch, Bursa (1855a, 1855b), Gemlik (1857), Yenice-Gönen (1953, Ms: 7.2) and Manyas (1964, Ms: 6.8) earthquakes have occurred within last 150 years (McKenzie, 1972, 1978; Taymaz et al., 1991; Taymaz, 2000; Ambraseys, 2002; Tan et al., 2008; Kalafat et al., 2011).

During instrumental period (1900- recent), the seismic activity observed in Gemlik- Dokurcun areas of NAF is quite low (Üçer et al., 1997; Ito et al., 2002; Tan et al., 2008; Kalafat et al., 2011). Figure 3, shows recent earthquakes M>4,0 that have occurred within last century between İznik Lake and Gemlik Bay (Ergin et al., 2000; Eyidoğan et al., 2000; Özalaybey et al., 2002; Tan et al., 2008; Kalafat et al., 2011). The fault plain solution related to the earthquake in 2006 November 24th which is the latest medium size earthquake associated with Gemlik fault (Mw: 5.1) indicates a right lateral strike slip rupture mechanism and its focal depth was suggested as 14.3 km (Figure 3; Kalafat et al., 2011).

4. The Geometry and Segment Characteristics of Eastern side of the Northern Branch

The Southern branch of NAF separates from main branch in Dokurcun valley. Southern branch is approximately 160 km between Dokurcun and Gemlik Bay, and restricts Armutlu block in South. Pamukova, İznik Lake and Gemlik bay have developed along this branch and are in the character of pull-apart basin. These three basins are connected to each other with morphological grooves that have developed along the fault. The Southern branch that developed between Dokurcun and Gemlik was formed by three fault segments which separated from each other by rightward stepovers where pull-apart basins had developed. These are namely the Geyve, İznik and Gemlik faults from east to west (Figures 2, 3, 4). The length of fault segments varies between 40 and 57 km.

4.1. Geyve Fault

Geyve fault, which is located at the easternmost part of the Southern branch, is 57 km long and has an approximate trend of N70-80°E. Nearly a 25 km section of the fault lying between Dokurcun valley and Pamukova basin at East passes through a mountainous area. As for the western side, the fault morphologically restricts the Pamukova basin in South (Figure 4). To the west of Pamukova basin, Geyve and İznik faults separate from each other by 1.2

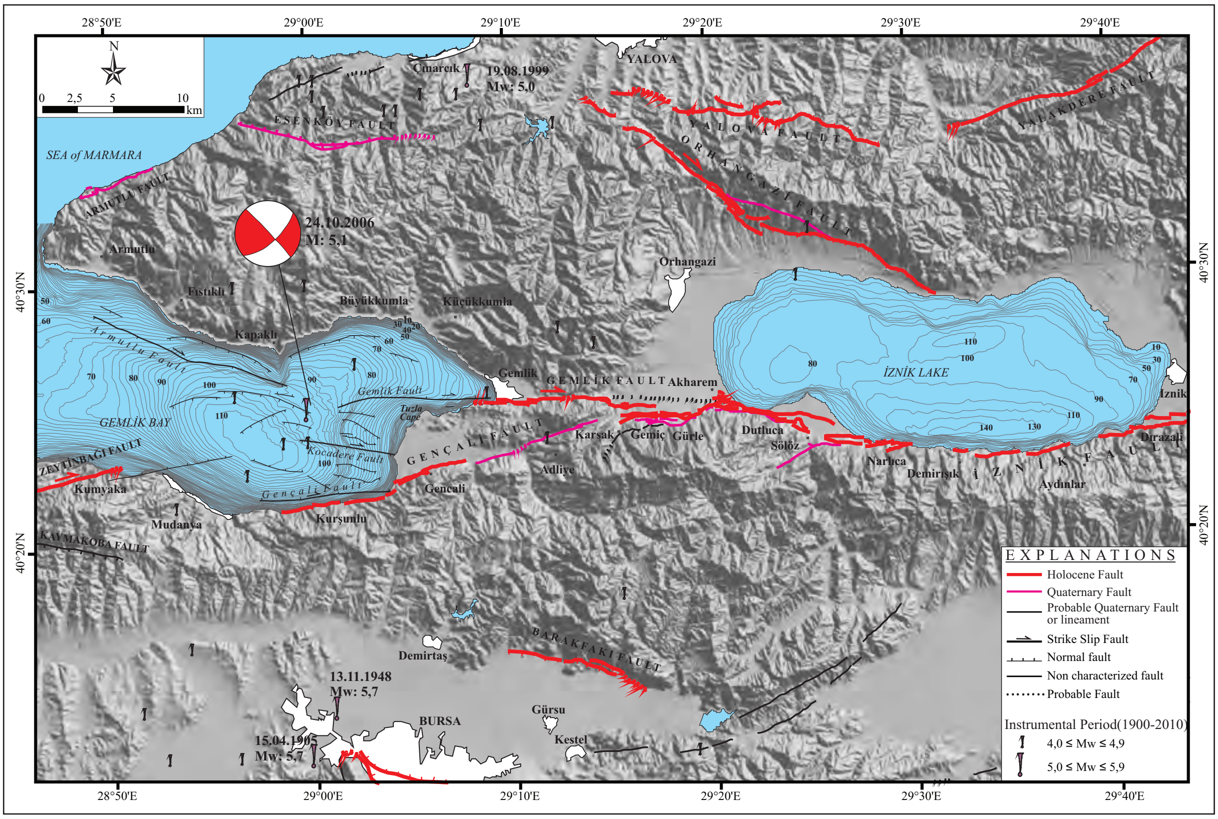

Figure 3 – Neotectonic faults of Gemlik and its vicinity (faults on land from Emre et al. (2011b), faults in Gemlik bay and the bathymetrical map from Kuşçu et al. (2009), the bathymetrical map of İznik Lake from Ikeda et al. (1991); seismological data from Kalafat et al. (2011)).

km wide and 9 km long Mekece releasing stepover. In this stepping, the western end of Geyve fault between Ciciler and Bozören villages is formed by subsegments separated from each other by rightward en echelon type stepover and these minor faults have a normal dip slip component (Figure 4). Pamukova basin has been shaped as a pull-apart basin developed in an extensional stepover between Geyve and İznik segments (Koçyiğit, 1988). The floor of basin was filled with Quaternary deposits of Sakarya River. Geyve fault restricts the basin from South. Fresh fault scarps, shutter ridges and right lateral offsets of drenaige observed along the fault can be quite clearly seen (Şaroğlu et al., 1987; Yoshioka and Kuşçu, 1994). The development of surface faulting in Late Holocene was encountered during paleoseismological trench studies carried out at SE of Pamukova basin (Yoshioka and Kuşçu, 1994).

Sakarya River in Pamuokva basin was right laterally offset by Geyve fault. According to assessments made in previous studies, a total offset varying in between 22-26 km is suggested in river bed (Sipahioğlu and Matsuda, 1986; Şaroğlu et al., 1987; Koçyiğit, 1988; Barka, 1992; Şengör et al., 2005). However, a total offset value of 16±1 km was obtained in this study in Sakarya River bed along Geyve fault. This value was estimated on either blocks of the fault by considering the geometric relation of the strait which is emplaced in Sakarya River with the fault (Figure 4). The age of primary deposition of the Sakarya River drainage is known as Late Pliocene (~3,000,000-3,500,000 years) (Tanoğlu and Erinç, 1956; Bilgin, 1968; Emre et al., 1998). Total of 16±1 km displacement along the Southern branch suggests an approximate slip rate of 5.3-4.5 mm/year for Late Pliocene – Recent, geomorphologically and this value is compatible with GPS data (Meade et al., 2002).

4.2. İznik Fault

İznik fault segment which is located between Pamukova basin and İznik Lake is 56 km long and has a strike of N80°-85°E in East and is in E-W direction at west. It is restricted by pull-apart basins on both ends. Ofsetted drainage, sag ponds, fresh fault scarps, shutter ridge along the fault are morphological formations showing the Quaternary – Holocene activity of the fault (Tsukuda et al., 1988; Honkura and Işıkara, 1991). The fault follows the

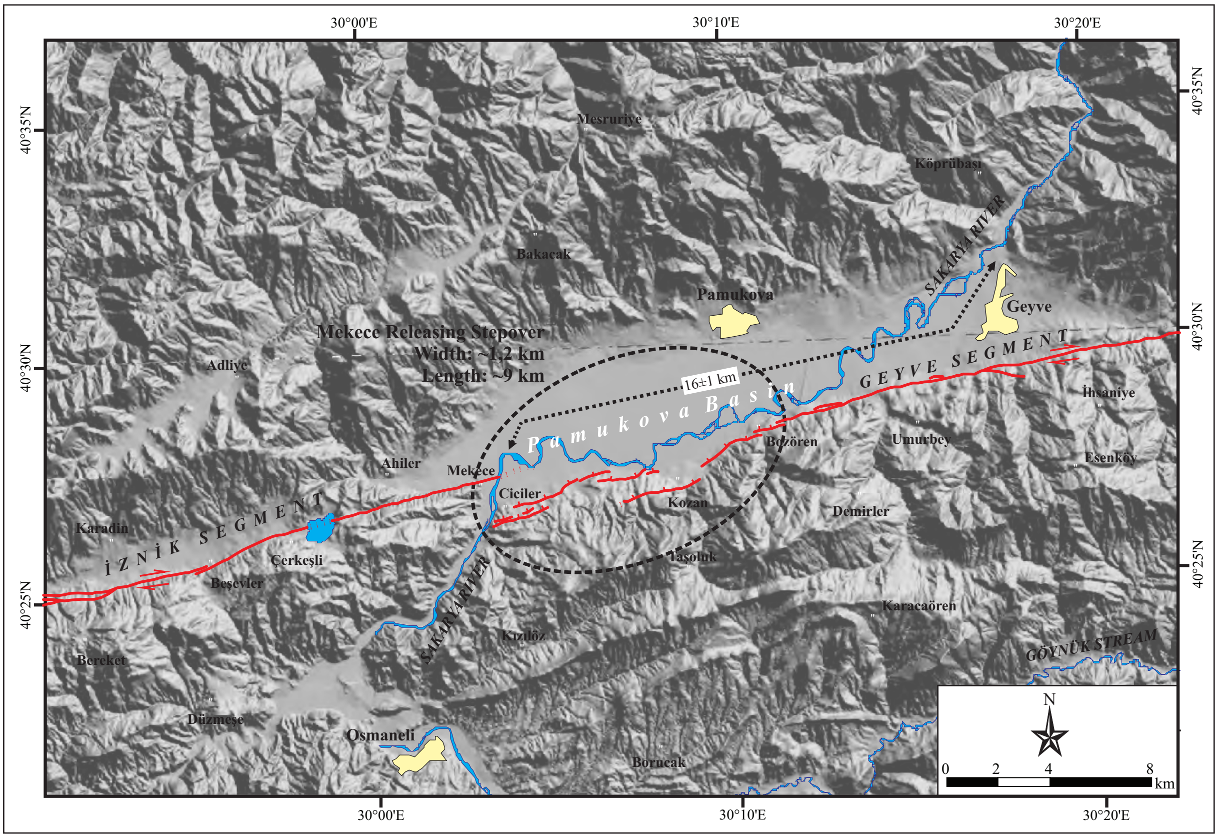

Figure 4 – The geometry of Mekece releasing stepover between İznik and Geyve segments and the right lateral movement observed in Sakarya River in Pamukova Basin.

southern margin of a groove in which the strike slip morphology is dominant and is filled with Quaternary deposits between Mekece and İznik Lake. The fault zone is divided into sub sections with a rightward stepping geometry along the southern margin of İznik Lake. The lake depression area formed within pull-apart basin was generated at a releasing stepover between Gemlik and İznik segments (Figure 3) (Barka and Kadinsky-Cade, 1988; Koçyiğit, 1988; Emre et al., 1998). Öztürk et al., (2009) state that the fault follows the southern margin of this basin within İznik Lake. İznik and Gemlik fault segments separate from each other with a releasing stepover at SW of the lake. This structure which is explained by the Sölöz releasing stepover is nearly 3 km wide and 12 km long (Figure 5). Three terrace surfaces were defined in these sections around the lake (Tanoğlu and Erinç, 1956; Bilgin, 1968). These extending terraces along the southern coast of the lake take place on the southern block of the fault which is at a higher level than the northern coast because of the normal component of the fault in this section. This situation approves that the fault has dip slip component at south of İznik Lake (Ikeda et al., 1991).

4.3. Gemlik Fault

Gemlik fault segment is located between İznik Lake and Gemlik bay pull-apart basins (Figure 3). The fault is E-W trending and has a length of 15 km section on land but reaches a length of 40 km with section below the sea (Figure 3).

The fault scarp extending parallel to Gemlik-İznik motorway at east is very distinctive. The Northern block of the fault in areas where it cuts through alluvial fans is morphologically lower than the Southern block. Back tilting and flexural morphology were observed in the Southern block. (Ikeda et al., 1989). The height of the fault scarp increases from west to east and reaches up to 5 meters heigh in the vicinity of Akharem village at east. Along the scarp, morphological findings related to strike slip faulting is very limited. At a cut in Karsak stream, it is clearly observed that the fault zone reach up to the level of culture.

The fault zone is in the position of a mountain pass along metamorphic rocks in Karsak stream. This valley was opened by a capture as an outlet of

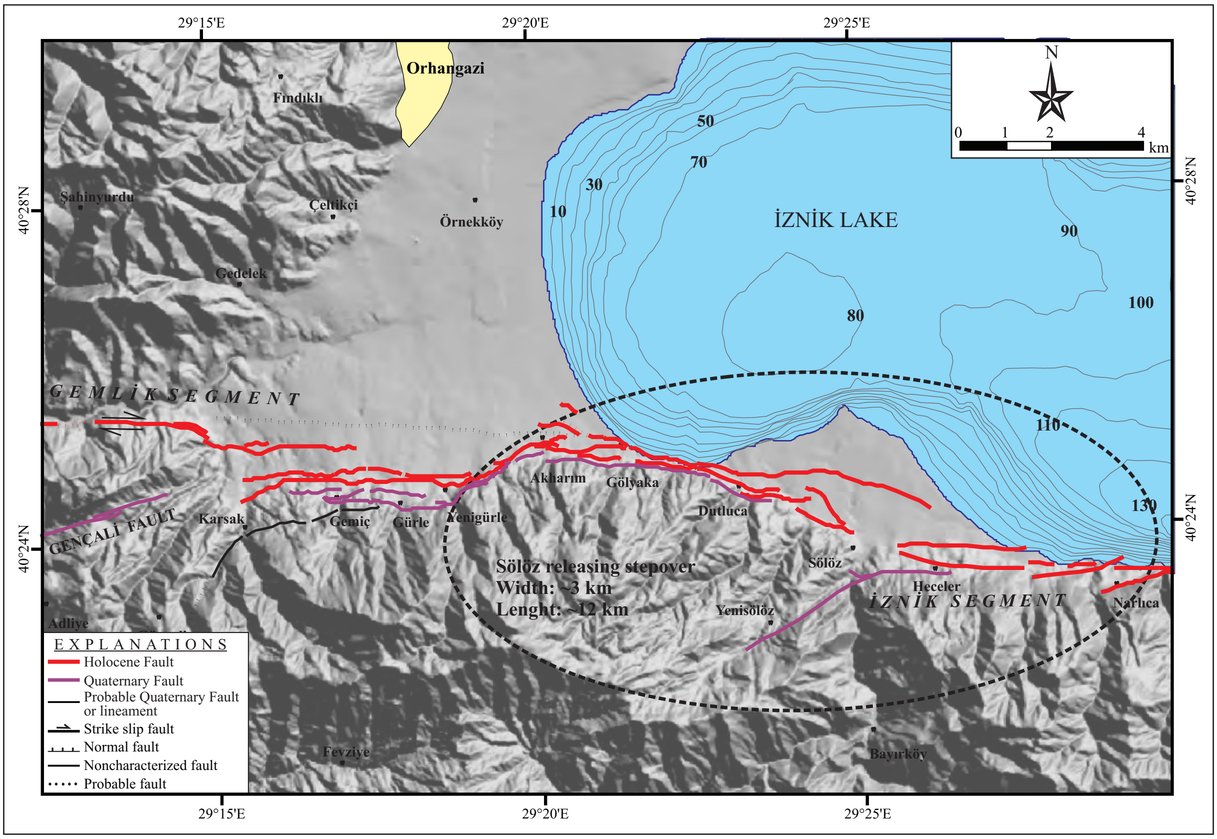

Figure 5 – The geometry of Sölöz releasing stepover between Gemlik and İznik segments. The bathymetrical map of İznik Lake was taken from Ikeda et al. (1991).

İznik Lake (Tanoğlu and Erinç, 1956). Erosional terraces on the Northern block through valley have gained an eastward inclination. The Southern block is morphologically above and exhibits a high topography in the form of steep slopes along fault. It is assumed that this fault has a reverse fault component because of its morphology. In westernmost part, the fault morphologically restricts Gemlik plain in south. In southeastern part of the plain, the fault generates from a sequence of normal faults which forms a contact between alluvial and basement rocks. Some of these cut Late Holocene alluvial fan deposits consisting of ceramic fragments. To the south of Gemlik, it was observed that hot springs were aligned along 2 km section of the fault where the fault cut flood plain deposits of Karsak stream. As the original topography at this section has been changed by human activity, aerial photographs taken in 1950 were used for mapping the fault. Accordingly; the Northern block of the fault is morphologicelly below. However, the vertical component in trench at the excavation site could not be clearly observed. The fault dives into the Sea of Marmara at south of Gemlik. The SW coasts of Gemlik bay has a linear topography. Especially, this lineament is quite clearly observed between alluvial and Eocene basement rocks in the vicinity of Tuzla Cape. High resolution shallow seismic data indicate that this lineament at southern coast of Gemlik plain extends in the same direction (Özalp et al., 2002; Okamura et al., 2003; Kuşçu et al., 2009).

5. Paleoseismological Studies

Trenching studies were attempted in the area where Terme hot spring is located in order to carry out paleoseismological assessments on Gemlik segment. In selecting the trench location, fault scarps which might be a surface fault related to historical earthquakes were taken as a basis for using aerial photographs. Terme area takes place at the central part of segment in Gemlik town (Figure 6).

Total of 7 charcoal and shell samples were taken from this trench in order to carry out C14 analysis in the Accelerator Mass Spectrometer (AMS) to clearly reveal the trench stratigraphy and ages of outcropping units in Terme hot spring. Analyses were performed in Geochron Laboratory in Massachusetts, USA. All ages were calibrated using OxCal 3.10 (Bronk Ramsey, 1998) and CALIB Rev. 5.0.1 (Stuiver and Reimer, 1993) software.

5.1. Terme Trench

Terme trench was excavated on Gemlik fault segment and the location is at the eastern part of the old Gemlik State Hospital which is beside Orhangazi – Bursa motorway (Figure 6). Along the section which lies between trench location and the Gemlik bay at west, the fault passes through settlement area, and several buildings and the hospital has been constructed over fault zone. The trench area and the primary morphology of its close vicinity have been demolished by human activity. Therefore, the fault in trench area was mapped using aerial photographs. The fault trace in aerial photographs is quite typical and the Southern block is topographically above with respect to the Northern block. The fault in the close vicinity of excavation site exhibits a zonal structure formed by rightward stepping sub sections. These faults cut across Holocene alluvial fan. The length of Terme trench is 10 meters long and 2 meters wide as being perpendicular to fault. The alluvial fan and faults cutting cross fluvial deposits were encountered in the trench. The trench was dug down to 2.8 meters as the groundwater level is high (Figure 7).

5.1.1. Trench Stratigraphy

On the walls of trench, there were observed fan deposits on top and fluvial deposits at the bottom and 5 stratigraphic units were divided in trench stratigraphy except the artificial fill (Figure 7). There are four erosional surfaces between the units. Unit 1, cropping out at the bottom, consists of coarse pebble, pebble, coarse sand and sand which are the characteristics of fluvial channel deposits of Karsak stream. Recent channel of the stream is located at 50 meters north of the excavation site. The dominant lithology in northern block is pebble and the material size is coarser than the Southern block. Whereas; coarse sand and sand are dominant on the southern block, and these layers seldom contain pieces of tiny tile and brick. The upper surface of the unit is in the form of groove marks and the deepest part corresponds with fault line. Although this groove is probably an erosional channel which developed due to post depositional stream its deepest section coincides with fault zone (Figure 7). Unit 2 overlies the lower gravel layer with an erosional contact. In general, at the base of the unit which is composed of silt and silty clay (mud), yellowish colored, well-sorted, middle-fine sand layer is situated. On both walls, sand layer is lensing within the silt, which is dominant lithology of the unit. However, it is cut by fault in the west wall. Silty layer rarely consists of sub-rounded pebbles and small charcoal fragments. Sandy layer of the unit is deposited as a channel deposits, while silty layer is deposited as a flood plain deposits. Two charcoal samples from the upper part of the unit were dated as 820 ± 40 (BP : Before Present) and 1070 ± 40 (BP) years (Table 2, figure 8). Calibrated 2 sigma age range

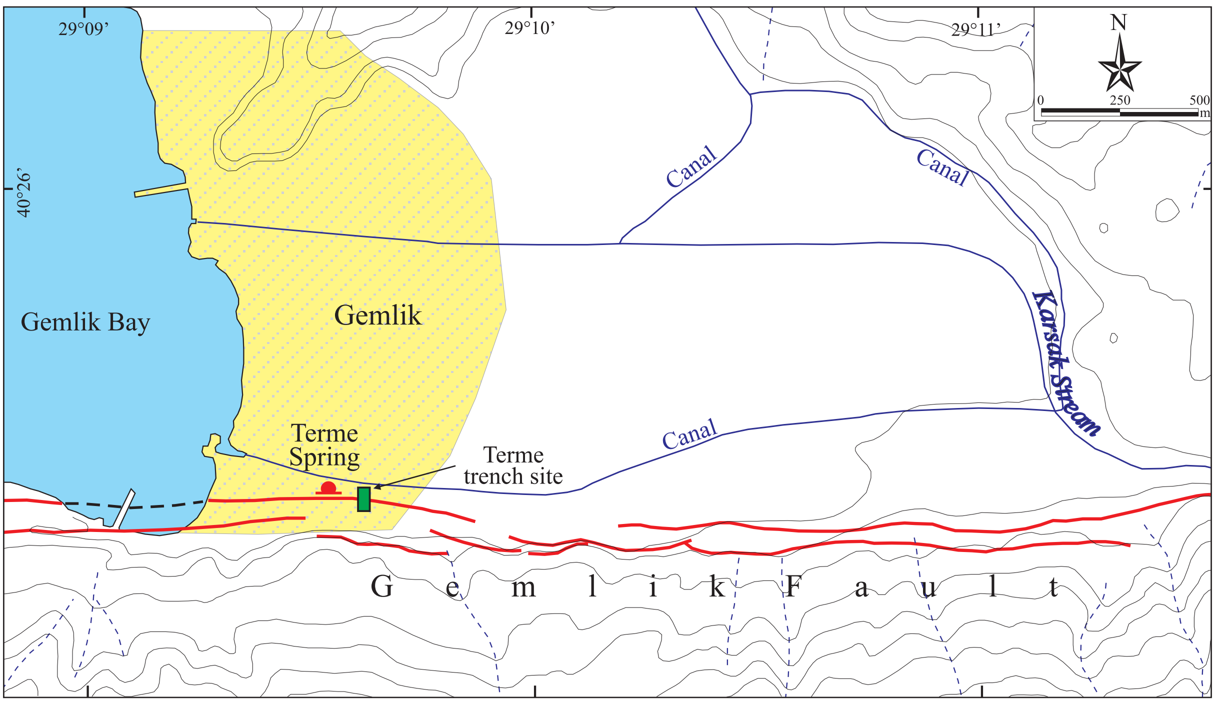

Figure 6 – Active fault map of Gemlik, its surround and the location of Terme trench site (contour interval is 20 m).

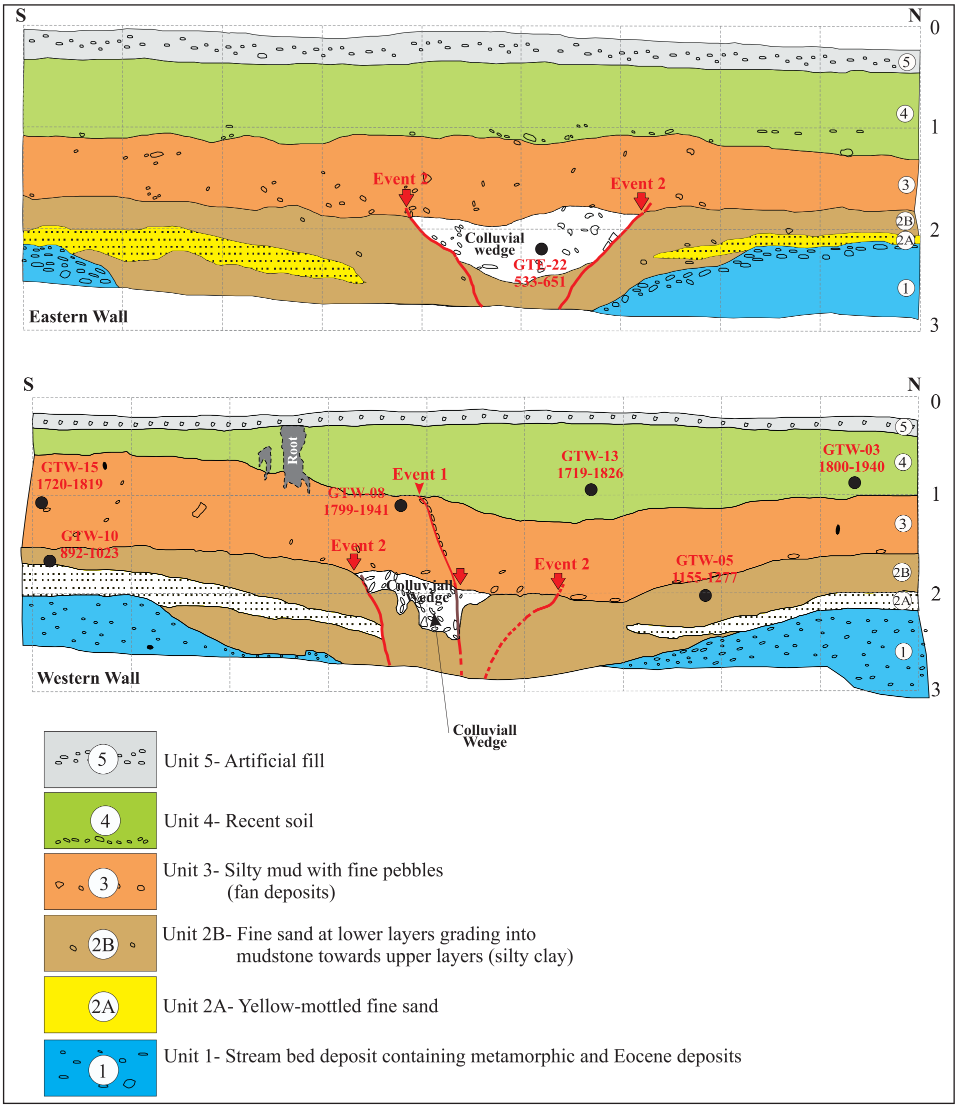

Figure 7 – Logs of Terme trench. The log of the eastern wall was inverted for correlation.

of the youngest one from AD 1155 to 1277 (Table 2). On both walls, a colluvial wedge is observed between Unit 2 and 3, and is developed just along the fault zone. It is located on a groove-shaped base on the eastern wall, while it is overlaid on an irregular base surface on the western wall (Figure 7). Pebbles within colluvial wedge which show a chaotic deposition in silts in Unit 2 are poorly sorted, rounded to subrounded and angular. Long axes of pebbles on western wall are generally vertical. The colluvial wedge represents a fault wedge that developed by a sudden deposition within micro topography. This micro topography was formed by the surface faulting which cuts Unit 2. One coal sample collected from the unit was dated as 1480 ± 40 (BP) (Table 2) but, this sample which is older than Unit 2 should have been transported. Unit 2 and the colluvial wedge are unconformably overlain by the bottom contact of Unit 3. Unit 3 has the character of alluvial fan deposit which consists of black to brown, fine pebbly, silty mud. This unit separates from Unit 2 and from the colluvial wedge at bottom by unclear pebbly soil (alteration) zone. The upper levels of the unit consist of transported marine molluscs, tile and ceramic fragments. Carrying out C14 analysis for two charcoal samples taken at this level, the ages younger than 220 years (180 ± 40 (BP) and 120 ± 40 (BP)) were obtained. This unit is overlain by Unit 4 which forms the recent soil cover, dark black, consisting of much organic fragments and thick root traces in patches. Again performing C14 method, two ages younger than 210 years were obtained as (170 ± 40 (BP) and 110 ± 40 (BP)) by taking samples from the bottom of this uppermost soil zone.

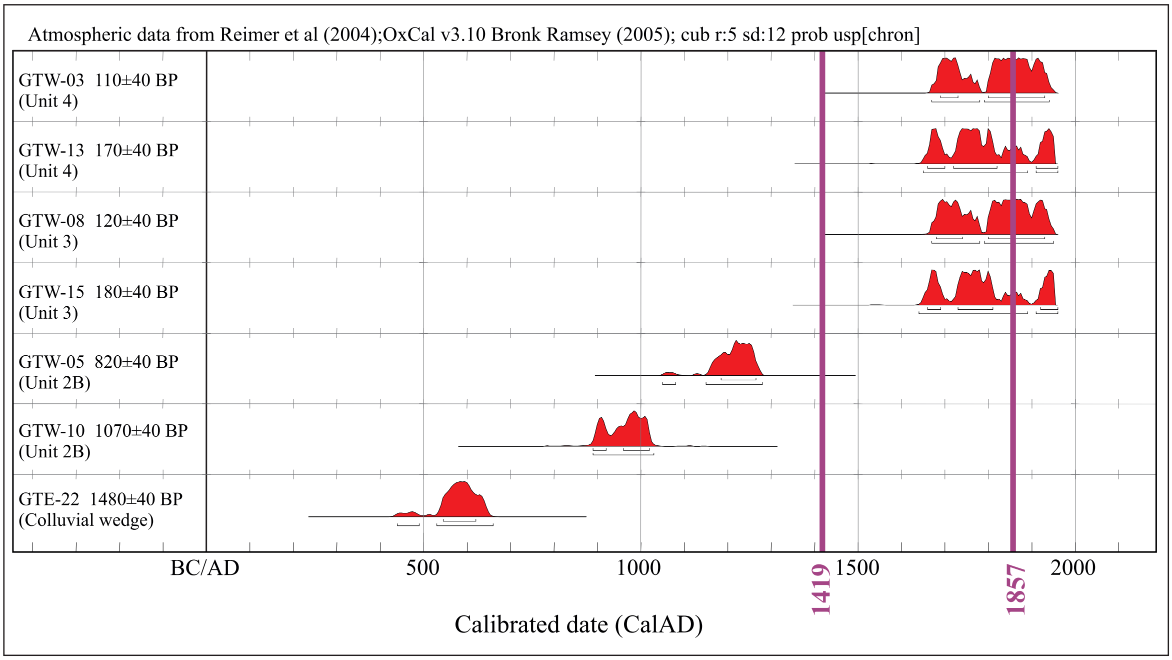

Figure 8 – Probability distribution of calibrated 14C ages (Table 2) obtained from radiocarbon dates (BP) using OxCal 3.10 software (Bronk Ramsey, 1998) for Terme Trench.

Table 2- Radiocarbon dates on samples recovered from Terme Trench.

Sample No	Laboratory No	Stratigraphic Unit	Material	$\delta^{13}C$ (‰)	14C Age (BP)	Calibrated Age Range (2σ)
GTW-03	GX-27285-AMS	Unit 4 (soil)	charcoal	-24.7	110 ± 40	AD 1677-1765 (.33) 1772-1776 (.007) **1800-1940 (.65)** 1951-1954 (.008)
GTW-13	GX-27288-AMS	Unit 4 (soil)	charcoal	-25.6	170 ± 40	AD 1655-1707 (.19) **1719-1826 (.49)** 1832-1886 (.13) 1912-1953 (.18)
GTW-08	GX-27287-AMS	Unit 3 (silt-mud)	charcoal	-24.8	120 ± 40	AD 1676-1777 (.37) **1799-1941 (.62)** 1951-1953 (.008)
GTW-15	GX-27289-AMS	Unit 3 (silt-mud)	charcoal	-26.0	180 ± 40	AD 1649-1706 (.21) **1720-1819 (.50)** 1824-1825 (.002) 1832-1883 (.10 1914-1953 (.18)
GTW-05	GX-27286-AMS	Unit 2B (mudstone)	charcoal	-22.5	820 ± 40	AD 1058-1072 (.01) **1155-1277 (.98)**
GTW-10	GX-27454-AMS	Unit 2B (mudstone)	charcoal	-26.1	1070 ± 40	AD **892-1023 (1.0)**
GTE-22	GX-27455-AMS	Cooluvial wedge	charcoal	-27.4	1480 ± 40	AD 441-455 (.01) 460-484 (.03) **533-651 (.95)**

Ages reported by radiocarbon laboratory based upon the Libby half-life (5570 years) for 14 C. The 2σ errors are presented in terms of probabilities (.97=97%) based on Calib Rev. 5.0.1 (Stuiver and Reimer, 1993).

5.1.2. Faulting Events and their Interpretation

Two faulting events were determined on the tectonostratigraphy of trench walls. The fault geometry and deformation structures indicate that the fault is strike slip, but since trench is in two dimensional, the amount of lateral displacement related to these two faulting could not be detected. The strike of the fault in trench is in E-W direction and approximately 4 m wide deformation zone is observed. Although the last earthquake (Event-1) is observed between the units 3 and 4 only on western wall of the trench, there is not any finding related to this earthquake on eastern wall of the trench (Figure 7). This situation was interpreted as the eastern wall corresponded to stepping area. The faulting related to Event-1 which is observed on the western wall cuts Units 2 and 3 with a colluvial wedge that have developed in penultimate earthquake and is overlain by recent soil located at the uppermost level (Figure 7). The fault trace is clearly observed in colluvial wedge which separates into two branches by the fault. The faulting related with this event can be defined by big and small pebble sequences emplaced in the shearing zone within Units 2 and 3. Calibrated C14 ages indicate that upper layers of Unit 3 which had been cut by the fault related with this event were deposited between 18th and 19th centuries (Figure 7 and 8, Table 2). So; it can be stated that the last earthquake has occurred within this time period. This result is compatible with the archeological age obtained from ceramic pieces proposed for the last earthquake which is at eastern part of the Gemlik fault (mid of 18th century) (Ikeda et al., 1991). This surface faulting can be correlated with historical earthquake (in 1857; M:?) which is believed that it had macroseismically occurred around Gemlik region.

The faulting related to penultimate earthquake (Event-2) on the other hand was observed on either walls of the trench. Faults related to this event in trench stratigraphy cut two units at bottom, but are overlain by Units 2 and 3. Thus, the interval between Units 2 and 3 was defined as event horizon. The colluvial wedge which is observed on both walls developed in fault zone. The event horizon corresponds to an erosional surface in trench stratigraphy. Faults and the colluvial fault wedge related to this event were eroded by erosion surface. The width of the deformation zone that has developed in this earthquake is 2 meters at top, but it gets narrower at lower levels. On the southern wall, faults related to this event are distinctive in sand layer which is being a reference layer at the bottom of Unit 2. The youngest carbon sample taken from Unit 2 was dated as 820 ± 40 (BP). This calibrated age value can be dated as in between AD 1155 and 1277 (Figure 8, Table 2). As mentioned above, Unit 3 on top can be dated as in between 18th and 19th centuries. Penultimate earthquake (Event-2) can be dated as in between AD 13th and 19th centuries according to calibrated C14 ages.

Event-2 can macroseismically be correlated with 1419 Earthquake which is interpreted that it had occurred in the section (between Gemlik bay and Dokurcun valley) of the southern branch of NAF (Ambraseys and Finkel, 1991; Ambraseys and Jackson, 1998; Ambraseys, 2002). Surface faulting related to 1419 Earthquake was approved paleoseismologically also in İznik segment of the southern branch (Honkura and Işıkara, 1991). There is not any record related to a destructive earthquake on Gemlik fault except for 1419 Earthquake between 13th-18th centuries. Hence, surface faulting related to Event-2 detected in Terme trench can be correlated with 1419 Earthquake.

6. Discussion and Results

The southern branch which separated from the main branch of NAF in Dokurcun Valley is approximately 160 km long up to Gemlik Bay. The southern branch that developed between Dokurcun and Gemlik was formed by three fault segments which separated from each other by rightward stepovers where pull-apart basins had developed. These are namely the Geyve, İznik and Gemlik faults from east to west. The length of fault segments varies in between 40 and 57 km. As a result of Terme trench studies carried out over Gemlik segment, both historical and paleoseismological data were assessed together and the seismic hazard of the southern branch was interpreted.

Findings obtained from Terme trench excavation explain that two large earthquakes have occurred as a result of surface faulting over Gemlik fault within 600 years period which covers a time interval of 13th century to recent. Radiometric ages indicate that the latest and second surface faulting on fault are dated as; 18th-19th and 13th-18th centuries, respectively. Sample GTW-05 indicates an earthquake that has occurred after AD 1216 ± 61, whereas; the sample GTW-15 indicates an earthquake which has occurred after AD 1770 ± 50. So, it can be said that the penultimate earthquake had occurred between these two dates based on this data. According to historical records on the southern branch of NAF, 1296 and 1419 earthquakes have been within this period (Table 1). According to Soysal et al. (1981) and Ambraseys (2002), Geyve segment has originated from 1296 Earthquake. It was interpreted that, this latest surface faulting defined during paleoseismological excavations in İznik segment was dated back to 200-500 years and corresponds to 1419 earthquake (Honkura and Işıkara, 1991). The surface faulting related to Event-1 defined in this study in Gemlik fault as well can be correlated with 1419 Earthquake. This correlation explains that, the surface faulting has developed on both the İznik and Gemlik faults in 1419 Earthquake and the faulting is approximately 95 km long. Using empirical equations between surface faulting length and earthquake magnitude, it can be stated that the magnitude of 1419 Earthquake is Mw: 7.3 (Wells and Coppersmith, 1994). As being compatible with this approach, Ambraseys (2002) indicates the magnitude of 1419 Earthquake as Mw: 7.2.

The last earthquake determined in Terme trench can be assessed within an earthquake series generated from 5 destructive earthquakes between the years 1850-1863 in Kemalpaşa-Bursa-Gemlik-İznik regions in 19th century in historical records. This earthquake series proceeding from west to east along active faults in Southern Marmara Region are formed from earthquakes of 1850 April 19th, 1855 February 28th, 1855 April 11th, 1857 September 17th and 1863 November 6th (Ambraseys and Finkel, 1991; Ambraseys, 2002). According to damage distribution (Ambraseys and Finkel, 1991), it is probable that earthquake in 1850 April 19th, in 1855 February 28th and 1855 April 11th originated from Kemalpaşa, Uluabat and Bursa faults which are in normal fault character, respectively. Damages in 1857 Earthquake has become intensive along Gemlik fault. Bursa fault which is the origin of 1855 Earthquake is located in the apex of an active fault system which is convex southward (Emre et al. 2011a, 2013). Gemlik fault restricts the hanging block of this fault in north. Because of this relationship, it is highly probable that 1857 Earthquake was triggered by 1855 Earthquake that had occurred on Bursa fault.

The recurrence time between last two earthquakes on Gemlik fault is 438 years. Yet, the time elapsed since the latest earthquake till today is 595 years in İznik segment and 717 years in Geyve segment (Ikeda, 1988; Yoshioka and Kuşçu, 1994). This situation explains that fault segments on the Southern branch of NAF have earthquakes with recurrence periods different than each other. However, 1419 Earthquake shows that these fault segments have been ruptured together in the same earthquake. Therefore, it can be asserted that, fault segments on the southern branch do not have a typical earthquake behavior. When 5 mm/year slip rate and duration elapsed since recent earthquakes till today are taken into consideration, it can be stated that there is a strain deformation corresponding to displacements of 3.5 m in Geyve fault and 3.0 m in İznik fault. Later than the earthquakes in 1999 there is a general consensus that the earthquake migration from east to west in NAF within the last century would continue along the main branch and the seismic hazard has increased a lot especially for the section of the Sea of Marmara. Nevertheless, the findings in this study show that fault segments on the southern branch of NAF produced large earthquakes that have not regular recurrence period. This study also indicates that the southern branch has a close or an equivalent potential to produce earthquake as well as the northern branch.

Acknowledgements

This study has been supported by the General Directorate of Mineral Research and Exploration. During excavation and drainage of trenches logistical support was taken from Gemlik Municipality. We are thankful to all organizations and executives, and to reviewers for their critics and supports.

Received: 10.12.2012
Accepted: 06.08.2013
Published: December 2013

References

Alpar, B., Çizmeci, S. 1999. Seismic hazard assessment in the Gemlik Bay region following the 17 August Kocaeli Earthquake. *Turkish Journal of Marine Sciences* 5, 3, 149-166.

Ambraseys, N.N. 1970. Some characteristic features of the North Anatolian Fault. *Tectonophysics* 9, 143-165.

Ambraseys, N.N. 1988. Engineering seismology. *Journal of Earthquake Engineering and Structural Dynamics* 17, 1-105.

Ambraseys, N.N. 2002. The seismic activity of the Marmara Sea region over the last 2000 years. *Bulletin of the Seismological Society of America* 92, 1, 1-18.

Ambraseys, N.N., Finkel, C.F. 1991. Long term seismicity of İstanbul and of the Marmara region. *Terra Nova* 3, 527-539.

Ambraseys, N.N., Jackson, J.A. 1998. Faulting associated with historical and recent earthquakes in the Eastern Mediterranean region. *Geophysical Journal International* 133, 390-406.

Ambraseys, N.N., Jackson, J.A. 2000. Seismicity of the Sea of Marmara (Turkey) since 1500. *Geophysical Journal International* 141, F1-F6.

Armijo, R., Meyer, B., Hubert, A. and Barka, A. 1999. Westward propagation of the North Anatolian fault into the northern Aegean: Timing and kinematics. *Geology*, 27, 3, 267–270.

Armijo, R., Meyer, B., Navarro, S., King, G. and Barka, A. 2002. Asymmetric slip partitioning in the Sea of Marmara pull-apart: a clue to propagation processes of the North Anatolian Fault? *Terra Nova* 14, 2, 80-86.

Barka, A.A. 1992. The North Anatolian Fault. *Annales Tectonicae* 6, 174-195.

Barka, A.A. 1997. Neotectonics of the Marmara region. In: Schindler, C., Pfister, M. (Eds.), Active Tectonics of Northwestern Anatolia-The Marmara Poly-Project, vdf Hochschulverlag AG an der ETH Zürich, 55-87.

Barka, A.A., Kadinsky-Cade, K. 1988. Strike-slip fault geometry in Turkey and its influence on earthquake activity. *Tectonics* 7, 3, 663-684.

Barka, A.A., Kuşçu, İ. 1996. Extents of the North Anatolian Fault in the İzmit, Gemlik and Bandırma bays. *Turkish Journal of Marine Sciences* 2, 93-106.

Bilgin, T. 1968. Samanlı Dağları. İst. Üniv. Coğ. Enst. Yayl. 50, 196 s.

Bronk Ramsey, C. 1998. Radiocarbon Calibration and Analysis of Stratigraphy: the OxCal Program. *Radiocarbon*, 37, 425-430.

Doğan, B., Tüysüz, O. 2011. Kuzey Anadolu Fay Sistemi Güney Kolunun Geyve-Gemlik arasındaki kesiminin tektonostratigrafik evrimi. İtü dergisi/d, Mühendislik, 10/4, 107-118.

Emre, Ö., Erkal, T., Tchepalyga, A., Kazancı, N., Keçer, M., Ünay, E. 1998. Neogene-Quaternary evolution of the Eastern Marmara Region, Northwest Turkey. *Bulletin of the Mineral Research and Exploration*, 120, 119-145.

Emre, Ö., Sugai, T., Doğan, A., Özalp, S., Okuno, M., Yıldırım, C., Masaaki, Y. 2002. Paleoseismological findings on the penultimate faulting of the Arifiye segment; 1999 İzmit earthquake, North Anatolian Fault. *Eos Transactions AGU* 83, 47, Fall Meet. Suppl., F1015.

Emre, Ö., Awata, Y. 2003. Neotectonic characteristics of the North Anatolian Fault System in the eastern Marmara region. In: Emre, Ö., Awata, Y., Duman, T.Y. (Eds.), Surface Rupture Associated with the August 17, 1999 İzmit Earthquake. *General Directorate of Mineral Research and Exploration of Turkey*, Special Publication Series: 1, 31-39, Ankara.

Emre, Ö., Doğan, A., Yıldırım, C., Şaroğlu, F. 2005. Active fault pattern and bend kinematics in NW Anatolia. *International Symposium on the Geodynamics of Eastern Mediterranean: Active Tectonics of the Aegean Region*, 15-18 June 2005, Kadir Has University, Abstracts, p. 98, İstanbul, Turkey.

Emre. Ö., Doğan, A., Özalp, S., Yıldırım, C. 2011*a*. 1:250.000 Ölçekli Türkiye Diri Fay Haritası Bandırma (NK 35-11b) Paftası. *MTA 1:250.000 Ölçekli Diri Fay Haritaları Serisi*, Seri No: 3, 55 s., Ankara.

Emre. Ö., Doğan, A., Duman, T.Y., Özalp, S. 2011*b*. 1:250.000 Ölçekli Türkiye Diri Fay Haritası Serisi, Bursa (NK 35-12) Paftası. Seri No: 9, *Maden Tetkik ve Arama Genel Müdürlüğü*, Ankara.

Emre, Ö., Duman, T.Y., Özalp, S., Elmacı, H., Olgun, Ş., Şaroğlu, F., 2013. Açıklamalı Türkiye Diri Fay Haritası, Ölçek 1:1.250.000. *Maden Tetkik ve Arama Genel Müdürlüğü, Özel Yayın Serisi*: 30, 89 s., Ankara.

Erdik, M., Demircioğlu, M., Sesetyan, K., Durukal, E., Siyahi, B. 2004. Earthquake hazard in Marmara Region. Turkey. *Soil Dynamics and Earthquake Engineering*, 24, 605–631.

Ergin, K., Güçlü, U., Uz, Z. 1967. Türkiye ve civarının deprem kataloğu (Milattan Sonra 11 yılından 1964 sonuna kadar). *İTÜ, Maden Fakültesi, Arz Fiziği Enstitüsü Yayınları*, No: 24, 169s.

Ergin, M., Özalaybey, S., Aktar, M.T., Tapırdamaz, C., Yörük, A., Biçmen, F. 2000. Aftershock analysis of the August 17, 1999 İzmit, Turkey, Earthquake. Barka, A., Kozacı, Ö., Akyüz, S., Altunel, E. (Eds.), The 1999 İzmit and Düzce earthquakes: preliminary results. *İstanbul Technical Univ. Press,* İstanbul, pp. 171-178.

Eyidoğan, H., Haessler, H., Polat, O., Cisternas, A., Gürbüz, C., Frogneux, M., Aktar, M., Üçer, B., Bouchon, M., Comte, D., Philip, H., Kaypak, B., Ergin, M., Karabulut, H., Akıncı, A., Kuleli, S., Yörük, A. 2000. August 17, 1999, Kocaeli (İzmit) Earthquake: before, during and after. In: Barka, A., Kozacı, Ö., Akyüz, S., Altunel, E. (Eds.), The 1999 İzmit and Düzce earthquakes: preliminary results. *İstanbul Technical Univ. Press*, İstanbul, pp. 161-169.

Guidoboni, E., Comastri, A., Traina, G. 1994. Catalogue of ancient earthquakes in the Mediterranean area up to the 10th century. *Instituto Nazionale di Geofisica,* Roma, 502 pp.

Hartleb, R.D., Dolan, J.F., Akyüz, H.S., Yerli, B., 2003. A 2000-Year-Long Paleoseismologic Record of Earthquakes along the Central North Anatolian Fault, from Trenches at Alayurt, Turkey. *Bulletin of the Seismological Society of America*, 93, 5, 1935–1954.

Hartleb, R.D., Dolan, J.F., Kozacı, Ö., Akyüz, H.S., Seitz, G.G., 2006. A 2500-yr-long paleoseismologic record of large, infrequent earthquakes on the North Anatolian fault at Çukurçimen, Turkey. *Geological Society of America Bulletin*, 118, 7/8, 823–840.

Honkura, Y., Işıkara, A.M. 1991. Multidisciplinary research on fault activity in the western part of the North

Anatolian Fault Zone. *Tectonophysics*, 193, 347-357.

Ikeda, Y. 1988. Geomorphological observations of the North Anatolian fault, west of Mudurnu. In: Honkura, Y., Işıkara, A.M. (Eds.), Multidisciplinary research on fault activity in the western part of the North Anatolian fault zone. *Tokyo Institute of Technology*, Tokyo, 6-14.

Ikeda, Y., Suzuki, Y., Herece, E. 1989. Late Holocene activity of the North Anatolian fault zone in the Orhangazi plain, Northwestern Turkey. In: Honkura, Y., Işıkara, A.M. (Eds.), Multidisciplinary research on fault activity in the western part of the North Anatolian fault zone (2). *Tokyo Institute of Technology*, Tokyo, 16-30.

Ikeda, Y., Suzuki, Y., Herece, E., Şaroğlu, F., Işıkara, A.M., Honkura, Y. 1991. Geological evidence for the last two faulting events on the North Anatolian Fault Zone in the Mudurnu Valley, Western Turkey. *Tectonophysics*, 193, 335-345.

Ito, A., Üçer, B., Barış, S., Nakamura, A., Honkura, Y., Kono, T., Hori, S., Hasegawa, A., Pektaş, R., Işıkara, A.M. 2002. Aftershock activity of the 1999 İzmit, Turkey, earthquake revealed from microearthquake observations. *Bulletin of the Seismological Society of America*, 92, 1, 418-427.

Jackson, J., McKenzie, D.P. 1984. Active tectonics of the Alpine-Himalayan belt between western Turkey and Pakistan. *Geophysical Journal of the Royal Astronomical Society*, 77, 185–264.

Kalafat, D., Güneş, Y., Kekovalı, K., Kara, M., Deniz, P., Yılmazer, M. 2011. Bütünleştirilmiş Homojen Türkiye Deprem Kataloğu (1900-2010); M≥4.0). *Boğaziçi Üniversitesi, Kandilli Rasathanesi ve Deprem Araştırma Enstitüsü*, Yayın No: 1049, 640 s., Bebek-İstanbul.

Ketin, İ. 1948. Uber die tektonisch-mechanischen Folgerungen aus den grossen anatolischen Erdbeben des letzten Dezenniums. *Geologische Rundschau*, 36, 77-83.

Ketin, İ. 1957. Kuzey Anadolu Deprem Fayı. *İstanbul Teknik Üniversitesi Dergisi*, 15, 49-52

Koçyiğit, A. 1988. Tectonic setting of the Geyve basin: age and total displacement of Geyve fault zone. *Middle East Technical University Journal of Pure and Applied Sciences*, 21, 81-104.

Koçyiğit, A., Özacar, A.A. 2003. Extensional Neotectonic Regime through the NE edge of the outer Isparta Angle, SW Turkey: new field and seismic data. *Turkish Journal of Earth Sciences*, 12 (1), 67-90.

Kozacı, Ö., Dolan, J.F., Finkel, R.C., 2009. A late Holocene slip rate for the central North Anatolian fault, at Tahtaköprü, Turkey, from cosmogenic 10Be geochronology: Implications for fault loading and strain release rates. *Journal of Geophysical Research*, 114, B01405.

Kozacı, Ö., Dolan, J.F., Yönlü, Ö., Hartleb, R.D., 2011. Paleoseismologic evidence for the relatively regular recurrence of infrequent, large-magnitude earthquakes on the eastern North Anatolian fault at Yaylabeli,Turkey. *Lithosphere*, 3, 37-54.

Kurtuluş, C., Canbay, M.M. 2007. Tracing the middle strand of the North Anatolian Fault Zone through the southern Sea of Marmara based on seismic reflection studies. *Geo-Mar Letters*, 27, 27–40.

Kuşçu, İ., Okamura, M., Matsuoka, H., Yamamori, K., Awata, Y., Özalp, S. 2009. Recognition of Active Faults and Stepover Geometry in Gemlik Bay, Sea of Marmara, NW Turkey. *Marine Geology*, 260, 90-101.

Langridge, R. M., Stenner, H. D., Fumal, T. E., Christofferson, S. A., Rockwell, T. K., Hartleb, R. D., Bachhuber, J., Barka, A. A. 2002. Geometry, slip distribution, and kinematics of surface rupture on the Sakarya fault segment during the 17 August 1999 İzmit earthquake, Turkey. *Bulletin of ther Seismological Society of America*, 92, 1, 107–125.

McClusky, S., Reilinger, R., Mahmoud, S., Ben Sari, D., Tealeb, A. 2003. GPS constraints on Africa (Nubia) and Arabia plate motions. *Geophysical Journal International*, 155, 126-138.

McKenzie, D. 1972. Active tectonics of the Mediterranean region. *Geophysical Journal of the Royal Astronomical Society*, 30, 109-195.

McKenzie, D. 1978. Active tectonics of the Alpine-Himalayan Belt: The Aegean Sea and surrounding regions. *Geophysical Journal of the Royal Astronomical Society*, 55, 217-254.

Meade, B.J., Hager, B.H., McClusky, S.C., Reilinger, R.E., Ergintav, S., Lenk, O., Barka, A., Özener, H. 2002. Estimates of seismic potential in the Marmara region from block models of secular deformation constrained by GPS measurements. *Bulletin of ther Seismological Society of America*, 92(1), 208-215.

Okamura, M., Matsuoka, H., Kuşçu, İ., Özalp, S., Kinjo, S., Yamamori, K., Awata, Y. 2003. Submarine faults activities in the Gulf of İzmit and Gemlik Bay, NW Turkey: high-resolution shallow seismic survey and earthquake recurrence studies. *Eos Transactions AGU* 84 (46), Fall Meet. Suppl., F1367.

Okay, A.İ., Kaşlılar-Özcan, A., İmren, C., Boztepe-Güney, A., Demirbağ, E., Kuşçu, İ. 2000. Active faults and evolving strike-slip basins in the Marmara Sea, northwest Turkey: a multichannel seismic reflection study. *Tectonophysics*, 321, 189-218.

Özaksoy, V., Emre, Ö., Yıldırım, C., Doğan, A., Özalp, S., Tokay, F., 2010. Sedimentary record of Late Holocene seismicity and uplift of Hersek restraining-bend along the North Anatolian Fault in the Gulf of İzmit. *Tectonophysics*, 487, 33-45.

Özalaybey, S., Ergin, M., Aktar, M., Tapırdamaz, C., Biçmen, F., Yörük, A. 2002. The 1999 İzmit earthquake sequence in Turkey: Seismological and tectonic aspects. *Bulletin of the Seismological Society of America*, 92, 1, 376-386.

Özalp, S., Kuşçu, İ., Okamura, M., Matsuoka, H., Yamamori, K., Nakaido, T., Özer, C., Emre, Ö. 2002. Gemlik Körfezindeki Aktif Faylar-Ön Bulgular. *Aktif Tektonik Araştırma Grubu Altıncı Toplantısı* (ATAG-6), 21-22 Kasım 2002, Bildiri Özleri, s.63, Ankara.

Özalp, S., Doğan, A., Emre, Ö. 2003. The last two faulting events on the southern strand of the North Anatolian Fault Zone, NW Turkey. *Eos Transactions AGU* 84 (46), Fall Meet. Suppl., F1003.

Öztürk, K., Yaltırak, C., Alpar, B. 2009. The Relationship Between the Tectonic Setting of the Lake İznik Basin and the Middle Strand of the North Anatolian Fault. *Turkish Journal of Earth Sciences*, 18, 209–224.

Parsons, T., Toda, S., Stein, R.S., Barka, A., Dieterich, J.H. 2000. Heightened Odds of Large Earthquakes Near Istanbul: An Interaction-Based Probability *Calculation. Science*, 288, 661-665.

Pınar, N., Lahn, E. 1952. Türkiye depremleri izahlı katoloğu. Bayındırlık Bakanlığı, Yapı ve İmar İşleri Reisliği Yayınları, 6, 36, 153s, Ankara.

Reilinger, R., McClusky, S., Vernant, P., Lawrence, S., Ergintav, S., Cakmak, R., Ozener, H., Kadirov, F., Guliev, I., Stepanyan, R., Nadariya, M., Hahubia, G., Mahmoud, S., Sakr, K., ArRajehi, A., Paradissis, D., Al-Aydrus, A., Prilepin, M., Guseva, T., Evren, E., Dmitrotsa, A., Filikov, S.V., Gomez, F., Al-Ghazzi, R., Karam, G. 2006. GPS constraints on continental deformation in the Africa-Arabia-Eurasia continental collision zone and implications for the dynamics of plate interactions. *Journal of Geophysical Research*, 111, B05411.

Rockwell, T., Barka, A., Dawson, T., Akyüz, S., Thorup, K., 2001. Paleoseismology of the Gaziköy-Saros segment of the North Anatolia fault, northwestern Turkey: Comparison of the historical and paleoseismic records, implications of regional seismic hazard, and models of earthquake recurrence. *Journal of Seismology*, 5, 433-448.

Rockwell, T., Ragona, D., Seitz G., Langridge, R., Aksoy, M.E., Uçarkuş, G., Ferry, M., Meltzner, A.J., Klinger, Y., Meghraoui, M., Şatır, D., Barka, A., Akbalık, B. 2009. Palaeoseismology of the North Anatolian Fault near the Marmara Sea: implications for fault segmentation and seismic hazard. In: Reicherter, K., Michetti, A.M. & Silva, P.G. (Eds) Palaeoseismology: Historical and Prehistorical Records of Earthquake Ground Effects for Seismic Hazard Assessment. *The Geological Society, London*, Special Publications, 316, 31–54.

Sipahioğlu, S., Matsuda, T. 1986. Geology and Quaternary fault in the İznik-Mekece area. In: Işıkara, A.M., Honkura, Y., (Eds.), Electric and Magnetic Research on Active Faults in the North Anatolian Fault Zone. *Tokyo Institute of Technology*, Tokyo, pp. 25-41.

Soysal, H., Sipahioğlu, S., Kolçak, D., Altınok, Y. 1981. Türkiye ve çevresinin tarihsel deprem kataloğu, M.Ö. 2100 – M.S. 1900. TÜBİTAK Proje No. TBAG 341, İstanbul, 87s.

Stein, R.S., Dieterich, J.H., Barka, A.A. 1996. Role of stress triggering in earthquake migration on the North Anatolian Fault. *Physics and Chemistry of the Earth*, 21, 4, 225-230.

Stuiver, M., Reimer, P.J. 1993. Extended 14C database and revised CALIB radiocarbon calibration program. *Radiocarbon*, 35, 215-230.

Şaroğlu, F., Emre, Ö., Boray, A. 1987. Türkiye'nin Diri Fayları ve Depremsellikleri. *Maden Tetkik ve Arama Genel Müdürlüğü,* Rapor no: 8174, Ankara, 394s.

Şaroğlu, F., Emre, Ö., Kuşçu, İ. 1992. Türkiye Diri Fay Haritası. MTA Genel Müdürlüğü, Ankara.

Şengör, A.M.C. 1979. The North Anatolian Transform Fault: its age, offset and tectonic significance. *Geologial Society of London*, 136, 269–282.

Şengör, A.M.C. 1980. Türkiye›nin neotektoniğinin esasları. Türkiye Jeol. Kur. Yayl., 40s.

Şengör, A. M. C., Görür, N., Şaroglu, F. 1985. Strike-slip faulting and related basin formation in zones of tectonic escape: Turkey as a case study. In Biddle, K.T., Christie-Blick, N. (Eds.). Strike-Slip Deformation, Basin Formation and Sedimentation. *Society of Economic Poleontologistr and Mineralogists* Special Publication 37, 227-264

Şengör, A.M.C., Tüysüz, O., İmren, C., Sakınç, M., Eyidoğan, H., Görür, N., Le Pichon, X., Rangin, C. 2005. The North Anatolian Fault: A new look. *Annual Revieue of Earth and Planetary Sciences*, 33, 37-112.

Tan, O., Tapırdamaz, M.C., Yörük, A. 2008. The earthquake catalogues for Turkey. *Turkish Journal of Earth Sciences*, 17, 405-418.

Tanoğlu, A., Erinç, S. 1956. Garsak Boğazı ve Eski Sakarya. *İstanbul Üniversitesi Coğrafya Enstitüsü Dergisi*, 4 (7), 17-30.

Taymaz, T. 2000. Seismotectonics of the Marmara region: Source characteristics of 1999 Gölcük-Sapanca-Düzce earthquakes. In: Barka, A., Kozacı, Ö., Akyüz, S., Altunel, E. (Eds.), The 1999 İzmit and Düzce earthquakes: preliminary results. *İstanbul Technical University* Press, İstanbul, pp. 79-97.

Taymaz, T., Jackson, J.A., McKenzie, D. 1991. Active tectonics of the North and Central Aegean Sea. *Geophysical Journal International*, 106, 433-490.

Toda, S., Tsutsumi, H., Duman, T.Y., Emre, Ö., Okuno, M., Özalp, S., Doğan, A., Haraguchi, T., Kondo, H., Sugito, N., Nakamura, T., Parlak, O., Çıplak, R. 2001. Recurrence Interval of the İzmit-Type Earthquakes along the Western North Anatolian. *Eos Transactions AGU* 82 (47), Fall Meet. Suppl., F929.

Toksöz, M.N., Shakal, A.F., Michael, A.J. 1979. Space-time migration of earthquakes along the North Anatolian Fault zone and seismic gaps. *Pure and Applied Geophysics*, 117, 1258-1270.

Tsukuda, E., Herece, E., Kuşçu, İ. 1988. Some geological evidence on activity of the western North Anatolian fault, Geyve, İznik, Gemlik area, research on Quaternary crustal movement and earthquake prediction. Report of International *Research and Development Cooperation ITIT Project*, 8513, Tokyo, pp. 69-91.

Uçarkuş, G. 2002. Gemlik Fay Zonu'nun Aktif Tektoniği. İstanbul Teknik Üniv., Avrasya Yer Bilimleri Enstitüsü, Yüksek Lisans Tezi, İstanbul, 82 s.

Utkucu, M., Budakoğlu, E., Durmuş, H. 2011. Marmara Bölgesinde (KB Türkiye) Depremsellik ve Deprem Tehlikesi Üzerine Bir Tartışma. *Yerbilimleri*, 32 (3), 187-211.

Üçer, B., Eyidoğan, H., Gürbüz, C., Barka, A., Barış, Ş. 1997. Seismic investigations of Marmara region. In: Schindler, C., Pfister, M. (Eds.), Active Tectonics of Northwestern Anatolia-The Marmara Poly-Project, vdf Hochschulverlag AG an der ETH Zürich, pp. 89-99.

Wells, D., Coppersmith, K. 1994. New empirical relationships among magnitude, rupture length, rupture width, rupture area and surface displacement. *Bulletin of the Seismological Society of America*, 84, 974-1002.

Yaltırak, C., Alpar, B. 2002. Evolution of the middle strand of North Anatolian Fault and shallow seismic investigation of the southeastern Marmara Sea (Gemlik Bay). *Marine Geology*, 190, 1-2, 307-327.

Yıldırım, C., Emre, Ö. 2004. Drainage evolution along the North Anatolian Fault zone, Eastern Marmara-Turkey. *Geological Society of America* (GSA), Denver Annual Meeting, 7-10 November 2004, Abstracts with Programs, 36 (5), 51, Denver, Colorado, USA.

Yoshioka, T., Kuşçu, İ. 1994. Late Holocene faulting events on the İznik-Mekece fault in the western part of the North Anatolian fault zone, Turkey. *Bulletin of the Geological Survey of Japan*, 45, 11, 677-685.

Bulletin of MTA (2013) 147: 19-29

Bulletin of the
Mineral Research and Exploration

http://bulletin.mta.gov.tr

THE TECTONO-STRATIGRAPHIC FEATURES OF METAMORPHITES IN ALACAHAN-ÇETİNKAYA REGION (KANGAL, SIVAS)

Metin BEYAZPİRİNÇ*, [a] and Ali Ekber AKÇAY[a]

[a] *General Directorate of Mineral Research and Exploration, Department of Geological Researches, 06800, Ankara, Turkey*

Key words:
Tectono-stratigraphy,
Bolkardağı Nappe,
Karaböğürtlen
Formation, Taurus
Mountains, Kangal

ABTRACT

The study area covers Alacahan, Çetinkaya and Kangal regions. Allochthonous and autochthonous rock units are present in the region. Metamorphic rocks exposed in the region have been studied in detail as formation and member and have been incorporated into the Bolkardağ Nappe. Bolkardağ nappe which deposited in Late Devonian-Late Cretaceous and metamorphosed in green schist facies, has been distinguished into Late Devonian Düzce formation, Carboniferous Kınalar formation, late Permian Çayderesi formation, (?)Middle/ Late Triassic-Cretaceous Kayaköy formation and Cretaceous Karaböğürtlen formation from base to top. The quartzites found at the base of the Kınalar formation and meta-conglomerates at the base of the Karaböğürtlen formation has been defined as 'Bakırtepe Member' and 'meta-conglomerate Member' respectively. Bolkardağ Nappe internally has numbers of imbricated structures. Yeşiltaşyayla complex consisting of blocks and slices of Gülbahar nappe, Güneş ophiolite and Munzur nappe overlies the Bolkardağ nappe with a tectonic contact. On the other hand Hekimhan formation, Kangal formation, Yamadağ group volcanics, Göbekören basalts and Plio-Quaternary cover units overlie the Bolkardağ nappe with an angular unconformity.

1. Introduction

Study area is in the Kangal, Çetinkaya, Alacahan region, in Sivas in the North Eastern part of the Eastern Taurus (Figure 1). Kurtman (1973), Bayhan (1980), Bayhan and Baysal (1982), Tunç et al (1991), Gürer (1992, 1994), İnan et al (1993), Gültekin (1993), Sayar and Gültekin (1993, 1995), Yılmaz (1994), Öztürk et al (1996), Yalçın and Bozkaya (1997), Yılmaz et al (2001) and Yılmaz and Yılmaz (2004) carried out general geological studies in various parts of the study area.

Gültekin (1993) carried out a study in the Alacahan-Çetinkaya-Divriği area and appointed Middle-Late Devonian-early Carboniferous age to the metamorphic units and considered them as Kangal Formation. Gültekin (1993) indicate that Late Jurassic-Early Cretaceous Kıratgediği re-crystallized limestones overlie the Kangal formation with an angular unconformity and ophiolites emplaced during Middle-Late Campanian and Saya formation were deposited during middle-late Campanian-early-middle Maastrichtian.

Gürer (1994) studied the stratigraphy of the Hekimhan-Hasançelebi area, evolution of Hekimhan basin and its position within the regional geology. Gürer (1994) stated that Hocalıkova ophiolite which is believed to have been transported from the north to the south in late Campanian, forms the bedrock of the area. Hekimhan basin opened up following the ophiolite emplacement. Karadere formation is composed of fluvial, deltaic and shallow-marine sediments deposited during late Campanian-early Maastrichtian and unconformably overlie ophiolites. Gürer (1994) indicated also that late Campanian-late Maastrichtian Hekimhan formation which is transitional with the units of the Karadere formation was deposited in tectonic controlled transgressive marine environments.

* *Corresponding author: M. BEYAZPİRİNÇ, metinbeyazp@hotmail.com*

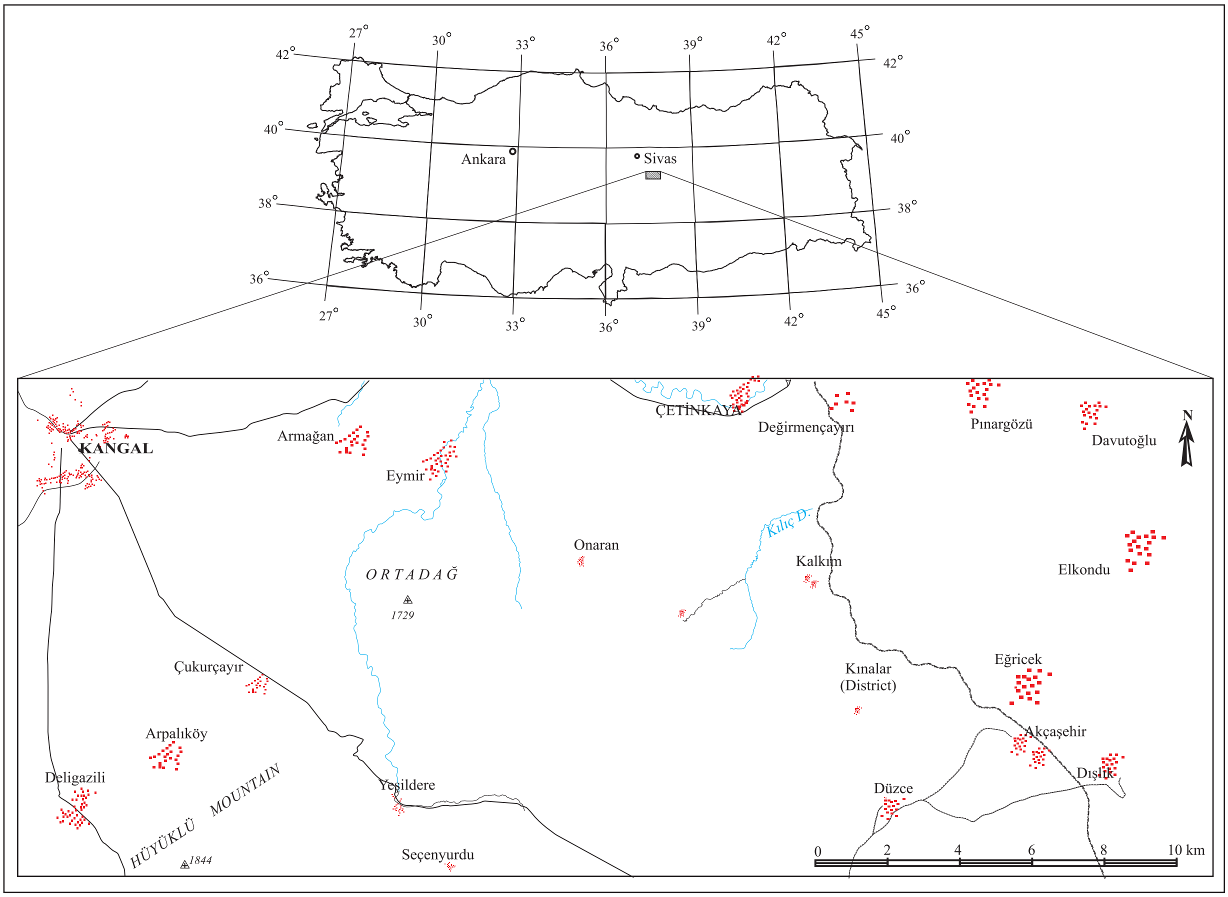

Figure 1-Location map of the study area

Yalçın and Bozkaya (1997) studied the burial and thrust mechanism relations of the Late Palaeozoic metamorphic rocks in the area. They determined that detritic parts of the Middle Devonian-early Carboniferous Kangal formation from base to the top have different lithological, textural and mineralogical charactertics as a result of burial and thrusting.

In this study tectono-stratigraphic features of the metamorphic rocks in the region have been studied.

2. Regional Geology

The study area is located in the Eastern Part of the Taurus Belt which started developing during the Alpine orogeny. Along the Taurus Belt there are numbers of units such as 'Geyikdağı Unit', 'Aladağ Unit', 'Bolkardağ Unit' and 'Bozkır Unit' represented by different stratigraphic, structural and metamorphic environmental conditions but also have tectonic relations with each other (Özgül 1976). Plate movements and oceanic crust development in the Eastern Taurus quite likely started in Late Jurassic-Early Cretaceous (Titonian-Berriacian) (Tarhan 1982). The ophiolites in the area are considered to be belong to the Southern branch of the Neo-Tethys and some parts have inner Tarus Oceanic origin (Şengör and Yılmaz 1981). In the area, oceanic crust started to develop and continued its development until Late Cretaceous as a result of rifting between Taurid-Anatolid platform and Bitlis-Pütürge massifs (Şengör and Yılmaz 1981). At the beginning of Late Cretaceous (Cenomanian-Turonian) the compressional regime started to develop in the crust (Yazgan 1981, 1983).

Özgül (1976) conducted a detailed study of the Taurus belt and indicated that the Taurus belt consisted of 6 units. Among these units Geyikdağı Unit is autochthonous; Aladağ, Bozkır, Antalya and Alanya Units are allochthonous.

The detailed descriptions of Geyikdağı, Aladağ and Bolkardağı units were defined by Özgül (1997) in the Central Taurus. He reported that Aladağ and Bolkardağı units consist of shelf type carbonate and detritic rocks deposited in Late Devonian-Late Cretaceous and flysch with Senonian olistoliths.

In the eastern part of the Eastern Taurus Belt, Alan et al. (2007) defined 5 structural units quite different from each other. Bolkardağ Unit is one of those structural units. In this structural unit they identified Carboniferous Aykuşdere formation, early Permian Erenlersırtı formation, late Permian Dumlutepe formation, Early-Middle Triassic Bastırık formation, Middle-Late Triassic Tozlutepe formation, Late Triassic Metrisyayla formation, Jurassic-Cretaceous Koçakkaletepe formation and Late Cretaceous Kaledere formation.

Bedi et al. (2009) carried out geological study in the western part of the Eastern Taurus Belt. They defined allochthonous rock units of different ages and representing different environments, tectonic relations with each other and autochthonous rock units. Tectono-stratigraphically from the base to the top it includes; Late Cretaceous Dağlıca complex, Late Jurassic-Cretaceous Kömürhan ophiolites and Bodrum nappe. Campanian-Maastrichtien Baskil granitoids intrude into the Kömürhan ophiolites and Bodrum Nappe. In the Binboğa mountain, units of the Lycian Nappe cover large areas in the south as well as in the north. These rock units display different stratigraphic and structural characters. From the base to the top are Gülbahar Nappe, Köseyahya Nappe and Munzur Nappe (Bedi et al. 2009).

From the base to the top the Bodrum Nappe consists of Late Devonian-Carboniferous Yoncayolu Formation, Late Permian Çayderesi formation, Early Triassic Alıçlı formation, (?) Middle-Late Triassic-Late Cretaceous Kayaköy formation, Ula formation with recrytallized limestones and intercalated dolomitic limestones. From Dogger onwards Kaya formation has horizantal and vertical transitions with Ula Formation. Late Cretaceous Karaböğürtlen formation with meta flysch comes to the top as a cover for the metamorphic units (Bedi et al 2009).

In the study area all of the geological features appear to have acquired their position in the area bound with the Taurid platform, Arabian platform, Northern branch of Neo-Tethys in the North and Southern branch of Neo-Tethis in the South.

During geodynamic evolution of the area some important geological events and related structural and stratigraphic features developed. These features are considered to have developed in three stages such as; pre-Maastrichtian stage, Maastrichtien stage, and Miocene-present stage. In the pre-Maastrichtien stage, it appears two basins were present, one in the north of Gürün Göreli autochthon, the other one in the south. Here northern and southern Ophiolites which were bound by the Gürün para-autochthone started plunging northwards under the Taurid and Anatolid platforms during pre-Maastrichtien (late Santonian-Campanian) stage. This development initiated the closing of the inner Taurid Ocean and northern branch of Neo-Tethys. Closing of the oceanic crust initiated large scale nappe developments. The successions of the Bolkardağ Nappe, particularly near to the Oceanic crust side of the platform (in accretionary prisms) and in the parts where crustal thickening were highly effective, were subjected to burial metamorphism. In the parts where burial mechanism was not effective (not much affected by the nappe developments) platform deposits and ophiolites of the Munzur and Gülbahar Nappes have not been affected by metamorphism (Bedi et al 2009).

The braided-river, deltaic and shallow-marine sediments of the Davutoğlu Member of the Hekimhan Formation deposited as a result of uplifts of the region and related sea-level fall in Maastrichtian (Beyazpirinç et al 2010).

In late Campanian-early Maastrichtian as a result of slowing down of subduction in the Southern ocean and subduction movement changed into transform fault and North-South compressional tectonic regime was replaced by extensional tectonic regime (Gürer 1992). Volcanisms have accompanied to sedimentation of Davutoğlu Member which is consisting of continental-shallow marine sediments at the base of the Hekimhan formation.

Nappe movements were quite effective until Maastrichtian and oceanic crust started closing and nappes in the thinning areas (Güneş ophiolite, Yeşiltaşyayla complex, Munzur nappe, Gülbahar nappe, Bolkardağı nappe) started acquiring their present day positions. In Maastrichtian in the opened up basins Hekimhan Formation has developed (Gürer 1992, 1994).

In the period between Miocene-present; along with shallow water, continental sedimentations have developed. Collisions and/or post collision volcanisms and deep faults related to volcanisms have also become effective (Beyazpirinç et al 2010).

3. Stratigraphy

Autochthonous and allochthonous units are present in the study area (Figure 2).

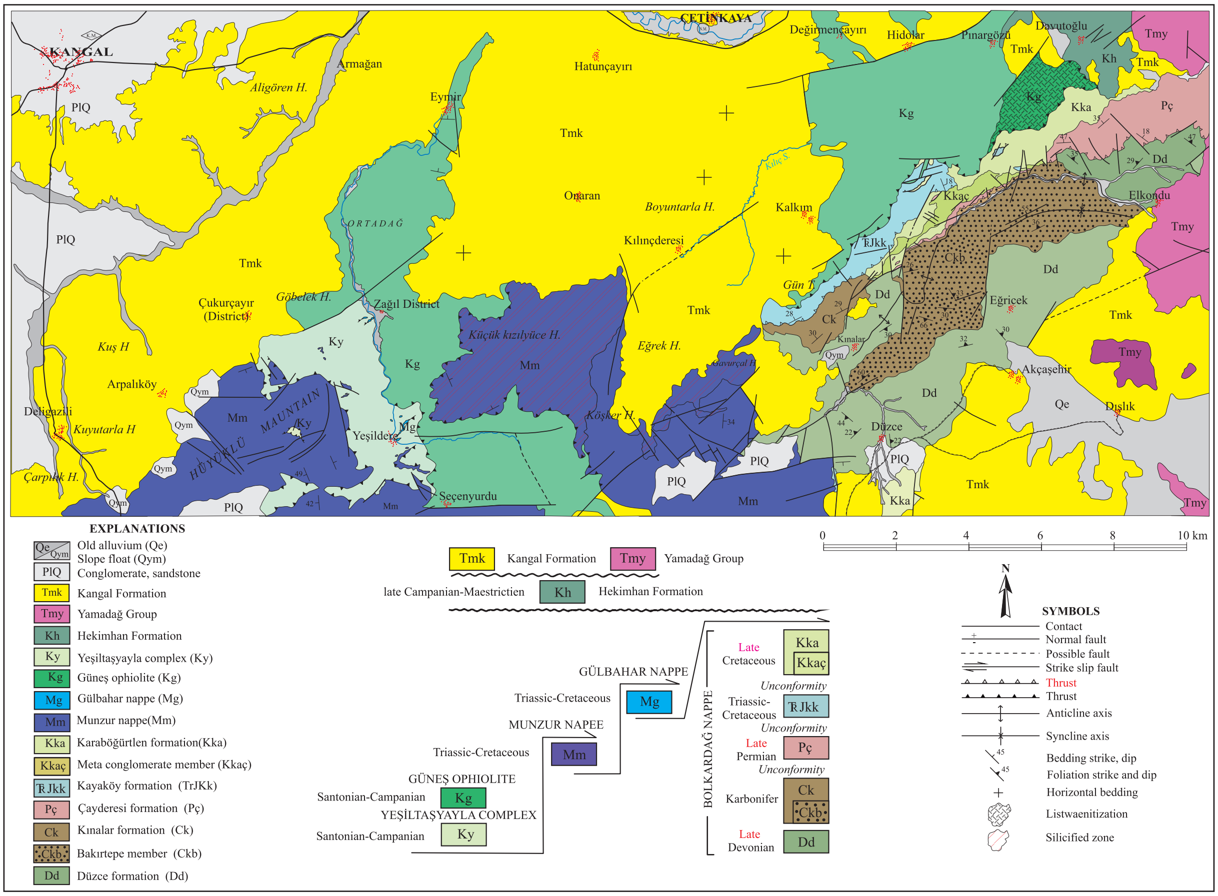

Figure 2- Geological map of the study area .

Bolkardağı Nappe (Özgül, 1976; Beyazpirinç et al 2010), Munzur Nappe (Bedi et al 2004, 2009) Yeşiltaşyayla Complex (Erkan et al 1978) and Gülbahar Nappe are present in the Yeşiltaşyayla Complex (Poisson 1977; Bedi et al 2004, 2009; Şenel et al, 1989) and Güneş Ophiolite (Bayhan, 1980) are allocthonous units emplaced in the area as nappes in pre Late Maestrichtian. Bolkardağ Nappe form the bedrock of the study area. Munzur Nappe and Yeşiltaşyayla Complex which also includes Gülbahar Nappe and Güneş ophiolite have been found with tectonic contacts on the top of Bolkardağ Nappe from bottom to top. Yeşiltaşyayla Complex includes tectonic blocks and slices of Gülbahar nappe and Munzur Nappe. Autochthones units overlie the older units with angular unconformity. They are; Hekimhan formation (Gürer, 1992, 1994), Kangal formation (Aktimur et al., 1988), Yamadağ group volcanics (Beyazpirinç et al., 2010), Göbekören basalts (Atabey, 1993) and Plio-Quaternary units (Figure 3).

Metamorphic rocks present in the study area have been defined as Bolkardağ Nappe. In this work tectono-stratigraphic features of the Bolkardağ Nappe have been studied.

3.1. Bolkardağ Nappe

Metamorphic rocks in the study area have been studied at member level in detail. They were previously named as Kangal formation (Gültekin 1993, Yalçın and Bozkaya 1997) and Alacahan Group (Öztürk et al 1996). Similar studies carried out for the metamorphic rocks at similar facieses in the Taurus belt have been named as Keban metamorfites (Perinçek, 1979*a*, *b*), Kabaktepe and Cağılhan metamorfites (Tarhan, 1982, 1984), Keban and Malatya Nappes (Yazgan, 1983), Malatya metamorfites (Perinçek and Kozlu, 1984*a*, *b*; Yıldırım, 1989; Yiğitbaş, 1989), Engizek group (Baydar, 1989), Keban-Malatya unit (Yılmaz et al 1992), Bodrum nappe (Bedi et al, 2009). Metamorphic rocks in the area are quite similar to the Bolkardağ group studied by Özgül (1976, 1997) in Central Taurus. Units of the Bolkardağ group which deposited during Late Devonian-Late Cretaceous interval consist of shelf type carbonates and detritic rocks which have undergone low grade metamorphism.

In this study, unit defined as Bolkardağ Nappe mainly consists of schist intercalated with marble,

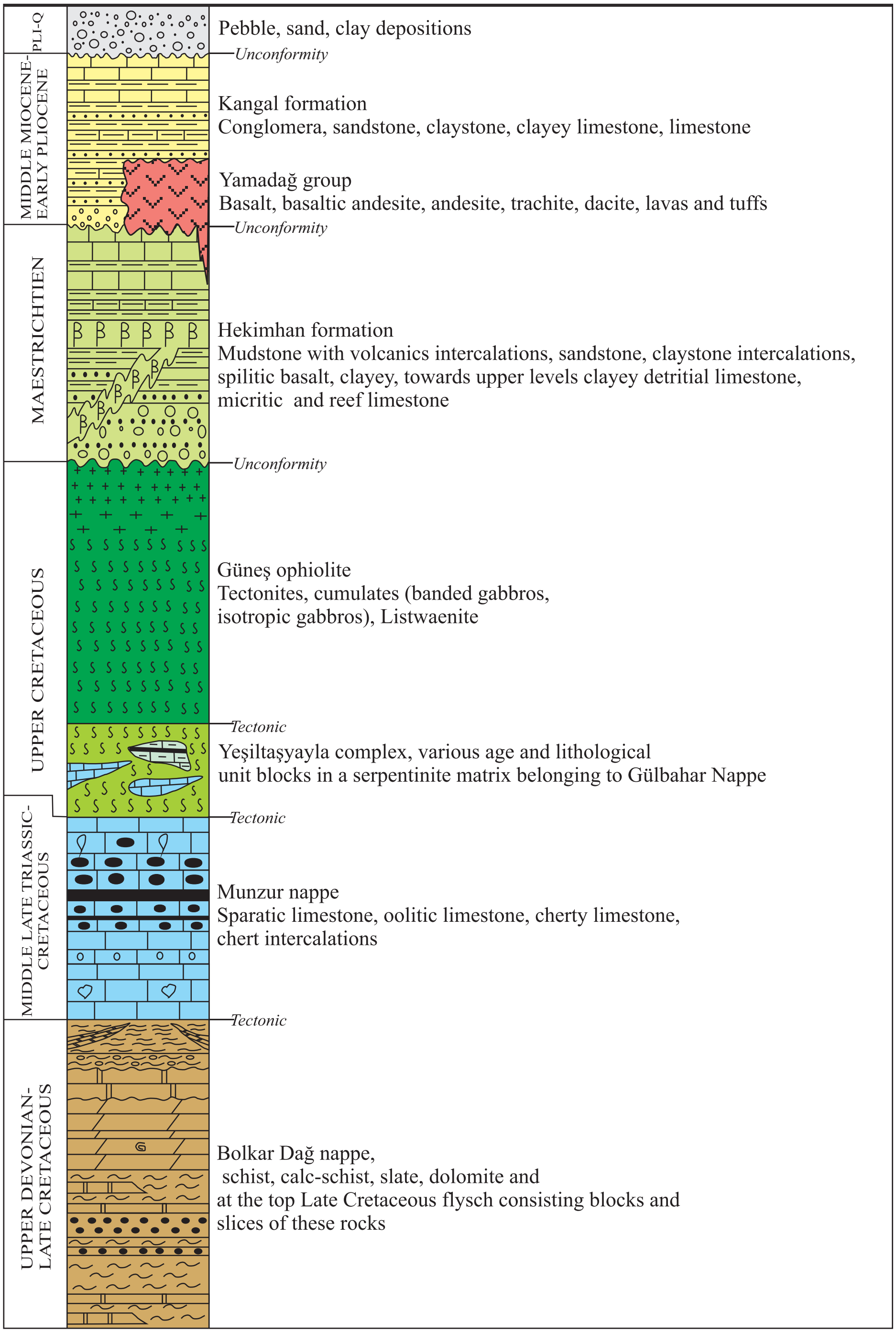

Figure 3- Generalized tectono-stratigraphic columnar section of the study area.

calc-schist, slate, re-crystallized limestone, quartzite and marble lithofacies.

Bolkardağ Nappe was deposited during Late Devonian - Late Cretaceous interval and has been subjected to green schist type metamorphism. From the base to the top it consists of late Devonian Düzce formation (Dd), Carboniferous Kınalar formation (Ck), Late Permian Çayderesi formation (Pç), (?) Middle-late Triassic-Cretaceous Kayaköy formation (TrJKk) and Late Cretaceous Karaböğürtlen formation (Kka) (Figure 4). Quartzites at the base of the Kınalar formation have been defined as ‘Bakırtepe Member’; Meta conglomerates at the base of the Karaböğürtlen formation have been defined as ‘Meta conglomerate Member’. Early Triassic level of the Bolkardağ Nappe has not been observed in the study area.

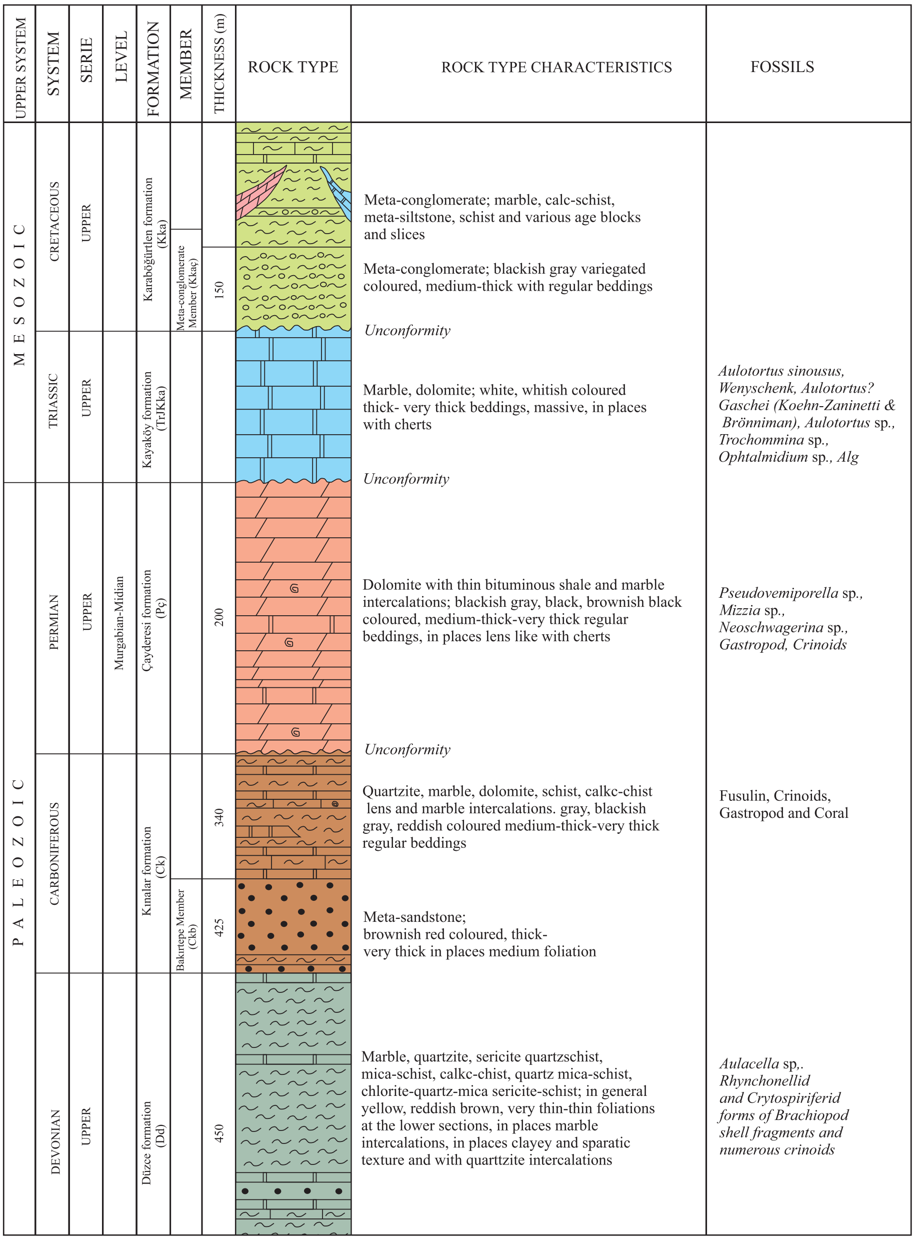

Figure 4- Generalized columnar section of the Bolkardağ Nappe.

3.2. Düzce Formation (Dd)

In the Kangal formation 'Düzce re-crytallized limestone Member' of Gültekin (1993) is the same as the 'Hocalar formation' described by Özgül (1997). In this study this unit is re-named as the 'Düzce formation'. It forms the base of the Bolkardağ Nappe and consists of meta -sandstones with calc-schist-marble intercalations, schist, slate.

The unit displays reference quality type sections in the North of Düzce village (Suluyurt Dere), also in Kınalar Village and on the southern slopes of the Kıratgediği Tepe. It consists of quartzites; sericite quartzites; chlorite, quartz mica-schist; slate; mica quartzs-chist, mica-schist,, quartz mica-schist, calc-schist.

At the top it has meta-sandstones and schist-slate intercalations. The unit is thinly foliated and has yellow, brownish red colour. In the lower sections it has locally intercalated with marble.

Weathered marbles are yellowish gray, pinkish coloured; fresh broken surfaces in places are rough, yellow, beige, coffee, reddish coloured. In places it displays, medium-thick scale good beddings. It has in places sparitic textures, has quartzite intercalations. It has knotted and flow structures, rich in fossils (Crinoids, Corals, Brachiopods). Weathered sandy-clayey calc-chists display yellowish gray colour, fresh fracture surfaces have yellow colour, in places have sericite smearings, and have thin-medium scale good beddings. 20-30 cm thick calc-schist intercalations in parts are rich in fossils (Crinoids, Brachiopods and shell fragments).

The measurable thickness of the Düzce formation is 450 m (At Kıratgediği Tepe)

Paleontological studies conducted on the samples collected from the Düzce formation showed the presence of Brachipod shell fragments *Aulacella* sp., Rhynchonellid and Cyrtospiriferid forms (determined by Dr. Gonca Nalcıoğlu). The presence of rich Crinoid's fossils shows that Düzce formation is likely to be at Late Devonian age. Sayar and Gültekin (1993) appointed Middle Devonian-Late Devonian age by the paleontological studies. All these data indicate that Düzce formation is possibly at Late Devonian age.

Düzce formation resulted from the green-schist facieses metamorphism of detritial and pelitic rocks in shallow water-slope environments.

3.3. Kınalar Formation (Ck)

Gültekin (1993) described this unit as Kınalar Member of the Kangal formation. In this study it is considered as formation and has been described as such.

The unit crops out in the area between North of Kınalar Village (Southern slopes of Cinalibaşı Tepe), Mollaosmançalı Tepe, Karadağ Tepe and Bakır Tepe. It mainly consists of quartzite, marble, dolomite, schist and calc-schist. Weathered surfaces of the marbles have gray colour, the freshly fracture surface is blackish gray, reddish colour, has good, medium-thick-very thick beddings. They have karstic cavities, are fractured, have calcite filled veins and has sparatic texture.

Marbles are in the form of lenses and interlayers and in places has cherty nodular, dolomitic character. They contain fossils (Fusulina, Crinoids, Gastropods and Corals). Quartzite's at the base of the succession have been named as Bakırtepe Member and described accordingly.

Measured thickness of the Kınalar formation in the upper part is 340 m. When the thickness of the Bakırtepe Member in the Cinalbaşı Tepe is included it amounts to 765 m. Continuation of the unit has not be observed, laterally it exhibits variations, in places it has carbonate lenses and layers.

Kangal formation can partly be correlated with the Kınalar formation but Özgül (1997) could not find any fossil data to appoint an age to the Kınalar formation. On the other hand fossils as such Fusulina, Crinoid and Corals found on the fresh rock faces of the marbles and calkschists indicate Early Carboniferous age (Sayar and Gültekin 1993). Stratigraphic position and correlations with the units of similar facies in the Taurus range, Carboniferous age fits reasonably well to the Kınalar formation.

Kınalar formation is represented by the metamorphic rocks of the sandstones, limestones and mudstones. It is suggested that these lithologies deposited in a shallow-marine and slope environment according to the rock types and metamorphosed in a green schist facies.

3.3.1. Bakırtepe Member (Ckb)

Quartzite and meta-sandstones in the study area were defined by Gültekin (1993) as 'Bakırtepe metaquartzite Member' of the Kangal formation. In this study quartzites and meta-sandstones have been considered in the Kınalar formation and re named as 'Bakırtepe Member'.

Bakırtepe unit consists mainly of quartzites with lesser amount of meta-sandstones. Reference quality type sections can be seen in Bakır Tepe. Weathered surface of the quartzites have blackish, reddish brown colour, fresh fracture surfaces are reddish brown, lead gray colours. They have lineated textures, are massive, and thickly foliated, small-medium in places with large crystals, heavily iron oxide stained and in places with quartz discharge.

In Bakır Tepe, 'Bakır Tepe Member' has 425 m known thickness. It does not display lateral continuations and it is at lens form at the bottom of the Kınalar formation.

'Bakır Tepe member' does not have any fossils. But as it is concordant with the Düzce Formation at the top and is situated at the bottom of the Carboniferous Kınalar formation, based on the stratigraphic position and its correlations with the similar unit facies in Taurids, Carboniferous is the assumed age for the 'Bakırtepe Member'.

In general quartzites are the main rock type. The origin of the quartzites is considered to be quartz rich sandstones deposited in shore-beach environment.

3.4. Çayderesi Formation (Pç)

Özgül et al (1981) carried out geological studies in the Keban-Malatya area and named the limestone unit as 'Çayderesi Limestone'. Yılmaz et al (1992) used the 'Çayderesi formation' name. In the study area the unit for the first time defined and 'Çayderesi formation' name has been adopted.

Çayderesi formation extends from Saraydüzü, Kulluk Tepe, Northern slopes of Kıratgediği Tepe, Naldöken Tepe to southern slopes of Naldöken Tepe and Çal Tepe in the area.

Main rock type of the 'formation' is dolomite; towards the top of the succession it includes thin bituminous shale intercalations. It is generally blackish gray, black and ash coloured, massive, medium-thick and sometimes displays regular beddings. Bituminous shale's have thin-medium beddings. It has calcite fillings, fractured-cracked, folded, in places with chert nodules and has fossils (Gastropod, Algae, Crinoids, Mizzia, Hemigordius).

The thickness of the 'Çayderesi formation' has been measured to be 200 m in the Kıratgediği Tepe. Rock types show lateral variations and have gastropod and crinoid pieces, Mizzia and Hemigordious fossils in various parts.

Paleontological studies carried out on the collected samples identified the presence of *Mizzia* sp., *Pseudovemiporella* sp., *Neoschwagerina* sp fossils, indicating Late Permian (Murgabian-Midian) age.

Dolomitized carbonates of 'the formation' indicate reasonably quite shallow marine environments.

3.5. Kayaköy Formation (TrJKk)

This unit was first identified in Munzur Mountains and named as 'Kale Tepesi Limestone' by Özgül (1981). It was then named as 'Kayaköy formation' by Bedi (2009). In this study 'Kayaköy formation' name is used.

Rock units of the 'Kayaköy formation' crop out on the southern slope of Cinalibaşı Tepe, on Saylak Tepe, Naldökenin Çal Tepe and in the Hanife Öreni area. It is also found as 25-30 m thick tectonic slices in the Karaböğürtlen formation in Naldöken Tepe region. Güneş Ophiolite overlies 'Kayaköy formation' with a tectonic contact.

The unit is generally represented by re-crystallized platform type carbonates. Rock types are marble and dolomite with cherts in the upper levels. Gray, blackish, in places cream, white coloured, with massive, thick-very thick beddings, fine crystals, fractured, karstic voids, calcite veins, upper levels with chert nodules. Marbels have mostly been dolomitized. Samples collected from the lower level of the Kayaköy formation have *Aulotortus sinousus* Wenynschenk, *Aulotortus*? g*aschei* (Koehn-Zaninetti & Brönnimann), *Aulotortus* sp., *Trochammina* sp., *Ophthalmidium* sp., Alg fossils indicating Late Triassic age. Bedi et al (2004, 2009) determined (?) Middle-Late Triassic-Late Cretaceous age to the 'Kayaköy Formation'.

'Kayaköy formation' consists of platform type carbonates. Data indicates that from Middle-Late Triassic age; onwards the units were deposited in a reasonably quite, shallow marine environment.

3.6. Karaböğürtlen Formation (Kka)

The unit was first defined and named by Philippson (1915) in Western Taurus. Although the 'blocky flysch' (bloklu filiş) described by Philippson (1915) is not metamorphosed but still the meta-flysch in the study area are considered to be the metamorphosed equivalents of them, so 'Karaböğürtlen formation' name has been kept.

Blocky parts of the 'Karaböğürtlen formation' crop out in the North of Damyeri and the others having tectonic slices are in the west part of Naldöken Tepe. They are also found on the Eastern side of Karahöyük Tepe, southern slopes of Saylak Tepe, Naldökençal Tepe and in Kavak Tepe.

The 'Karaböğürtlen formation' in the study area was first determined by this study. It mainly consists of meta-conglomerates, meta-siltstones, calc-schists, re-crystallized limestones and marbles. It also includes blocks and tectonic slices of units of 'Kayaköy' and 'Çayderesi' formations. Meta-conglomerates at the bottom have been defined as 'Member'.

No fossil data has been found to appoint an age to the 'Karaböğürtlen formation'. But it includes blocks and slices of (?) Middle-Late Triassic-Cretaceous units and unconformably overlies the older units such as Pre and Late Permian. It suggested therefore that Karaböğürtlen Formation has developed as a result of low grade (green schist facieses) metamorphism of Late Cretaceous age blocky flysch.

3.6.1.Metaçakıltaşı (Meta-conglomerate) Member (Kkaç)

This unit has been defined and named for the first time in this study. It is consists of meta-conglomerate and is located at the base of the Karaböğürtlen formation.

It crops out in the Naldökeninçal Tepe and in the North of Damyeri. It exhibits typical sections in the South Eastern slopes of Naldökeninçal Tepe.

Weathered surface of the meta-conglomerates have gray, beige like, blackish gray, pinkish colours. Freshly fracture surfaces display variegated - blackish colours. It has thin-medium-thick regular beddings, with karstic cavities and chert nodules. In the elongated matrix chert, dolomite and marble pebbles are present. Pebbles are 2-30 mm in size and display distinct lineation. They include pebbles belonging to 'Kayaköy formation' and also from older units.

Meta-conglomerates are 150 m thick and do not exhibit lateral continuity. No fossil data have been found for the meta-conglomerates forming the base of the 'Karaböğürtlen formation'

Meta-conglomerates at the base of the blocky flysch are believed to have developed at the early stage of the transgression. They were subjected to low grade metamorphism and are the covering unit of the Bolkardağ Nappe.

4. Results And Discussion

Metamorphic rock outcrops in the study area have been evaluated within the Taurus belt and considered as Bolkardağ Nappe. Tectono-stratigraphic character of the Bolkardağ Nappe has been determined. New data has produced for the metamorphic rocks present in the study area. Within light of this new data, metamorphic rocks have been defined as 'Formation' and 'Member' levels. The presence of Late Cretaceous meta-flysch has been brought to light and meta conglomerates in the meta-flysch have been defined at 'Member' level. The presence of Late Carboniferous has been shown in the field as well as proved with the paleontological data.

The metamorphic rocks in the study area were previously defined as crystalline rocks. Gültekin (1993) considered that metamorphic rocks were re-crystallized Kıratgediği Limestones of Jurassic-Cretaceous age overlying Carboniferous-Devonian Kangal formation with angular unconfirmity and he classified these rocks as 'Bakırtepe meta-quarzite Member' and 'Düzce re-crystallized limestone Member' by considering them within the 'Kangal formation'. Regional geological settings and geographical distribution of metamorphic rocks in the area do not fit to the definition of 'Kangal formation'. In this study metamorphic schists in the area have been defined as 'Bolkardağ Nappe' of similar facies in the Central Taurus (Özgül 1976).

Acknowledgment

This paper includes some of the field study findings on the 'Geodynamic Evolution of Central Taurus (Sivas-Malatya-Kahramanmaraş-Kayseri) The project was conducted by the Geological Studies Department of Mineral Research and Exploration (MTA). Our thanks are due to the Directorate of the Geological studies Department of MTA. To the assoc. Prof. Dr. Cengiz Okuyucu and Dr. Erkan Ekmekçi (MTA) who carried out paleontological studies. Dr. Gonca Nalcıoğlu (MTA) conducted brachiopod definitions. Mr. Halil Keskin (MTA) read and edited the manuscript.

Received: 06.12.2012
Accepted: 06.08.2013
Published: December 2013

References

Aktimur, T., Atalay, Z., Ateş, Ş., Tekirli, M.E., Yurdakul, M.E. 1988. Munzur dağları ile Çavuş dağı arasının jeolojisi. *Maden Tetkik Arama Genel Müdürlüğü Rapor No*: 8320, 102s. Ankara (unpublished).

Alan, R., Şahin, Ş., Keskin, H., Altun, R.; Bakırhan, B., Balcı, V., Böke, N., Saçlı, L., Pehlivan, Ş., Kop, A., Hanilçi, N., Çelik, Ö., F., 2007. Orta Torosların Jeodinamik Evrimi, Ereğli (Konya)-Ulukışla (Niğde) - Karsantı-(Adana)-Namrun (İçel) Yöresi, *Maden Tetkik ve Arama Genel Müdürlüğü Rapor No*: 11006, Ankara (unpublished)

Atabey, E. 1993. Gürün otoktonunun stratigrafisi (Gürün-Sarız arası), Doğu Toroslar-GB Sivas. *Türkiye Jeoloji Bülteni*, 36, 99-113.

Baydar. O. 1989. Berit-Kandil Dağları (Kahramanmaraş) ve civarının jeolojisi. İstanbul Üniversitesi Doktora Tezi, 248 s. İstanbul (unpublished).

Bayhan, H. 1980. Güneş-Soğucak (Divriği) jeolojik, mineralojik, petrografik, petrolojik ve metalojenik incelemesi. Doktora Tezi, Hacettepe Üniversitesi, Ankara, 206s. (unpublished).

Bayhan, H., Baysal, O. 1982. Güneş-Soğucak (Divriği-Sivas) yöresinin petrografik ve petrolojik incelemesi. *Türkiye Jeoloji Kurumu Bülteni*, 25/1, 1-13.

Bedi, Y., Şenel, M., Usta, D., Özkan, M. K., Beyazpirinç M. 2004. Binboğa Dağları'nın Jeolojik Özellikleri ve Batı-Orta Toroslar'daki Benzer Birimler ile Deneştirilmesi, 57. *Türkiye Jeoloji Kurultayı Bildiri Özleri*, s. 271-272.

Bedi, Y., Yusufoğlu, H., Beyazpirinç, M., Özkan, M. K., Usta, D., Yıldız, H. 2009. Doğu Toroslar'ın jeodinamik evrimi (Afşin-Elbistan-Göksun-Sarız dolayı). *Maden Tetkik Arama Genel Müdürlüğü Rapor No*: 1150, 388s. Ankara (unpublished).

Beyazpirinç, M., Akçay, A. E., Metin, Y., Taptık, M. A., Öcal, H., Çobankaya, M., Çoban, M., Doğan, A., Bağcı, U., Rızaoğlu, T. 2010. Doğu Toroslar'ın Jeodinamik Evrimi (Sivas-Malatya-Kahramanmaraş-Kayseri) 2008 Yılı Arazi Raporu. *Maden Tetkik Arama Genel Müdürlüğü Rapor No*: 11331,143s. Ankara (unpublished).

Erkan, E. N., Özer, S., Sümengen, M., Terlemez, İ. 1978. Sarız, Şarkışla, Gemerek, Tomarza arasının temel jeolojisi. *Maden Tetkik Arama Genel Müdürlüğü Rapor No*: 5641, Ankara (unpublished).

Gültekin, A. S. 1993. Alacahan-Çetinkaya-Divriği (Sivas) arasında kalan alanın jeolojisi. Doktora Tezi, İstanbul Üniversitesi, 180s, İstanbul (unpublished).

Gürer, Ö. F. 1992. Hekimhan-Hasançelebi (Malatya) dolayının jeoloji incelemesi. İstanbul Üniversitesi, Fen Bilimleri Enstitüsü Doktora Tezi, 323s. (unpublished).

Gürer, Ö. F. 1994. Hekimhan-Hasançelebi yöresinin Üst Kretase stratigrafisi ve havza evrimi. *Türkiye Jeoloji Bülteni*, 37/2, 135-148.

İnan, S., Öztürk, A., Gürsoy, H. 1993. Ulaş-Sincan (Sivas) yöresinin stratigrafisi. *Doğa-Türk Yerbilimleri Dergisi*, 2, 1-15.

Kurtman, F. 1973. Sivas-Hafik Zara ve İmranlı bölgesinin jeolojik ve tektonik yapısı. *Maden Tetkik ve Arama Dergisi*, 80, 1-33.

Özgül, N. 1976. Toroslar'ın bazı temel jeoloji özellikleri. *Türkiye Jeoloji Kurumu Bülteni*, 19/1: 65-78, Ankara.

Özgül, N. 1997. Bozkır-Hadim-Taşkent (Orta Toroslar'ın kuzey kesimi) dolayında yer alan tektono-stratigrafik birliklerin stratigrafisi. Maden Tetkik ve Arama Dergisi, 119, 113-174.

Özgül, N., Turşucu, A., Özyardımcı, N., Şenol, M., Bingöl, İ., Uysal, Ş. 1981. Munzur Dağları'nın Jeolojisi. *Maden Tetkik ve Arama Genel Müdürlüğü Rapor No*: 6995, Ankara (unpublished).

Öztürk, A., Boztuğ, D., Yalçın, H., İnan, S., Gürsoy,H., Bozkaya, Ö., Yılmaz, S., Uçurum, A. 1996. Hekimhan (KB Malatya) ve Kangal (GD Sivas) yörelerinde mevcut maden yataklarının jeolojik ve madencilik açısından değerlendirilmesi çalışmaları. DPT 89 K 120450 No'lu Teknolojik Araştırma Projesi.

Perinçek, D. 1979*a*. Geological investigation of the Çelikhan-Sincik-Koçali area (Adıyaman Province). İst. Üni. Fen Fak. Mecmuası, Seri B 44: 127-147, İstanbul.

Perinçek, D. 1979*b*. İnterrelations of the Arabian and Anatolian Plates. Guide Book For Excursion 'B' First Geological Congress On Middle East, the Geological Society of Turkey, 17 p. Ankara.

Perinçek, D., Kozlu, H. 1984*a*. Afşin-Elbistan-Doğanşehir dolayının stratigrafisi ve bölgedeki birliklerin yapısal ilişkileri. TPAO Rapor No. 1909 (unpublished).

Perinçek, D., Kozlu, H. 1984*b*. Stratigraphic and structural relations of the units in the Afşin-Elbistan-Doğanşehir Region (Eastern Taurus). In Tekeli, O., and Göncüoğlu, M.C. (Eds), Geology of Taurus Belt, 181-198, Ankara-Turkey.

Phillipson, 1915. Reisen und Forschungen İm Westlichen Kleinasien. Pett, Mitt., H., 167.

Poisson, A. 1977. Recherches geologique dans Ie Tauridis Occidentales (Turquie). These Üniversite du Paris-Sud Orsay, 795 p. (unpublished).

Sayar, C., Gültekin, A. S. 1993. Kangal (Sivas) çevresi yeşilşist fasiyesinde Devoniyen-Karbonifer Brakiyopodları. 46. Türkiye Jeoloji Kurultayı Bildiri Özleri, s. 136.

Sayar, C., Gültekin, A. S. 1995. The stratigraphy, age and faunal community of Kangal formation (greenschist), Sivas, Turkey. Second International Turkish Geology Workshop, September 6-8, Cumhuriyet University, p.99, Sivas, Turkey.

Şenel, M., Selçuk, H., Bilgin, Z. R., Şen, M. A., Karaman, T., Dinçer, M. A., Durukan, E., Abraş, A., Örçen, S., Bilgi, C. 1989. Çameli (Denizli)- Yeşilova (Burdur)-Elmalı (Antalya) ve dolayının jeolojisi. Maden Tetkik ve Arama Genel Müdürlüğü Rapor No. 9429, Ankara (unpublished).

Şengör, A. M. C., Yılmaz, Y. 1981. Tethyan evolution of Turkey. A Plate Tectonic Approach. Tectonophysics, 75, 181-241.

Tarhan, N. 1982. Göksun-Afşin-Elbistan Dolayının Jeolojisi. Maden Tetkik ve Arama Genel Müdürlüğü Rapor No. 7296, 63s. Ankara (unpublished).

Tarhan, N. 1984. Göksun-Afşin-Elbistan Dolayının Jeolojisi. Jeoloji Mühendisliği, 19, 3-9, Ankara.

Tunç, M., Özçelik, O., Tutkun, Z. ve Gökçe, A. 1991. Divriği-Yakuplu-lliç-Hamo (Sivas) yöresinin temel jeoloji özellikleri. Doğa-Türk Müh. Çevre Bilimleri Dergisi, 15, 225-245.

Yalçın, H., Bozkaya, Ö. 1997. Kangal-Alacahan yöresi (Sivas) Üst Paleozoyik yaşlı meta-sedimanter kayaçlarda gömülme ve bindirme ile ilişkili çok düşük dereceli metamorfizma. Türkiye Jeoloji Bülteni, 40, 2, 1-16.

Yazgan, E. 1981. Doğu Toroslar'da etkin bir paleo-kıta etüdü. Yerbilimleri Dergisi, 7, 83-104, Ankara.

Yazgan, E. 1983. A geotraverse between the Arabian Platform and the Munzur nappes. International Symposium on the *Geology of the Taurus Belt, Guide*

Yıldırım, M. 1989. K. Maraş kuzeyindeki (Engizek-Nurhak Dağları) tektonik Birliklerin jeolojik, petrografik incelemesi. İ.Ü. Ph.D. Thesis, İstanbul (unpublished).

Yılmaz, A., Bedi, Y., Uysal, Ş., Aydın, N. 1992. Doğu Toroslar'da Uzunyayla ile Berit Dağı arasının jeolojik yapısı. *Maden Tetkik ve Arama Genel Müdürlüğü Rapor No*. 9453, Ankara (unpublished).

Yılmaz, A. 1994. Çarpışma sonrası bir çanak örneği: Sivas Havzası. Türkiye 10. Petrol Kongresi Bildirileri (Jeoloji), Hilton International, 13, 21-33s. Ankara.

Yılmaz, H., Arıkal, T., Yılmaz, A. 2001. Güneş Ofiyolitinin (Divriği-Sivas) Jeolojisi. 54. Türkiye Jeoloji Kurultayı, Bildiri Özleri, Bildiri No. 54-65, 15-16s. Ankara.

Yılmaz, H. ve Yılmaz, A. 2004. Divriği (Sivas) yöresinin jeolojisi ve yapısal evrimi. Türkiye Jeoloji Bülteni, 47,13-45.

Yiğitbaş, E. 1989. Engizek Dağı (K.Maraş) dolayındaki tektonik birliklerin petrolojik incelenmesi. İ.Ü. Ph.D. thesis, 347 s., İstanbul (unpublished).

Bulletin of MTA (2013) 147: 31-55

Bulletin of the
Mineral Research and Exploration

http://bulletin.mta.gov.tr

FIRST DETERMINATION OF RUDISTS (BIVALVIA) FROM NE IRAQ: SYSTEMATIC PALAEONTOLOGY AND PALAEOBIOGEOGRAPHY

Sacit ÖZER[*,a], Kamal Haji KARIM[b] and Dereen Mohamad SADIQ[b]

[a] *Dokuz Eylül University, Engineering Faculty, Geological Engineering Department, 35160 Tınaztepe-Buca Campus, İzmir, Turkey,*
[b] *University of Sulaimani, Department of Geology, Sulaimaniya, IRAQ*

Key words:
Rudists,
Maastrichtian,
systematic
palaeontology,
palaeobiogeography,
Iraq.

ABSTRACT

The Maastrichtian Aqra Formation around Mawat-Chwarta (Sulaimaniya city) in NE Iraq consists mainly of coarse grained detrital limestone, locally containing terrigenous clastics, and is characterized by abundant rudists in life position. The rudist biostromes are very common in the formation and benthic foraminifers, gastropods and non-rudist bivalves with scarcer echinoderms and solitary corals are associated with the rudists. This first determination of rudists from NE Iraq recognizes the following species, *Dictyoptychus* aff. *morgani*, *Sauvagesia somalica*, *Hippurites cornucopiae*, *Praeradiolites subtoucasi* and *Lapeirousia jouanneti,* as well as some indeterminable radiolitid sections. This rudist fauna is assigned to the *Hippurites cornucopiae* interval zone indicating a mid to Late Maastrichtian age. *Dictyoptychus* is an endemic rudist genus for the Arabian Plate, to which *Sauvagesia somalica* also seems to be limited. Other determined species are recorded mostly from the central-eastern Mediterranean Tethys, and to a lesser extend from the Arabian Plate. The determination of rudists from NE Iraq fills an important gap in terms of the taxonomic database and palaeobiogeography. The data on the rudist fauna reveals the existence of a shallow marine dispersal route for rudist larvae during the Maastrichtian along the area of the present Zagros fold-thrust belt from SE Turkey across NE Iraq towards SW Iran.

1. Introduction

Our knowledges of the Upper Cretaceous rudists of northern Iraq is limited by the absence of systematic studies. Only one or two genera or species have been documented so far, as follows: *Eoradiolites liratus* Conrad and *Caprinula* sp. were announced by Dubertret (1966) from the Cenomanian beds around Ga'ara and Rutbah (western Iraqi, Syrian Deserts) and some radiolitids and hippuritids were cited from the type area of the Maastrichtian Aqra Formation in northern Iraq by Bellen et al. (1959), Buday (1980), Karim (2004) and Sadiq (2009).

The rudist specimens of the present study were extracted from the three following measured stratigraphic sections of the Aqra Formation in the Mawat-Chwarta area, north-northeast of Sulaimaniya city (Figure 1):

1- Khewata section: West of Khewata village at 6 km south of Mawat town at the intersection of latitude (35° 48' 25.06" N) and longitude (45° 26' 34.35" E).

2- Sura Qalat section: 2km to the northwest of Suraqalat town and 8 km to the south of Mawat town at the intersection of latitude (35° 47' 5.10" N) and longitude (45° 26' 32.50" E).

3- Sherawezha section: 1km west of Sherawezha village at south east of Chwarta town, along the

[*] *Corresponding author: S. ÖZER, sacit.ozer@deu.edu.tr*

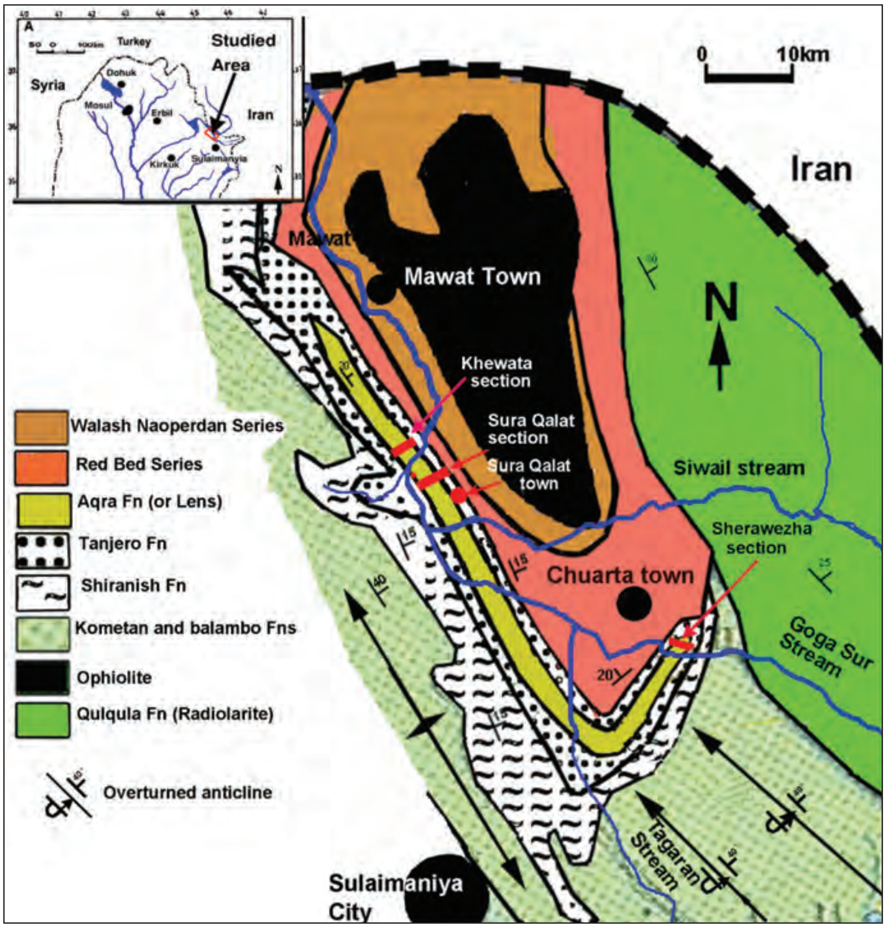

Figure 1- Location map of the studied area (inset top left) and geological map (modified from Maala, 2008 and Sadiq, 2008) showing the measured-stratigraphic sections.

eastern and western banks of the Qalachwallan stream at the intersection of latitude (35^{o} 41^{-} 21.90$^{=}$ N) and longitude (45^{o} 36^{-} 20.63$^{=}$ E).

The aim of this study is mainly to describe the rudists collected from NE Iraq and also to show their palaeobigeographic importance in the Arabian platform. Isolated rudist specimens are held in the S. Özer collection in Dokuz Eylul University, İzmir, Turkey.

2. Geological Setting And Stratigraphy

The studied area represents the northeastern margin of the Arabian Plate, where the previous Early Cretaceous platform was transformed to a foreland basin during the Late Cretaceous. This transformation was due to either ophiolite obduction (Buday, 1980; Buday and Jassim,1987; Jassim and Goff, 2006) or to the continental collision of the Iranian and Arabian plates (Karim, 2004; Karim and Surdashy, 2006). According to Karim (2005), the Mawat-Chwarta area consists of a large graben which was formed by two transverse normal faults. Geographically, the northern part of the area is occupied by ophiolite (Late Cretaceous) and Naoperdan Series thrust sheets while the northeastern part is covered by the Qulqula Formation (Early Cretaceous). The carbonates of Early and Middle Cretaceous age are exposed in the south and southwest of the study area (Figure 1).

The rudist-bearing Aqra Formation crops out as a narrow L-shaped strip about 35 km wide alongside the Qalachuallan-Mokaba stream (downstream of Goga Sur stream) to the south of Mawat and Chwarta towns (Figure 1). Due to imbrication, overturned synclines and anticlines are recognized and all the strata dip about 25 degrees towards the northeast (Figures 1, 2). The Aqra Formation has two stratigraphic manifestations due to the lateral change of the Tanjero Formation (Buday, 1980; Karim, 2004; Al-Barziniy,

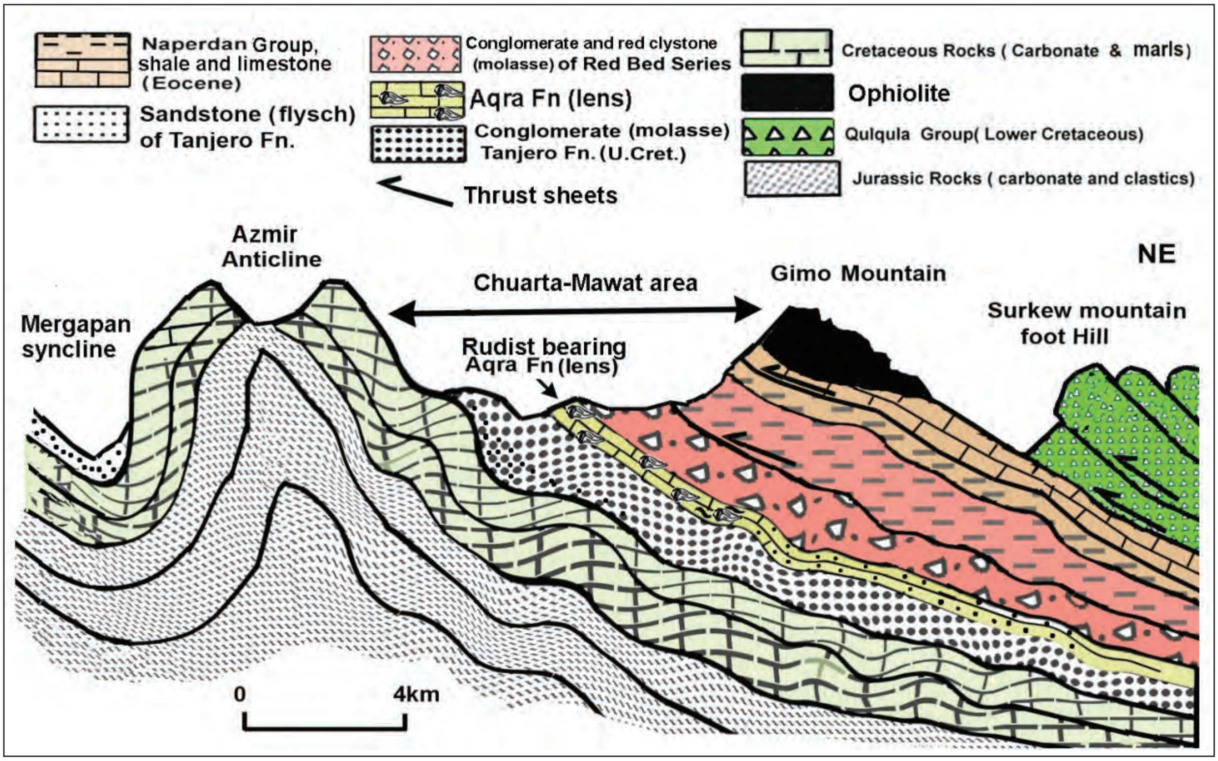

Figure 2- Simplified geological cross section of the studied area (after Karim et al., 2007).

2005; Sadiq, 2009). The first outcrop is located between the Tanjero Formation (Maastrichtian), at its base, and a Red Bed Series (Paleocene) at its top (Figures 2, 4). The second outcrop is located along the southern boundary where the Aqra Formation is located inside the upper part of the Tanjero Formation (Figure 3).

The Tanjero Formation consists mainly of thick successions of gravel conglomerate with a thickness of 20-500m in the northern and eastern part of the studied area (in the proximal part of the Cretaceous foreland basin), whereas it consists of calcareous shale and channelized sandstone and pebbly sandstone in the southern and western part of the studied area.

The Aqra Formation consists mainly of coarse grained detrital limestones, which contains in many places terrigenous clastics, and its thickness varie from 20 m to 150 m. It is characterized by abundant rudists and also benthic foraminifers, gastropods and non-rudist bivalves, the echinoderms and solitary corals are very sparse (Karim, 2004; Sadiq, 2009). The formation is very fossiliferous in the northern part of the studied area (proximal area), but much less so in the southwestern area (outer shelf or distal part). The benthic foraminifera have been determined as as *Orbitoides medius* (d'Archiac), *Omphalocyclus macroporus* (Lamarck) and *Loftusia* sp. and a Maastrichtian age was suggested for the Aqra Formation by Al-Kubaysi (2008), Sadiq (2009) and

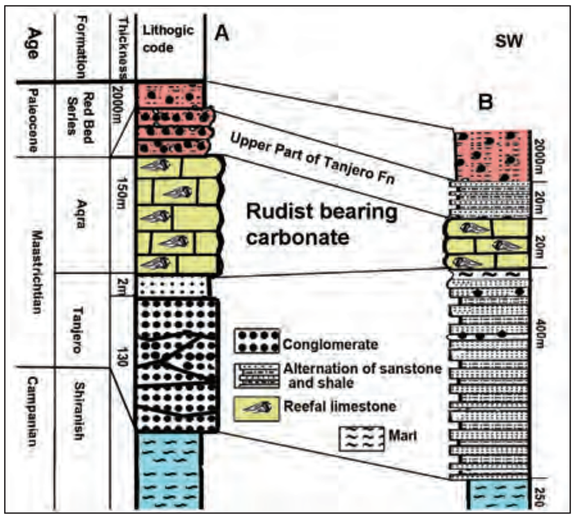

Figure 3- Stratigraphic columns showing the setting of the Aqra Formation in the succession at Mawa-Chuarta area (after Karim et al., 2007). A. The column for the northern boundary of the studied area (Khewata section). B. The column for the southern boundary of the studied area reflecting Suraqalat and Sherawazha sections.

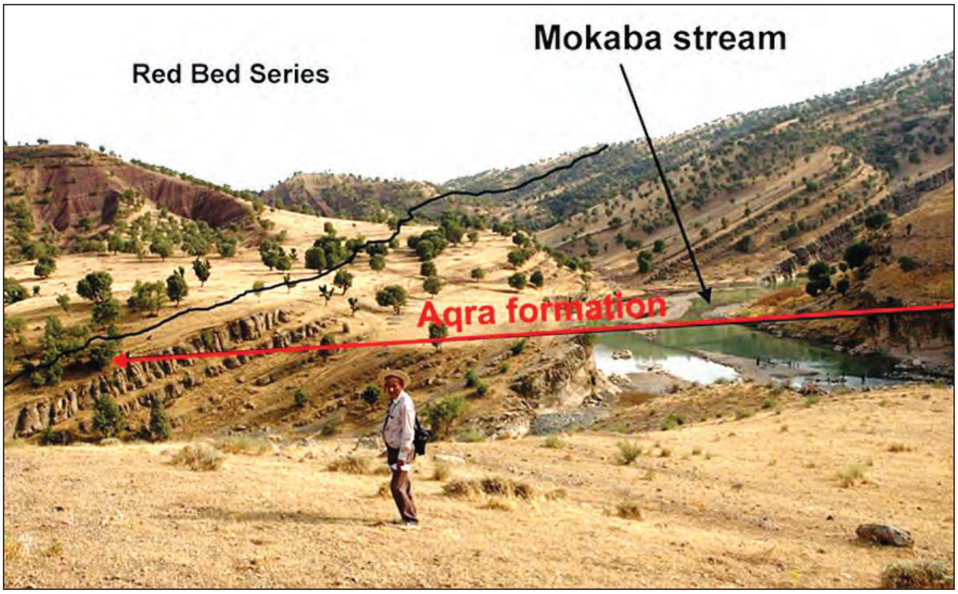

Figure 4- Khewata section showing the relationship of the Aqra Formation with Red Bed Series in the northern boundary of the studied area, looking southeast.

Zebari (2010). The rudists are found life in position in two places along both Suraqalat and Khewata sections, where the *Hippurites cornucopiae* Defrance biostromes are commonly observed (Figure 5).

The Red Bed Series (or Red Bed Group) consist mainly of alternations of thick beds of red claystone, sandstone and conglomerate, Paleocene-Eocene in age (Figures 3, 4).

Figure 5- *Hippurites cornucopiae* biostrome, top view, Sura Qalat section, Aqra Formation.

3. Systematic Palaeontology

The classification scheme and terminology for rudist higher taxa used follows Skelton (2013).

Abbreviations: LV, left valve; RV, right valve; Ab, anterior radial band; Pb, posterior radial band; Ib, interband; L, ligament ridge; ma, anterior myophore; mp, posterior myophore; at, anterior tooth; pt, posterior tooth; ct, central tooth; ac, accessory cavity; pp, posterior pillar, ap, anterior pillar; Pp, posterior pseudopillar, Ap, anterior pseudopillar; cv, body cavity; ol, outer (calcitic) shell layer; il, inner (originally aragonitic) shell layer; op, outer (celluloprismatic calcitic) shell layer of the RV (in radiolitids).

Class BIVALVIA Linnaeus, 1758

Order : Hippuritida Newell, 1965

Superfamily : Radiolitoidea d'Orbigny, 1847

Family : Trechmannellidae Cox, 1933

Genus : *Dictyoptychus* Douvillé, 1905

Type species: *Polyptychus morgani* Douvillé, 1904

Dictyoptychus aff. *morgani* (Douvillé, 1904)

(plate I, figures A-I)

1904 *Polyptychus Morgani* Douvillé, page 520, text-figures 1, 2.

1933 *Trechmanella morgani* (Douvillé), Cox, page 388.

1995 *Dictyoptychus morgani* (Douvillé), Morris and Skelton, page 282, plate 1, figure 3.

2010*a Dictyoptychus morgani* (Douvillé), Özer, pages 587-592, plates 1-4.

2012 *Dictyoptychus morgani* (Douvillé), Steuber and Schlüter, page 52, figure 10 B.

Material: Three specimens with both valves (Nos. Kh1, Kh2 and Kh3) from Khewata section, and three RV (Nos. Sh6, Sh9 and Sh10) from Sherawezha section.

Description: The LV is depressed conical with dorsally eccentric apex and it has very thin ol, around 1 mm. The longitudinal sections of the radial canals of the il are observed where the ol has been eroded away (Plate I, Figures B, C, D).

The RV is conical to cylindro-conical in shape, slightly curved towards the ventral part and of length varying from 35 mm to 65mm. The surface of the valve is smooth (Plate I, Figure A); however dense and fine growth lamellae can be observed in some specimens (Plate I, Figure E). Two shallow swellings representing Ab and Pb can be observed only in one specimen. The ol of the valve is thick, about 15 mm (Plate I, Figures H, I). Due to the intense sediment infilling, the pallial canals of the il and also the cardinal apparatus are badly preserved. However, the large canal sections can be observed in some specimens (Plate I, Figures G, H). The transverse section too close to commissure of one of the specimens shows also the basal attachement of the myocardinal arc within the LV (Plate I, Figure F). The myophores can be partially observed in the another section of the same specimen, from 10 mm below the precedent, but the individual teeth can not be clearly determined due to the recrystallization. The L is absent.

Discussion: The absence of L, the presence of radial and pallial canals in the il of LV and RV respectively, the greater thickness of the ol in the RV than that of LV, the very simple ornementation of the RV and the shallow structure of the radial bands show that these specimens belong to the Afro-Arabian endemic rudist genus, *Dictyoptychus* (Douvillé, 1904, 1905; Karacabey-Öztemür, 1979; Özer, 1986, 1992 a, b, 2005, 2010 a; Pons et al., 1992; Morris and Skelton, 1995; Skelton and Smith, 2000; Khazaei et al., 2010; Steuber and Schlüter, 2012). *Dictyoptychus* has recently been revised by Özer (2010 a), who showed the variability of the canal shapes and the cardinal apparatus of the RV, and demonstrated that all of the previous determined species such as *D. leesi* (Kühn), *D. paronai* (Kühn), *D. persicus* (Cox), *D. euphratica* Karacabey-Öztemür and *D. orontica* Karacabey-Öztemür are synonymous with *D. morgani* (Douvillé), excepting only *D. striatus* (Douvillé), *D. quadrizonalis* Özer and *D. vanensis* Özer. The Iraqi specimens show close similarities with *D. morgani* determined from SE Anatolia (Karacabey-Öztemür, 1979; Özer, 1986, 2010 a), Zagros region (Khazaei et al., 2010; Asgari Pirbaluti et al., 2012), and also the UAB-Oman region (Morris and Skelton, 1995; Steuber and Schlüter, 2012).

Family : Radiolitidae d'Orbigny, 1847

Genus : *Praeradiolites* Douvillé, 1902

Type species : *Sphaerulites ponsiana* d'Archiac 1835

Praeradiolites subtoucasi Toucas, 1907

(plate II, figures A-F; plate III, figures A-H)

1907 *Praeradiolites subtoucasi* Toucas, page 31, plate 3, figures 8, 9.

1954 *Praeradiolites subtoucasi* Toucas, Astre, pages 61, 76-77, 83, plate 6, figures 1, 2.

1965 *Praeradiolites subtoucasi* Toucas, Pamouktchiev, page 37, plate 4, figure 1, text-figure 6.

1976 *Praeradiolites subtoucasi* Toucas, Lupu, page 126, plate 17, figures 4,5a-b, plate 39, figure 6.

1977 *Praeradiolites subtoucasi* Toucas, Pons, page 69, plate 50, figures 1a-d.

1992 *Praeradiolites subtoucasi* Toucas, Vicens, page 201, plate 75, figures 1-15, plate 76, figures 3-4, plate 79, figures 1-5.

1995 *Praeradiolites* cf. *subtoucasi* Toucas, Morris and Skelton, page 292, plate 6, figures 3, 4.

1999 *Praeradiolites subtoucasi* Toucas, Fenerci, pages 90-94, text-figures 3.28, 3.29, plate VII, figures 1-7.

2001 *Praeradiolites* cf. *subtoucasi* Toucas, Götz, page 69, plate 7, figures 17.

2006 *Praeradiolites subtoucasi* Toucas, Pons and Vicens, pages 15,16, figure 13 F, figure 14 G.

2008 *Praeradiolites subtoucasi* Toucas, Pons and Vicens, pages 219-234, figure 1 F (copy of 2006 *Praeradiolites subtoucasi* Toucas, Pons and Vicens, page 15, figure 13 F), figure 14 G (copy of 2006 *Praeradiolites subtoucasi* Toucas, Pons and Vicens, page 16, figure 14 G).

Material: Seven specimens with both valves (Nos. Sh1, Sh2, Sh3, Sh 4, Sh5, Sh7 and Sh8) and two RV (Nos. Sh13 and Sh14) from Sherawezha section.

Description: The RV is generally cylindro-conical and robust, however a single specimen is very long and acute and another one is conical in shape (Plate II, Figures A, B, D; Plate III, Figures A, B, E). The length of the valve varies from 80mm to 170 mm and its surface is ornamented with horizontal growth lines. The growth lamellae are continuously observed around the ventral part of the valve, while they show undulations in the radial band area (Plate II, Figures A, B, D; Plate III, Figure A).The valve is characterized by three very pronounced longitudinal costae and both the Ab and Pb are represented by two deep longitudinal grooves (Plate II, Figures A, D; Plate III, Figures A, E). The radial bands show approximately the same width. The Ib is represented by longitudinal costae and has a width ranges from 7 mm to 10 mm. The ventral and posterior bands are represented by longitudinal costae (Plate II, Figures C, E, F; Plate III, Figures A, E, F, H).

The transverse section of the RV is of rounded triangular form and its diameter ranges from 45x60 mm to 55x110 mm (Plate II, Figures C, E, F; Plate III, Figures D, F, H). However, some specimens show round transverse sections (Plate III, Figure G). The op is generally thicker (16 mm) on the dorso-ventral side than in the posterior part (10 mm), and it consists essentially of closely packed rectangular cells. But, some polygonal or pentagonal cells are also observed around the pb. The growth lamellae are continuously stacked in the dorso-ventral side of the valve (Plate II, Figures E, F; Plate III, Figures G, H). However, compact structure is also observed in the outermost margin of the growth lamellae. The inner margin of the op shows slight indentations next to the radial bands (Plate II, Figures C, E, F; Plate III, Figures D, G, F, H). The L is long (15 mm), has a thin stem (0.5 mm), and is rounded at its extremity. But, it is broken-off in some specimens (Plate II, Figures E, F; Plate III, Figures G, H). The cardinal apparatus is well developed and preserved; the at is bigger than the pt (Plate II, Figures E, F; Plate III, Figure G).

The LV is very flat or slightly convex and consists of growth lamellae (Plate II, Figures A, B, D; Plate III, Figures A, B, C, E). The ol is 10 mm thick in the transverse section of the valve. The myophore apophyses, teeth and L are partially preserved.

Discussion: The specimens show some similarity to *Praeradiolites aristidis* (Munier-Chalmas), however the radial bands of our specimens are deeper and better-developed than those of the latter species. Anyway, it is regarded as synonymous with *Praeradiolites subtoucasi* Toucas by Vicens (1992). Because of the sub-triangular transverse section of the RV, approach *Praeradiolites toucasi* (d'Orbigny), but they have less developed radial bands. The radial bands of our specimens may also be compared with those of *Praeradiolites boucheroni* (Bayle), but their L is long while that of latter species is small and triangular.

Genus : *Sauvagesia* Choffat, 1886

Type species : *Sphaerulites sharpei* Bayle, 1857

Sauvagesia somalica Tavani, 1949

(plate IV, figures A-C)

1949 *Sauvagesia somalica* Tavani, page 17, plate 1, figure 4, plate 4, figure 4.

1949 *Sauvagesia attenuata* Tavani, page 17, plate 1, figures 8, 9, plate 2, figure 2, plate 4, figure 11.

1971 *Sauvagesia somalica* Tavani, Vogel, pages 62, 72.

1992 *Sauvagesia somalica* Tavani, Pons et al., page 237, text-figures 20 a-b.

2012 *Sauvagesia* cf. *somalica* Tavani, Asgari Pirbaluti et al., page 60, plate 4, figure 2.

Material: A single specimen with both valves (No. Sh12) from Sherawezha section.

Description: The RV is cylindro-conical. The apex having broken off, the present length of the valve is about 65 mm (Plate IV, Figure A). The surface of the valve is ornamented with densely longitudinal costae and grooves. The radial bands are very well preserved, the Pb and Ab are slightly concave limited by 5 mm thick longitudinal costae and Pb is wider than Ab (Plate IV, Figure A). The transverse section across the RV very close to commissure, is semicircular with diameters of 50x60 mm (Plate IV, Figure C). The op is thick (15 mm) and composed of very small polygonal cells with prismatic pattern. But, some compact structure (Pons and Vicens, 2008) can be observed in the radial bands area and towards the outer part of op. The L is present, 2 mm long and truncated at its extremitiy.

The LV is conical, approximately 10 mm height, and presents radial costae. The transverse section of the valve shows thin lamellar, compact ol with some sections ressembling the orifices and also a few fusiform structures in the il flanking the myophores (Plate IV, Figure B).

Discussion: The presence of the L, the structure of the op, the ornamentation of the RV and the shape of the radial bands indicate that this specimen has the characteristic of the genus *Sauvagesia* Choffat. The radial bands of the specimen present very similar structure with those of the *Sauvagesia somalica* determined by Tavani (1949). The specimen shows also the same characters of *Sauvagesia attenuata* Tavani, however this species is synonymous with *Sauvagesia somalica* as proposed by Pons et al., (1992). The structure of the op and the radial bands show very close resemblance with Fig. 20 b of Pons et al. (1992).

A few orifices like sections across radial canals situated within the ol, and fusiform structures like pallial canals in the il of the LV, they may be compared with those of *Kurtinia* illustrated by Karacabey-Öztemür (1980). These features suggest the possibility of a relationship of studied specimen with *Kurtinia*. However, the determination here based on a single specimen, so it needs another well-preserved LVs for proving this similarity.

Genus : *Lapeirousia* Bayle, 1878

Type species : *Sphaerulites jouanneti* Des Moulins, 1826

Lapeirousia jouanneti (Des Moulins, 1826) Bayle, 1878

(plate IV, figures D-F)

1826 *Sphaerulites* Des Moulins, page 99, plate 3, figures 1, 2.

1850 *Radiolites Jouanneti* d'Orbigny, Orbigny, page 223, plate 564.

1878 *Lapeirousia Jouanneti* (Des Moulins), Bayle, plates CX, CXI.

1886 *Lapeirousia jouanneti* (Des Moulins), Douvillé, page 403, text-figure 19.

1900 *Lapeirousia Jouanneti* (Des Moulins), Parona, page 17, plate 2, figure 6.

1908 *Sphaerulites Jouanneti* Des Moulins, Toucas, page 58, plate 10, figures 4-5.

1910 *Lapeirousia jouanneti* (Des Moulins), Douvillé, page 26, plate 6, figures 2, 3; text-figures 25, 26.

1929 *Lapeirousia jouanneti* (Des Moulins), Klinghardt, page 98, plate 13, figures 4, 5; plate 14, figure 2.

1969 *Lapeirousia jouanneti* (Moulins), Pamouktchiev, page 75, plate 1, figures 1, 2, plate 2, figures 1, 2, text-figures C, D.

1992*a* *Lapeirousia jouanneti* (Des Moulins), Özer , page 139, plate 1, figure 10.

1993 *Lapeirousia jouanneti* (Des Moulins), Plenićar, page 57, plate 11, figures 1, 2.

1995 *Lapeirousia jouanneti* (Des Moulins), Morris and Skelton, page 302, figures 7 a, b.

Material: Five right valve sections from the field photographs of Khewata section and four right valves (Nos. Su2, Su3, Su11 and Su 12) selected from many specimens of Sura Qalat section.

Description: The RV is conical, flat-based, probably 55 mm high and its transverse section is ovaloid, approximately 60x70 mm (Plate IV, Figures D, F). The Pp and Ap are lensoid in section and demarcated within op by a layer 1 mm thick (Plate IV, Figure E).

Discussion: The structure of the op and the presence of the pseudopillars show that these specimens are belong to *Lapeirousia* Bayle. The pseudopillars present the typical characteristics of the species.

Family : Hippuritidae Gray, 1848

Genus : *Hippurites* Lamarck, 1801

Type species : *Hippurites bioculatus* Lamarck, 1801

Hippurites cornucopiae Defrance, 1821

(plate IV, figure G)

1821 *Hippurites cornucopiae* Defrance, page 195, plate 58, figures 1 a, b.

1897 *Hippurites cornucopiae* Defrance, Douvillé, page 223, plate 22, figures 11, 12, text-figure 72.

1900 *Hippurites comucopiae* Defrance, Parona, page 10, plate 1, figure 1.

1910 *Hippurites (Hippuritella) cornucopiae* Defrance, Douvillé, page 79, plate 7, figures 3-5.

1933 *Hippurites cornucopiae* Defrance, Kühn, page 159, plate 1, figure 3.

1949 *Hippurites (Hippuritella) cornucopiae* Defrance, Tavani, page 13, plate 4, figures 7, 9.

1949 *Hippurites (Hippuritella) somalicus*, Tavani, page 14, plate 4, figure 6.

1961 *Hippurites (Hippuritella) cornucopiae* Defrance, Devidé-Nedela and Polsak, pages 364, 373, plate 3, figure 4, text-figure 4.

1972 *Hippurites (Hippuritella) comucopiae* Defrance, Sladić-Trifunović, plate 11, figures 2, 3.

1983 *Hippurites cornucopiae* Defrance, Camoin, page 223, plate 7, figure 1.

1983 *Hippurites cornucopiae* Defrance, Özer, page 17, plate 3, figures 6, 7.

1988 *Hippurites cornucopiae* Defrance, Accordi et al., page 140, text-figure 5, plate 1, figure 12.

1992*b* *Hippurites cornucopiae* Defrance, Özer, page 77, plate 1, figures 1, 2.

1992 *Hippurites cornucopiae* Defrance, Pons et al., page 284, plate 3, figures 1-3, text-figures 3/1a-c, 2a-b.

1994 *Hippurites cornucopiae* Defrance, Pons and Sirna, page 274, plate 1, figures 1-2, plate 2, figures 1-6, plate 3, figures 1-7.

1995 *Hippurites cornucopiae* Defrance, Morris and Skelton, page 292, plate 5, figures 4-7.

1999 *Hippurites cornucopiae* Defrance, Steuber, page 124, text-figures 46a-c, e-f.

2010 *Hippurites cornucopiae* Defrance, Khazei et al., page 706, text-figures 2, tb. 1, 2, plate 1, figures 3-5, plate 2, figures 2, 3.

2012 *Hippurites cornucopiae* Defrance, Steuber and Schlüter, pages 49, 50, 52, figure 10 A.

2012 *Hippurites cornucopiae* Defrance, Asgari Pirbaluti et al., plate 4, figures 5-7.

Material: Numerous specimens of the RV (see Figure 5) and a specimen (No. Su1) showing a cluster of orientated individuals from Sura Qalat section. A few specimens of the RV (Nos. Kh4 and Kh5) from Khewata section.

Description: The RV is cylindro-conical in shape, the length is 120 mm and the surface of the valve is generally smooth with two pillars that are represented by longitudinal grooves. The transverse section is generally circular and the diameter varies from 10 mm to 20 mm. The L is reduced. The pp is open at the base, however the ap is pinched at the base and it is better developed than the posterior one, and recurved towards the posterior part of the valve in some sections (Plate IV, Figure G). Different growth stages show a variation in pinching of the ap, but the posterior one is always open at the base. The cardinal apparatus is partly preserved. The ol is approximately 1 to 2 mm and it shows radial ribbings.

The LV is generally absent or partly preserved.

Discussion: The pillars of the specimens are characteristic for the species and also show clear similarities with those of Somalia, the UAE-Oman region, Iran and SE Anatolia (Tavani, 1949; Pons et al., 1992; Özer, 1992 b; Morris and Skelton, 1995; Khazaei et al., 2010; Steuber and Schlüter, 2012).

4. Age Of The Rudist Fauna

The species of the rudist fauna from NE Iraq vary in abundance according to measured stratigraphic sections (Figure 6). The Arabian Plate endemic genus *Dictyoptychus* is abundantly found in the Khewata section, where *Lapeirousia jouannetti* is represented also in abundance, however the specimens of *Hippurites cornucopiae* are very rare. The latter species and *Lapeirousia jouanneti* are very abundant in the Sura Qalat section, where the specimens of *Praeradiolites subtoucasi* are abundant, but those of *Dictyoptychus* are very rare. The Sherawazha section is characterized by the high abundance of *Praeradiolites subtoucasi. Hippurites cornucopiae* and *Dictyoptychus*, but *Lapeirousia jouanneti* and *Sauvagesia somalica* are very rare in this section.

Hippurites cornucopiae seem to be a unique species within the rudist fauna showing a wide distribution and indicating a Maastrichtian age; whereas the other determined species were found in the late Campanian-Maastrichtian or Maastrichtian formations of the central and eastern Mediterranean Tethys and Arabian Plate (Steuber, 2002).

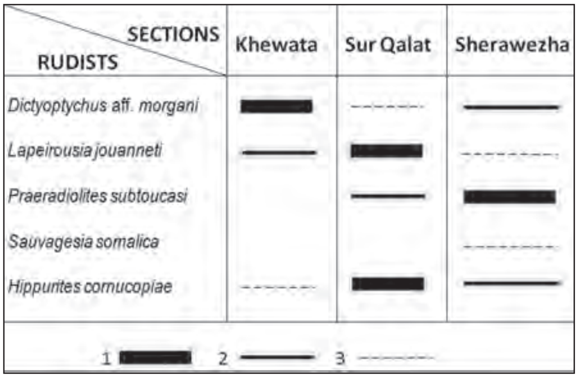

Figure 6- The abundance distribution of the rudists according to the measured- stratigraphic sections. 1-very abundant, 2-abundant, 3-rare.

Rudist biozones have recently been proposed for the central-eastern Mediterranean Tethys and Arabian plate based on Sr-isotope data and numerical ages of the rudist shells by Steuber and Schlüter (2012). Because of the presence of Arabian endemic rudists in the NE Iraq fauna, the Arabian plate biozones of these authors are considered in this study. Three rudist biozones for mid-Campanian-Maastrichtian interval have been suggested by Steuber and Schlüter (2012):

1-*Torreites*/*Vaccinites* aff. *vesiculosus* interval biozone: Middle Campanian. The base of this biozone is determined by the first occurrence of *Torreites* Palmer and *Vaccinites* aff. *vesiculosus* (Woodward) in the Simsima Formation (Oman) (Grubić, 1979; Skelton and Wright, 1987; Morris and Skelton, 1995; Simonpietri et al., 1998; Schumann, 1995, 2010) and the top with the lowest occurrence of *Dictyoptychus* in the Terbüzek Formation (Alidamı-Adıyaman) (Schlüter, 2008; Özer et al., 2008; Steuber et al., 2009).

2- *Dictyoptychus* interval biozone: uppermost Campanian-Lower Maastrichtian. The Sr-isotope analysis and numerical ages of rudist shells (Schlüter, 2008; Özer et al., 2008; Steuber et al., 2009) from the shallow marine rudist-bearing limestone lenses in the Terbüzek Formation cropping out around Alidamı village-Adıyaman (Yalçın, 1976; Karacabey-Öztemür, 1979; Meriç et al., 1985; Özer, 1986, 1992*c*, 2002, 2010*a*; Özcan, 2007; Özer et al., 2009) and the first occurrence of *Dictyoptychus* characterize the base of the biozone. The first occurrence of *Hippurites cornucopiae* in the locality of Oman, Buraimi, Jebel As Saifr determine the top of the biozone (Morris and Skelton, 1995). This biozone contains also two rudist genera endemic to the Arabian plate, *Vautrinia* (Vautrin) and *Paracaprinula* Piveteau, while *Hippuritella lapeirousei* Goldfuss and *Pseudosabinia* Morris and Skelton have been found in the Kahta, Besni-Adıyaman, Gölbaşı-KahramanMaraş, Yayladağı-Antakya, Çermik-Diyarbakır and Körkandil-Siirt in SE Anatolia (Erentöz, 1949; Karacabey-Öztemür, 1979; Karacabey-Öztemür and Selçuk, 1981; Özer, 1986, 1991, 2002, 2010*a, b*; Steuber et al., 2009).

3- *Hippurites cornucopiae* interval biozone: mid-Upper Maastrichtian. The base of this biozone is determined by the first occurrence of *Hippurites cornucopiae* in the locality of Oman, Buraimi, Jebel As Saifr. *Hippurites cornucopiae* was found in the SE Anatolia, Zagros-Iran, Oman Mountains (the border of the UAE and Oman), Somalia and Yemen (Steuber, 2002). The top of the biozone can not defined, but some little hippuritids were found a few metres below of the K/T boundary in the Oman Sur Qualhat locality, apparently belonging to *Hippurites cornucopiae* (Schlüter et al., 2008). *Dictyoptychus* Douvillé, *Vaccinites* aff. *oppeli* Douvillé and *Pseudosabinia* Morris and Skelton accompanied this zone.

The numerical ages data play an important role for the determinations of the biozones as explained above, obtained from the rudist shells of SE Anatolia, located in the northernmost part of the Arabian Plate. The presence of *Hippurites cornucopiae* indicates a Maastrichtian age for the NE Iraq rudist fauna. The rudist fauna determined here, is assigned to the *Hippurites cornucopiae* interval biozone of Steuber and Schlüter (2012) and so of mid- to Late Maastrichtian age. The paleontologic reports on the benthic foraminifers of the Aqra Formation (Al-Kubaysi, 2008; Sadiq, 2009; Zebari, 2010), including the presence of *Racemiguembelina fructicosa* (Egger) indicate an earliestLate Maastrichtian age. Moreover, many planktonic foraminifers, which were recently determined from the Tanjero Formation (Sharbazheri, 2008; personal report of K.H. Karim, 2013) of the NE Iraq, support this age.

5. Palaeobiogeography

The Zagros fold-thrust belt was formed from the convergence between the Arabian and Eurasian plates, and because of the closing of the Mediterranean Tethys during the Late Cretaceous, ophiolitic material cropsout widely in northeastern Iraq (Buday, 1980; Buday and Jassim,1987; Jassim and Goff, 2006; Karim, 2004; Karim and Surdashy, 2006; Karim et al., 2007). The Campanian-Maastrichtian rudist-bearing formations (or platforms) of northeastern Iraq are developed over these rocks (Buday, 1980; Karim, 2004, 2005; Al-Barzinjy, 2005; Sadiq, 2008) and located on the northern border of the Arabian platform (Figure 7), about 20° or 21° N paleolatitude (Dercourt et al., 1986). Due to insufficient data about the shallow marine carbonate platforms, northeastern Iraq was included in the thin continental crust in the previous palaeogeographic reconstructions (Dercourt et al., 1986; Camoin et al., 1993). The recently obtained stratigraphic data (Karim, 2004, 2005; Al-Barzinjy, 2005; Sadiq, 2008) and also new data presented in this study allowed us, by contrast, to add the presence of carbonate platforms around northeastern Iraq to the palaeogeographic map of Dercourt et al. (1986) (Figure 7). This has important implications for the palaeobigeography of the northern side of Arabian plate as indicated below.

Although the rudist fauna of NE Iraq has a low diversity, it contains both some species that show a wide distribution in the Mediterranean Tethys and Afro-Arabian region, and *Dictyoptychus*, which is endemic to the Arabian plate (Özer, 1986, 2010*a*; Morris and Skelton, 1995; Steuber and Schlüter, 2012), as well as *Sauvagesia somalica*, which shows a geographic distribution likewise limited to the same plate according to present knowledges (Tavani, 1949; Pons et al., 1992; Steuber, 2002; Asgari Pirbaluti et al., 2012). Indeed, the Arabian Plate rudist fauna consists of, beside *Dictyoptychus,* endemic genera such as *Vautrinia* (Vautrin), *Paracaprinula* Piveteau, *Eodictyoptychus* Skelton and El-Asa'ad and *Semailia* Morris and Skelton and species like *Hippurites syriaca* Vautrin and *Pironaea syriaca* (Vautrin), which have not so far been observed in the Mediterranean Tethys (Özer, 1991, 1992*c, d*, 2002, 2010*a*; Özer et al., 2008, 2009; Skelton and El-Asa'ad, 1992; Morris and Skelton, 1995; Schlüter, 2008; Steuber et al., 2009; Steuber and Schlüter, 2012). The main reason for the absence of such Arabian Plate endemic rudists, other than *Dictyoptychus*, from the NE Iraq rudist fauna may be that they are limited to the latest Campanian-Early Maastrichtian age formations as indicated by Steuber and Schlüter (2012).

The biogeographic and stratigraphic distributions of the rudists of NE Iraq are as follows:

Dictyoptychus is abundantly represented in the Late Campanian-Maastrichtian formations of the Afro-Arabian region such as in SE Turkey (Karacabey-Öztemür, 1979; Karacabey-Öztemür and Selçuk, 1981; Özer, 1986, 1991, 1992*c, d*, 2005, 2010*a*; Özer et al., 2008, 2009), Iran (Douvillé, 1904, 1910; Kühn, 1933; Cox 1933, 1934; Khazaei et al.,

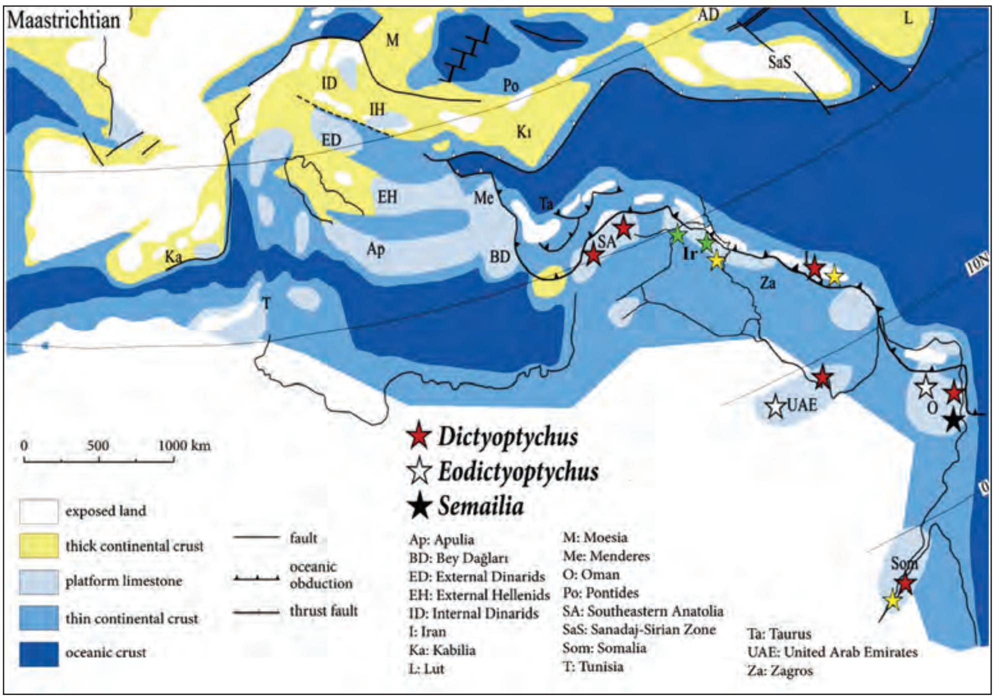

Figure 7- Maastrichtian palaeogeographical reconstruction of the Mediterranean area (simplified and partly modified after Dercourt et. al., 1986) showing the distribution of endemic rudists *Dictyoptychus* (green asterisks for localities in Iraq) and Sauvagesia somalica (yellow asterisks) and also *Eodictyoptychus* and *Semailia* in the Afro-Arabian plate (after Özer, 2010*a*). Ir indicates NE Iraq.

2010; Asgari Pirbaluti et al., 2012), Saudi Arabia, the UAE, Oman (Kühn, 1929; Morris and Skelton, 1995; Skelton and Smith, 2000; Steuber and Schlüter, 2012) and Somalia (Tavani, 1949; Pons et al., 1992).

Sauvagesia somalica seems to be also endemic to the Arabian platform. It was first determined from the Maastrichtian of Somalia (Tavani, 1949; Pons et al., 1992), and reported from the Maastrichtian of Iran and Afghanistan (Vogel, 1971). It was recently also determined from the Maastrichtian of the Central Zagros region of Iran (Asgari Pirbaluti et al., 2012).

Other determined rudists show a very wide geographic distribution in the Mediterranean Tethys as follows:

Hippurites cornucopiae is abundantly represented in the Maastrichtian of the central and eastern Mediterranean Tethys (Steuber, 2002) and also SE Turkey, Iran, Oman, the UAE, Somalia and Yemen of the Arabian Plate (Özer 1992 b, Özer et al., 2009; Pons and Sirna, 1994; Morris and Skelton, 1995; Khazaei et al., 2010; Steuber and Schlüter, 2012; Asgari Pirbaluti et al., 2012).

Praeradiolites subtoucasi is mainly represented in the Campanian-Maastrichtian of the Mediterranean Tethys from Spain to Turkey (Steuber, 2002), but has also been recorded from the mid-Maastrichtian of Oman (Morris and Skelton, 1995).

Lapeirousia jouanneti shows very a similar distribution to that of *Praeradiolites subtoucasi.* It is mainly recorded from the Campanian-Maastrichtian of the Mediterranean Tethys (Steuber, 2002), but is also found in the Maastrichtian of Iran (Douvillé, 1904). Some *Lapeirousia* specimens showing resemblance to this species were also demonstrated from the Maastrichtian of the UAE-Oman border region (Morris and Skelton, 1995) and Zagros region in Iran (Khazaei et al., 2010; Asgari Pirbaluti et al., 2012).

These data show that all of the determined rudists of NE Iraq have a distribution in the Maastrichtian formations of the Arabian Plate.

Although the Maastrichtian rudist-bearing formations are well known from the SE Anatolia-Turkey and SW Iran along the Zagros fold-thrust belt (Özer, 1986, 1992*c*, *d*, 2002, 2010*a*, *b*; Özer et al., 2008, 2009; Steuber et al, 2009; Khazaei et al, 2010), the palaeobiogeographic relationships of these regions were attributed to faunal resemblances (Özer, 1992*c*, *d*; Özer et al., 2008) because of our insufficient knowledge about NE Iraq. So, the palaeobiogeographic approaches have been limited in the northern border of the Arabian Plate. But, the discovery of the rudist-bearing formations in this study fills an important palaeobiogeographic gap between SE Turkey and Iran and allows us to identify the presence of a path-way for larval distribution during the Maastrichtian along the Zagros fold-thrust belt from SE Turkey across NE Iraq towards SW Iran (Figure 7). The relationship of this path-way with other rudist localities such as Oman, the UAE and Somalia of the Arabian Plate is not yet known, but a connection in the Maastrichtian is implied by the presence also *Dictyoptychus* and *Hippurites cornucopiae* in these localities. According to the increase our knowledge in the following years the migration routes in the Arabian Plate will be better interpreted.

6. Conclusions

The Aqra Formation cropping out around Sulaimaniya city-NE Iraq consists mainly of detrital limestones. Three stratigraphic sections at Khewata, Sura Qalat and Sherawezha are characterised by abundant rudist associations. The rudist fauna consists of *Dictyoptychus* aff. *morgani*, *Praeradiolites subtoucasi*, *Sauvagesia somalica*, *Lapeirousia jouanneti* and *Hippurites cornucopiae*, which are determined from the NE Iraq for the first time.

The age of the rudist fauna is considered to be mid- to Late Maastrichtian based on the *Hippurites cornucopiae* interval zone proposed by Steuber and Schlüter (2012) for the Arabian Plate.

Dictyoptychus and *Sauvagesia somalica* are characteristic endemic rudists for the Arabian Plate. Other rudists are seen mainly in the central-eastern Mediterranean Tethys, but also in the Arabian Plate. The determination of rudists from NE Iraq both augments the palaeobiogeographic and taxonomic database and indicates a palaeobiogeographic relationship between SE Turkey, NE Iraq and SW Iran during the Maastrichtian involving larval dispersion along the Zagros fold-thrust belt.

Acknowledgements

Authors would like to thank Peter W. Skelton for his valuable constructive comments and English corrections that helped to improve the quality of the manuscript. Thanks also to Feride Özyol (DEÜ-İzmir) for the organisation of the rudist photos in the plates.

Received: 01.03.2013
Accepted: 23.07.2013
Published: December 2013

References

Accordi, G., Carbone, F., Sirna, G., Catalano, G., Reali, S. 1988. Sedimentary events and rudist assemblages of Maiella Mt. (central Italy): Paleobiogeographic implications. *Geologica romana* 26, 135-147.

Archiac, A. de. 1835. Mémoire sur la formation crétacée du Sud-Ouest de la France. *Mémoires de la Société géologique de France* 2, 157-192.

Al-Barzinjy, S. T. M. 2005. Stratigraphy and basin analysis of Red Bed Series from northeastern Iraq-Kurdistan Region. Ph.D. thesis, University of Sulaimani (unpublished)

Al-Kubaysi, K. N. 2008. Biostratigraphy of Aqra, Tanjero and Shiranishs Formation in Chwarta Area, Sulaimanyah Governorate, NE-Iraq. *Iraqi Bulletin of Geology and Mining* 4, 1-23.

Asgari Pirbulati, B., Khazaei, A., Jafarian, M. A., Khosrow-Tehrani, K., Afghah, M., Abiyat, A. 2012. Biostratigraphy of the Tarbur Formation in Tang-e-Zendan section, Sabzeh kuh (Southwest Borujen) based on Foraminifera and Rudists. *Journal of Sciences Esfahan University–Research stratigraphy and sedimentology* 45, 49-64.

Astre, G. 1954. Radiolitidés nord-pyrénéens. *Mémoires de la Société géologique de France*, N.S., 71, 140 p.

Bayle, E. 1878. Fossiles principaux des terrains. *Mémoire pour servir à l'Explication de la Carte géologique de la France* vol. 4b.

Bellen, R. C. Van, Dunnington, H. V., Wetzel, R., Morton, D. 1959. Lexique Stratigraphique International. Asie, Iraq 3c, 10a, 333 p.

Buday, T. 1980. Regional Geology of Iraq: Vol. I, Stratigraphy: Kassab, I. I., Jassim, S. Z. (Ed.). *Publication of Establishment of Geological Survey of Iraq, Baghdad* 445p.

Buday, T., Jassim, S. Z. 1987. The Regional Geology of Iraq: Tectonic Magmatism, and Metamorphism. Kassab, I.I., Abbas, M.J. (Ed.). *Geosurv, Baghdad* 2, 445 p.

Camoin, G. 1983. Plates-formes carbonatées et récifs à rudistes du Crétacé de Sicile. *Travaux du Laboratoire de Géologie historique et de Paléontologie* 13, 244 p.

Camoin, G., Bellion, Y., Dercourt, J., Guiraud, R., Lucas, J., Poisson, A., Ricou, L. E., Vrielynck, B. 1993. Atlas Tethys Palaeoenvironmental Maps, Explanatory Notes. Dercourt, J., Ricou, L. E., Vrielynck, B. (Ed.). *Gauthier-Villars* Paris, 179-196.

Cox, L. R. 1933. The evolutionary history of the rudists. *Proceedings of the Geologists' Association* 44, 379-388.

Cox, L. R. 1934. On the structure of the Persian rudist genus *Trechmanella* (formerly *Polyptychus*), with the description of a new species. *Proceedings of the Malacological Society of London* 21, 42-66.

Defrance, J. L. M. 1821. Hippurites. Defrance, J. L. M. (Ed.). *Dictionnaire des sciences naturelles* 21, 195-197.

Dercourt, J., Zonenshain, L. P., Ricou, L. E., Kazmin, V. G., Le Pichon, X., Knipper, A. L., Grandjacquet, C., Sbortshikov, I.M., Geyssant, J., Lepvrier, C., Pechersky, D.H., Boulin, J., Sibuet, J.-C., Savostin, L.A., Sorokhtin, O., Westphal, M., Bazhenov, M.L., Lauer, J.P., Biju-Duval, B., 1986. Geological evolution of the Tethys belt from the Atlantic to the Pamirs since the Liassic. *Tectonophysics* 123, 241-315.

Des Moulins C. 1826. Essai sur les sphérulites qui existent dans les collections de MM. F. Jouannet, membre de l'Académie royale des Sciences, belle Lettres et Arts de Bordeaux, et Charles Des Moulins. *Bulletin d'Histoire naturelle de la Société Linnéenne de Bordeaux* 5, 1, 148-303.

Devidé-Nedela, D., Polsak, A. 1961. Sur la présence du Maestrichtien dans la région de Bespelj au nord de Jajce (Bosnie). *Geoloski Vjesnik* 14, 355-374.

D'Orbigny, A. de.1847. Paléontologie française, Terrains crétacés. II-III, Lamellibranchia. 1-807.

Douvillé, H. 1886. Essai sur la morphologie des rudistes. *Bulletin de la Société géologique de France* 3, 14, 389-404.

Douvillé, H. 1897. Etudes sur les rudistes. Distribution régionale des Hippurites. *Mémoires de la Société géologique de France, Paléontologie* 6, 6, 187-230.

Douvillé, H. 1902. Classification des Radiolites. *Bulletin de la Société géologique de France* 4, 2, 461-477.

Douvillé, H. 1904. Mollusques fossiles. Morgan, J. de : Mission scientifique en Perse, volume 3, Etudes géologiques, partie 4, Paléontologie, 191–380.

Douvillé, H. 1905. Observations. Morgan, J. de : Notes sur la géologie de la Perse et sur les travaux paléontologiques de H. Douvillé sur cette region. *Bulletin de la Société géologique deFrance* 5, 170–189

Douvillé, H. 1910. Etudes sur les rudistes. Rudistes de Sicile, d'Algérie, d'Egypte, du Liban et de la Perse. *Mémoires de la Société géologique de France* 41, 83 p.

Dubertret, L. 1966. Liban, Syrie et bordure des pays voisins. Première partie. Tableau stratigraphique, avec carte géologique au millionième. *Notes et Mémoires sur le Moyen-Orient* 8, 251-385.

Erentöz, L. 1949. Note sur la repartition stratigraphique des quelques *Hippurites* provenant du Sud-Est de la Turquie. *Bulletin of the Geological Society of Turkey* 2, 1, 14-28.

Fenerci, M. 1999. Cretaceous rudist fauna of Kocaeli Peninsula and Western Pontides, Ph D. Thesis, Dokuz Eylül Üniversitesi, 232 p. İzmir-Turkey.

Götz, S. 2001. Rudisten-Assoziationen der keltiberischen Oberkreide SE-Spaniens: Paläontologie, Palökologie und Sediment-Organismus-Wechselwirkungen. *Bayerische Akademie der Wissenschaften, Mathematisch-Naturwissenschaftliche* Klasse, *Abhandlungen* N. F. 171, 1-112.

Grubić, A. 1979. *Torreites milovanovici* sp. nov. from Oman, *T. coxi* sp. nov. and *T. chubbi* sp. nov. from Jamaica, a new description of the genus *Torreites* Palmer, and a reference to the significance of its palaeogeographic distribition. *Vesnik Geologija, A37. Zavod za geoloska i geofizicka Istrazivanja* 81–95.

Jassim, S.Z., Goff, J. C. 2006. Geology of Iraq. *Dolin, Prague and Moravian Museun, Berno,* 341p.

Karacabey-Öztemür, N. 1979. Two new species of the genus *Dictyoptychus* in Turkey. *Bulletin of the Mineral Research and Exploration Institute of Turkey* 92, 35-39.

Karacabey-Öztemür, N. 1980. Two new genera of Radiolitidae (*Balabania* n. gen. *Kurtinia* n. gen.) from Turkey. *Geological Bulletin of Turkey* 23, 79-86.

Karacabey-Öztemür, N., Selçuk, H. 1981. A new genus and two new species of rudists from Hatay, Turkey. *Bulletin of the Mineral Research and Exploration Institute of Turkey* 95/96, 97-105.

Karim, K. H. 2004. Basin analysis of Tanjero Formation in Sulaimaniya area, NE-Iraq, Ph.D. thesis, University of Sulaimani (unpublished) 131p.

Karim, K.H. 2005. Some sedimentary and structural evidence of possible graben in Chuarta-Mawat area, Sulaimaniya area, NE-Iraq. *Iraqi Journal of Earth Science* 5, 9-18.

Karim, K.H., Surdashy, A.M. 2006. Sequence Stratigraphy of Upper Cretaceous Tanjero Formation in Sulaimaniya area, NE-Iraq, Kurdistan Academician Journal, 4, 10-28.

Karim, K. H., Surdashy, A. M., Al-Barzinjy, S. T. 2007. Concurrent and lateral deposition of flysch and molasse in the foreland basin of Upper Cretaceous and Paleocene from NE-Iraq, Kurdistan Region. *2nd International Conference on Geo-Resources in the Middle East and North Africa (GERMENA II), Cairo University* 757-769.

Khazaei, A.R., Skelton, P.W., Yazdi, M. 2010. Maastrichtian rudist fauna from Tarbur Formation, (Zagros region, SW Iran), Preliminary observations. Özer, S., Sarı, B., Skelton, P. W. (Ed.). Jurassic-Cretaceous Rudists and Carbonate Platforms, Part (A), 8th International Rudist Congress. *Turkish Journal of Earth Sciences* 19, 703–719.

Klinghardt, F. 1929. Die stammesgeschichtliche Bedeutung, innere Organisation und Lebensweise von *Eoradiolites liratus* Conrad sp. *Palaeontographica* 72, 95-101.

Kühn, O. 1929. Beiträge zur Palaeontologie und Stratigraphie von Oman (Ost-Arabien). *Annalen des Naturhistorischen Museums in Wien* 43, 13-33.

Kühn, O. 1933. Rudistae from eastern Persia. *Records of the Geological Survey of India* 46, 151-179.

Linnaeus, C. 1758. Systema Naturae. 10th ed. , *Holmiae (Salvius)* 1, 824 p.

Lupu, D. 1976. Contributions à l'étude des rudistes sénoniens des Monts Apuseni. *Institut de Géologie et Géophysique, Mémoires* 24, 83-151.

Ma,ala, K. A. 2008. Geological map of the Sulaimaniyah Quadrangle, sheet N1-38-3, scale 1:20000. Published by Establishment of Geological Survey of Iraq, Badgdad.

Meriç, E., Oktay, F. Y., Özer, S. 1985. Besni Formasyonu'nun Alidamı (Kahta-Adıyaman) kuzeybatısındaki stratigrafik gelişimi ile ilgili yeni gözlemler. *Jeoloji Mühendisliği* 25, 51-54.

Morris, N. J., Skelton, P. W. 1995. Late Campanian-Maastrichtian rudists from the United Arab Emirates-Oman border region. *Bulletin of the British Museum (Natural History), Geology Series* 51, 277-305.

Newell, N. D. 1965. Classification of the Bivalvia. *American Museum Novitates* 2206, 125.

Özcan, E. 2007. Morphometric analysis of the genus *Omphalocyclus* from the Late Cretaceous of Turkey: new data on its stratigraphic distribution in Mediterranean Tethys and description of two new taxa. *Cretaceous Research* 28, 621—641.

Özer, S. 1983. Les formations à rudistes du Sénonien supérieur d'Anatolie centrale (Turquie). *Travaux du Laboratoire de Stratigraphie et de Paleoécologie* N.S. 1, 32 p.

Özer, S. 1986. Faune de Rudistes maestrichtienne de I'environ de Kahta-Adıyaman (Anatolie sud-est). *Bulletin of the Mineral Research and Exploration Institute of Turkey* 107, 101-105.

Özer, S. 1991. Yayladağı (Hatay) Mestrihtiyen rudist faunası ve biyocoğrafyası. Yetiş, C. (Ed.). Ahmet Acar Jeoloji Sempozyumu, Çukurova Üniversitesi, Bildiriler 145-152.

Özer, S. 1992*a*. Deux nouvelles espèces du genre *Miseia* (rudistes) en Turquie. Remarques systématiques et phylogénétiques. *Palaeontographica* A, 220, 131-140.

Özer, S. 1992*b*. Presence of rudist-bearing limestone blocks derived from the Arabian platform in Gevaş (Van) ophiolite. *Bulletin of the Mineral Research and Exploration* 114, 75-82.

Özer, S. 1992*c*. Rudist carbonate ramp in southeastern Anatolia, Turkey. Simo, J. A. T., Scott, R. W., Masse, J.-P. (Ed.). Atlas of Cretaceous Carbonate Platforms. *American Association of Petroleum Geologist Bulletin* Memoir 56, 163-171.

Özer, S. 1992*d*. Stratigraphic setting and biogeographic characteristics of rudists in SE Anatolia. *Turkish Association Petroleum Geoloical Bulletin, Special issue for M.Ozan Sungurlu* 4, 47-58.

Özer, S. 2002. Distributions stratigraphiques et géographiques des rudistes du Crétacé superieur en Turquie. Sladic-Trifunović, M., Grubić, A. (Ed.). Proceedings-First International Conference on rudists (Beograd, 1988). *USGY, Memorial publication* 173-187.

Özer, S. 2005. Two new species of canaliculate rudists (Dictyoptychidae) from southeastern Turkey. *Geobios* 38, 2, 235-245.

Özer, S. 2010*a*. *Dictyoptychus* Douvillé: taxonomy, revision, phylogeny and biogeography. Özer, S., Sarı, B., Skelton, P. W. (Ed.). Jurassic-Cretaceous Rudists and Carbonate Platforms, Part (A), 8th International Rudist Congress. *Turkish Journal of Earth Sciences* 19, 5, 583-612.

Özer, S. 2010*b*. Campanian-Maastrichtian *Pseudosabinia* from Turkey: Descriptions and taxonomic problems. Özer, S., Sarı, B., Skelton, P. W. (Ed.). Jurassic-Cretaceous Rudists and Carbonate Platforms, Part (A), 8th International Rudist Congress. *Turkish Journal of Earth Sciences* 19, 5, 643-669.

Özer, S., Sarı, B., Önal, M. 2008. Campanian-Maastrichtian rudist-bearing mixed silisiclastic-carbonate transgressive-regressive system tracts of the eastern and southeastern Anatolia: faunal correlation, depositional facies and palaeobiogeographic significance. Eighth International Congress on Rudists June 23-25 2008 İzmir-Turkey, Pre-meeting Field Trip (1) Excursion Guide, *Dokuz Eylul University* 1-28.

Özer, S., Meriç, E., Görmüş, M., Kanbur, S. 2009. Biogeographic Distributions of Rudists and Benthic Foraminifera: An Approach to Campanian-Maastrichtian Palaeobiogeography of Turkey. *Geobios* 42, 623-638.

Pamouktchiev, A. 1965. Faune rudiste du Maëstrichtien de l'arrondissement du Breznik (II). *Annuaire de l'Université de Sofia, Faculté de Géologie et Géographie, Livre 1, Géologie* 58, 25-46.

Pamouktchiev, A. 1969. Représentants maëstrichtiens du genre *Lapeirouseia*, Bulgarie de l'Ouest. *Izvestija na geologicheskija Institut, Serija Paleontologija* 18, 71-81.

Parona, C. F. 1900. Sopra alcune rudiste senoniane dell'Appennino meridionale. *Memorie dell'Accademia delle Scienze di Torino, Classe di Scienze fisiche, matematiche e naturali* 50, 1-23.

Plenićar, M. 1993. *Radiolites* from the Cretaceous beds of Stranice near Slovenske Konjice (Slovenia). *Slovenska Akademija Znanosti in Umetnosti, Razred za naravoslovne Vede, Razprave* 34, 45-103.

Pons, J.M. 1977. Estudio estratigráfico y paleontológico de los yacimientos de rudistidos del Cretácico sup. del Prepirineo de la Prov. de Lerida. *Universidad Autónoma de Barcelona, Publicaciones de Geología* 3, 105 p.

Pons, J.M., Sirna, G. 1994. Revision of *Hippurites cornucopiae* Defrance and proposal of a neotype. Matteucci, R. et al. (Ed.), Studies on ecology and paleoecology of benthic communities, *Bollettino della Società paleontologica italiana* Spec. Vol. 2, 269-278.

Pons, J. M., Vicens, E. 2006. Field Guide to Pyrenean Rudist Bivalves, International Congress on Bivalvia July 22-26. 2006, Barcelona, Organism Diversity and Evolution 6. *Electronic Supplement 16* part 3, 1-18.

Pons, J. M., Vicens, E. 2008. The structure of the outer shell layer in radiolitid rudists, a morphoconstructional approach. *Lethaia* 41, 219-234.

Pons, J.M., Schroeder, J.H., Höfling, R., Moussavian, E. 1992. Upper Cretaceous rudist assemblages in northern Somalia. *Geologica Romana* 28, 219–241.

Sadiq, D. M. 2009. Facies analysis of Aqra Formation in Chwarta-Mawat Area from Kurdistan Region, NE−Iraq. MSc thesis, College of Science, University of Sulaimani, 98 p. (unpublished).

Sharbazheri, K. M. I. 2008. Biostratigraphy and paleoecology of Cretaceous/Tertiary boundary in the Sulaimani region, Kurdistan, NE-Iraq. Phd thesis, College of Science, University of Sulaimani, 122 p. (unpublished).

Schlüter, M. 2008. Late Cretaceous (Campanian-Maastrichtian) rudist-bearing carbonate platforms of the Mediterranean Tethys and the Arabian plate. Phd Thesis, Fakultät für Geowissenschaften der Ruhr-Universität Bochum, 99 p.

Schlüter, M., Steuber, T., Parente, M., Mutterlose, J. 2008. Evolution of Maastrichtian-Paleocene tropical shallow-water carbonate platform (Qualhat, NE Oman). *Facies* 54, 513-527.

Schumann, D. 1995. Upper Cretaceous rudists and stromatoporoid associations of central Oman (Arabian Peninsula). *Facies* 32, 189-202.

Schumann, D. 2010. The morphology and function of the upper valve of *Vaccinites vesiculosus* (Woodward). Özer, S., Sarı, B., Skelton, P. W. (Ed.). Jurassic-Cretaceous Rudists and Carbonate Platforms, Part (B), 8th International Rudist Congress. *Turkish Journal of Earth Sciences* 19, 6, 791–798.

Simonpietri, G., Philip, J., Platel, J.-P., 1998. Etude statistique des espèces du genre *Vaccinites* (Hippuritacea, Hippuritidae) du Campanien du Sultanat d'Oman. Masse, J.-P., Skelton, P.W. (Ed.).

Quatrième Congrès International sur les Rudistes. *Geobios* Mémoire spécial, 22, 313–329.

Skelton, P. W. 2013. Rudist classification for the revised Bivalvia volumes of the 'Treatise on Invertebrate Paleontology'. *Carribean Journal of Earth Science* 45, 9-33.

Skelton P.W., Wright, V.P. 1987. A Caribbean rudist bivalve in Oman: island hopping across the Pacific in the Late Cretaceous. *Palaeontology* 30, 505–529.

Skelton, P.W., El-Asa'ad, G. M. A. 1992. A new canaliculate rudist bivalve from the Aruma Formation of central Saudi Arabia. *Geologica romana* 28, 105-117.

Skelton, P.W., Smith. A. B. 2000. A preliminary phylogeny of rudist bivalves: sifting clades from grades. Harper, E.M., Taylor, J.D., Crame, J.A. (Ed.). The evolutionary biology of the Bivalvia. *Geological Society, London* Special Publications, 177, 97-127.

Sladić-Trifunović, M. 1972. Senonian limestones with orbitoides and rudists from Kozluk (Northeastern Serbia). *Geoloski Anali balkanskoga Poluostrva* 37, 2, 111-150.

Steuber, T. 1999. Cretaceous rudists of Boeotia, central Greece. *Special Papers in Palaeontology* 61, 229 p.

Steuber, T. 2002. A palaeontological database of Rudist Bivalves (Mollusca: Hippuritoidea,Gray1848). http://www.ruhr-uni-bochum.de/sediment/rudinet/intro.htm.

Steuber, T., Özer, S., Schlüter, M., Sarı, B. 2009. Description of *Paracaprinula syriaca* Piveteau (Hippuritoidea, Plagioptychidae) and a revised age of ophiolite obduction on the African-Arabian Plate in southeastern Turkey. *Cretaceous Research* 30, 41-48.

Steuber, T., Schlüter, M. 2012. Strontium-isotope stratigraphy of Upper Cretaceous rudist bivalves: biozones, evolutionary patterns and sea-level change calibrated to numerical ages. *Earth-Science Reviews* 114, 42-60.

Tavani, G. 1949. Rudiste ed altri Molluschi cretacei della lligiurtinia (Africa orientale). *Palaeontographia Italica* 66, 1–40.

Toucas, A. 1907. Etudes sur la classification et l'évolution des radiolitidés: *Agria* & *Praeradiolites*. *Mémoires de la Société géologique de France, Paléontologie* 36, 14, 1-46.

Toucas, A. 1908. Etudes sur la classification et l'évolution des radiolitidés: *Sphaerulites* & *Radiolites. Mémoires de la Société géologique de France, Paléontologie* 36, 16, 47-78.

Vicens, E. 1992. Estudio de la fauna de rudistas (Hippuritidae y Radiolitidae) de los materiales cretácicos del Pirineo oriental: implicaciones bioestratigráficas. Universidad Autónoma de Barcelona, Publicaciones de Geología, Phd Thesis, 255 p.

Vogel, K. 1971. On the Upper Cretaceous in east Iran and in west and north Afghanistan. *Geological Survey of Iran* Report, 20, 56-79.

Yalçın, N. 1976. Geology of the Narince-Gerger area (Adıyaman province) and its petroleum possibilities. *Revue de la Faculté des Sciences de l'Université d'İstanbul* B 41, 57-82.

Zebari, B.G.A. 2010. Sedimentology of Aqra Formation (Upper Cretaceous) in selected sections in the Kurdistan region-Iraqi. MSc thesis, Salahaddin University (unpublished). 135p.

PLATES

PLATE - I

Dictyoptychus aff. *morgani* (Douvillé).

A**-C.** Khewata section, No. Kh 2.

A**-** Both valves, ventral side. Note robuste conical, very smooth surface of the RV and very depressed LV.

B- Top view of the partly preserved LV.

C- Enlargement of the LV showing thin longitudinal radial canals (arrow) observed beneath the eroded parts of the ol.

D- Upper view of LV. Note thin ol and longitudinal radial canals (arrow) in the eroded parts. Sherawezha section, No. Sh 6.

E, F. Khewata section, No. Kh 3.

E- Both valves, anterior side. Note the dense and fine growth lamellae (arrow) in the RV. The LV is very depressed.

F- Transverse section of the RV passing too close the commissure showing the basal attachement of the myocardinal arc within the LV. Some badly preserved canals of the il can be observed.

G- Transverse section of the RV passing 10 mm below of the commissure. Sherawezha section, No. Sh 9.

H- Transverse section of the RV passing 10 mm below of the commissure. The il contains some badly preserved canals. Sherawezha section, No. Sh 10.

I- Bivalve specimen, field photograph, in life position. Note thick ol. Khewata section, No. Kh 1.

Scale indicates 10 mm.

PLATE - I

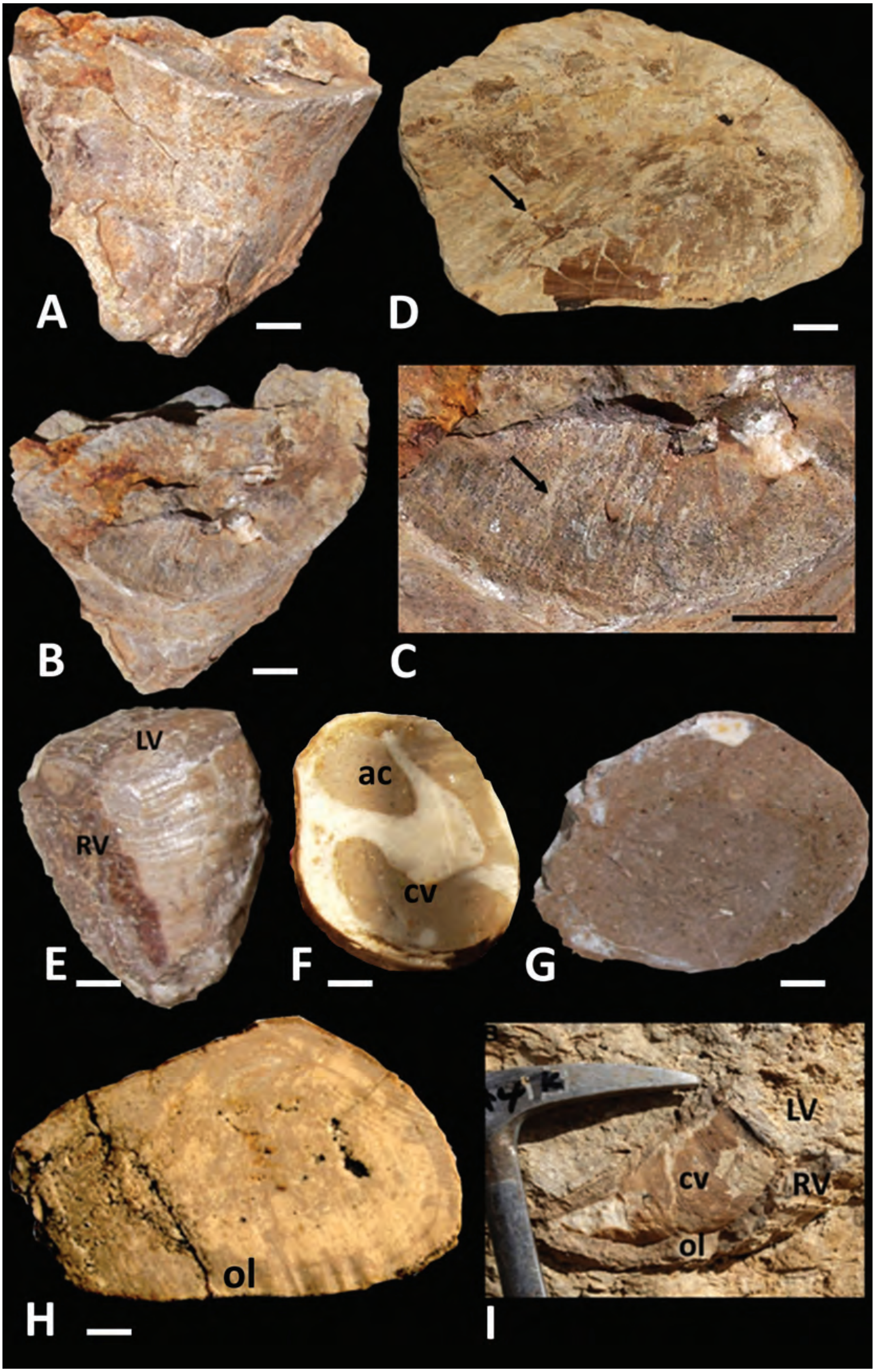

PLATE - II

Praeradiolites subtoucasi Toucas.

A-C. Sherawezha section, No. Sh 3.

A- Both valves showing two radial bands (Ab, Pb) delimited by three very pronounced longitudinal costae. Note very robust RV and flattened LV.

B- Ventral part. Note horizontal growth lamellae.

C- Transverse section of the RV passing 20 mm below of the commissure. L is present, but broken off. Note very thick op and radial bands (Ab, Pb).

D-F. Sherawezha section, No. Sh 2.

D- Both valves showing three very pronounced longitudinal costae and two radial bands (Ab, Pb). Horizontal growth lamellae are well-preserved. Note flat LV consisting of horizontal growth lamellae showing resemblance to those of RV.

E, F- Transverse sections of the RV passing 15 mm below of the commissure. Note the long L and well-preserved cardinal apparatus.

Scale indicates 10 mm.

PLATE - II

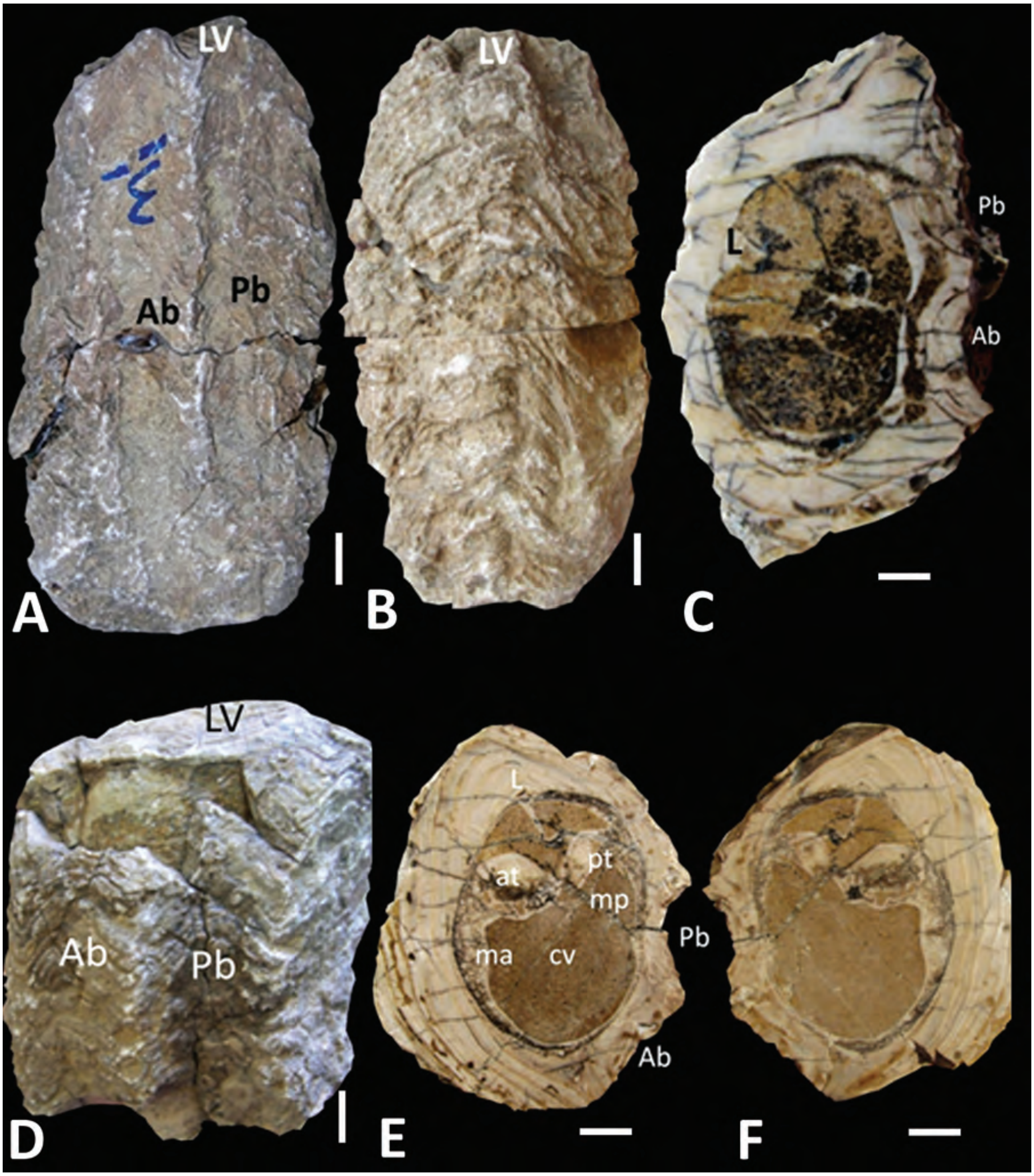

PLATE - III

Praeradiolites subtoucasi Toucas.

A-D. Sherawezha section, No. Sh 4.

A- Both valves showing two radial bands. Compare the radial bands and longitudinal costae with those of plate II, figures A and D.

B- Both valves, ventral side. Note the strong development of the growth lamellae in both valves.

C- LV, top view, growth lamellae are very well-preserved.

D- Transverse section of the RV passing 15 mm below of the commissure. The L is broken off.

E, F. Sherawezha section, No.Sh 5.

E- Both valves showing two radial bands. Note the greater length and lesser width of the RV compared with other specimens of the species.

F- Transverse section of the RV passing 10 mm below of the commissure. The L is partly preserved. Three longitudinal costae and radial bands can be well-observed.

G- Transverse section of the RV passing 10 mm below of the commissure. The L and cardinal apparatus are well-observed. Note the circular section of the valve compared with the other specimens of the species. Sherawezha section, No. Sh 7.

H. Transverse section of the RV passing 10 mm below of the commissure, juvenil form. Sherawezha section, No. Sh 8.

Scale indicates 10 mm.

PLATE - III

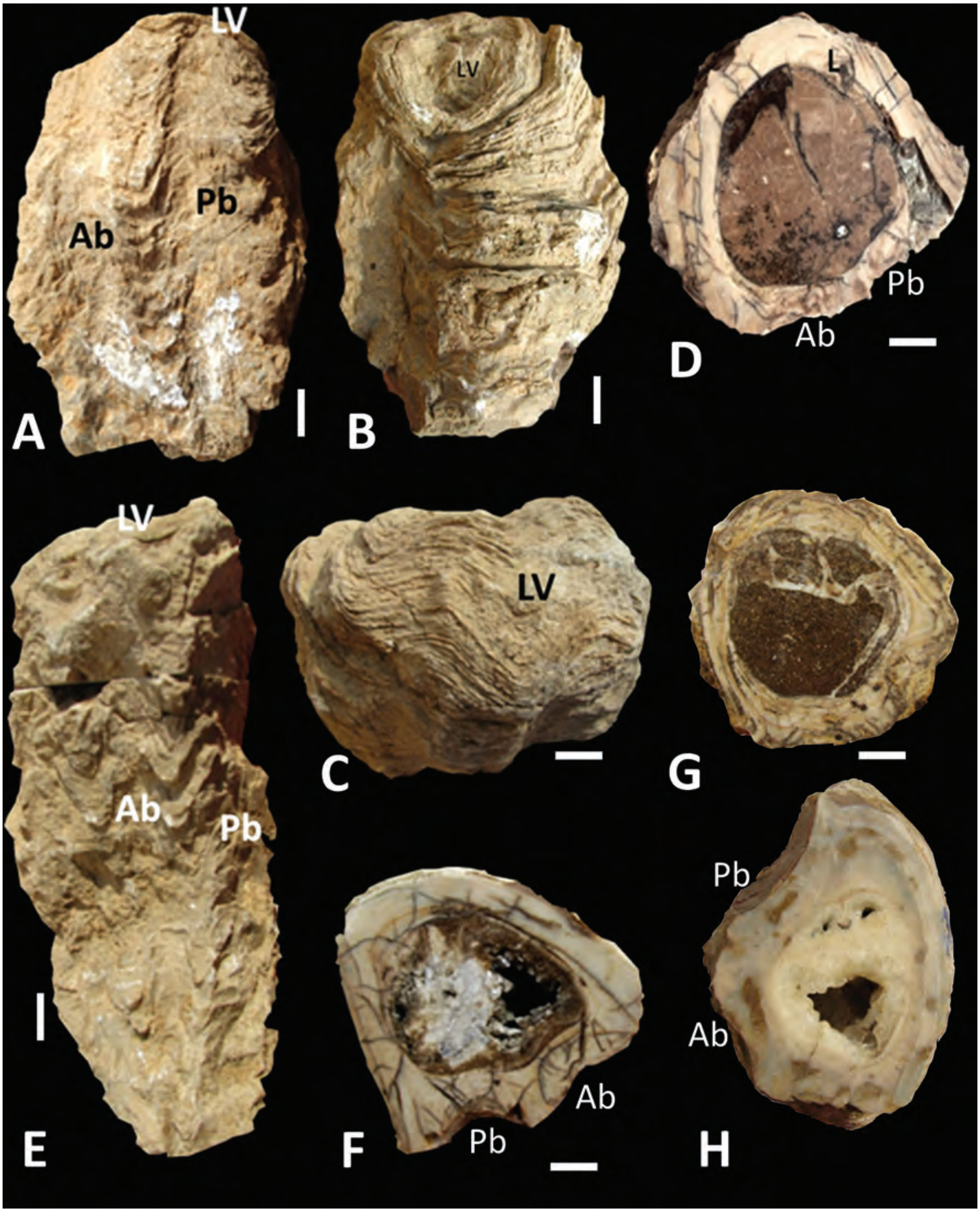

PLATE - IV

Sauvagesia somalica Tavani.

A-C. Sherawezha section, No. Sh 12.

A- Both valves showing two slightly concave radial bands limited by longitudinal costae.

B- LV, top view. Note a few orifices like sections across radial canals situated within the ol, and fusiform structures like pallial canals in the il flanking the myophores.

C- Transverse section of the RV passing 10 mm below of the commissure. Note thick op composed of very small polygonal cells in prismatic pattern.

Lapeirousia jouanneti (Des Moulins)

D-F. Sura Qalat section, No. Su 12.

D- Upper view of the RV showing the pseudopillars (Ap, Pp).

E- Enlargement of the pseudopillars showing spout-like shape. Note their demarcation by a compact layer (arrows) within the op.

F- Field photograph showing the typical outer shell layer and pseudopillars of the species. Khewata section.

G- *Hippurites cornucopiae* Defrance, from biostrome of Sura Qalat section, No. Su 1. Transeverse sections of RVs. The pillars can be clearly observed.

Scale indicates 10 mm.

PLATE - IV

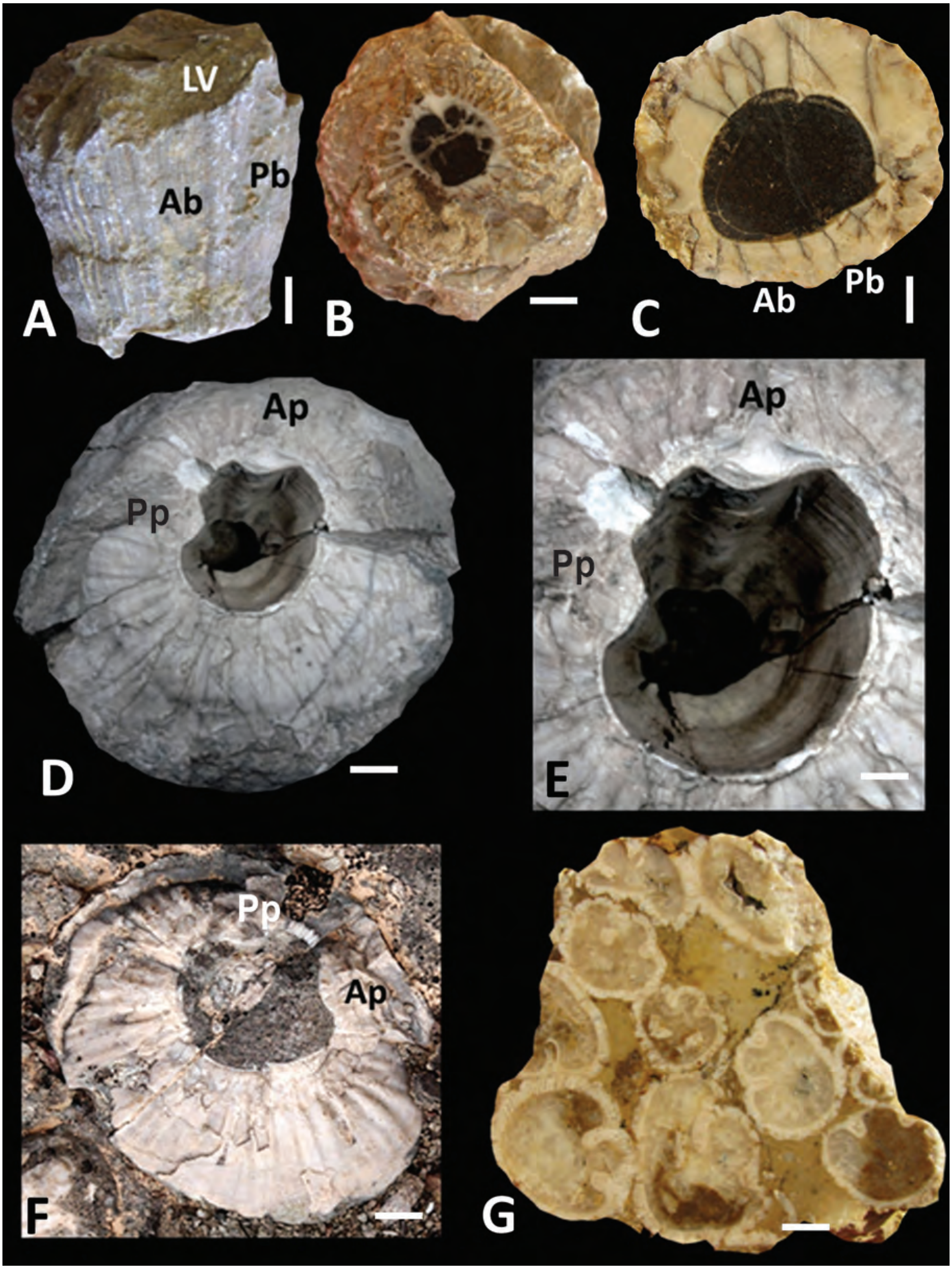

Bulletin of MTA (2013) 147: 57-71

Bulletin of the
Mineral Research and Exploration

http://bulletin.mta.gov.tr

MARINE MICRO AND MACRO FAUNAS OF HOLOCENE DEPOSITS OF ANADOLU HİSARI (ANATOLIAN CASTLE, BOSPHORUS) AND THE PRESENCE OF XANTHO PORESSA (OLIVI) (Crustacea: Decapoda: XanthIdae)

Engin MERİÇ[a], Hüsamettin BALKIS[b], Niyazi AVŞAR[c], Atike NAZİK[c] and Feyza DİNÇER[d]

[a] *Moda Hüseyin Bey Sokak No: 15/4, 34710 Kadıköy, İstanbul*
[b] *İstanbul University, Faculty of Science, Department of Biology, 34459, Vezneciler-İstanbul*
[c] *Çukurova University, Faculty of Engineering and Architecture, Department of Geological Engineering, 01330, Balcalı, Adana*
[d] *Nevşehir University, Faculty of Engineering and Architecture, Department of Geological Engineering, 50300, Nevşehir*

Keywords:
Xantho poressa (Olivi),
Anadolu Hisarı,
Küçüksu Palace,
Bosphorus, Holocene.

ABSTRACT

The presence of *Xantho poressa* (Olivi), known as the recent fossil, from Crustacea-Decapoda in Holocene deposits of Anadolu Hisarı has been revealed inthis study. This crab species is known as ranging from Mediterranean Sea to Black Sea and from Canary Islands to Portugal in Northeast Atlantic within depths of 0-15 meters in tidal and shallow subtidal environments. Remnants of broken crab shells with benthic foraminifera, ostracoda, bryozoan, pelecypoda and gastropoda were found in 78 samples which were collected from different levels of 8 of the cores taken from the basement of Küçüksu Palace at the Anadolu Hisarı. It was determined that the remnants of these crabs belonged to *Xantho poressa* (Olivi). ^{14}C value from the bottom levels of deposits of the investigation area was estimated as 6.644±48 BP. It is understood that this carp type and the other faunal assemblage reflecting the Mediterranean and Black Sea assemblages investigated in the study area had been continuing their lives within the same environmental conditions for 6.644 years.

1. Introduction

Core drillings reaching the main rock were carried out by DSİ (State Hydraulic Works) in 1982 and 1983 due to the settlements that occurred at the basement of Küçüksu Palace which was constructed in 1856 between Küçüksu and Göksu rivers in Anadolu Hisarı. In order to investigate the formation of Bosphorus, 98 samples bearing foraminifers, ostracods, byrozoans, pelecypods and gastropods taken from drills SK-1, SK-3, SK-6, PRSK-4, PRSK7, PRSK-8 and PRSK-9 made in Kuşdili Formation were investigated (Meriç et al., 1991). Only SK-6 and PRSK-7 drills were assessed together as they had some missing parts but are very close to each other as locality. Several shell fragments of the crab namely the "*Xantho poressa* (Olivi)" were encountered in 78 of the samples (Figures 1 and 2, Plate 1). The purpose of this study is to discuss reasons of the presence of *Xantho poressa* (Olivi) by means of environmental and age data. Therefore; micro and macro faunas which were observed with crabs in samples were assessed together.

2. Material And Method

H_2O_2 with a 10% concentration was added on each dry sample as weighing 10 gr for 98 samples that had been collected during drilling investigation performed by DSI between the years of 1982-1983 around Küçüksu Palace. These samples were left drying 24 hours then washed on 0.063 mm sized sieve. These

* *Corresponding author: E. MERİÇ, ienginmeric@hotmail.com, barutif@istanbul.edu.tr*

Figure 1- View of Küçüksu Palace (looking east) (www.millisaraylar.gov.tr).

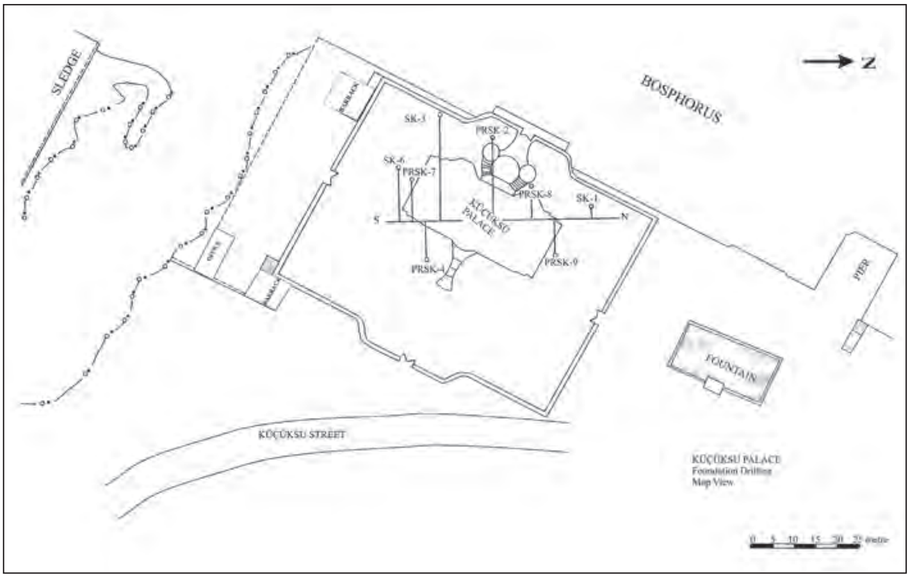

Figure 2- Map of drilling locations (from Meriç et al., 2000*b*).

samples were again dried at a temperature of 50°C and sieved on 2.00, 1.00, 0.5, 0.25 and 0.125 sized sieves. Then foraminifera, ostracoda, bryozoa, mollusk and crabs were defined studying samples under binocular microscope.

Furthermore; shells of *Modiolus* sp. from pelecypods collected from the bottom of SK-3 drill were dated as 6.644±48 years at the University of Arizona (USA) performing ^{14}C radiometric dating (Meriç and Algan, 2007) and related assessments were made using this age data.

3. Crab Findings

Xantho poressa (Olivi) mollusks were encountered in significant amounts in 78 samples collected from drill cores in the study area (SK-1, SK-3, SK-6, PRSK-2, PRSK-4, PRSK-7, PRSK-8 and PRSK-9). Within these samples there was not detected any sample belonging to the main body namely the "carapas". Crab pieces obtained are the remnants of Cheliped and pereopod forming generally the cardinals (Plate 1). The most significant characteristics of this crab for the investigation area is its presence in great amounts at places where Küçüksu and Göksu rivers reach the sea during 6.644 years between the meters of 24.90 and 3.90 within approximately 25 meters thick sedimentary deposit (Figure 3).

So far, there have not been obtained any data related to this crab at northern and southern marine drillings in Bosphorus, in Holocene Kuşdili formation during on land drillings in Kuşdili paddock and in Dilovası at Anatolian side, in Ayamama River at Rumeli side, in Holocene Kuşdili formation obtained at land drillings in Bakırköy and within sedimentary deposits obtained from marine drillings which belong to the Holocene of Haliç (Estuary) and in İzmit Bays (Meriç, 1990; Meriç et al., 1991*a* and *b*; Meriç, 1995; Meriç et al., 1998*a* and *b*; 2000*a*; 2003; Şafak et al., 1999; Meriç and Algan, 2007).

Xantho poressa (Olivi) is a widely observed crab type on shallow areas at depths not deeper than 0.1 and 0.30 meters along shores of Atlantic Ocean and Mediterranean shores of the countries such as; Turkey, Spain, Greece and Israel (Gonzalez-Gordillo et al., 1990; D'Udekem D'Acoz, 1999; Reuschel and Schubart, 2007, Spivak et al., 2010). Nowadays; it represents a wide distribution along the shores of Mediterranean (Holthuis, 1961; Kocataş, 1981; Kocataş and Katağan, 2003), the shores of Aegean (Kocataş, 1971; Ergen et al., 1988, Balkıs et al., 2001, 2002; Kocataş and Katağan, 2003), along the straits of Turkey (Heller, 1863; Ostroumoff, 1896; Ninni, 1923; Holthuis and Göttlieb, 1958; Holthuis, 1961; Caspers, 1968; Kocataş, 1981; Müller, 1986, Okuş, 1989, Balkıs, 1994; Balkıs et al., 2002; Kocataş and Katağan, 2003; Yurdabak, 2004; Çelik et al., 2007) and along the Black Sea coasts (Holthuis, 1961) (Figure 4).

This species was observed generally between the depths of 0.1-5 meters, on rocky surfaces and pebbles, on pier pillars, on rock surfaces covered with algae, on stony and sandy floors, on meadows of Posidonia, sometimes in regions where salinity is low, on stony areas with mussel and in regions full of mussels, in sandy and muddy areas which its depth reaches down to 30 meters (Holthuis and Göttlieb, 1958; Holthuis 1961; Kocataş, 1971; Ramadan and Dowidar, 1972; Kattoulas and Koukouras, 1975; Lewinshorn and Holthuis, 1986; Ergen et al., 1988; Balkıs, 1994; Petrescu and Balaşescu, 1995; Kevrekidis and Galil, 2003; Yurdabak, 2004; Bilgin and Çelik, 2004; Çelik et al., 2007; Özcan, 2007).

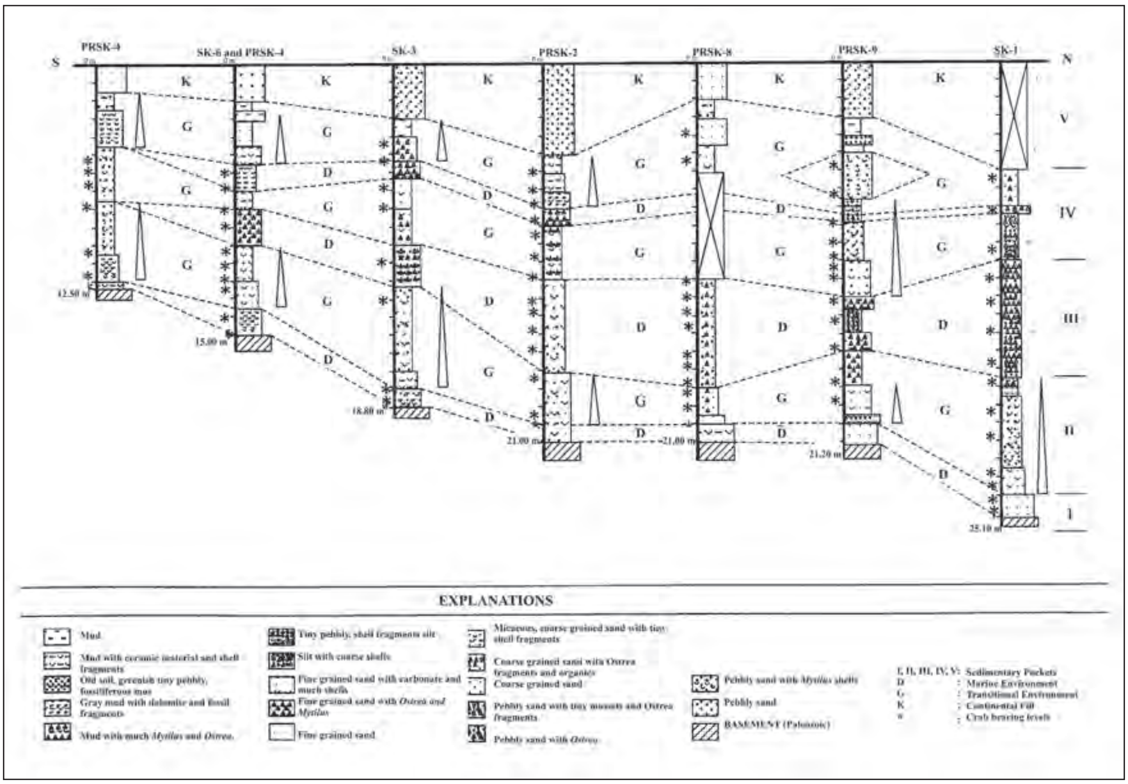

Figure 3- Lithofacies assemblages of Küçüksu Palace drillings (Anadolu Hisarı) and levels of Xanto poressa (Olivi) (modified from Meriç et al., 2000*b*).

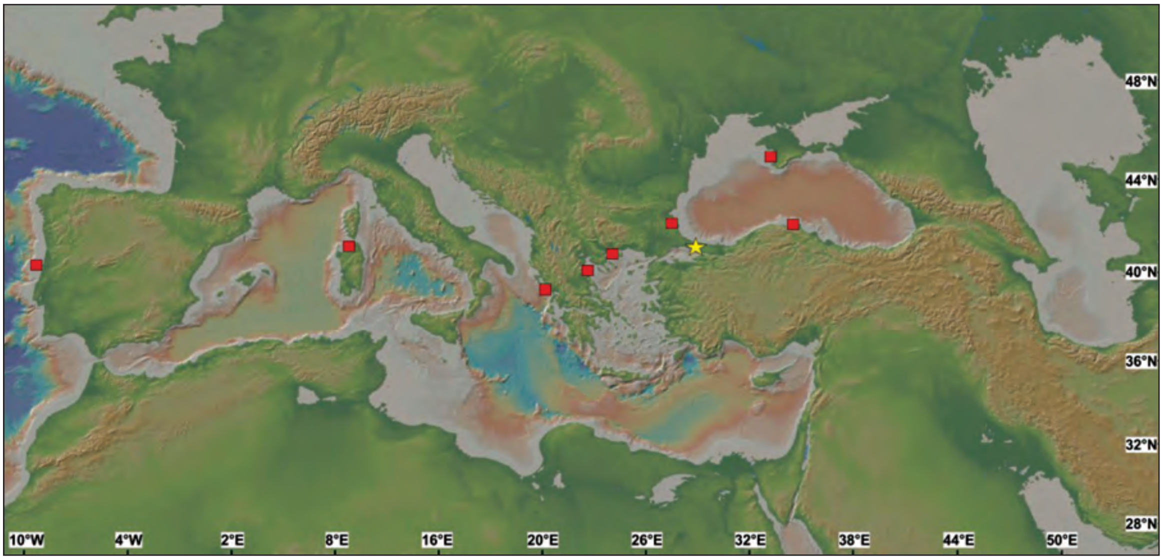

Figure 4- Distribution of Xanto poressa (Olivi) along Turkish coasts and in Mediterranean.

4. Micro and Macro Fauna Observed With *Xantho Poressa* (Olivi)

4.1. Foraminifers

Total of 31 genera and 52 species were detected in 78 of 98 samples as foraminiferal assemblage in the deposit. These were described as; *Spiroplectinella sagittula* (d'Orbigny), *Textularia bocki* Höglund, *T.* cf. *pala* Czjzek, *T. sagittula* Defrance, *T. truncata* Höglund, *Spirillina vivipara* Ehrenberg, *Lachlanella undulata* (d'Orbigny), *Massilina secans* (d'Orbigny), *Quinqueloculina laevigata* d'Orbigny, *Q. lamarckiana* d'Orbigny, *Q. seminula* (Linné), *Miliolinella elongata* Kruit, *M. labiosa* (d'Orbigny), *M. subrotunda* Montagu, *Pseudotriloculina laevigata* (d'Orbigny), *Triloculina marioni* Schlumberger, *T. plicata* Terquem, *Dentalina inornata* d'Orbigny, *Polymorphina* sp., *Globigerina bulloides bulloides* d'Orbigny, *Globigerinoides ruber* (d'Orbigny), *G. seigliei* Bermudez ve Bolli, *Cassidulina carinata* Silvestri, *Bulimina elongata* d'Orbigny, *B. marginata* d'Orbigny, *Stomatorbina concentrica* (Parker and Jones), *Rosalina bradyi* Cushman, *R. floridensis* (Cushman), *R. globularis* d'Orbigny, *Cibicides advenum* (d'Orbigny), *C. floridanus* (Cushman), *Cibicidina walli* Bandy, *Lobatula lobatula* (Walker and Jacob), *Planorbulina mediterranensis* d'Orbigny, *Acervulina* cf. *inhaerens* Schultz, *Sphaerogypsina globula* (Reuss), *Nonionella* sp., *Astrononion stelligerum* (d'Orbigny), *Aubignyna perlucida* (Heron-Allen and Earland), *Ammonia ammoniformis* Colom, *A. compacta* Hofker, *A. parkinsonmiana* (d'Orbigny), *A. tepida* Cushman, *Cribroelphidium poeyanum* (d'Orbigny), *Porosononion subgranosum* (Egger), *Haynesina anglica* (Murray), *H. depressula* (Walker and Jacob), *Elphidium aculeatum* (d'Orbigny), *E. advenum* (Cushman), *E. complanatum* (d'Orbigny), *E. crispum* (Linné), *E. jenseni* (Cushman), *E.* cf. *limbatum* (Chapman), *E. macellum* (Fichtel and Moll) and most of them are Mediterranean genera and species in origin (Meriç et al., 2000b) (Plates 2 and 3).

4.2. Ostracods

Total of 40 species belonging to 24 genera was described as Ostracod assemblage. *Cytherella* sp., *Bairdia corpulenta* G.W. Müller, *B. longevaginata* G.W. Müller, *Microcytherura* sp., *Leptocythere bisulcata* Stancheva, *L. castanea* Sars, *L. levis* G.W. Müller, *L. pellucida* Baird, *L. rara* G.W. Müller, *L. rastrifera* Ruggieri, *Callistocythere mediterranea* G.W. Müller, *C. montana* Doruk, *C. pallida* G.W. Müller, *Cyprideis sohni* Bassiouni, *C. torosa* (Jones), *Pontocythere elongata* (Brady), *Costa edwardsii* (Roemer), *Carinocythereis antiquata* (Baird), *C. carinata* Roemer, *Falunia quadridentata* (Baird), *F. rugosa* (Costa), *Falunia* sp., *Aurila convexa* (Baird), *Urocythereis favosa* Roemer, *U. margaritifera* G.W. Müller, *Tyrrhenocythere amnicola* (Sars), *T. praeazerkbairdjania* (Livantel), *Loxoconcha ancilla* Stancheva, *L. mediterranea* G.W. Müller, *L. rhomboidea* Fischer, *L. tumida* Brady, *Hirschammina* sp., *Paracytheridea depressa* (G.W. Müller), *Semicytherura acuticostata* (Sars), *S. ruggieri* G.W. Müller, *Eucytherura* sp., *Xestoleberis aurantia* (Baird), *X. communis* G.W. Müller, *X. depressa* Sars, *Paradoxostoma triste* G.W. Müller, *Sclerochilus contortus* (Norman), *Argilloecia conoidea* Sars, *Propontocypris prifera* G.W. Müller, *Candona paralella pannonica* Zalanyi, *Candona (Pseudocandona) sp., Cyclocypris sp.* were widely detected almost in all samples in drillings made (Nazik, 1998; Nazik et al., 1999; Meriç et al., 2000*b*).

4.3. Bryozoans

Crisia cf. *eburnea* (Linné), *C.* cf. *denticulata* (Lamarck), *Crisia* sp., *Electra* cf. *crustulenta* (Palas), *Conopeum seurati* (Canu), *Cryptosula pallasiana* (Moll), *Scrupocellaria scruposa* (Linné) were detected in 60 samples obtained from drillings as the assemblage of Bryzoans (Meriç et al., 2000*b*) and these indicate that Mediterranean Sea affected this area 6.6644 years ago.

4.4. Mollusks

The presence of *Modiolus (M.)* cf. *adriaticus* (Lamarck), *Mytilaster lineatus* (Linné), *Cerastoderma edule* (Linné), *C. edule lamarcki* (Reeve), *Ostrea (O.) edulis* (Linné), *Dreissena polymorpha* (Palas), *D. polymorpha pontocaspia* (Andrussow), *Lentidium (L.) mediterranea* (Costa), *Paphia (P.) rugata* (B.D.D.), *P. (P.) rugata proclivis* (Milaschevitsch), *Polymesada (P.) coroliniana* (Basc), *Chlamys (C.) varia* (Linné), *Spisula (S.) subtruncata triangula* (Reiner) from pelecypods; and *Hydrobia (H.) acuta* (Draparnaud), *Pseudamnicola (P.) anatina* (Draparnaud), *Assiminea (M.) francesi* (Gray), *Bittium (B.) reticulatum* (Da Costa), *Trochus (C.) tiaratus* (Qway and Gaimard), *T. (T.) moculatus* (Linné), *Tegula (T.) pellisserpentis* (Wood), *Gibbula (G.) adansoni* (Payradeau), *Cittarium pica* (Linné), *Hinia (H.) reticulata* (Linné) from gastropods that belong to mollusk group were observed in 81 samples studied (Meriç et al., 2000*b*).

5. Results

The presence of *Xantho Poressa* (Olivi) in the Sea of Marmara, the fauna in which this species lived, the environmental and age determinations were assessed in this study. Environmental characteristics according to foraminifers, ostracods, bryzoans and mollusks which were observed with the species studied can be interpreted as follows.

When foraminiferal fauna of the samples belonging to drills made around Küçüksu Palace was studied, it was clearly observed that there had been a distinct change in environmental conditions from bottom to top. Despite the presence of two marine stages both at bottom and top, there was observed a transitional period and the dominancy of continental facies at the topmost layer (Figure 3) (Meriç et al., 2000*b*). Among ostracods; *Tyrrhenocythere* and *Cyprideis* indicate the brackish water environment, *Xestoleberis* and *Loxoconcha* indicate the transitional environment of brackish-marine waters; and *Aurila, Callistocythere, Pontocythere* and *Paradoxostoma* indicate a marine environment. Ostrocod assemblage is rich in terms of both genus and species diversity, and findings obtained in the sequence approve the presence of a marine – brackish – marine transitional environment in the region which is called as Göksu Paddock in recent (Figure 3) (Nazik, 1998; Nazik et al., 1999; Meriç et al., 2000*b*). When the fauna of Bryozoan was taken into consideration, it was seen that this assemblage was Atlantic in origin and there was an environment of which the salinity ratio had sometimes changed in this area during Holocene time (Meriç et al., 2000*b*). *Dreissena* sp. in pelecypods as the fauna of mollusk characterizes the freshwater environment. This genus which is present in upper levels of the sequence in SK-3 and PRSK-2 drills indicates the presence of an alluvial flow towards the study area. However; the other genera and species typically symbolize the marine environment (Meriç et al., 2000*b*).

All these faunal data indicate that very shallow and transitional environments alternatively developed for the investigated area. Therefore; it is understood that the crab mentioned was observed at different levels of the Holocene deposit as a result of rework, biological cycle and changes in water level. It was detected that the age was detected as 6.644±48 years as a result of radiometric dating (^{14}C) obtained from the bottom of the sequence and the waters of the Mediterranean Sea had been affective in the region since that time. According to the sedimantological findings, the sea level changes were detected twice and it was determined that marine fauna and brackish water types were dominant when the sea level increased and decreased, respectively (Meriç et al., 2000*b*).

Xantho poressa (Olivi) is known as a crab type which lives between the depths of 1.00 and 23.00 meters, at a salinity of ‰19-29 and at a temperature of 6-24°C in the Sea of Marmara (Balkıs, 1994). It is clearly understood that this species has continued its life time by adopting itself to varying living condition 6.644 years long in the area where Küçüksu and Göksu rivers reach the sea.

As mentioned above, the presence of this species was not encountered in studies made in Holocene sediments in Istanbul and in its close vicinity. For this crab to be represented with many individuals only in Anadolu Hisarı and around Küçüksu Palace makes us consider that the environmental conditions were different for crabs. There has not been any thermal source which is considered to have affected environmental conditions during 6.6444 years in and around the study area. If there had been a thermal source then, as foraminifers being the first, it would have an effect on all faunas as it had been detected in Haliç (estuary) (Meriç et al., 2003; Suner et al., 2012). As a result; it is considered that the effect of currents in this area in Istanbul Strait have decreased and crabs have continued their lives in places where feeding opportunities are great and accordingly they have increased their population in a still environment.

Received: 19.02.2013
Accepted: 20.06.2013
Published: December 2013

References

Balkıs, H. 1994. Crabs in the Sea of Marmara. *İstanbul University Journal of Biyology*, 57, 71-111 pp.

Balkıs, H., Balkıs, N., Altınsaçlı, S. 2001. The crab species found on the coasts of Gökçeada (Imbroz) Island in the Aegean Sea. *Hydrobiologia*, 449, 99-103 pp.

Balkıs, N., Albayrak, S., Balkıs, H. 2002. Check list of the crustacea fauna of the Bosphorus. *Turkish Journal of Marine Sciences*, 8, 157-164 pp.

Bilgin, S., Çelik, E. Ş. 2004. Karadeniz'in Sinop kıyıları (Türkiye) yengeçleri. *Fırat Üniversitesi Fen ve Mühendislik Bilimleri Dergisi*, 16 (2), 337-345 pp.

Caspers, H. 1968. La macrofaune benthique du Bosphore et les problémes de l'infiltration des éléments méditerranéens dans la Mer Noire. *Rapport de la Commission Internationale pour l'Exploration Scientifique de la Mer Méditerranée*, 19 (2), 107-115 pp.

Çelik, E. Ş., Ateş, A. S., Akbulut, M. 2007. A survey on the Brachyura (Decapoda) in the Dardanelles. *Turkish Journal of Zoologie*, 31, 181-183 pp.

D'Udekem D'Acoz C. 1999 Inventaire et distribution des crustacés décapodes de l'Atlantique nord-oriental, de la Méditerranée et des eaux continentales adjacentes au nord de 258N. Collection Patrimoines Naturels. *Muséum National d'Histoire Naturelle*, Paris, France 40, 383 pp.

Ergen, Z., Kocataş, A., Katağan, T., Önen, M. 1988. The distribution of Polychaaeta and crustacea fauna found *Posidonia oceanica* meadows of Aegean coast of Turkey. *Rapport de la Commission Internationale pour l'Exploration Scientifique de la Mer Méditerranée*, 31 (2), 25 p.

Gonza´lez-Gordillo J.I., Cuesta J.A., Pablos F. 1990. Adiciones al conocimiento de los crusta´ceos deca´podos de las zonas mediolitoral e infralitoral de las costas suratla´nticas andaluzas (Suroeste Espan˜a). I Brachyura. *Cahiers de Biologie Marine* 31, 417–429 pp.

Heler, C. 1863. Die crustaceen des südlichen Europa. Crustacea Podophtalmia. 336 p, Wilhelm Braumüller, Wien.

Holthuis, L.B., Göttlieb, E. 1958. An annotated list of the decapod Crustacea of the Mediterranean coast of Israel, with an appendix listing the Decapoda of the eastern Mediterranean. *Bulletin of the Research Council of Israel, B, Zoology*, 7B (1-2), 1-126.

Holthuis, L. B. 1961. Report on a collection of Crustacea Decapoda and Stomatopoda from Turkey and the Balkans. *Zoologische verhandelingen / uitgegeven door het Rijksmuseum van Natuurlijke Historie te Leiden*, 47, 1-67 pp.

Kattoulas, M., Koukouras, A. 1975. Benthic fauna of the Evvoia coast and Evvoia Gulf. VI. Brachyura (Crustacea, Decapoda). Scientific Annals Faculty of Physics and Mathematics, University of Thessaloniki, 15, 291-312 pp.

Kevrekidis, K., Galil, B. S. 2003. Decapoda and Stomatopoda (Crustacea) of Rodos Island (Greece) and the erythrean expansion NW of the Levantaine Sea. *Mediterranean Marine Science*, 4 (1), 57-66 pp.

Kocataş, A. 1971. İzmir Körfezi ve civarı yengeçlerinin "Brachyura" taksonomisi ve ekolojisi üzerine araştırmalar. Doktora Tezi, Ege Üniversitesi, 115 p., İzmir.

Kocataş, A. 1981. Liste preliminaire et répartition des crustacés décapodes des eaux turques. *Rapport de la Commission Internationale pour l'Exploration Scientifique de la Mer Méditerranée*, 27 (2), 161-162 pp.

Kocataş, A., Katağan, T. 2003. The decapod crustacean fauna of the Turkish seas. *Zoology in Middle East*, 29, 63-74 pp.

Lewinsohn, Ch., Houlthuis, L.B. 1986. The Crustacea Decapoda of Cyprus. *Zoologische verhandelingen / uitgegeven door het Rijksmuseum van Natuurlijke Historie te Leiden*, 230 (12), 1-64 pp.

Meriç, E. 1990. İstanbul Boğazı güneyi ve Haliç'in Kuvaterner (Holosen) dip tortulları (Ed. E. Meriç), 114 p., İstanbul.

Meriç, E., Oktay, F. Y., Sakınç, M., Gülen, D., Ediger, V. S., Meriç, N., Özdoğan, M. 1991*a*. Kuşdili (Kadıköy-İstanbul) Kuvaterner'inin sedimanter jeolojisi ve paleoekolojisi. *Cumhuriyet Üniversitesi Mühendislik Fakültesi Dergisi, Seri A, Yerbilimleri*, 8 (1), 83-91 pp., Sivas.

Meriç, E., Oktay, F. Y., Sakınç, M., Gülen, D., İnal, A. 1991*b*. Ayamama (Bakırköy-İstanbul) Kuvaterner istifinin sedimanter jeolojisi ve paleoekolojisi. *Cumhuriyet Üniversitesi Mühendislik Fakültesi Dergisi, Seri A, Yerbilimleri*, 8 (1), 93-100 pp., Sivas.

Meriç, E. 1995. İzmit Körfezi Kuvaterner istifin (Ed. E. Meriç), 355 p., İstanbul.

Meriç, E., Kerey, E., Avşar, N., Tunoğlu, C., Taner, G., Kapan-Yeşilyurt, S., Ünsal, İ., Rosso, A. 1998*a*. İstanbul Boğazı yolu ile Marmara Denizi-Karadeniz bağlantısı hakkında yeni bulgular. *Sualtı Bilim ve Teknolojisi Toplantısı (SBT) Proceedings*, 82-97 pp., Çapa-İstanbul.

Meriç, E., Kerey, İ. E., Avşar, N., Nazik, A. 1998*b*. Dilovası (Gebze-Kocaeli) Kuvaterner istifi. Çukurova Üniversitesi *Yerbilimleri (Geosound)*, 32, 199-218 pp., Adana.

Meriç, E., Kerey, İ. E., Avşar, N., Tunoğlu, C., Taner, G., Kapan-Yeşilyurt, S., Ünsal, İ., Rosso, A. 2000*a*. Geç Kuvaterner (Holosen)'de İstanbul Boğazı yolu ile Marmara Denizi-Karadeniz bağlantısı hakkında yeni bulgular. *Türkiye Jeoloji Bülteni*, 43 (1), 73-118 pp., Ankara.

Meriç, E., Kerey, İ. E., Avşar, N., Taner, G., Akgün, F., Ünsal, İ., Rosso, A., Nazik, A., Koral, H., 2000*b*. Anadolu Hisarı (Doğu Boğaziçi-İstanbul) Kuvaterneri. *Çukurova Üniversitesi Yerbilimleri* (Geosound), 36, 135-184 pp., Adana.

Meriç, E., Kerey, İ. E., Avşar, N., Tuğrul, A. B., Suner, F., Sayar, A. 2003. Haliç (İstanbul) kıyı alanlarında (Unkapanı-Azapkapı) gözlenen Holosen çökelleri hakkında yeni bulgular. *Hacettepe Üniversitesi Yerbilimleri*, 28, 9-32pp., Ankara.

Meriç, E., Algan, O. 2007. Paleoenvironments of the Marmara Sea (Turkey) coasts from paleontological and sedimentological data. *Quaternary International*, 167-168, 128-148 pp.

Müller, G.J. 1986. Review of the hitherto recorded species of Crustacea Decapoda from the Bosphorus, the Sea of Marmara and the Dardanelles. *Cercetari Marine (Institutul Roman de Cercetari Marine-Constanta)*, 19, 109-130 pp.

Nazik, A. 1998. Küçüksu Kasrı (Anadolu Hisarı-İstanbul) Kuvaterner istifinin ostrakod faunası. *Çukurova Üniversitesi Yerbilimleri (Geosound)*, 32, 127-146 pp., Adana.

Nazik, A., Meriç, E., Avşar, N. 1999. Environmental interpretation of Quaternary sediments: Küçüksu Palace (Asian side of Bosphorus, Anadolu Hisarı-Turkey). *Hacettepe Üniversitesi Yerbilimleri*, 21, 105-113 pp., Ankara.

Ninni, E. 1923. Primo contributo allo studio dei pesci e della pesca nelle acque dell'Impero Ottomano. 5. Premiate Officine Grafishe Caralo Ferrari, Venezia.

Okuş, E. 1989. Marmara Adası (Kuzey) littoralinde yapılan araştırmalar. *İstanbul Üniversitesi Deniz Bilimleri ve Coğrafya Enstitüsü Bülteni*, 6 (6), 143-166 pp.

Ostroumoff, A. 1896. Comptes-rendus des draggages et du plancton de l'expédition de *"Seljanik"*. *BULLETIN de l'Academie Imperiale des Sciences de Saint-Pétersbourg*, 5 (5), 33-92 pp.

Özcan, T. 2007. Türkiye'nin Akdeniz kıyılarında dağılım gösteren littoral dekapod (Crustacea) türleri ve biyo-ekolojik özellikleri. Doktora Tezi, Ege Üniversitesi, 328 p., İzmir.

Petrescu, I., Balasescu, A. M. 1995. Contributions to the knowledge of decapod fauna (Crustacea) from the Romanian coast of the Black Sea. *Travaux du MUSÉUM d´Histoire Naturelle "GRIGORE ANTIPA"*, 35, 99-146 pp.

Ramadan, Sh. E., Dowidar, N.M. 1972. Brachyura (Decapoda Crustacea) from the Mediterranean waters of Egypt. *Thalassia Jugoslavica*, 8 (1), 127-139 pp.

Reuschel S., Schubart C.D. 2007. Contrasting genetic diversity with phenotypic diversity in coloration and size in *Xantho poressa* (Brachyura: Xanthidae), with new results on its ecology. *Marine Ecology* 28, 296–305 pp.

Spivak, E.D., Arevalo, E., Cuesta, J.A., Gonzalez-Gordillo, J.I. 2010. Population structure and reproductive biology of the stone crab *Xantho poressa* (Crustacea: Decapoda: Xanthidae) in the 'Corrales de Rota' (south-western Spain), a human-modified intertidal fishing area. *Journal of the Marine Biological Association of the United Kingdom*, 90(2), 323–334 pp.

Suner, F., Meriç, E., Avşar, N., Önal, B. Ç., Avşar, N. 2012. Haliç (İstanbul-Kuzeybatı Türkiye) Holosen çökellerinde jips oluşumu ile bentik foraminifer ve ostrakod topluluğu ilişkisi, T*ürkiye Petrol Jeologları Derneği Bülteni*, Ankara (in print).

Şafak, Ü., Avşar, N., Meriç, E. 1999. Batı Bakırköy (İstanbul) Tersiyer çökellerinin ostrakod topluluğu. *Maden Tetkik ve Arama Dergisi*, 121, 17-31.

Yurdabak, F. 2004. Crustaceans collected in upper-infralittoral zone of the Gallipoli Peninsula, Turkey. *Pakistan Journal of Biological Sciences*, 7 (9), 1513-1517 pp.

PLATES

PLATE - I

Xanto poressa (Olivi), all photos belong to drillings of Anadolu Hisarı Küçüksu Palace.

Linear Scale: 2 mm.

1. Cheliped, upper and lower views, PRSK-2, 7.00-7.10 m.
2. Cheliped, upper and lower views, PRSK-9, 11.90-12.00 m.
3. Cheliped, upper and lower views, SK-1, 11.90-12.00 m.
4. Cheliped, upper and lower views, SK-3, 6.90-7.00 m.
5. Cheliped, upper and lower views, SK-6, 8.00-8.10 m.
6. Cheliped, upper and lower views, PRSK-9, 9.90-10.00 m.

PLATE - I

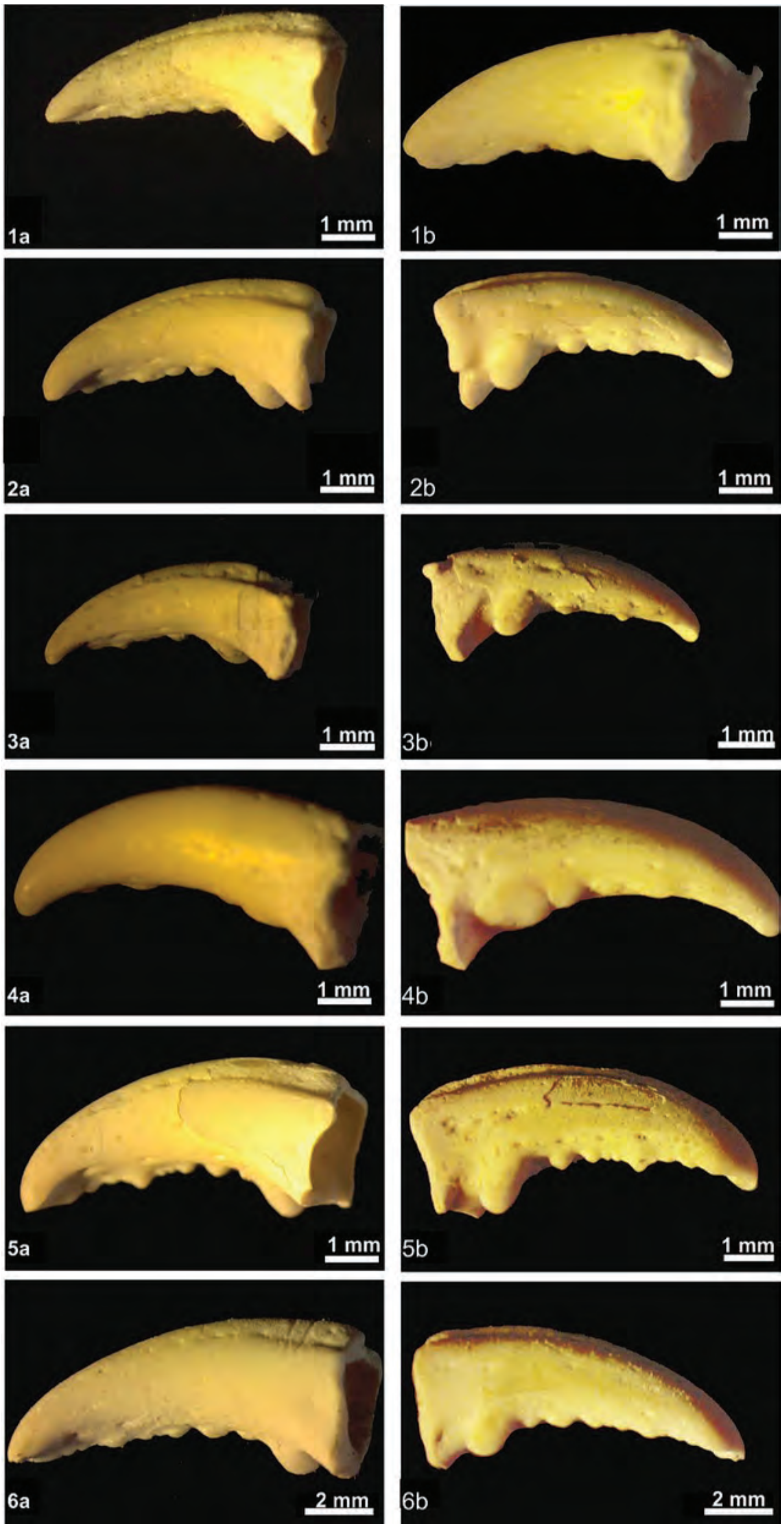
1a
1 mm
1b
1 mm
2a
1 mm
2b
1 mm
3a
1 mm
3b
1 mm
4a
1 mm
4b
1 mm
5a
1 mm
5b
1 mm
6a
2 mm
6b
2 mm

PLATE - II

All photos belong to examples of foraminifers taken from drillings of Küçüksu Palace at Anadolu Hisarı.

Linear scale: 100 µ.

1. *Spiroplectinella sagittula* (d’Orbigny). External view, SK-1, 10.40-10.50 m.
2. *Spiroplectinella sagittula* (d’Orbigny). External view, PRSK-8, 20.00-20.10 m.
3. *Textularia bocki* Höglund. External view, SK-1, 10.40-10.50 m.
4. *Textularia bocki* Höglund. External view, PRSK-8, 20.00-20.10 m.
5. *Textularia* cf. *pala* Czjzek. External view, SK-1, 23.30-23.40 m.
6. *Textularia truncata* Höglund. External view, PRSK-8, 20.00-20.10 m.
7. *Quinqueloculina seminula* (Linné). External view, SK-3, 5.40-5.50 m.
8. *Miliolinella subrotunda* Montagu. External view, PRSK-8, 20.00-20.10 m.
9. *Triloculina marioni* Schlumberger. a) external view and b) view from mouth, SK-1, 10.40-10.50 m.
10. *Triloculina marioni* Schlumberger External view, PRSK-7, 14.90-15.00 m.
11. *Bulimina elongata* d’Orbigny. External view, PRSK-7, 12.40-12.50 m.
12. *Bulimina marginata* d’Orbigny. External view, SK-3, 16.30-16.40 m.
13. *Stomatorbina concentrica* (Parker and Jones). External view, spiral side, PRSK-8, 19.00-19.10 m.
14. *Rosalina bradyi* Cushman. External view, spiral side, SK-1, 6.50-6.60 m.

PLATE - II

PLATE - III

All photos belong to examples of foraminifers detected in drillings of Küçüksu Palace at Anadolu Hisarı.

Linear scale: 100 μ.

1. *Rosalina bradyi* Cushman. a and b external views; a) spiral side and b) detailed view of periphery on sprial side, SK-3, 5.40-5.50 m.

2. *Rosalina floridensis* (Cushman). External views; a) spiral and b) umbilical sides, PRSK-8, 20.00-20.10 m.

3. *Lobatula lobatula* (Walker and Jacob). External views; a) spiral side, SK-1, 23.30-23.40 m. and b) umbilical side, PRSK-7, 14.00-14.10 m.

4. *Cibicides advenum* (d'Orbigny). External view, spiral side, PRSK-8, 20.00-20.10 m.

5. *Planorbulina mediterranensis* d'Orbigny. External view, free surface, SK-1, 10.40, 10.50 m.

6. *Ammonia ammoniforkmis* Colom. External views; a) spiral side and b) umbilical side, PRSK-14.90-15.00 m.

7. Ammonia tepida Cushman. External views; a) spiral and b) umbilical sides, SK-3, 4.40-4.50 m.

8. *Cribroelphidium poeyanum* (d'Orbigny**).** External view, SK-1, 10.40-10.50 m.

9. *Elphidium limbatum* (Chapman). External view, PRSK-8, 21.90-22.00 m.

10. *Elphidium limbatum* (Chapman). External view, PRSK-7, 14.90-15.00 m.

PLATE - III

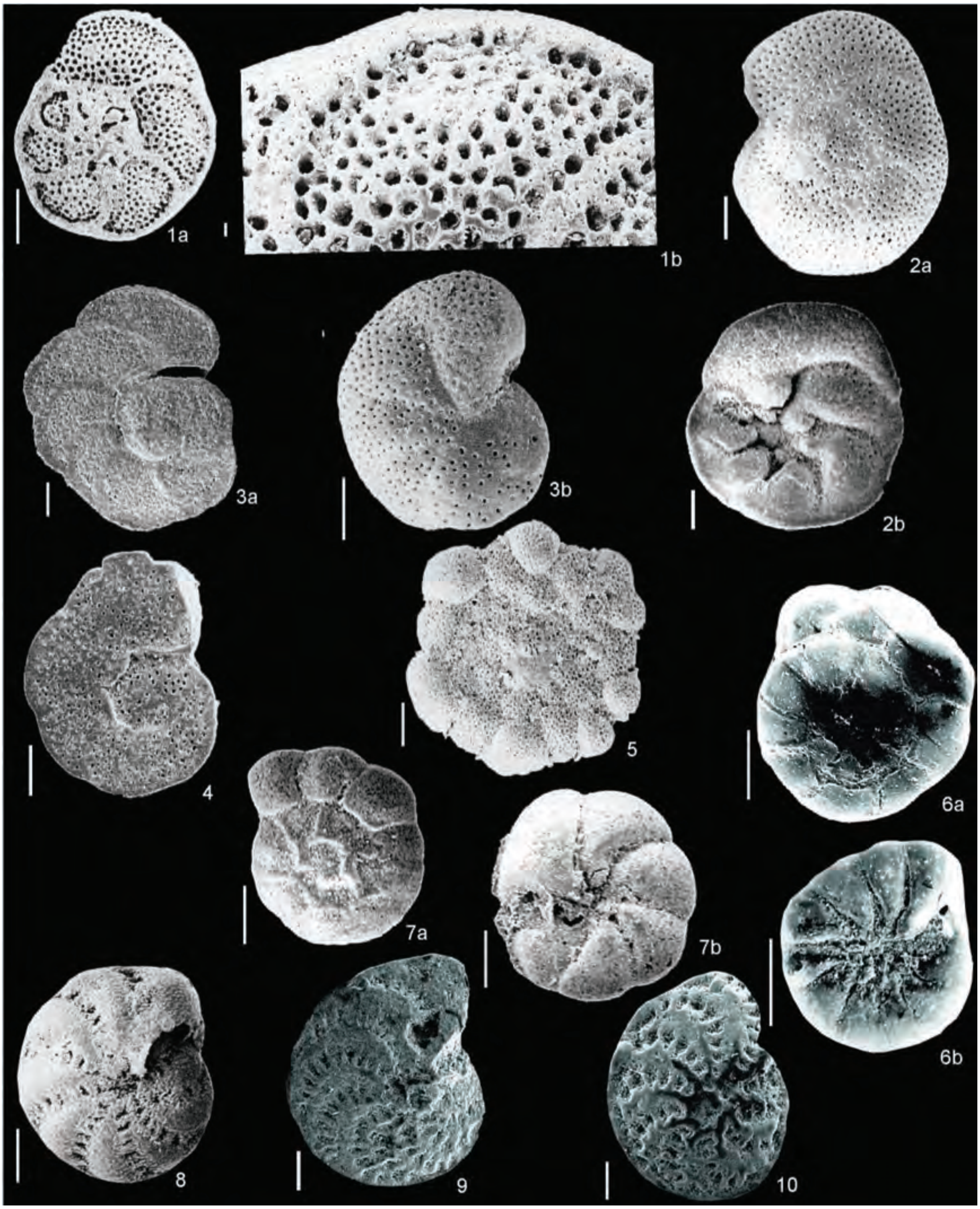

Bulletin of MTA (2013) 147: 73-89

Bulletin of the
Mineral Research and Exploration

http://bulletin.mta.gov.tr


BULLETIN OF THE
MINERAL RESEARCH AND EXPLORATION

CONTENTS

ORIGINAL FINDINGS ON THE ORE-BEARING FACIES OF VOLCANOGENIC MASSIVE SULPHIDE DEPOSITS IN THE EASTERN BLACK SEA REGION (NE TURKEY)

M.Kemal REVAN[a], Yurdal GENÇ[b], V. Valery MASLENNIKOV[c], Taner ÜNLÜ[d],
Okan DELİBAŞ[a] and Semi HAMZAÇEBİ[e]

[a] *Department of Mineral Research and Exploration, General Directorate of Mineral Research and Exploration (MTA), 06800 Ankara, Turkey*
[b] *Hacettepe University, Department of Geological Engineering, 06800 Beytepe, Ankara, Turkey*
[c] *Institute of Mineralogy, Russian Academy of Sciences, Ural Division and National Research South Ural State University, Miass, Russia*
[d] *Ankara University, Department of Geological Engineering, 06100 Tandoğan, Ankara, Turkey*
[e] *General Directorate of Mineral Research and Exploration (MTA), Trabzon Branch, Turkey*

Keywords:
Pontides, ore facies,
sulphide sandstone,
clastic ore, tube worm,
sulphide chimney

ABSTRACT

In the massive sulphide deposits of the eastern Black Sea region, there are ore facies and ore-bearing sedimentary facies. The former are subdivided into hydrothermal-metasomatic, seafloor hydrothermal, and biological facies. Hydrothermal-metasomatic facies refer to sub-seafloor processes and include network-disseminated, massive vein, and massive lens facies. The precipitation of sulphide minerals within pre-existing volcano-sedimentary rocks occurs largely beneath the seafloor, and these ores form an important component of some deposits. The term seafloor hydrothermal facies refers to sulphide accumulation on the seafloor and is characterised by hydrothermal chimneys and clastic sulphide ores. Clastic sulphide ores can be subdivided into proximal and distal facies. Ore-bearing sedimentary facies are characterised by relatively thin ferruginous chert (exhalite?) beds that occur along the uppermost part of the ore horizon. The biological facies is represented by fossil vent fauna, which are diagnostic for seafloor sulphide formation.

The VMS ores of the eastern Black Sea region have well-preserved facies characteristics, especially in terms of texture and components. Some massive sulphide deposits accumulated via molasse/mass flow on the seafloor, whereas others formed via sub-seafloor replacement processes. Clastic sulphide textures and some sedimentary structures indicate that these deposits formed in a highly active setting. Clastic sulphide textures, sulphide chimney fragments, ferruginous cherts and fossil vent fauna (tube worms) recognised in the Pontide deposits are diagnostic and support the seafloor origin of VMS deposits.

1. Introduction

The North Anatolian metallogenic belt has long been the focus of researchers due to a large number of economic, sub-economic deposits and prospects. The eastern part of this belt, referred to as the Eastern Pontides (e.g., Ketin, 1966; Yılmaz et al., 1997; Okay and Şahintürk, 1997), contains five operating volcanogenic massive sulphide (VMS) mines and is host to a number of sub-economic deposits and prospects (Figure 1). Of the many deposits and prospects in the district, only two deposits currently in production (Çayeli-Rize and Murgul-Artvin) contain significant tonnage. In addition to the known deposits, numerous volcanogenic-related alteration zones are present in the district, emphasising the possibility of hidden deposits. Porphyry-, vein- and skarn-type deposits are also present in the belt but are economically less significant than the VMS deposits. Due to their nonmetamorphosed nature, Late Cretaceous VMS deposits in the eastern Black Sea region are well-preserved in terms of their primary structures and

* *Corresponding author: M. K. REVAN, kemalrevan@gmail.com)*

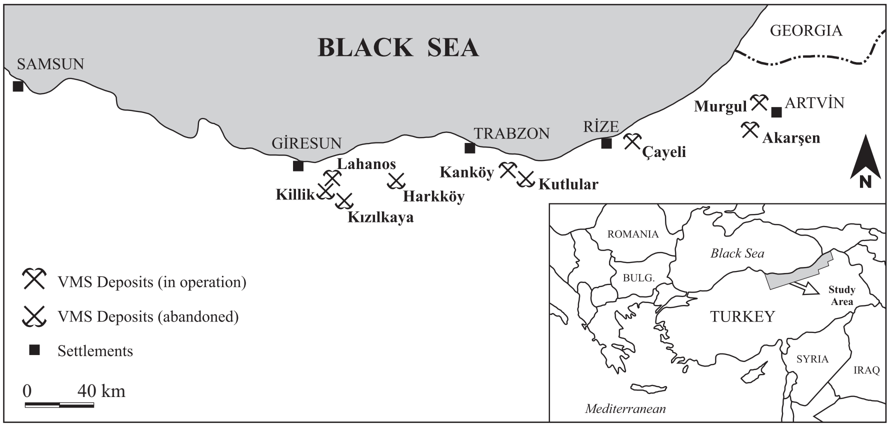

Figure 1- Site location of some major VMS deposits in the eastern Black Sea region.

textures. VMS deposits of this metallogenic province have a number of characteristics in common with Kuroko (Japan) and Uralian (Urals) deposits.

The purpose of this paper is to describe the ore and ore-bearing facies of VMS deposits in this region and to describe the environment in which the VMS deposits formed.

2. Regional Geology and VMS Deposits

The Anatolian Peninsula lies in the Alpine-Himalayan orogenic belt. Four tectonic belts trend east-west; from north to south, these are the Pontides, Anatolides, Taurides and Border Folds (Ketin, 1966). The North Anatolian tectonic belt, also known as the Pontide, has three different sectors, referred to as the western, central, and eastern Pontides (Yılmaz et al., 1997). The bimodal-felsic VMS deposits are located in the eastern Black Sea tectonic belt. The basement of the eastern Pontides is composed of the Palaeozoic metamorphics and granitic rocks that intersect these metamorphics (Schultze-Westrum, 1961). A thick volcano-sedimentary sequence ranging in ages from Palaeozoic to Quaternary overlies these basement rocks (Figure 2).

Three main magmatic periods between the Mesozoic and Tertiary were identified in the eastern Black Sea region (Okay and Şahintürk, 1997). The first period is Early to Middle Jurassic and is most likely tholeiitic in character and related to rifting. Magmatism of the Turonian-Maastrichtian, the second period, is subalkaline and related to

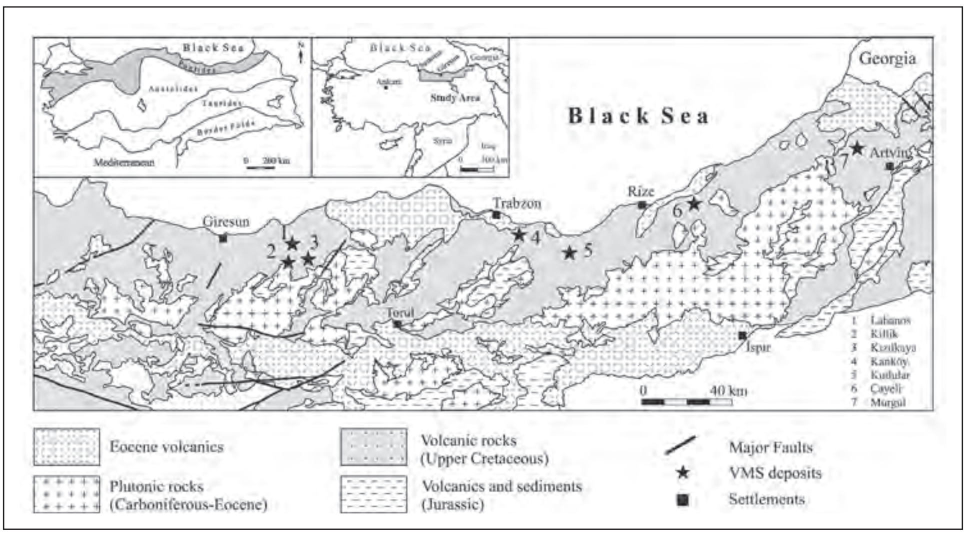

Figure 2- Site location and simplified regional geologic maps of major VMS deposits in the eastern Black Sea region. The inset shows major tectonic belts of Anatolia (from Ketin, 1966) and the location of the study area.

subduction. This Cretaceous volcanism is completely submarine, mostly subalkaline and a product of typical island arc formation (Peccerillo and Taylor, 1975; Gedikoğlu, 1978; Akın, 1979; Eğin et al., 1979; Manetti et al., 1983; Akıncı, 1984, Gedik et al., 1992). The third period, during the Middle Eocene, features calc-alkaline volcanism and is most likely related to regional extension (Adamia et al., 1977; Eğin et al., 1979; Kazmin et al., 1986; Çamur et al., 1996).

VMS deposits derived from Cretaceous bimodal volcanism are related to circular structures and fault-controlled subsidence, which developed in an island-arc setting (Tüysüz, 2000). These structure-controlled VMS deposits formed proximal to dacitic/rhyolitic domes. All massive sulphide deposits described in the eastern Black Sea belt occur in relatively thin dacitic/rhyolitic rocks and are overlain by a sequence composed of dacite, andesite, basalt, and volcano-sedimentary sequences of various thicknesses. The ore deposits are commonly located at the uppermost contact of the dacitic/rhyolitic pile or within the lowermost part of the overlying sequences (Revan, 2010).

3. Ore Facies and Facies Analyses

The geological setting of the massive sulphide deposits noticeably features ore facies and ore-bearing sedimentary facies. In the context of VMS deposits, ore facies refer to ore deposition on and/or beneath the seafloor. In this context, ore facies may be divided into four associated groups: hydrothermal-metasomatic, seafloor hydrothermal, clastic ore, and biological facies. The hydrothermal-metasomatic facies, forming a central part of the ore bodies and stockwork zones, has been investigated in detail (e.g., Yarosh, 1973; Kuroda, 1983; Eldridge et al., 1983; Buslaev et al., 1992; Gemmell and Large, 1992). The literature on hydrothermal-metasomatic facies emphasises replacement processes. Among these processes, the seafloor hydrothermal facies (hydrothermal vent chimneys), clastic ores, and biological facies are very important for understanding the sedimentation conditions in the massive sulphide paleohydrothermal fields, but these processes have not been studied sufficiently. Ore-bearing facies, including gossan, umber, jasper, and exhalites, are very special formations, reflecting seafloor alteration (halmyrolysis) within the massive sulphide paleohydrothermal fields.

3.1. Hydrothermal-metasomatic Facies (Stockwork, Massive vein and Massive lens)

Most of the VMS deposits in the eastern Black Sea region (e.g., Murgul, Kızılkaya, Çayeli, Lahanos, Kutlular, Harkköy, Killik, Pesansor, and İsraildere) are predominantly syn-volcanic accumulations of sulphide minerals that precipitated from hydrothermal fluids below the seafloor. In these deposits, hydrothermal fluids ascended along channelways formed by structural discontinuities. This resulted in the stockwork and sub-seafloor replacement ores via infiltration and precipitation in open spaces before reaching the seafloor. Ore types that formed largely sub-seafloor are primarily vein, disseminated and network type rather than massive ore bodies. These sub-seafloor zones are characterised by intense silicification and contain disseminated-network zones (Figure 3a to d), massive lenses (Figure 3e), and massive veins (Figure 3f). Discordance with the enclosing host rocks and the presence of strong host rock alteration, similar in style and intensity to footwall alteration, are diagnostic of sub-seafloor replacement.

In the Harkköy deposit, hydrothermal-metasomatic facies are represented by stockwork and possibly massive vein type mineralisations. Dacitic/rhyolitic footwall rocks, including stockwork ores, are characterised by intense silicification and sericite alteration, and the primary textures of the host rocks are unrecognisable. The thickness of ore veins (where sphalerite abundance is greater than galena) is variable and, in places, attains thicknesses of 15 cm. In the Killik deposit, the hydrothermal-metasomatic facies is represented by stockwork and a massive ore lens. A massive ore lens is nearly tabular and discordant with the enclosing host rocks. Massive pyritic ore has a completely homogeneous texture, shows no evidence for reworking of the transported ore, and does not contain any clastic components. This small massive ore body is approximately 3 m in thickness and, 10 m in length and is located approximately 700 m to the north of the main Killik orebody. In the Kızılkaya deposit, network-dissemination and massive vein type mineralisations have a large lateral and vertical extent. Massive ore veins found within footwall rocks are up to 60 cm in thickness. The massive ore veins (where pyrite abundance is greater than chalcopyrite) are discordant with the enclosing host rocks and the orientations of well-exposed ore veins are nearly vertical. In the Çayeli deposit, a well-developed stockwork sulphide zone is present beneath the stratiform massive orebody. Intense silicification occurs in the core of the stockwork zone and primary textures of this zone have been

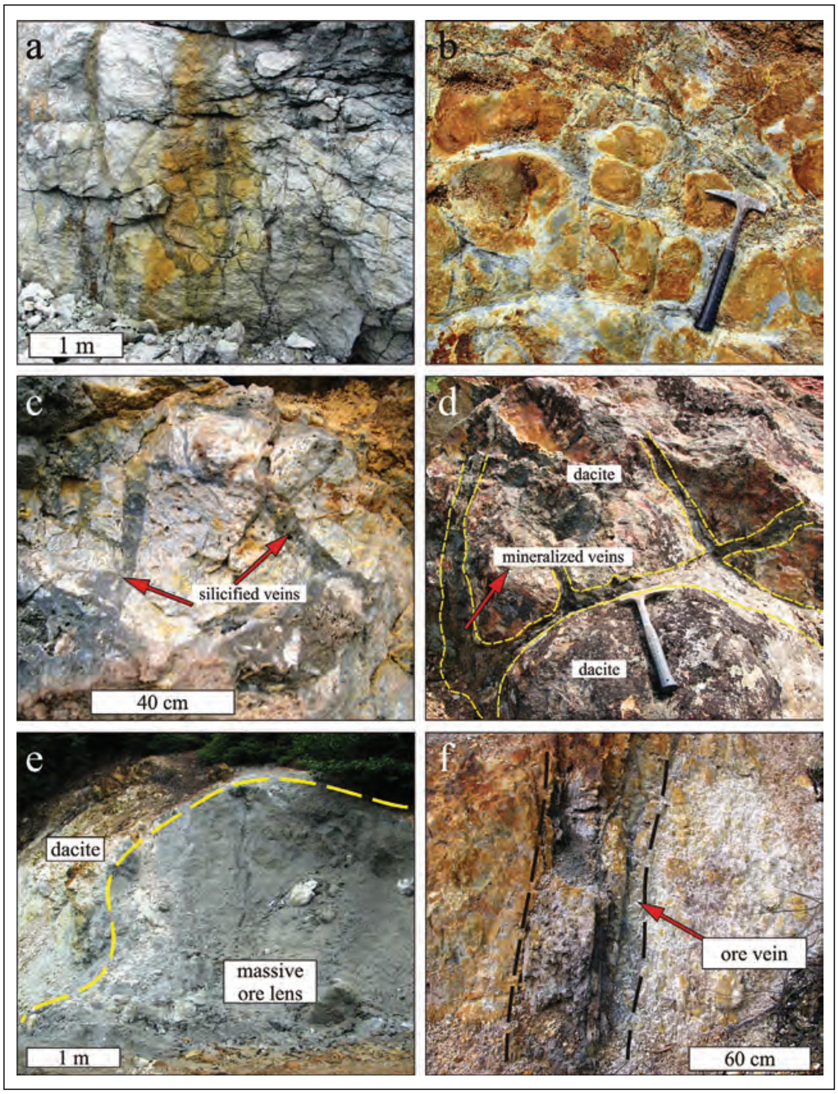

Figure 3- Examples of hydrothermal-metasomatic facies. Footwall rocks and associated stockwork zones of Murgul (a) and Lahanos (b) deposits. (c) The disseminated sulphide-bearing silicified veins in the footwall rocks of Kızılkaya deposit. (d) Stockwork mineralization of the Harkköy deposit. (e) Massive pyritic sulphide lens of the Killik deposit. (f) Sulphide vein in the footwall rocks of the Kızılkaya deposit.

altered beyond recognition. Massive mineralised veins (mainly pyrite, with minor chalcopyrite and sphalerite) up to 50 cm thick are common, especially close to the massive stratiform orebody. These thicker veins are economically mined. At Lahanos, this facies, represented by stockwork zones, has a limited lateral and vertical extent. Stockwork zones are developed below the stratiform massive ore body and characterised by intense silicification and sericite alteration. Primary textures are commonly well-preserved at some distance from the massive ore body due to progressively decreasing alteration intensity. The average thickness of mineralised sulphide veins is several centimetres, with some reaching up to 15 cm. The Murgul deposit hosts stockwork mineralisation, massive ore veins and possibly lenses. The thicknesses of these mineralised veins (pyrite-chalcopyrite) are variable and rarely reach 70-80 cm. These veins contain significant mineralisations of economic interest.

3.2. Seafloor Hydrothermal Facies: Hydrothermal Vent Chimneys

All fragments of the paleo-hydrothermal chimneys in massive sulphide deposits of the eastern

Black Sea region are found in the clastic sulphide ores (Maslennikov et al., 2009; Revan, 2010). The diameters of the mineralised chimney fragments range from a few millimetres to ~8 centimetres. The sizes of the well-preserved chimney wall fragments are variable and generally vary from a few millimetres to a few centimetres. Most well-preserved chimney fragments were collected from Çayeli deposit. These well-preserved samples are up to 8 cm (Figure 4a) and are found in a clastic sulphide matrix. The chimney fragments collected from the Killik deposit are also well-preserved (Figure 4b, c). The sizes of these fragments are up to 5 cm and are also found in a clastic sulphide matrix.

The chimney samples from the Lahanos deposit are partially well-preserved samples (Figure 4d, e), and the mineralogical zoning can be clearly observed in some samples. The well-preserved chimney fragments are 6-7 cm in diameter. The sizes of the well-preserved chimney wall fragments generally range from a few millimetres to a few centimetres. The chimney fragments were collected as clasts in sulphide-rich breccias. The hydrothermal chimney samples from Kızılkaya, Kutlular, and Akarşen deposit are not well-preserved. In the Kutlular deposit, only two partially well-preserved chimney fragments were found (Figure 4f), and chimney wall fragments

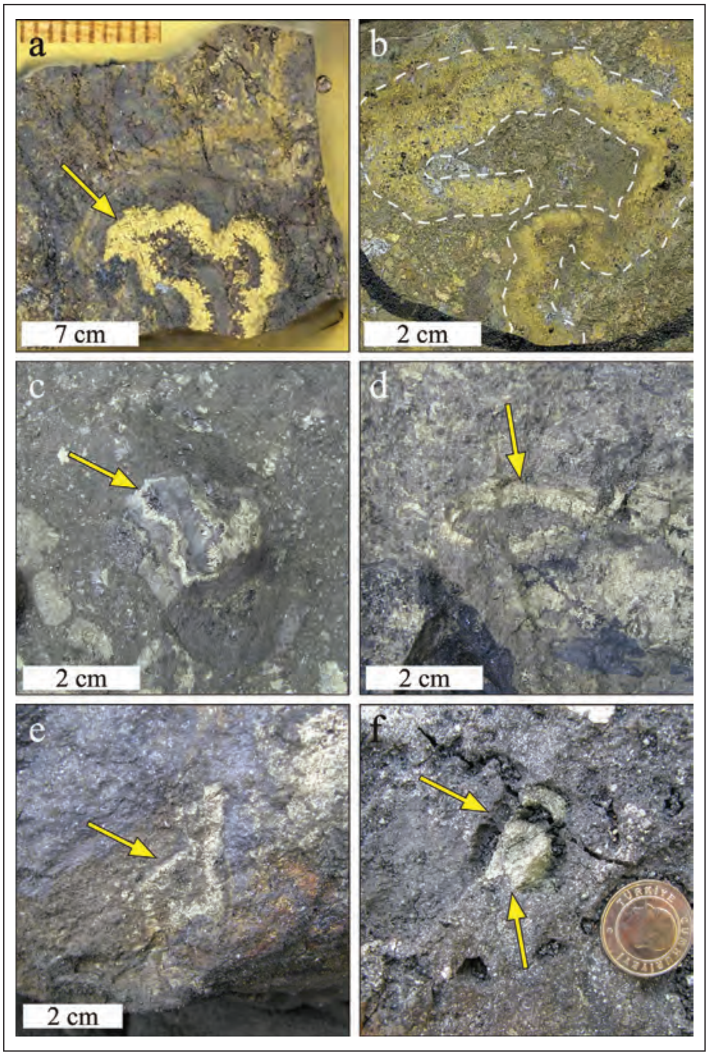

Figure 4- The seafloor hydrothermal facies of VMS deposits in the eastern Black Sea region. (a) The well-preserved sufide chimney fragment in the Çayeli orebody. (b) and (c) The well-preserved sulphide chimney fragments in the Killik orebody. (d) and (e) Sulphide chimney fragments in the Lahanos orebody. (f) Partially well-preserved sulphide chimney fragment in the Kutlular orebody.

are more abundant. The presence of concentric zones is clearly observed in a partially preserved sample.

Hydrothermal vent chimneys have concentric zones composed of Zn-, Cu- and Fe-sulphides and the well-preserved chimney fragments are clearly zoned (Figure 5). Each concentric zone is characterised by certain dominant mineral abundances. The outer zones are generally enriched in Fe- and Zn-sulphides, whereas Cu- and minor Fe-sulphides are abundant in the inner zones. Numerous examples of what appear to be chimney wall fragments have porous textures (Figure 6a). Some chimney fragments display a thin alteration rim, indicative of oxidising conditions on the seafloor (Figure 6b).

3.3. Clastic Ore Facies

Samples collected from VMS deposits (Kızılkaya, Kutlular, Çayeli, Lahanos, Killik, Kanköy, Akarşen, Kuvarshan) in the eastern Black Sea region exhibit clastic textures and are heterogeneous (Figure 7). Rounded, subhedral, and anhedral sulphide minerals with various compositions are present in the sulphide matrix. The size of individual sulphide minerals vary from micrometre to centimetre scale. Sulphide fragments are generally composed of pyrite, chalcopyrite, sphalerite, bornite, and galena. The chimney fragments and, to a lesser extent, fossil fauna fragments form the major constituents of clastic sulphide ores. Rarely, relics of the host facies (volcanic and sedimentary rock fragments) occur

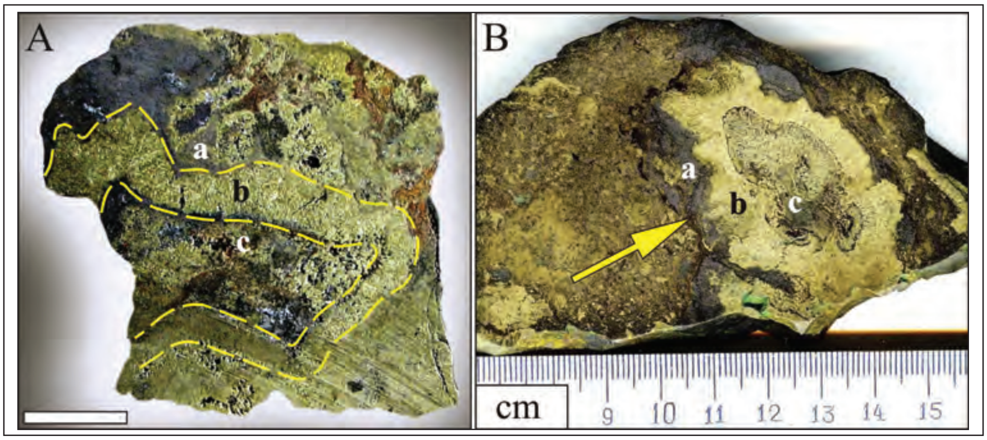

Figure 5- Mineralogical zoning in the chimney sample collected from Killik (A) and Lahanos (B) mines. Fe- and Zn-sulphide are abundant within the outer zones (a). Fe-and Cu-sulphide are abundant within the inner zones (b). The axial conduits (c) are commonly filled by barite gangue and pyrite, with minor amounts of fahlore, sphalerite, chalcopyrite, and galena. Scale bar is 2 cm in figure A.

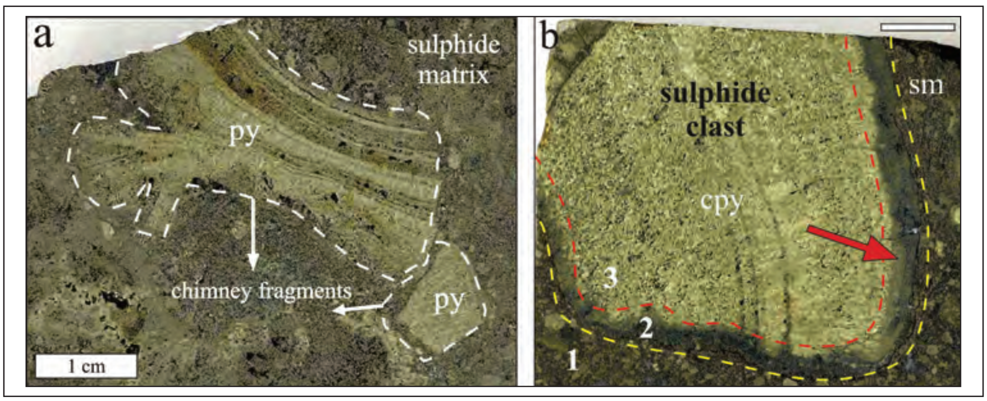

Figure 6- Examples of seafloor hydrothermal facies. (a) The subhedral, laminated cavernous chimney walls' sulphide (pyrite) fragment are up to 4 cm in size in the Lahanos mine. (b) An alteration rim around a chimney sulphide fragment (cpy) in a sulphide matrix, which is indicative of oxidizing conditions. The sample is from the Killik mine. (1 or sm: sulphide matrix, 2: alteration rim, 3: chalcopyrite fragment). Scale bar is 0.5 cm in figure b.

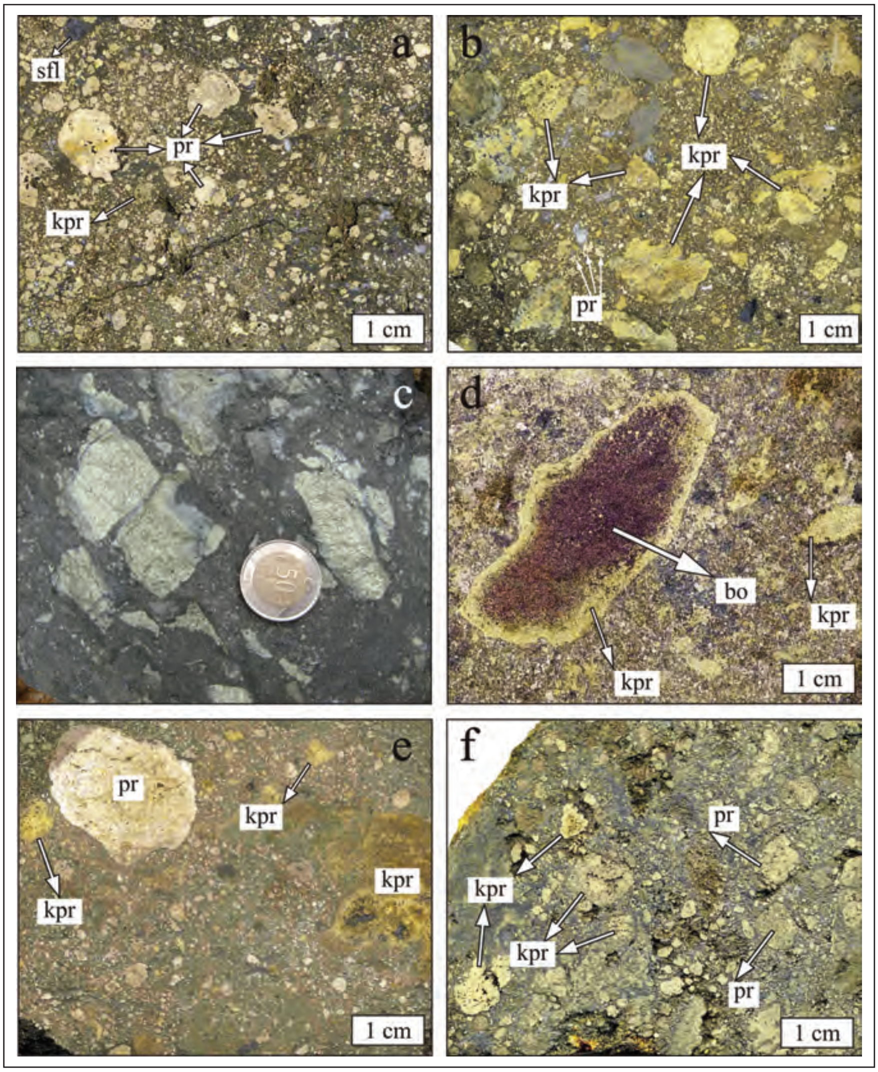

Figure 7- Examples of seafloor hydrothermal facies. (a), (b) and (c) Clastic ore facies from Killik deposit. Sulphide fragments with variable sizes within the sulphide matrix. (d) Sulphide fragments up to 5 cm in a sulphide matrix of the Çayeli orebody. (e) Sulphide fragments up to 2 cm in a sulphide matrix of the Kutlular (e) and the Kızılkaya (f) deposits (cpy-chalcopyrite, py-pyrite, bo-bornite, sph-sphalerite).

within the massive orebody and may also contribute to the constituents of clastic sulphide ores. Large and small fragments are found together (Figure 8a). While the proportion of coarse-grained components is higher than fine-grained components in some samples, fine-grained components predominant in other samples. Fractures are commonly observed in coarse-grained sulphide clasts (Figure 8b). The grain size of the clasts decreases from vent channels outward, with coarse-grained components predominating close to vent channels. As a result of reworking, the grain size decreases to sand size during transport, and a deposition of sulphide sandstone composed mostly of sulphide material takes place at a specific distance from the vent channel.

When the structures and textures of some samples taken from different places of the Lahanos deposit are analysed, it is observed that coarse-grained sulphide (pyrite) components are up to 4 cm in proximity to vent channels and decrease to millimetre then micrometre scale with increasing distance. This deposition of sulphide sandstone results from disintegration and precipitation. The situation is the same in the Kutlular deposit. Coarse-grained sulphide fragments (~3 cm in diameter) were deposited near the vent channel, while finer fragments accumulated in the more distal part of system (Figure 9).

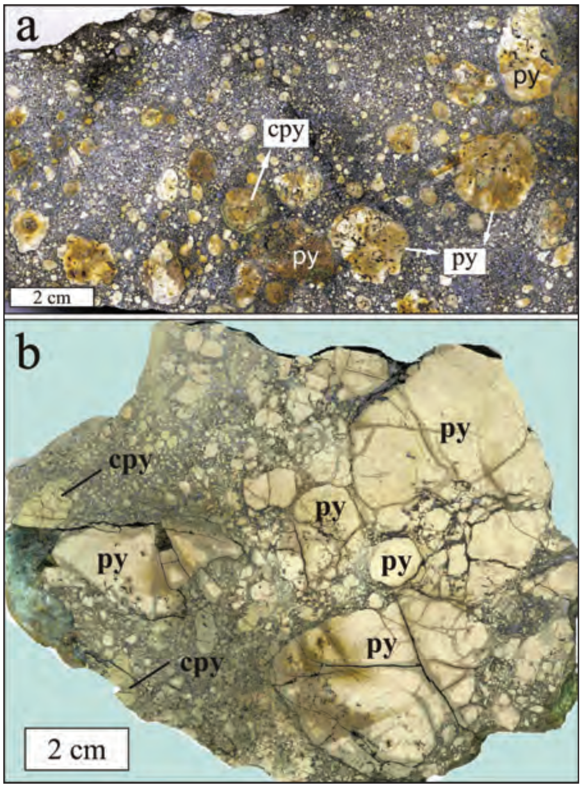

Figure 8- Examples of clastic ore facies. (a) Sulphide fragments with variable sizes within the fine grained-sulphide matrix (matrix>grain)-Çayeli deposit. (b) Large sulphide fragments within the fine grained-sulphide matrix (grain>matrix)-Akarşen deposit (cpy-chalcopyrite, py-pyrite).

The formation of clastic (brecciated) ores has been studied numerous times. Diverse hypotheses for the origin of these clastic ores, such as tectonic, tectonic-metasomatic, magmatic-explosive, hydroexplosive, and erosional origins, have been offered to date (e.g., Eldridge et al., 1983; Maslennikov, 1991). Based on the observation of the destruction of a modern sulphide mound, it is possible to confirm the erosional hypothesis of brecciated ore formation during and after hydrothermal activity attenuation (Maslennikov, 1999; Herrington et al., 2005). A number of different subfacies of clastic ores have been proposed based on the erosional origin hypothesis. These facies are the following: (1) eluvial ore, (2) colluvial ore, (3) proximal turbidity ore, and (4) distal turbidity ore. These subfacies form the lithological-facies range, based on the degree of distance from the sulphide mound. Areas near the sulphide mound are in the form of coarse-grained, brecciated ore (eluvial ore and colluvial ore), while regions far from the sulphide mound are composed of relatively small components (proximal turbidity ore and distal turbidity ore). In some examples, clastic ores almost completely compose the ore deposit as in the Alexsandrinskoye deposit in the Urals (Tesalina et al., 1993). The interaction between the seafloor and sea water is the major factor influencing the massive sulphide mound, and these processes are described as seafloor alteration (halmyrolysis). These processes are highly effective in open systems, causing disintegration of the sulphide mound and adjacent sedimentary facies (Herrington et al., 2005). Depending on the effect of these processes on the components in the system, different facies types may result.

The fragmental nature of sulphide ores is confirmed by the following facts: (1) the co-occurrence of fragments with different composition, texture and structure; (2) the cutting of the crystals' zonality and the textural fabric of the ore bodies; (3) the decrease of the fragments' dimensions with increasing distance from the ore mound; and (4) the presence of volcanic fragments that have not been replaced by sulphides (Maslennikov, 1999).

Eldridge et al. (1983) listed several mechanisms that may cause such slumping, which include the following: (1) syndepositional or post-ore intrusion of dacite. This has been suggested by Hashiguchi (1983) as the major cause for various deformational features including clastic ore textures; (2) soft sediment deformation, such as the injection of muddy or tuffaceous footwall rocks into massive ores; (3) hydraulic lifting of the ore; (4) growth of the ore pile on the seafloor. Oversteepened slopes of ore piles may slump due to gravity or in response to seismic activity; (5) changes in volume associated with the dehydration of gypsum or hydration of anhydrite underlying the sulphide pile. This reversible reaction causes depression or elevation of the ores; (6) collapse of the sulphide pile in response to the removal of material by dissolution from within the ore blanket; and (7) sudden violent hydrothermal eruptions, as proposed by Clark (1971).

3.4. Biological Facies

The biological facies is characterised by the fossil remnants of symbiotic vent communities. All fragments of fossil fauna in the massive sulphide deposits are found in the clastic sulphide ores (Revan et al., 2010). Traces of fauna are well-preserved in the Lahanos, Killik, and Çayeli deposits. Fossil fauna from Kızılkaya, Kutlular, and Kanköy deposits are scarce and not well-preserved. The dimensions of the of the tube worm fossil traces found in the Lahanos deposit reach up to 2.5 cm in diameter

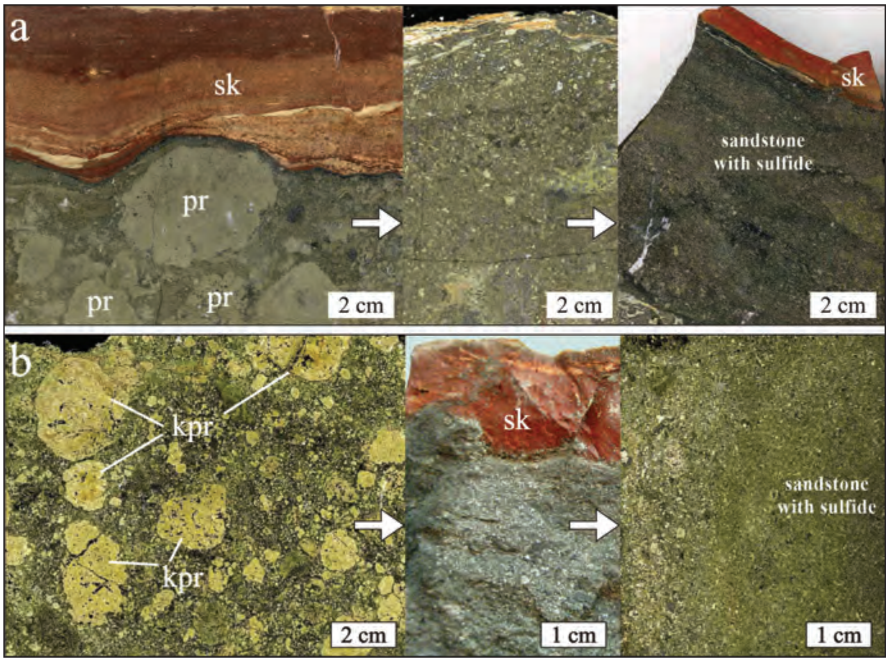

Figure 9- Clastic ore facies of VMS deposits in the eastern Black Sea region (Revan, 2010). (a) The coarse-grained sulphide (pyrite) components up to 5 cm in proximity to vent channels and decrease to sand size as a result of transport and reworking- the Lahanos mine. (b) Fragments up to 2 cm in proximity to vent channels and decrease to sand size after transport and reworking- the Kutlular mine (pr-pyrite; kpr-chalcopyrite; sc-siliceous carbonate).

and 8 cm in length. These fossils are preserved in a clastic sulphide matrix composed mainly of pyrite and sphalerite (Figure 10a). The interiors of the tube fossil traces are filled with variable minerals (such as pyrite, chalcopyrite, tetrahedrite, sphalerite, covelite, dolomite, barite, serpierite, goethite, jarosite, and gypsum). In the Killik deposit, mineralised tube worm samples are preserved in a brecciated sulphide matrix and their dimensions reach 2 cm in diameter and 7 cm in length (Figure 10b). The internal surfaces of the tubular samples are filled mainly with sulphide minerals (pyrite, sphalerite, chalcopyrite, and galena), while very few samples feature external replacement with opaque and gangue minerals. As much as it can be observed from axial and equatorial sections, these replacements cover all of the fossil trace in some samples. However, only the side sections and the internal part of the fossil trace is left in the shape of a cavity (Figure 10c, d). In some other samples from the Killik mine, outer sections of the tube fossil traces are replaced by barite, while the internal portions are filled with sulphide clasts.

In the Çayeli deposit, fossil traces are 5 cm long and 2 cm wide and are found in clastic sulphide matrix. In contrast to other deposits, one sample is preserved in clastic pyritic ore. A microscopic view of a sample from Çayeli mine is displayed in Figure 11. This sample is well-preserved and is in the clastic sulphide material (sulphide sandstone) in which clast sizes reach 1 mm. The innermost part, consisting of sulphide clasts (mostly pyrite, chalcopyrite, and sphalerite), displays moderate gradation. A sphalerite zone encircles the innermost part, while the outermost part, surrounding the sphalerite zone, is composed mainly of chalcopyrite.

The fossil tubes are infilled by sulphide and sulphate minerals, with lesser amounts of dolomite, serpierite, goethite, and jarosite minerals. In some examples, the morphologies of fossils are completely replaced and preserved, whereas some fossil traces form a cavity due to intense and extensive acidic leaching. Compared with the other VMS districts (such as the Urals, Cyprus, or Oman), traces of fossil fauna in massive sulphide deposits of the eastern Black Sea region are quite abundant and well-preserved.

3.5. Ore-bearing Sedimentary Facies

The ore-bearing sedimentary facies in the eastern Black Sea region is recognised by the red colour imparted by abundant iron oxides. There is only one form, bedded, which has been identified only in

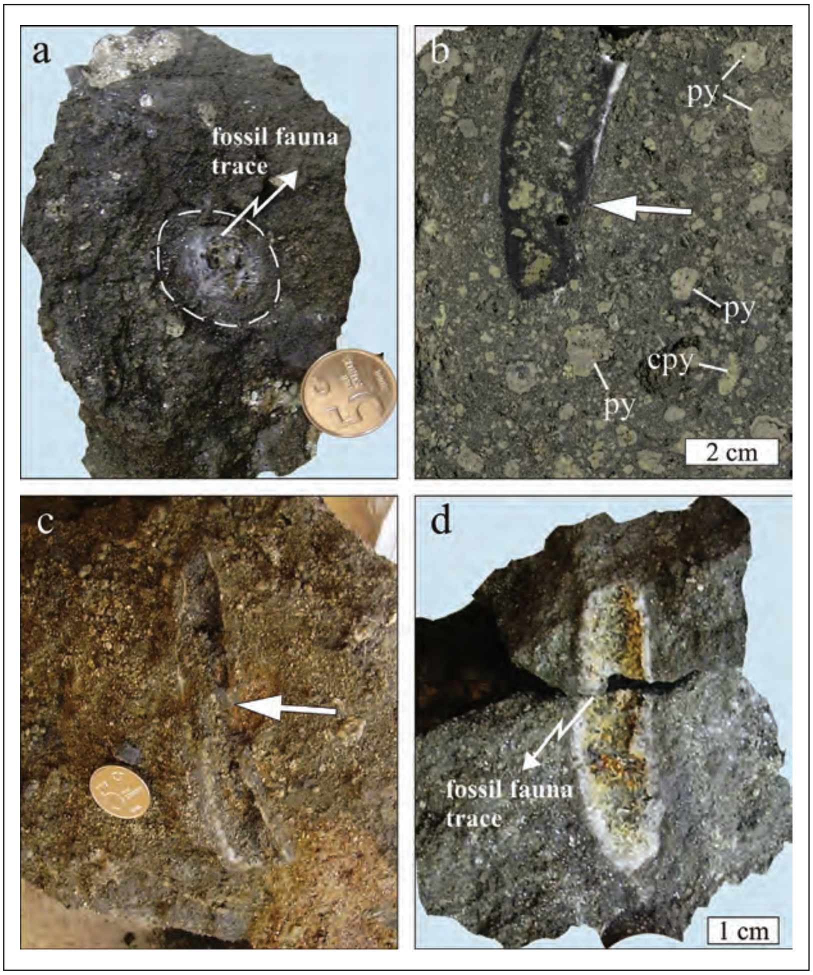

Figure 10- Biological facies of VMS deposits in the eastern Black Sea region (Revan, 2010). (a) Trace fossil from the clastic sulphide ore within the Lahanos orebody. Trace of fossil tube worm replaced by sulphide and sulphate minerals within the clastic sulphide ore of the Killik (b) and the Lahanos (c) deposits. (d) Tube worm replaced by various minerals (dolomite, barite, serpierite, goethite, jarosite, gypsum). py-pyrite; cpy-chalcopyrite.

the Lahanos, Kutlular, Çayeli, and Kanköy massive sulphide deposits. In the Lahanos mine, an ore-bearing sedimentary horizon directly overlies the massive sulphide ore. This typically red-coloured-layer ranges in thickness from < 1 cm to several meters (Figures 9a and 12a, b). In places, it contains ore fragments from the underlying massive ore and rock fragments (hyaloclastics) from the overlying horizon. The silicified layer covers the whole massive orebody (~300 m), despite the layer's variable thickness. In the Çayeli mine, this facies has the distinctive red colour (Figure 12c) and can be traced discontinuously for approximately 550 m atop the massive ore body. The thickness of this layer ranges from 2 cm to 2 m. This facies in the Kanköy mine is red coloured and reach 20 cm thick in some localities (Figure 12d). In the Kutlular mine, the ore-bearing horizon is the typical red and directly overlies massive ore. No data are available on its thickness and extent. However, observations in some locations indicate it is at least 20 cm thick. In the Kutlular mine, there are two varieties: (1) proximal horizons directly overlying massive sulphide ore (Figure 12e) and (2) distal horizons interlayered with massive sulphide ores (Figure 12f). In above-mentioned deposits, comprehensive analyses should be made in order to distinguish true hydrothermal chemical sediments (exhalite) from other sedimentary facies (e.g., mudstone or reworked clastic weathering products).

In the mineralised chemical sediment of Lahanos mine, glass shards, sericitic volcanic rock fragments,

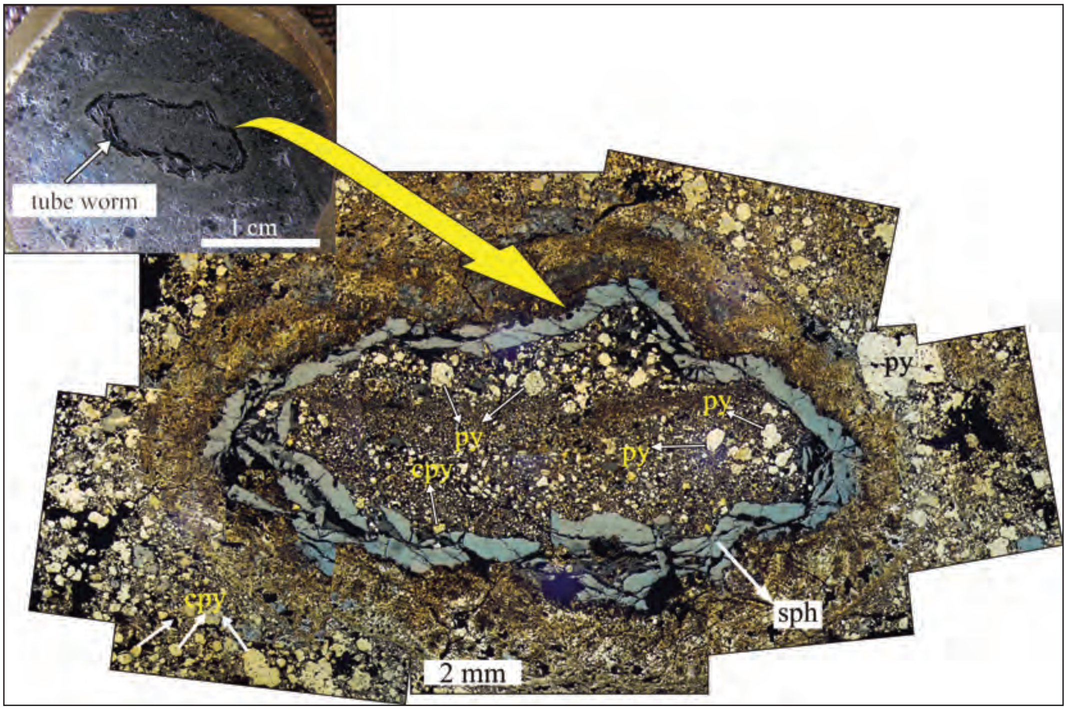

Figure 11- Trace of fossil fauna (vestimentiferan tube worm?) described in clastic sulphide orebody of the Çayeli deposit (Revan, 2010). Clastic sulphide fragments are mainly pyrite (py), chalcopyrite (cpy), and sphalerite (sph).

corroded quartz, and opaque minerals (pyrite, chalcopyrite) are present within a carbonate, silica, iron oxide, and iron hydroxide matrix (Figure 13a, b). Quartz crystals are both primary and secondary. Flow foliation is well-developed. Chloritisation and carbonate- and hematite-bearing alterations are common. The sediment is composed of the minerals, in order of abundance, kaolinite, siderite, barite, quartz, hematite and amorphous materials. The main ore minerals, in order of abundance, are chalcopyrite, pyrite, limonite, fahlores, rutile, and galena. Major element compositions of mineralised sediments from the Lahanos, Kutlular, Çayeli, and Kanköy deposits are given in table1. Silica and iron contents are quite high, and results of the analysis indicate intense seafloor alteration.

Volcanogenic massive sulphide deposits commonly display a spatial and genetic association with iron-rich horizons (sulphide and oxide facies), which is referred to in Japan as tetsusekiei or iron quartz (Kalogeropoulos and Scott, 1983) and elsewhere as ferruginous chert, cherty tuff, tuffite, and gossanite. Such sedimentary facies are generally known as exhalite (Ridley, 1971). This facies typically occurs at, or above, the ore horizon and can be useful in exploring for massive sulphide deposits. In old VMS districts, in which metamorphism has commonly obscured most primary textures (Kalogeropoulos and Scott, 1983; Kalogeropoulos, 1985), these facies have not been described and are nearly impossible to detect. Thus, this facies is not specific to all VMS districts. There remains uncertainty about their source and origin. It is rather difficult to determine which are true hydrothermal exhalites, which are reworked clastic weathering products and which are the products of regional weathering phenomena of volcanic rocks (Allen et al., 2002). Many researchers suggest that these exhalites may be attributed to the same hydrothermal system that formed the massive sulphide deposit (Large, 1977; Edmond et al., 1979; Kalogeropoulos and Scott, 1983; Tsutsumi and Ohmoto, 1983).

For the lithified analogues of such sediments, Zaykov et al. (1993) offer the term gossanites. With regard to “source” sulphides, gossanites are to be subdivided into autochthonous (deposited immediately atop the ores) and allochthonous (at some distance relative to the ore deposits) (Maslennikov, 1999). Gossanites have massive, brecciform, parallel-layered, cross-layered, or rhythmically-layered textures. The structures are usually small- and fine-grained and are sometimes pseudo-oolitic. Compared to the massive sulphide ores, they have relatively low contents of Cu, Zn, and Pb. Red-coloured gossanites

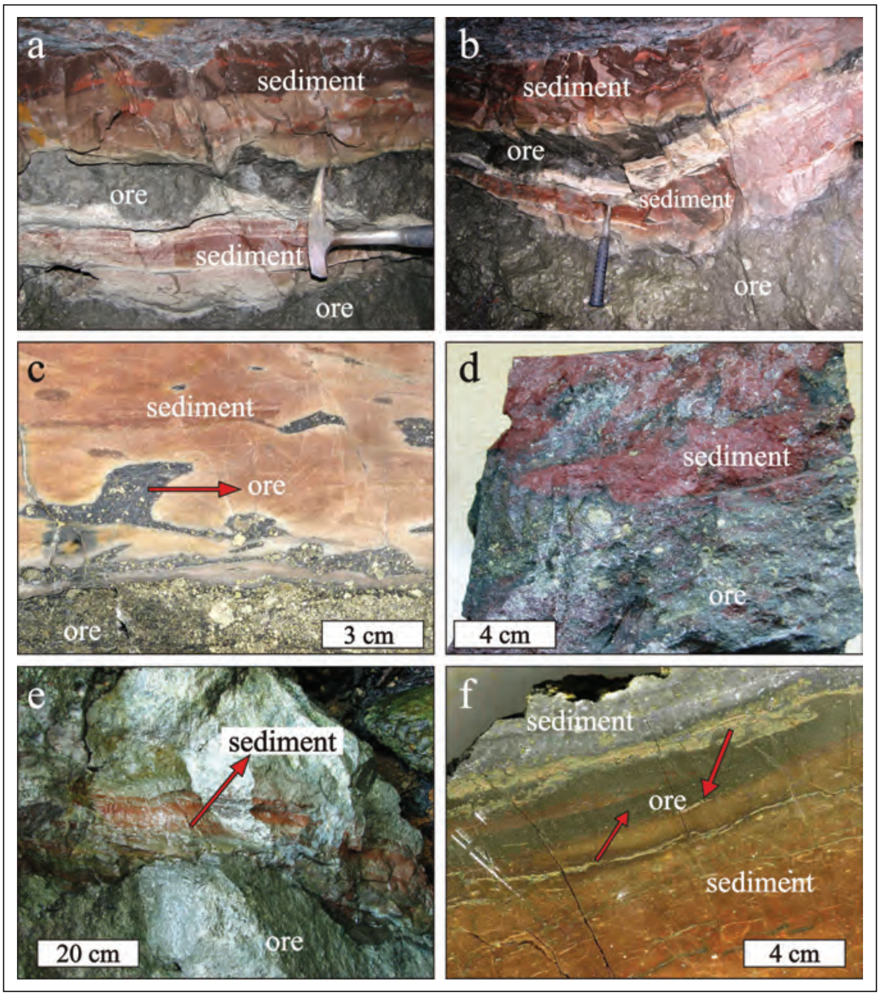

Figure 12- Ore-bearing sedimentary facies of VMS deposits in the eastern Black Sea region. Ferrigenous chert layers directly overlying massive ore body of the Lahanos (a-b), the Çayeli (c), the Kanköy (d) and the Kutlular (e-f) deposits, are typically red-coloured. This facies is interbedded with ore at the distal part of the Kutlular mine (f).

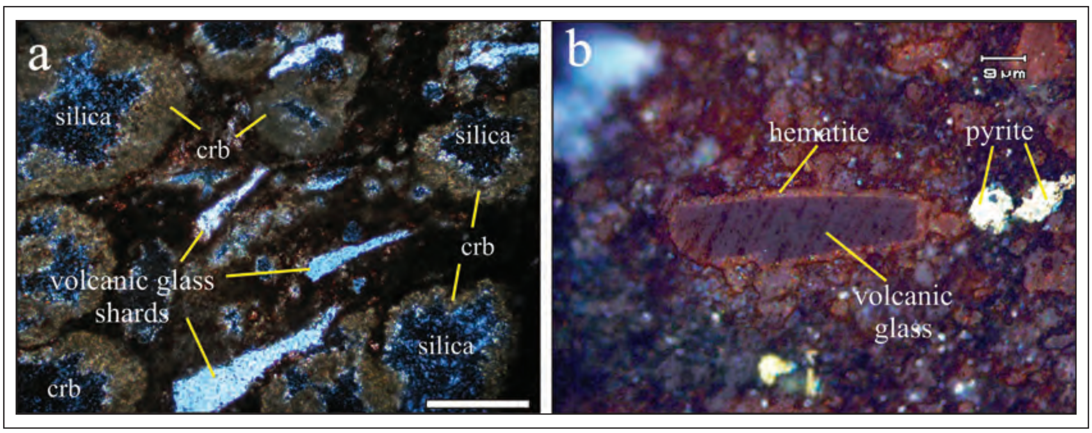

Figure 13- Photomicrographs of ore-bearing sedimentary facies overlying the Lahanos orebody. (a) Glass shards in carbonate (crb) and siliceous matrix. Scale bar is 40µm. (b) Ore minerals (pyrite) and hematitic rim around volcanic glass within the silica, carbonate, and kaolinite matrix.

Table 1- Major element compositions (%) of mineralized sediments of VMS deposits in the eastern Black Sea region. See Figure 12 for location of analyzed sediments.

Location and Sample No	Na_2O	MgO	Al_2O	SiO_2	P_2O_5	K_2O	CaO	TiO_2	MnO	Fe_2O	L.O.I	Total
Lahanos-1	0,07	2,76	13,51	39,9	0,47	0,14	1,76	0,53	0,10	21,9	16,3	**97,4**
Lahanos-2	<0,10	2,90	12,70	39,9	0,60	0,10	3,70	0,40	0,30	21,7	19,8	**102,2**
Çayeli-1	0,07	3,47	1,3	13,1	0,10	0,07	4,75	0,02	7,05	55,8	11,7	**97,4**
Kutlular-1	<0,01	0,18	0,22	48,2	<0,01	0,02	0,37	<0,01	0,01	14,7	12,2	**75,9**
Kutlular-2	0,01	0,52	1,94	43,3	0,41	0,05	0,50	0,04	0,04	34,9	5,5	**87,2**
Kanköy-1	0,20	2,50	4,70	13,9	0,80	<0,10	6,50	<0,10	0,10	40,3	12,5	**81,5**
Kanköy-2	0,20	2,20	3,80	10,9	0,70	<0,10	7,70	0,10	0,20	39,1	12,5	**77,4**

(Abbreviations: L.O.I: Loss on ignition)

of modern and ancient sulphide-bearing hydrothermal fields are characterised by significant compositional variations in Fe_2O_3 (20-87 %), P_2O_5 (0.1-1.5 %) and by the high proportions of nonferrous and noble metals (Telenkov and Maslennikov, 1995). Maslennikov (1999) proposed two main hypotheses for the origin of the ore-enclosing siliceous-ferruginous sediments: halmyrolytic and seafloor-hydrothermal. The common model, uniting these hypotheses, has been offered by Telenkov and Maslennikov (1995). In this model, the ore-enclosing rocks were proved to include at least three facies or genetic types: gossanites, umberites, and jasperites.

When ferruginous chert layers (ore-bearing sediments), which are common within massive sulphide deposits (Franklin et al., 1981; Kalogeropoulos et al., 1983; Allen et al., 2002), are evaluated with these characteristics, their primary traces appear well-preserved in the nonmetamorphosed eastern Black Sea region. Typical features of this facies at the Lahanos, Çayeli, Kutlular, and Kanköy deposits have been described generally. They typically have red colours and high silica contents. They vary in thickness from several centimetres to several meters and commonly cover at least an area of the orebody. At Lahanos, this layer extends continuously across the entire massive orebody, whereas, in Çayeli mine, it can be traced only discontinuously above the orebody. Their extents in other deposits have not been fully established. They contain mainly volcanic rock fragments, glass shards, quartz fragments, barite, chlorite, and abundant opaque minerals (pyrite, chalcopyrite, tennantite, sphalerite, and galena) in a matrix consisting of carbonate, silica, iron oxide, iron hydroxide, kaolinite, and montmorillonite.

4. Discussion

Based on variation in the texture and structures of the VMS deposits in the eastern Black Sea region, the types of deposits present include those that have accumulated sub-seafloor and those that formed via sulphide precipitation at the seafloor (Figure 14). The accumulation processes occurred over the life of the hydrothermal system. The hydrothermal-metasomatic facies is represented by stockwork zones and provides clear evidence for the sub-seafloor origin of deposits (Sangster, 1972; Franklin et al., 1981; Eldridge et al., 1983; Lydon, 1984*a,b*; Doyle and Allen, 2003). These zones are composed of networks and disseminations rather than massive replacements. Massive sulphide lenses/veins in this part of deposit form by replacement of the permeable zones within the dacitic/rhyolitic host rocks (Galley and Koski, 1999; Tornos, 2000; Doyle and Allen, 2003). Discordance between ore lenses/veins and the bedding of the enclosing host lithologies, homogeneous textures, the structure of massive sulphide lenses/veins and the presence of strong host rock alteration are all diagnostic features of sub-seafloor accumulation. The sizes and metal contents of stockwork mineralisations in the eastern Black Sea region are variable. At Murgul, there is a well-developed stockwork mineralisation in vertical and lateral orientations, whereas in other deposits (e.g., Lahanos, Killik, Kanköy, and Kutlular), the sizes of stockwork zones are relatively small. Some deposits (e.g., Çayeli and Peronit) have medium-sized stockwork zones compared to other deposits in the district. Because these parts of deposits are of no economic interest, except at Murgul, their sizes have not been studied well and are not fully known. Among the most important controlling factors on the size and metal content of these zones are the permeability of the host-rock and the duration of

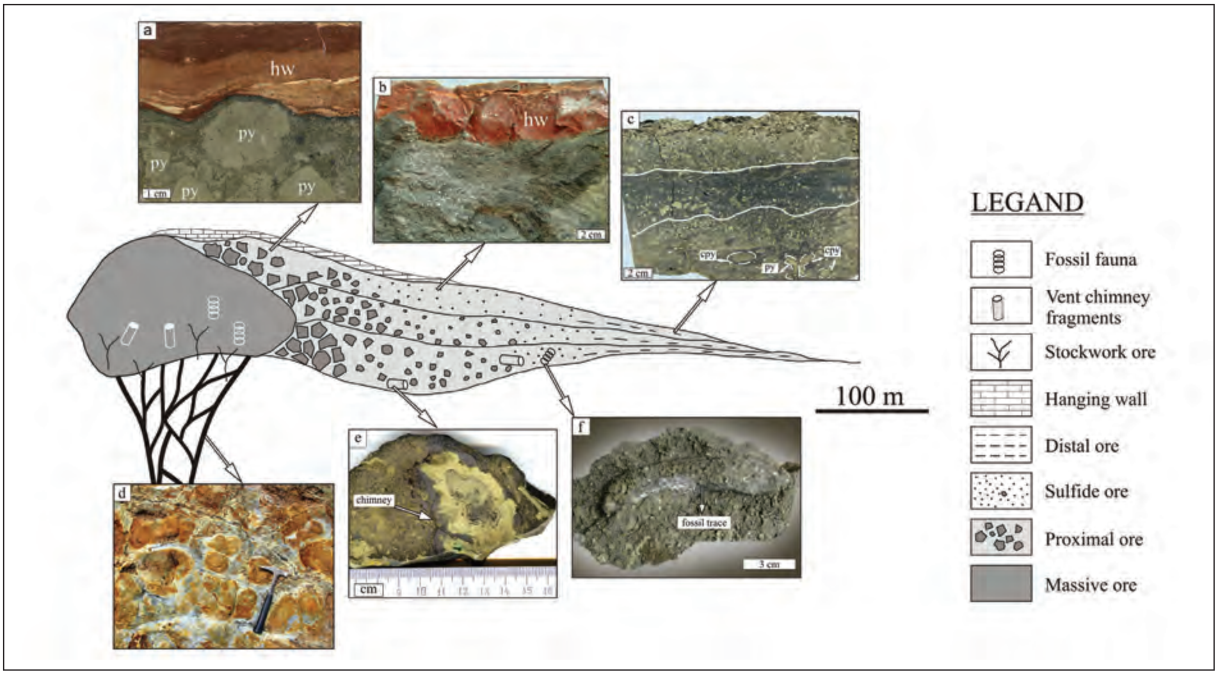

Figure 14- A schematic diagram illustrating possible locations of ore facies at the eastern Black Sea region. (a) Sulphide breccia (proximal ore). (b) Sulphide sandstone (distal ore). (c) Graded ore (distal ore). (d) Stockwork mineralization. (e) Hydrothermal vent chimney fragment. (f) Biological facies (cpy-chalcopyrite; py-pyrite).

the magmatic heat source (Large, 1992; Barrie and Hannington, 1999; Doyle and Allen, 2003). Factors affecting hydrothermal alteration mineralogy include rock composition, temperature, fluid composition, and salinity, but fluid pH appears to have the largest effect (Eldridge et al., 1983; Allen et al., 2002). The depths below the seafloor at which infiltration and replacement occur are mainly in the range of 10-200 m, with some reaching up to 500 m. The upper few tens to hundreds of metres in the volcano-sedimentary pile are the favoured depths for replacement. At these depths, clastic facies are wet, porous, and poorly consolidated, and, at greater depths, they become progressively more compacted, dewatered, altered, and less amenable to large scale infiltration and replacement by hydrothermal fluids (Doyle and Allen, 2003).

Some VMS deposits in this district (such as Kızılkaya, Çayeli, Kutlular, Lahanos, Killik, Kanköy, Akarşen, and Kuvarshan) provide critical evidence in support of a seafloor origin and are likely to have formed on the seafloor. Hydrothermal fluids ascending along structural discontinuities below the seafloor infiltrated and precipitated minerals within open spaces, which led to the stockwork and sub-seafloor replacement ores (Eldridge et al., 1983; Doyle and Allen, 2003). Metals that remain in solution are transported to the seafloor (Eldridge et al., 1983). The accumulation process starts with the initiation of hydrothermal flow from seafloor fractures into the overlying seawater. Mixing of hydrothermal fluids with seawater causes rapid deposition of sulphate and sulphides, which begins to form chimney walls. Based on observations, hydrothermal vent chimneys are the first products of the seafloor hydrothermal facies. The destruction of chimneys contributes to the formation of a mound of chimney talus. Chimney fragments also form the major constituents of clastic sulphide ores. The highly active and unstable setting at the seafloor leads to the disintegration of the seafloor sulphide mounds and redeposition following lateral sedimentary transport. Large (20-30 cm) and small (10 µm) fragments are found together, indicative of accumulation on the seafloor by debris (molasse) flow. The presence of some sedimentary structures, such as wavy structures, slump structures, and the diversity in the components (occasionally including wall rock and ore fragments), indicate that erosion and sedimentary processes were highly effective on the paleo-seafloor.

The clastic ore facies is represented by accumulated ore clasts resulting from disintegration of sulphide mounds and from reworking processes (seafloor alteration). Clastic ore textures, chimney fragments, fossil vent fauna, and alteration rims surrounding some ore fragments are clear evidence for seafloor mineralisation (Qudin and Constantinou, 1984; Doyle and Allen, 2003; Herrington et al., 2005). Some ore fragments display an alteration rim, indicative of seafloor oxidation. Such an oxidation zone around chimney fragments and post-depositional modifications can be attributed to submarine alteration (halmyrolysis). It is clear that halmyrolitic processes, such as oxidation, dissolution, and the resedimentation of disintegrated material (Maslennikov et al., 2012), were highly active on the paleo-seafloor.

Considering that modern massive sulphides are situated at depths >2500 m (Spiess et al., 1980; Qudin and Constantinou, 1984) near rift zones (Francheteau et al., 1979; Hekinian et al., 1980; Haymon, 1983; Goldfarb et al., 1983; Qudin and Constantinou, 1984; Hannington et al., 2005), it is likely that the hydrothermal black smoker chimneys formed at similar depths. From this, we conclude that the VMS deposits of the eastern Black Sea belt formed in a deep-sea extensional setting.

The ecological environment of the deposits also support a deep-sea setting. The ecological characteristics of the seafloor-related deposits, shed light on the environment and conditions of formation of modern and ancient-massive sulphide hydrothermal fields. Fauna found in massive sulphide deposits (possibly vestimentiferan tubeworms) live in highly unusual, hydrogen sulphide-rich (H_2S) conditions, which are not favourable for many other organisms. The organisms that survive in such a hydrothermal field are so specialised that it is almost impossible for them to live in any other environment (Lob'e, 1990). These ecological conditions are indicative of a deep-sea setting. In modern oceans, there are three main environments where the autogenic oxygen regime occurs: (1) the shallow ocean, which is saturated with oxygen; (2) the near-continental moderately deep-sea environment, where the seafloor has at least minimal oxygen (depths ranging from 100 m to 2000 m, averaging 800-1000 m), and (3) the deep-sea oxygen zone, formed as a result of the subsidence of oxygen-rich waters from the surface beds in zones of convergence and a lack of active oxygen consumers at depth (Murdmaa, 1987 from Maslennikov, 1999). This latter oxygen source explains the existence of the oxygen required for oxidation processes in a deep-sea setting.

The existence of ferruginous sediments (sch as ferruginous chert, jasper or exhalite) directly overlying the massive ore bodies in the eastern Black Sea belt is one of the important pieces of evidence indicating a paucity of volcanism on the seafloor. Active processes such as active volcanism on the seafloor are followed by quiescent periods in which sedimentation take places. However, wavy structures, sudden changes in thickness, soft sediment deformation and slump/collapse structures (Revan 2010) suggest that precipitation occurred in a highly active and unstable setting. One cause of this high level of activity is syndepositional or post-ore intrusion by dacite (Hashiguchi, 1983). Sulphide accumulations and/or sediments on the seafloor are deformed by the intruding felsic domes, often resulting in clastic (breccia) structure due to disintegration.

Detailed analysis of ore facies unique to massive sulphide deposits provides important data in understanding the physico-chemical environment and the processes of precipitation. The data obtained can be used in global comparisons of VMS deposits and/or districts. The eastern Black Sea VMS deposits are well-preserved deposits in term of ore texture/structure (clastic ores) and components (mineralised chimney fragments and fossil fauna). These primary structures and textures are largely preserved due to the region's nonmetamorphosed nature. Finally, in terms of ore characteristics, the eastern Black Sea Region VMS deposits have a number of characteristics in common with Kuroko and Uralian deposits (Revan, 2010).

Received: 20.06.2013
Accepted: 05.09.2013
Published: December 2013

References

Adamia, S.A., Zakariadze, C.S., Lordkipanidze, M.B. 1977. Evolution of the ancient active continental margin as illustrated by Alpine history of the Caucasus. *Geotectonica* 11/4, 20-309.

Akın, H. 1979. Geologie Magmatismus und Lagerstaettenbildung im ostpontischen Gebirge-Türkei aus der Sicht der Plattentektonik. *Geologische Rundschau* 68, 253-283.

Akıncı, Ö.T. 1984. The geology and the metallogeny of the Eastern Pontides (Turkey). *International Word Geological Congress Abstracts*, 197-198.

Allen, R.L., Weihed, P., The Global VMS Research Project Team, 2002. Global comparison of volcanic-associated massive sulphide districts. In: Blundel, D.J., Neubauer, F. and von Quadt, A. (eds.), The Timing and Location of Major Ore Deposits in an Evolving Orogen. *Geological Society, London*, Special Publication, 204, 13-37.

Barrie, C.T., Hannington, M.D. 1999. Classification of volcanic-associated massive sulfide deposits based on host-rock composition. In: Barrie, C.T. and Hannington, M.D. (Eds), Volcanic-associated

Massive Sulfide Deposits: Processes and Examples in Modern and Ancient Settings. *Rewievs in Economic Geology* 8, 1-10.

Buslaev, F.P., Kalegorov, B.A. 1992. The age of sulfide ore formation according to the K/Ar method. In: Prokin, V.A., Seravkin, I.B., Buslaev, F.P. et. Al. (eds). Copper-sulfide deposits of the Urals: conditions of formations. Russian Academy of science, Ural Branch. Ekaterinburg, 186-199 (in Russian).

Clark, L.A. 1971. Volcanogenic ores: Comparison of cupriferous pyrite deposits of Cyprus and Japanese Kuruko deposits. *Soc. Mining Geologists Japan*, Spec. Issue 3, 206-215.

Çamur, M.Z., Güven, İ.H., Er, M. 1996. Geochemical characteristics of the eastern Pontide volcanics, Turkey: An example of multiple volcanic cycles in arc evolution. *Turkish Journal Earth Science* 5, 123-144.

Doyle, M.G., Allen, L.A. 2003. Subsea-floor replacement in volcanic-hosted massive sulfide deposits. *Ore Geology Reviews* 23, 183-222.

Edmond, J.M., Measures, C., Mangum, B., Grant, B., Sclater, F.R., Collier, R., Hudson, A. 1979. On the formation of metal-rich deposits at ridge crests. Earth Planet. Sci. Letters, 46, 19-30.

Eğin, D., Hirst, D.M, Phillips, R. 1979. The petrology and geochemistry of volcanic rocks from the northern Harşit River Area, Pontid volcanic province, northeast Turkey. *Journal of Volcanology and Geothermal Research* 6, 105-123.

Eldridge, S.C., Barton, Jr. P.B., Ohmoto, H. 1983. Mineral textures and their bearing on formation of the Kuroko ore bodies. *Economic Geology Mon.* 5, 241-281.

Francheteau, J., Needham, H.D., Choukrone, P., Juteau, T., Seguret, M., Ballard, R.D., Fox, P.J., Normark, W.R., Carranza, A., Cordoba, D., Guerro, J., Rangin, C., Bougault, H., Cambon, P., Hekinian, R. 1979. Massive deep-sea sulfide ore deposits discovered on the East Pacific Rise. *Nature*, 277, 523-528.

Franklin, J.M., Lydon, J.W., Sangster, D.F. 1981. Volcanic-associated massive sulfide deposits. *Economic Geology, 75th Anniversary volume,* 485-627.

Galley, A.G., Koski, R.A. 1999. Setting and characteristics of ophiolite-hosted volcanogenic massive sulfide deposits. In: Barrie, C.T., Hannington, M.D. (Ed.), Volcanic-Associated Massive Sulfide Deposits: Processes and Examples in Modern and Ancient Settings. *Reviews in Economic Geology,* 8, 221-246.

Gedik, A., Ercan, T., Korkmaz, S., Karataş, S. 1992. Petrology of the magmatic rocks in the area between Rize, Fındıklı and Çamlıhemşin (eastern Black Sea region) and their distribution in the eastern Pontides. *Geological Bulletin of Turkey* 35, 15-38. (in Turkish).

Gedikoğlu, A. 1978. Harşit granite complex and neighbouring rocks (Doğankent-Giresun). Unpub. thesis, Black Sea Technical University, 176 s. (in Turkish).

Gemmell, J.B., Large, R.R. 1992. Stringer system and alteration zones underlying the Hellyer volcanic-hosted massive sulfide deposit, Tasmania, Australia. *Economic Geology* 87, 620-649.

Goldfarb, M.S., Converse, D.R., Holland, H.D., Edmond, J.M. 1983. The genesis of hot spring deposits on the East Pacific Rise, 21 ºN. *Economic Geology Monograph* 5, 184-97.

Hannington, M.D., de Ronde, C.E.J., Petersen, S. 2005. Sea-floor tectonics and submarine hydrothermal systems. *Economic Geology, 100th Anniversary volume*, 111-141.

Hashiguchi, H. 1983. Penecontemporaneous deformation of Kuroko ore at the Kosaka Mine, Akita, Japon. *Economic Geology Monograph* 5, 167-183.

Haymon, R. M. 1983. Growth history of hydrothermal black smoker. *Nature*, 301, 695-698.

Hekinian R., Fevrier M., Bischoff J.L., Picot, P., Shanks, W.C. 1980. Sulfide deposits from the East Pacific Rise near 21 °N. *Science*, 207, 1433-1444.

Herrington, R.J., Maslennikov, V.V., Zaykov, V.V., Seravkin, I.B., Kosarev, A.S., Bushmann, B., Orgeval, J-J., Holland, N., Tessalina, S.G., Nimis, P., Armstrong, R. 2005. Classification of VHMS deposits: Lessons from the Uralides. *Reviews in Economic Geology*, 203-237.

Kalogeropoulos, S.I. 1985. Discriminant analysis for evaluating the use of lithogeochemistry along the Tetsusekiei Horizon as an exploration tool in search for Kuroko type ore deposits. *Mineralium Deposita* 20, 135-142.

Kalogeropoulos, S.I., Scott, S.D. 1983. Mineralogy and Geochemistry of tuffaceous exhalites (Tetsusekiei) of the Fukazawa Mine, Hokuroku Districti Japan. *Economic Geology Monograph* 5, 412-432.

Kazmin, V.G., Sbortshikov, I.M., Ricou, L.E., Zonenshain, L.P., Boulin J., Knipper, A.L. 1986. Volcanic belts as markers of the Mesozoic-Cenozoic active margin of Eurasia. *Tectonophysics* 123, 123-152.

Ketin, İ. 1966. Anadolunun Tektonik Birlikleri. Bulletin of the *Mineral Research and Exploration of Turkey* 66, 20-34. (in Turkish).

Kuroda, H. 1983. Geological characteristics and formation environment of the Furutobe and Matsuki Kuroko deposits, Akita Prefecture, northeast Japon. *Economic Geology Monograph* 5, 149-166.

Large, R.R. 1977. Chemical evolution and zonation of massive sulfide deposits in volcanic terrains. *Economic Geology* 72, 549-572.

Large, R.R. 1992. Australian volcanic-hosted massive sulfide deposits: features, styles, and genetic models. *Economic Geology* 87, 471-510.

Lob'e, L. 1990. Oasises on the ocean flor. Moscow. *Hydrometeoizdat* 156 p. (in Russian).

Lydon, J.W. 1984*a*. Volcanogenic massive sulphide deposits. Part 1. Descriptive model. Geoscience Canada 11, 195-202.

Lydon, J.W. 1984*b*. Some observations on the morphology and ore texture of volcanogenic sulphide deposits of Cyprus. Current Research. Part A. Geological Survey of Canada, Paper 84-1A, 601-610.

Manetti, P., Peccerillo. A., Poli, G., Corsini, F. 1983. Petrochemical constrains on the models of Cretaceous-Eocene tectonic evolution of the eastern Pontic Chain (Turkey). *Cretaceous Research* 4, 159-72.

Maslennikov, V.V. 1991. Lithological control of copper massive sulfide ores (after the example of Sibay and Oktyabrskoye deposits, Ural). Sverdlovsk, UB of RAC USSR press, 139 p. (in Russian).

Maslennikov, V.V. 1999. Sedimentogenesis, halmyrolysis, ecology of massive sulfide-bearing paleohydrothermal fields (on the Southern Ural example). Miass: Geotur, 348 p.

Maslennikov, V.V., Zaykov, V.V., Monacke, T., Large, R.R., Danyushevsky, L.V., Maslennikova, S.P., Allen, R.L, Çağatay, N., Revan, M.K. 2009. Ore facies of volcanic massive sulfide deposits in Pontides. *2 th international symposium on the geology of the Black Sea region,* Turkey. Abstract Book, p.123.

Maslennikov, V.V., Ayupova, N.R., Herrington, R.J., Danyushevsky, L.V., Large, R.R. 2012. Ferruginous and manganiferous haloes around the massive sulphide deposits of the Urals. *Ore Geology Reviews*, 47, 5-41.

Murdmaa, I.O. 1987. Ocean facies. Moscow; Nauka, 304 p. (in Russian).

Okay, A.İ., Şahintürk, Ö. 1997. Geology of the eastern Pontides. *In*: Robinson A.G. (Ed.) Regional and Petroleum Geology of the Black Sea and Surrounding Regions. *American Association of Petroleum Geologist,* Memoirs 68, 291-311.

Peccerillo, A., Taylor, S.R. 1975. Geochemistry of Upper Cretaceous volcanic rocks from the Pontic chain, Northern Turkey. *Bull. Volcan.* 39/4, 557-569.

Qudin, E., Constantinou, G. 1984. Black smoker chimney fragments in Cyprus sulphide deposits. *Nature* 308, 349-353.

Revan, M.K., 2010. Determination of the typical properties of volcanogenic massive sulfide deposits in the eastern black sea region. Unpub. Ph.D. thesis, Hacettepe Univ., Ankara, 320 p. (in Turkish).

Revan, M.K., Genç, Y., Ünlü, T., Maslennikov, V.V., Karslı, Ş. 2010. Preliminary findings of fossil traces from massive sulfide deposits (Lahanos, Killik, Çayeli) of eastern Black Sea Region. *63th geological congress of Turkey. Abstract book*, 120-121.

Ridler, R.H. 1971. Analysis of Archean volcanic basin in the Canadian Shield using exhalite concept (abs.). *Canadian Inst. Mining Metal. Bull.* 64, No: 714, p. 20.

Sangster, D.F. 1972. Precambrian volcanic-hosted massive sulphide deposits in Canada: a review. Geological Survey of Canada, Paper 72-22.

Schultze-Westrum, H.H. 1961. Giresun civarındaki Aksu deresinin jeolojik profili; Kuzeydoğu Anadolu'da, Doğu Pontus cevher ve mineral bölgesinin jeolojisi ve maden yatakları ile ilgili mütalaalar. *Maden Tetkik ve Arama Dergisi,* 57, 63-71.

Spiess, F.N., Rise Group 1980. East Pacific Rise: Hot springs and geophysical experiments. *Science* 207, 1421-1433.

Telenkov, O.S., Maslennikov, V.V. 1995. Automatic Expert System for Typification of Siliceous-Ferruginous Rocks in Paleohydrothermal Fields of the southern Urals. Institute of Mineralogy, Urals Branch, *Russian Academy of Science*, Miass. 200 pp. (in Russian).

Tesalina S.G., Maslennikov V.V. 1993. Complete clastation of some sulfide mounds on the bottom of the Urals paleoocean. *L.P.Zonenshain memorial international conference on plate tectonics,* Moscow, p.143.

Tornos, F. 2000. Styles of mineralization and mechanisms of ore deposition in massive sulfides of the Iberian Pyrite Belt. In: Gemmell, J.B., Pongratz, J. (Ed.), Volcanic environments and massive sulfide deposits, Abstracts. CODES Special Publication, v. 3, 211-213.

Tsutsumi, M., Ohmoto, H. 1983. A preliminary oxygen isotope study of Tetsusekiei ores associated with the Kuroko deposits in the Hokuroko district, Japan. *Economic Geology Monograph* 5, 433-438.

Tüysüz, N. 2000. Geology, Lithogeochemistry and Genesis of the Murgul massive sulfide deposit, NE-Turkey. *Chemie der Erde* 60, 231-250.

Yarosh, P.Y. 1973. Diagenesis and metamorphism of massive sulfide ores in the Urals VMS deposits. Moscow, "Nauka" publishing house, 239 p. (in Russian).

Yılmaz, Y., Tüysüz, O., Yiğitbaş, E., Genç, Ş.C., Şengör, A.M.C. 1997. Geology and tectonic evolution of the Pontides. In: A.G. Robinson, A.G.(Ed), Regional and Petroluem Geology of the Black Sea and Surrounding Regions, *American Association Petroleum Geologist, Memoir 68, 183-226.*

Zaykov, V.V., Maslennikov, V.V., Zaykova, E.V. 1993. Volcanism and Metalliferous Deposits of Devonian Island Arc System of southern Urals. Institute of Mineralogy, Urals Branch, Russian Academy of Science, Miass. 146 pp. (in Russian).

Bulletin of MTA (2013) 147: 91-113

Bulletin of the
Mineral Research and Exploration

http://bulletin.mta.gov.tr

ORGANIC GEOCHEMICAL AND PETROGRAPHIC PROPERTIES OF HAZRO DADAŞ (DİYARBAKIR) COALS

Orhan KAVAK[a, *] and Selami TOPRAK[b]

[a] *Dicle University, Engineering Faculty, Mining Department, 21280-Diyarbakır*
[b] *General Directorate of Mineral Research and Exploration (MTA), Department of Mining Anolysis and Technologies, 06800 Ankara, Turkey*

Keywords:
Hazro coals, Organic Geochemistry, Oil generation, Organic Petrography, Permian Coal.

ABSTRACT

This study was carried out in Hazro-Dadaş (Diyarbakır) region which owns the only coal basin in the area. Chemical, petrographic analysis and organic geochemical evaluations of the Permian aged coals were taken into consideration. Coal quality investigation along with proximate (moisture, volatile matter, fixed carbon, ash) and elemental analyses (C, H, O, and S, N) were performed and revealed. The huminite reflectance of organically abundant matter and coal levels were found to be between 0.458 and 1.141 %. This parameter complies with fluorescence colors, calorific value (average original 3165 – 3432 Kcal/kg) and average T_{max} (418 °C). Hasbro coals show low grade maturity and own sub-bituminous, bituminous coalification ranks. This is thought to be resulted from thin overburden and its possible low lithostatic pressure. Rock Eval analysis results show that Type II/III and III kerogen, with average T_{max} value is 418 °C and corresponding to the immature and early-mature rank for hydrocarbon generation. The coals are characterized with their abundance of huminite maceral group and gelinite maceral, with small amount of liptinite and inertinite macerals. Mineral matters of the Hazro-Dadaş coals are clay, quartz and calcite minerals. Hazro-Dadaş coals are thought to have deposited in limnic environment swamps.

1. Introduction

Coal is an important natural energy resource of our country. With technological progresses, mankind increased the utilization of this source in various ways. Coal is mostly used in thermal power plants to produce electricity, thermal energy as fuels, coke for steel production and natural gas production. Utilization of coal in the nation, exhibit the same figure and takes a substantial share of it, in thermal power plants to produce electricity.

With rapid population growth and consumption rate of the energy resources, finding new and alternative energy sources become inevitable to be investigated and explored. Since petroleum is an exhaustible source and its reserve is limited, but usage of petrochemical materials are immense, studies to explore new resources besides the old ones, as well as hydrocarbon generation potential of coals are bound to get increased. Particularly, studies related with terrestrial sediments containing organic material, which have shown tendency to produce oil and gas with increasing thermal effect of burial, have been basis for detail investigations (Hubard, 1950).

As a result of various laboratory studies such as pyrolysis analysis, gas generation potential of humic propertied coals was recorded and the studies were concentrated on this (Durand and Paratte, 1983; Espitalié et al., 1977, 1985; Kalkreuth et al., 1998). According to rock correlation and basin modeling

* *Corresponding author: O. KAVAK, kavakorhan@gmail.com ; orkavak@dicle.edu.tr*

studies, coals aged in the interval between Jura and Tertiary periods tend to contain high petroleum generation potentials (Wilkins and George, 2002). Essentially, studies show that the petroleum generation is related with not completely coal but with coaly shales and the Upper Cretaceous-Tertiary humic coals of the Gipssland Basin, Australia and Indonesia Basins, Groningen in North Nederland, Cooper Basin in Australia were indicated to carry high gas generation potential areas (Hunt, 1995).

Small scaled coal deposits are operated by private companies, but do not carry properties to be used as economic and industrial energy resources. Due to increasing demand of energy, imported petroleum and their increasing prices brought in the study of proper utilization and hydrocarbon generation potential of coals to the agenda, in Turkey. For this, various studies were conducted and there are ongoing projects in this manner (İnan, 2007; Yalçın et al., 2007; Kavak and Toprak, 2011 and 2012).

Coal bearing formations in the nation is mostly located in West, Middle Anatolia and Trace. Southeast Anatolia, due to its geology, consists of water, petroleum, copper, chromium, iron, phosphate like underground resources but is not as lucky to consist the coals beds (Kavak, 2005). The only coal bearing units outcrop in Hazro anticline located in Dadaş and Gomaniibrik (Çökek su) villages of Hazro Town (Figure 1).

Figure 1- Location of the studied area

Paleozoic-Lower Mesozoic aged units in Diyarbakır-Hazro region, outcropped at the Hazro anticline center was known as Diyarbakır Tanin Çığlı units.

Of these lithostratigraphic units which are of Silurian-Lower Triassic age interval, Diyarbakır Group is represented by Dadaş (Upper Silurian-Lower Devonian) and Hazro (Lower Devonian) formations; Tanin Group, by Kaş and Gomaniibrik (Upper Permian) formations; Çığlı Group by Yoncalı, Uludere and Uzungeçit (Lower Triassic) formations among (Perinçek et al., 1991; Yılmaz and Duran, 1997; Günay, 1998; Bozkaya et al., 2009).

Upper Permian aged Gomaniibrik and Kaş Formations are the most essential coal bearing formations here (Lebküchner, 1961). The formation made of shale and sandstone succession consists of two main limnic coal seams (Figure 2 and 3). As a result of investigation and drillings, the coals are of 0.2-1.9 meter thickness, 1.2 % moisture, 30 % ash content and of 5100 Kcal/kg calorific value as well as 2.3 million ton total reserve (Gümüşsu, 1988).

The purpose of this study is to determine organic petrographic and coal quality properties of Hazro-Dadaş (Diyarbakır) coals and their relations. By means of this, not only industrial properties of the coals, also hydrocarbon generation potential of them were determined on mostly from surface samples.

2. Geology

The study area is located between Dadaş and Çökek su villages, in northern part of Hazro town of Diyarbakır city.

The coals were occasionally cut by drillings performed in this region by MTA. Diyarbakır-Hazro-Dadaş coals are of 0.2–1.9 meter thickness, and outcrop within Hazro anticline. The anticline is formed of Paleozoic aged units ascending in the middle of a Tertiary basin (Figure 3). The old formations aged from Devonian to Permian, represented with few rock units, compose the inner core of the Hazro Anticline (Lebküchner, 1961). Basement of Dadaş formation is not observed at the center of the anticline which is located at about 5 km away in northwestern of Hazro Town, but the upper units exhibit a conformable relation with the formation. A detail sampling was conducted along an about 460 m extended vertical section to include the whole lithologies typically. Basically the general outlook of the formation, formed of grayish-green colored shale, mudstone and sandstones; its bottom levels are composed of 10-15 cm thick gray sandstone and brownish green colored shale with rare limestone intercalations and the middle levels, of 40-50 cm thick but occasional successive brownish green colored shale with sandstone intercalations. Their upper level is represented by 30-40 cm thick green mud stones

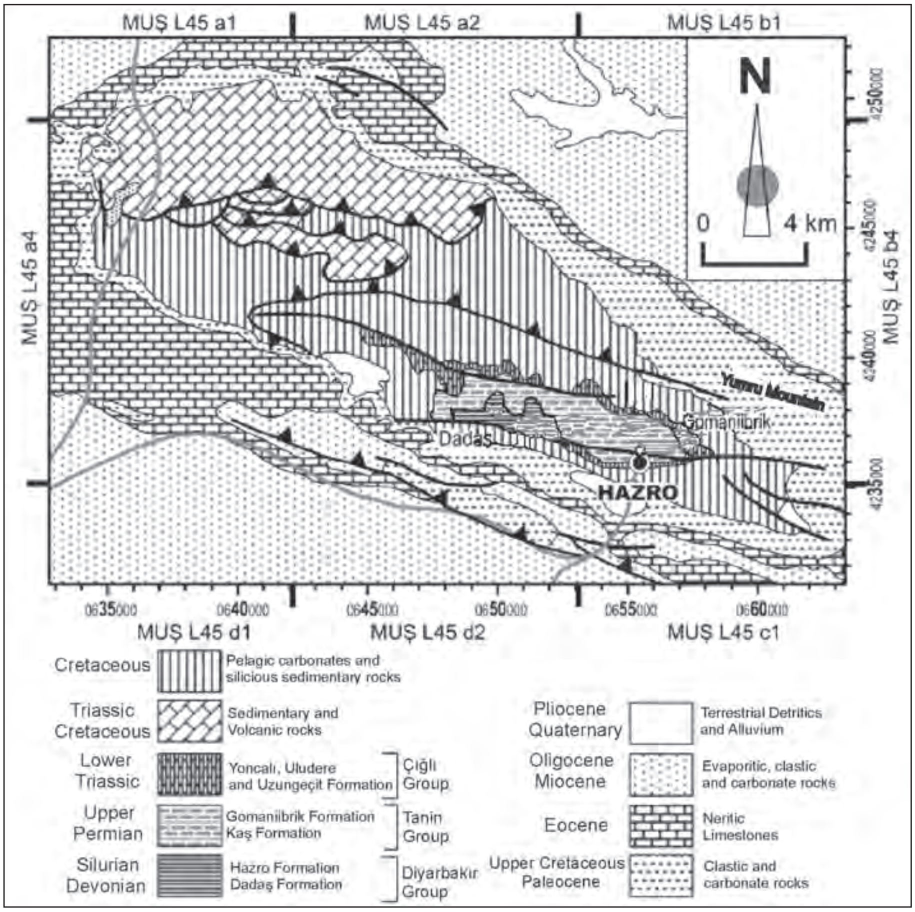

Figure 2- Geologic map of Hazro area (MTA, 2002; Bozkaya et al., 2009)

with a 15-20 cm thick yellowish-brown colored, worm traced sandstone and gray colored sandy limestone intercalations. The formation, which is a shelf deposited environment succession, starting with transgression but finishing with regression, exhibits a very well source rock property for petroleum due to its organic content and type (Bozdoğan et al., 1987; Kranendonk, 2004) (Figure 2).

Hazro formation is only outcropped in Diyarbakır City Hazro region of the Southeastern Anatolia. Typically observed unit, at around Hazro Town, Dadaş Village vicinity, is conformable with underlying Dadaş formation but not with Kaş formation at above. About 100 m thick, Lower Devonian aged formation is represented with different lithologies at the bottom, middle and top levels. The bottom levels are composed of about 5 m thick gray-green colored dolomitic marls with pinkish colored stiff sandy dolomite intercalations with between 10 and 50 cm but occasionally 3 m thicknesses. The middle levels start with 1 m thick brown-claret colored, loose cemented sandstone intercalation of a 2 m thick gray-green colored mudstones, transmitting to a 15 m thick white laminated cream colored sandstones, then a 10 m thick brown colored patchy green marl level covers all. The upper units are represented by 1.5-2 m thick, generally green colored, occasionally brown marl looking mudstones with 50 cm thick yellowish brown colored, occasional petroleum leakage containing loose cemented intercalations and a 5 m thick yellowish cream colored, stiff, textured dolomite strata (Bozkaya et al., 2009).

Upper Permian aged Kaş Formation, which overlies the upper parts of the Hazro Formation, contains coaly shale, siltstone, sandstones and also coal occurrences (Yalçın et al., 2010; Stolle et al., 2011). The unit exhibit typical outcrops at Kaş district, in the east of Dadaş Village, at the western part of Hazro Anticline. The lower boundary is disconformable with Hazro formation, but the upper, conformable with Gomaniibrik formation. To vertical section, the formation is of about 60 m thickness and rich of flora,

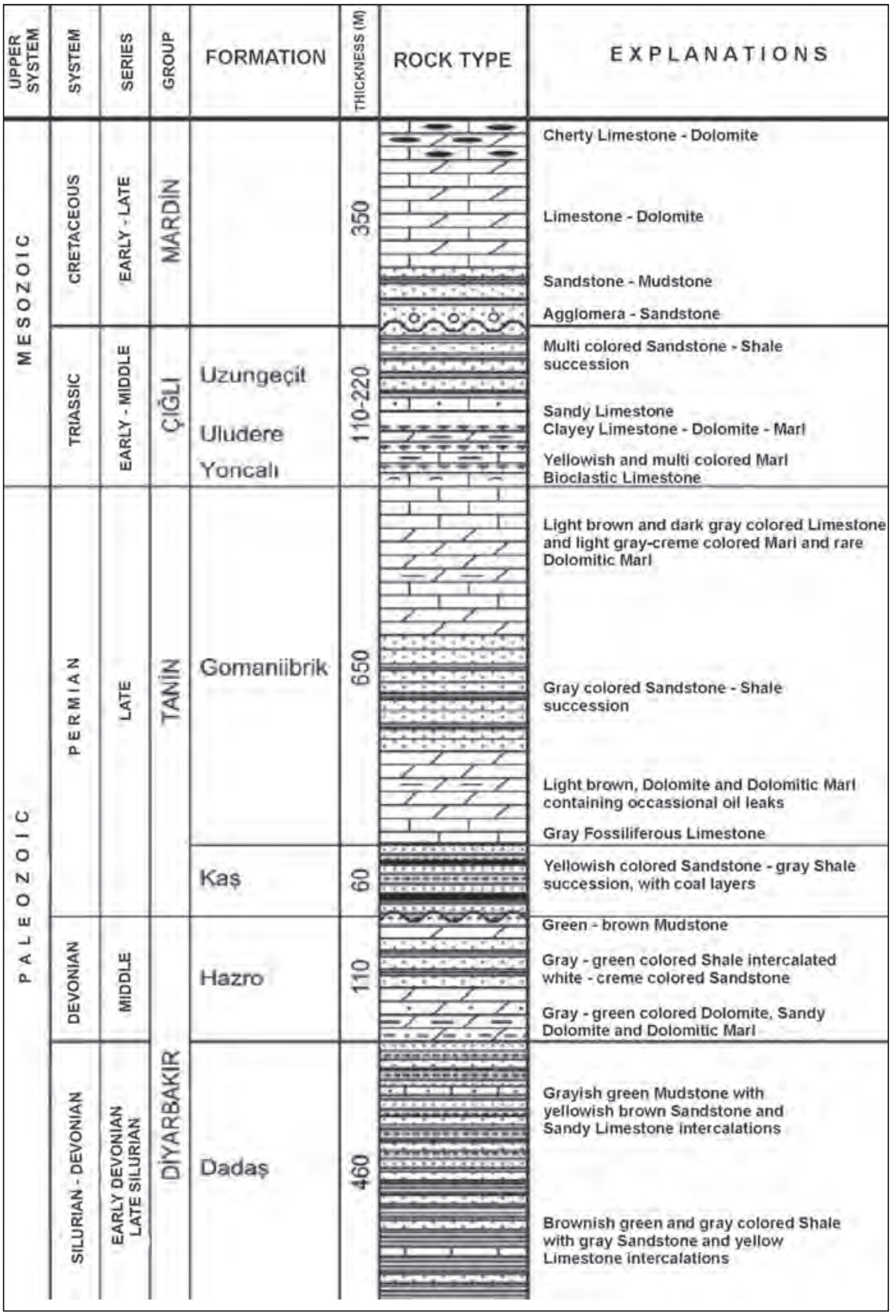

Figure 3- Generalized stratigraphic section of the visible autochthonous sequence from the Hazro anticline (not to scale) (Bozkaya et al., 2009).

abundant plant, coal, spore and pollen fragments (Ağralı and Akyol, 1967). According to spore and pollen investigations, the age of the formation was determined as Lower Permian (Ağralı and Akyol, 1967; Bozdoğan et al., 1987). The formation is mainly composed of gray-black coal and coaly shales with claret, yellow, pink and occasionally white sandstone intercalations. The sandstones exhibit a thickness between 0.7-2 m and shales, between 0.3-0.5 m. Pinkish claret colored sandstones within the middle levels is a characteristic nature of the formation. Coal rich levels exhibit 1 m thickness at bottom, 0.15 m at the middle and 0.3 as well as 1 m thicknesses at the top. Quartzarenite classified sandstones do not exhibit any lineation, are of medium-poorly sorted, angular-medium rounded ingredients. Silt sized quartz crystals were filled into the grain pores of the siliceous cemented sandstones. Sandstones with occasional clay matrix (>5%) were defined as clayey quartzarenite. Quartz, feldspar as well as clay/sericite and dolomite are common minerals in the silty shale or mudstones. Sparry textured dolomite (dolosparite, lithoclastic dolosparite) and limestones (lithosparite with dolomite and chert, dololitho-biomicrosparite) form carbonate rocks. Dolomitic rocks generally contain not only large sparry (sugar texture) dolomite crystals, but also chalcedonic quartz, glauconite and idiomorphic opaque minerals (likely to be pyrites). In some samples, algae fragments take parts in the center of idiomorphic dolomite crystals which exhibit zoning textures.

Upper Permian aged Gomaniibrik formation displays typical outcrops in the vicinity of Gomaniibrik Village, located in the northeastern of Hazro Town, and is conformable with underlying Kaş formation as well as with overlying Uludere formation belonging to Çığlı Group. The unit with about 650 m thickness, defined with vertical sections, was classified and observed as three facieses, as A, B, C, by Bozdoğan (1987). At the measured typical section, the bottom levels of the lithologies belonging to the unit are composed of carbonates with occasional oil leakages and these rocks are represented by gray fossiliferous limestone, gray-black dolomite, gray-black dolomitic marl and yellow clayey dolomites. The rocks, limestones with 2-3m, dolomites with 15-25cm, dolomitic marls with 0.5-1m thicknesses, form layers. Petroleum occurrences are found in the pores of 5-10cm diameter gray-black dolomite as in the form of being surrounded by calcite crystals. By this study, petroleum leakages of the Permian aged units are firstly mentioned. The middle level is essentially composed of clastic rocks which are mostly gray, pinkish colored and occasionally iron containing sandstones, tile colored mudstone and gray shales. The sandstones are of 10-20cm, occasionally 40cm thick, and clayey levels' forming units, of mudstone and shales with 30-50cm thick levels. Carbonate rocks are dominant at the upper levels, similar to the bottom levels. Lithologies in this level are generally yellowish or tile colored coated and represented with mainly grayish cream colored dolomite, green and greenish cream colored dolomitic marl and gray colored limestones. The dolomites are observed as with 30-40cm thick protruded forms, among clay levels. Clayey levels represented by dolomitic marls and clayey dolomites are much thicker (0.4-1.0m) than the dolomites. The bottom and upper parts of the formation indicate a shallow marine, but middle level, a river and an ebb-tide effective delta plain depositional environment (Bozkaya et al., 2009).

In dolosparitic dolomites, subidiomorphic dolomite crystals generally own large sparry (sugar texture) but partially microsparitic texture and include very little amount of quartz extra clasts. The biomicrite limestones are characteristics of containing abundant neritic fossil fragments. The limestones' not exhibiting any brecciated and stylolitic texture was thought as a sign of their having an early diagenetic evolution. The sandsones (quartzarenite) are composed mainly of loosely cemented, sub angular quartzes and exhibit medium grade sorting (Figure 3).

Gomaniibrik formation is one of the most important units which starts with light gray, gray colored sandstone unit with petroleum marks, at the bottom, gray shale at the middle and continues upwardly as with reddish yellow colored siltstone, sandstones. The formation presents its vastest spreading in the vicinity of Gomaniibrik (Çökek su) Village, to the northeast of Hazro Town and extends westward up to Dadaş Village.

The total coal reserve, found in the Permian aged Gomaniibrik and Kaş formation was determined as about 2.3 million coals with 12 500 ton of apparent, about 400 000 ton of probable, and 1.8 million ton of possible reserves. Though there are various utilization possibilities of the coals, operated in the region, the coals are only used for domestic heating (Gümüşsu, 1988). Geologic units outcropped in the region did not allow larger coal deposits take places (Figure 2, 3 and 4) (Lebküchner, 1969).

The coals outcrop in a line, running from Dadaş Village to Gomaniibrik Village. The upper coal presents an operable potential at Dadaş region but the lower seam at Gomaniibrik region. The coals have three seams but the middle one does not exhibit proper thicknesses and properties to be mined out (Lebküchner, 1976). The upper coal has about 0.80-1.20m and the lower one, about 0.20-1.90m thicknesses in the coal bearing formations. The coal level, operated in Gomaniibrik region is the lower one. The coal, in the region, was operated by private companies at the past but there is no operation in the region at the present time. Chemical properties of the coals are given on table 1. The coals have high calorific value (5000 Kcal/kg), the ash content as about 25 % and very low moisture content (averagely 2%). The only negative property of this coal is respectively high sulfur content.

Çığlı Group consists of three formations, namely as Yoncalı, Uludere and Uzungeçit, from bottom to up. In this study, the formations were not observed with

Table 1- Average of some chemical analysis of Diyarbakır Hazro region coals (Lebküchner, 1961).

Analyses	Variation interval
Low Calorific Value (Kcal/kg)	5049 – 5588
Moisture %	1.17 – 2.34
Sulfur %	5.66 – 10
Ash %	23 – 30

their vast spreading, therefore not classified in detail, but taken as groups. Çığlı Group is observed along the north and western part of Hazro, such as encircling Gomaniibrik formation. Although the bottom and upper parts were not observed, Çığlı Group presents a disconformity of its borders with Gomaniibrik formation and Mardin Group, at the bottom and top, respectively (Günay, 1998). Since Çığlı and Mardin Group have no important relation within our study, they are here not mentioned in detail.

3. Material And Methods

13 channel samples with 5-10cm intervals were taken systematically from the coal outcrops. Due to systematic sampling from certain intervals of the coal seams, organic geochemical and petrographic analyses represent the coals (Figure 4). In order to determine the properties of inorganic components of the coals, XRD analyses of 10 the whole rock samples were conducted at Ankara TPAO Research Laboratory (Figure 5).

For chemical and elementary analysis, the coal samples were ground as in ASTM standards. Firstly, they were ground to < 100 mesh size, then, homogenized and analyzed. The analyses were carried out in MTA General Directorate's MAT Department Laboratories. Chemical analysis (total moisture, ash, volatile matter, fixed carbon and calorific value) were conducted with IKA 4000 adiabatic calorimeter and in TUBİTAK MAM Laboratories. Elementary analysis, as total sulfur, carbon, hydrogen and nitrogen, were carried out in the same laboratory with LECO analyzer.

For coal petrographic analysis, 14 samples were prepared according to ICCP standard (1998 and 2001) techniques. In order to determine maceral and mineral contents, white, reflected and fluorescence lights were used. A Leitz MPV-SP microscope was used to determine petrographic and mineralogic properties as well as reflectance measurements of the samples. Reflectance values of the samples were performed with using 32x and 50x oil objectives, at 546 nm wavelengths. For each modal analysis, 500 point and for reflectance measurements 100 point measurements were taken as basis. The refractive index (n) of the oil, used for reflectance measurement is 1.518 and the reflectance value of the used standard, sapphire, is

Figure 4- Field views (a, b, c, d) of the studied coals.

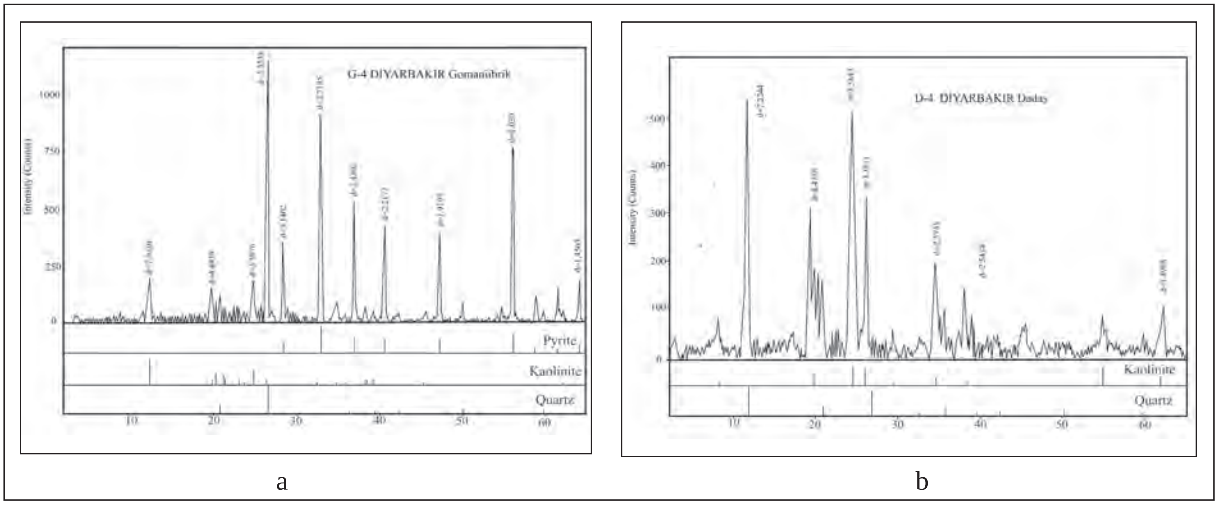

Figure 5a, b- XRD graphics of the studied coals.

0.548 %. MPV Geor software program was used for the reflectance measurements. Sample preparation, petrographic analyses and reflection measured all were carried out in MTA, MAT Department Laboratories (Ankara).

Standard palynologic methods (Durand and Nicaise, 1980; Tissot and Welte, 1984) were used to prepare kerogen slides of 5 samples, taken from the studied area. Kerogen spore alteration color indexes as well as organic content of the samples were determined with polarized microscope in the TPAO Research Center Laboratories (in Ankara). Hydrocarbon source rock properties of 14 samples were determined with TOC-Rock Eval pyrolysis analysis (Espitalié et al., 1985; Peters, 1986). For biomarker analysis, 5 samples differentiated with aid of Rock Eval, TOC results, were taken to dissolve in 40 hours within Dichloromethane in ASE 300 (Accelerated solvent Extraction). After dissolving, the leached materials were separated from asphalts with column chromatography and the dense material were analyzed with Agilent 6850 whole leachate GC, but gas chromatography mass spectrometer analysis were carried out in TUBİTAK MAM Laboratories with Agilent 7890A/5975C GC-MS instrument.

4. Findings And Discussions

4.1. Chemical and Elementary Analyses

Elementary analysis of coals include C, H, N+O and S. Elementary analysis of 10 samples showed the C ratio to be 23.11 – 25.11 %, H to be 2.12 - 2.32 %, N+O 10.85 – 12.97 %, S 0.60 - 0.65 %. Air dried samples tend to have C ratio as 35.16– 36.42 %; H content to be as 3.12 - 3.32 %; N+O, as 15.09 - 16.1 %; S, as 1.08 - 1.12 % (Table 2).

Table 2- Elementary Analysis of Hazro coals.

Sample	Original Sample				Dry Sample			
	C (%)	H (%)	(N+O) (%)	S (%)	C (%)	H (%)	(N+O) (%)	S (%)
G1	23.11	2.16	12.80	0.62	36.30	3.31	15.40	1.09
G2	24.43	2.12	10.85	0.64	36.42	3.15	15.63	1.11
G4	23.54	2.15	11.26	0.64	35.55	3.17	16.11	1.11
D4	24.71	2.32	12.30	0.61	35.72	3.14	15.56	1.07
D5	25.07	2.17	12.20	0.60	35.69	3.12	15.27	1.09
D6	24.10	2.20	12.97	0.65	36.01	3.32	15.12	1.12
D02	25.11	2.15	12.04	0.63	35.16	3.18	15.45	1.08
HDG	24.24	2.14	10,98	0.63	35.82	3.20	15.55	1.09
HDO	23,11	2.33	12.65	0.62	36.12	3.19	15.09	1.10
DO7	23.94	2.16	11.40	0.65	35.45	3.21	15.80	1.07

Ash content of 15 coal samples was determined, the dominant ingredient was found to be SiO_2 with 32.4 – 44.53 %. Al_2O_3+TiO_2 content is between 15.0 - 18.1 %, Fe_2O_3 between 7.6 - 8.77 %, CaO between 1.69 – 20.10 %, MgO between 4.45 - 5.80 %, SO_3 between 10.5 - 16.36 % and Na_2O+K_2O between 1.35 - 1.52 % (Table 3). High calcium rate stands for plant remnant's bacterial decay, gelinite and pyrite content of coals are thought to be derived from bacterial reduction of sulfates. Pyrite content of the coals and associated clays are considerably high and observed as framboidal at most. Minerals within macerals are observed with various shapes, thicknesses and as filling voids as well as veins. On Table 4, total moisture, ash, sulfur, volatile matter and calorific values and on Table 5, petrographic composition and huminite reflection (Rmax) values were exhibited in detail.

Ash content of the observed coals are considerably high (20.51–76.42 %, in original and 26.42–81.72 % in dry coals) which comply with petrographic composition as well. This data reveals the coal formation, mostly in brackish water conditions, high organic material decaying and abundant inorganic material composition as a result of these (Teichmuller et al., 1998). Sulfur content of the original samples vary between 0.07–10.25 for original, 0.08–10.43 for dry coal samples and this, together with the ash values indicate considerably raised terrestrial environment. The volatile matter content of the coals (16.67 – 33.82 % as original and 17.44 – 37.77 % as air dried), and the elementary analysis of the coals seem to comply with the coal rank (Table 4 and 5). As can be understood from the tables, the coalification rank of the coals complies with sub-bituminous and bituminous ranks (Stach et al., 1982). Partially obtained high coal rank was probably resulted from the tectonic activities taken places, close to the region. Upper calorific values of the coals vary between 1217- 5244 (averagely 3165) Kcal/kg of the original samples, as in air dried basis 1274 - 5329 (averagely 3432) Kcal/kg. In order to find ASTM colification rank, the calorific values were converted to BTU/lb as in dried, mineral matter free basis. Element analysis results, as seen on Tables 4 and 5, comply with coalification ranks and refer to Sub Bituminous B/C – Bituminous Coal types (ASTM 1983, D388-82) (Table 6).

High sulfur content of the coals may be resulted from lake water or brackish water conditions or high pH as well as low Eh conditions and sulphate ion abundances within the lake waters. It can also be derived from primary organic material as well as associated rocks (Stach et al, 1982)

4.2. Petrographic Evaluation

Dull bands and banded lihotype successions are predominantly observed in the studied coals. Petrographic evaluations, determinations of liptinite, huminite (vitrinite) and inertinite macerals were determined as in Stach et al. (1982) (Figure 6), and the depositional environment interpretation was realized with using Diessel (1986) graphic) (Figure 7).

The petrographic data were presented on the diagrams (Figure 8) and Tables (Table 5 and 6). As a result of petrographical analysis, coals tend to have huminite (vitrinite) macerals dominantly and limnic depositional environment. Petrographic observations also imply a heterogeneous material accumulation during the peat development. Huminite (vitrinite) maceral distribution of the coals vary between 33 - 55 % and is the predominant maceral. Gelinites are

Table 3- Ash components of Hazro coal samples.

Sample	SiO_2 (%)	$Al_2O_{3+}TiO_2$ (%)	Fe_2O_3 (%)	CaO (%)	MgO (%)	SO_3 (%)	Na_2O+K_2O (%)
G1	44.53	17.10	8.77	12.69	4.85	10.66	1.40
G2	32.40	17.1	8.20	20.05	4.50	16.33	1.42
G4	42.35	15.70	7.84	14.30	5.80	12.50	1.51
D4	33.49	18.11	8.10	18.09	4.50	16.36	1.35
D5	43.46	16.10	8.70	14.79	4.87	10.60	1.48
D6	35.44	15.00	8.22	20.10	4.60	16.24	1.40
D02	41.30	15.14	8.20	13.62	4.80	15.44	1.50
HDG	34.35	15.20	7.60	13.30	4.45	10.50	1.41
HDO	40.15	16.30	8.51	15.69	4.70	12.60	1.44
DO7	41.20	17.05	8.60	18.23	4.50	15.74	1.52

Table 4- Proximate analysis of Hazro coal samples

Sample	M %	VM %	Ash %	Total Sulfur %	UCV (Kcal/kg)	LCV (Kcal/kg
G1	6.49	17.08	76.42	0.07	-	-
G2	4.45	16.67	66.59	1.49	1217	1134
G4	1.61	33.82	32.10	10.27	5244	5028
D4	10.83	19.68	65.45	0.22	2	-
D5	8.85	17.57	72.83	0.12	1	-
D6	10.36	27.83	40.87	0.85	2747	2569
D02	8.58	27.36	51.61	1.15	1842	1693
HDG	22.38	29.32	20.51	0.75	3580	3314
HDO	2.62	22.75	48.73	1.87	3354	3215
DO7	2.47	26.74	42.77	1.74	4177	4005

Dried Sample

Sample	VM %	Ash %	Total Sulfur %	UCV (Kcal/kg)	LCV (Kcal/kg)
G1	18.27	81.72	0.08	-	-
G2	17.44	69.68	1.56	1274	1212
G4	34.37	32.62	10.43	5329	5120
D4	22.07	73.40	0.25	2	-
D5	19.27	79.90	0.13	1	-
D6	31.04	45.59	0.95	3065	2929
D02	29.93	56.45	1.26	2015	1904
HDG	37.77	26.42	0.97	4612	4428
HDO	23.36	50.04	1.92	3444	3316
DO7	27.41	43.85	1.78	4283	4121

M- Moisture; VM- Volatile Matter; UCV-Upper Calorific Value; LCV-Lower Calorific Value.

the macerals in huminite macerals which are jellified macerals showing no cellular structures. Detritic macerals, densinites are considerably, very common in the samples (Table 5). Inertinite and liptinite maceral group are rather less than huminite group macerals.

Liptinite contents were determined between 2 - 6 %, sporinite, alginate and cutinites are the most abundant liptinite macerals. Inertinite group macerals vary between 3-8 % and are mostly composed of macrinite and fusinites (Figure 5). Ratios of the maceral groups are shown on Table 5, coal maturity values on Figure 6 and the reflection values on Table 6. To these, the coals exhibit 0.458-1.141 % reflection values and sub-bituminous to bituminous coalification ranks. Considerably high variations of the reflectance are thought to be likely resulted from partial interactions of the tectonic activities in the region.

High gelinite content is a reflection of a characteristic nature of calcium rich coals and fusinite and macrinite like macerals indicate increase of oxidation and decrease of water levels within swamps (Figure 6 b, c and d) (Flores, 2002; Stach et al., 1982). The coals contain high amount of spores and clay minerals (Figure 6a and c) also which indicate abundant bacterial activities as well as decaying, in reed moor environment and underwater conditions. Mineral matter ratio changes between 14 - 30 % and mostly formed with carbonates, clays and silicate minerals which probably formed as a result of biologic activities in the region (Figure 6a and c). These levels indicate occasional inorganic material inputs instead of organic material, during peat development. High mineral matter content, detritic maceral inclusion and rare presence of the textures refer exposition of the materials to insitu transportations as well as tectonic activities. In figure 6, observation of desiccation cracks as micro traces indicates the abundance of high moisture absorbing mineral matter such as clay minerals and a high moisture loss. Slightly higher reflection values refer a short distance of the coal environment to the very important tectonic lineation (the Arabian plate suture zone and associated faults).

High calcium rate indicates alkaline depositional environment, bacteria the imply formations of humic

Table 5- Petrographical analysis of Hazro coal samples (as %).

No	Sample	Huminite								Liptinite				Inertinite			Pyrite				INOR (Cl+Qz +Ca)
		HTEL			DHUM		HCOL		TOT HUM	Sp	Alg	Cut	TOT LIP	Fus	Ma	TOT INER	Fr	Eu	Fil	TOT PYR	
		Tx	Tul	Eul	Att	Dn	Gel	Cor													
1	G1	6	5	4	2	6	28	1	52	3	1	1	5	1	3	4	3	1	1	5	34
2	G2	2	3	4	2	4	32	1	48	2	0	1	3	1	3	4	3	1	0	4	41
3	G4	3	4	5	2	7	28	1	50	2	2	1	5	1	3	4	2	1	1	4	37
4	X	3	3	4	2	5	29	1	47	2	1	1	4	1	3	4	3	1	0	5	36
5	D4	3	4	4	0	5	26	1	43	2	2	0	4	2	3	5	2	0	0	2	46
6	D5	1	2	3	0	3	24	0	33	2	0	0	2	0	3	3	2	0	0	2	60
7	D6	3	5	6	3	7	23	2	49	3	2	1	6	1	3	4	3	1	1	5	36
8	XX	2	4	5	2	7	26	2	48	2	2	1	5	1	3	4	3	1	0	4	35
9	D02	2	4	7	3	8	29	2	55	3	2	1	6	2	6	8	2	1	0	3	28
10	HDG	7	4	4	3	7	23	2	50	2	1	1	4	2	4	6	4	1	1	6	40
11	XXX	7	5	2	3	6	24	2	49	2	1	1	4	2	3	5	4	0	1	5	32
12	HDO	3	2	2	5	4	29	1	46	3	2	1	6	1	3	4	4	1	0	5	44
13	DO7	4	3	4	2	6	30	2	51	2	1	0	3	1	4	5	3	0	1	5	41

HTEL- Telohuminite; DHUM- Detrohuminite; HCOL- Gelohuminite; TOT- total; HUM- huminite; LIP- Liptinite; INER- Inertinit; PYR- Pyrite; Cl- Clay; Qz- Quartz; Ca- Calcite; INOR- inorganik material; Tx- Textinite; Tul- Texto-ulminite; Eul- Eu-ulminite; Att- Attrinite; Dn- Densinite; Gel- Gelinite; Cor- Corpohüminite; Sp- sporinite; Alg- Alginite; Cut- Cutinite; Fus- Fusinite; Ma- Macrinite; Fr.- Framboidal; Eu- Euhedral crystal; Fil.- Void and fracture filling pyrites.

Table 6- Reflection values of Hazro coal samples and their corresponding ranks.

No	Sample	Rmax %	Rmean %	Rmin %	St.D. %	Coalification Rank
1	G1	0.478	0.381	0.281	0.013	Sub bituminous claystone
2	G2	1.02	0.912	0.850	0.02	Clayey bituminous coal
3	G4	0.458	0.440	0.399	0.019	Sub bituminous clay
4	D4	0.527	0.496	0.412	0.014	Sub bituminous claystone
5	D5	1.141	0.992	0.864	0.019	Bituminous coaly claystone
6	D6	0.966	0.919	0.851	0.014	Bituminous coal
7	D02	0.922	0.888	0.820	0.019	Bituminous coal
8	HDG	1.076	1.003	0.968	0.038	Bituminous coal
9	HDO	0.569	0.539	0.518	0.013	Sub bituminous coal
10	DO7	0.658	0.613	0.493	0.014	Bituminous coal

gels, nitrogen and hydrogen rich coal products (Teichmuller et al., 1998). These properties were also observed in the Amynteo Basin Pliocene aged lignite as in the same way (lordanidis and Georgakopoulos, A., 2003). TPI (Tissue Preservation Index) and VI (Vegetation Index) values were used to determine the pale depositional environments according to Diessel (1986) (Figure 7). Low TPI values developed either

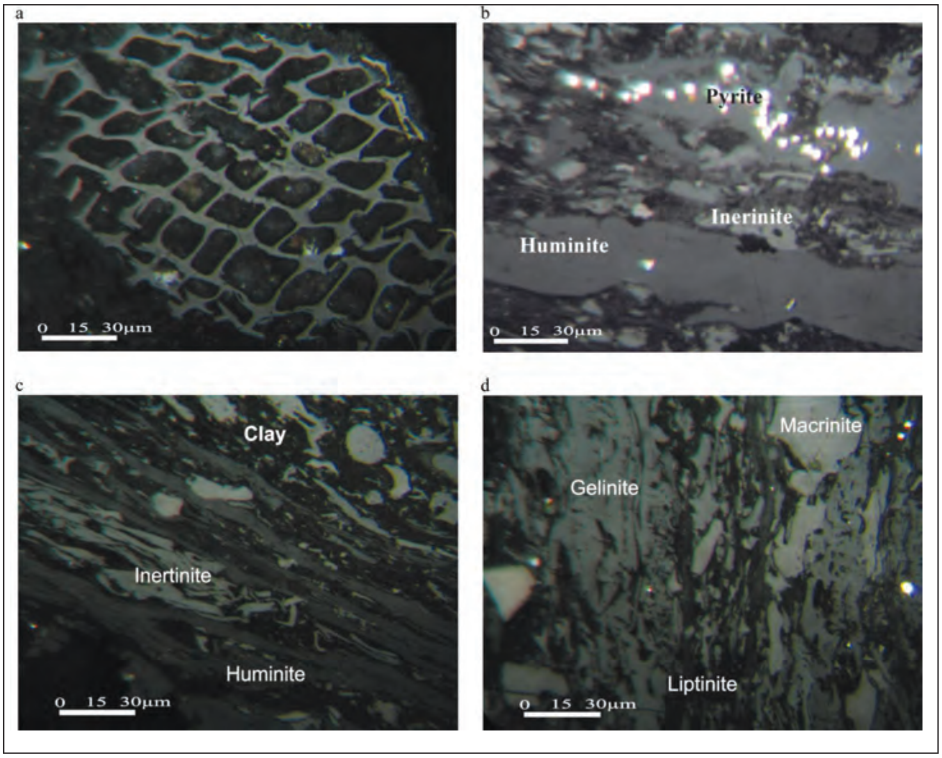

Figure 6- Petrographic images of Hazro Dadaş Coals.

a- Typical cell appearances of huminites (textinite), filled with dark colored clay minerals.
b- Gray colored common huminite maceral (gelinite) observed in the coals, white colored inertinites and pyrites.
c- Inertinite (macrinite) macerals observed commonly in the coals, common gray colored huminites and dark colored clay minerals.
d- Common gray colored maceral, gelinite and white colored macrinite macerals and thin dark gray colored liptinites.

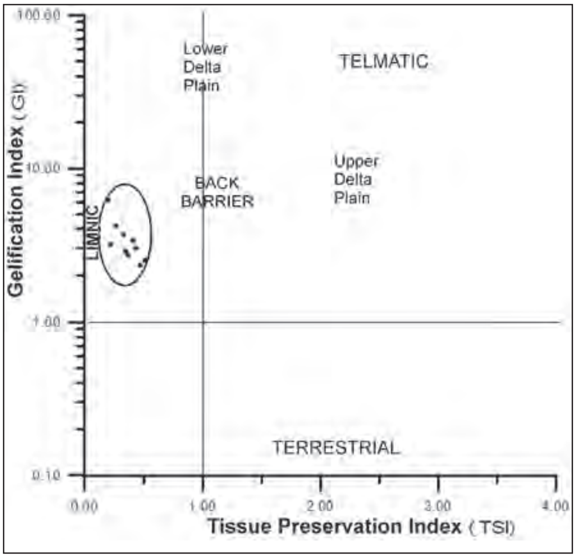

Figure 7- Located depositional environments of the Hazro coals on the Diessel (1986) graphics, based on the conducted petrographic analysis.

depending on the vegetation type (high angiosperm/gymnosperm ratio), or on low tissue preservation conditions (Kolcon and Sachsenhofer, 1999; Bechtel et al., 2005). TPI values for Hazro coals vary between 0.1 – 0.5 %. The GI value indicates underground water level and/or pH level. For jellification, regular water flow, bacterial activity and low acidic conditions are essentials (Kolcon and Sachsenhofer, 1999; Georgakopoulos, A. and Valceva, 2000). GI value changes between 2 and 7 for the Hazro coals (Figure 7).

TPI values being lower than 0.5 and GI values higher than 2, also pyrite content refer a limnic paleo-depositional environment. Coalification was developed in an underwater level with normal subsidence rate; taking places in autochthonous to hypoautochtonous conditions. Here, high alkalinity conditions were the case in point. Low TPI value indicates high bacterial activity and high pH value, in addition, common presence of gastropods are good supporting evidences for alkaline environmental conditions such as seen in Amyneto Basin (Greece) (Iordanidis and Georgakopoulos, A., 2003).

To the XRD results (Figure 5a and b), most of the inorganic contain clay minerals, quartz and pyrites. Pyrite and clay inclusions of the coals were also determined in the petrographical studies (Table 5 and Figures 6a, b, c).

4.3. Geochemical Evaluation

As geochemical evaluations, Total Organic Carbon (TOC), organic material type and for maturation, Rock-Eval Pyrolysis analysis was carried out. GC, GC-MS and GC-IRMS analysis were conducted to determine biomarker data of the samples in detail. Organic material abundance, organic type, diagenetic development and source rock potential of the organics were produced with Rock–Eval pyrolysis data. Though this technique is performed on carbonate shale like rocks, which are thought to have source rock potentials, since Rock-Eval device works well on coaly samples and has well additions to petrographical investigations, the usage of it became very common for coal researches, as well (Teichmuller and Durand, 1983; Durand and Nicaise, 1980; Durand and Parette, 1983; Fowler et al., 1991; Korkmaz and Gulbay, 2007; Erik, et al. 2008, Kavak and Toprak, 2010 and 2011).

4.4. Organic Matter Quantity (Total Organic Carbon)

Total Organic Carbon (TOC %) were carried out on 13 samples, the values tend to vary between 3.75–50.20 % (Table 7). The results reveals that Hazro coals are rich in organic content (TOC > 3.75) and able to be considered as source rocks.

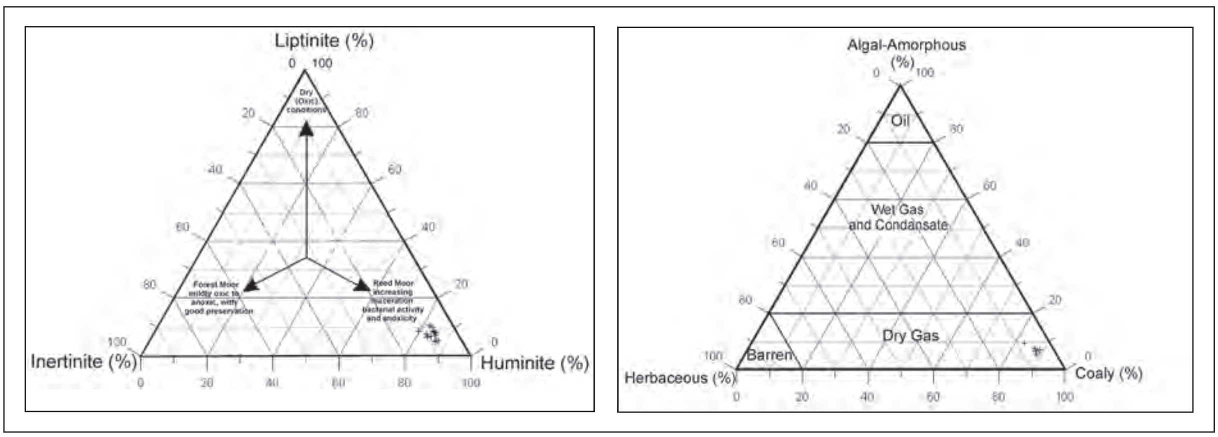

Figure 8a, b- Triangular diagrams of Organic matter types for Hazro Dadaş coal samples.

Table 7- Total organic carbon (TOC %) and Rock-Eval pyrolysis results of Hazro coal samples.

Sample	TOC	S1	S2	S3	S2/S3	Tmax	HI	Ol	Pl	PY
G1	3.75	0	0.06	3.01	0.019	537	2	80	0.01	0.06
G2	16.70	0.25	14.82	9.17	1.61	431	89	55	0.02	15.07
G4	50.20	6.88	172.04	0.99	173.7	343	343	2	0.99	178.92
G5	32.20	4,23	121,03	4,64	11,34	389	243	32	0,67	98,78
D4	9.12	0	0.92	7.68	0.11	441	10	85	0	0.92
D5	4.78	0	0.16	3.99	0.04	442	3	84	0.01	0.16
D6	30.86	0.21	18.31	21.76	0.63	435	60	71	0.01	18.52
D7	22,3	0,11	2,14	9,89	0,41	440	19	77	0,01	15,06
D02	23.70	0.09	7.34	17.08	0.42	438	31	73	0.01	7.43
HDG	40.64	0.54	22.55	24.51	0.92	438	54	60	0.02	23.09
HDH	30,01	0,32	16,36	18,03	0,71	426	42	66	0,01	23,06
HDO	36.10	1.24	80.18	0.83	96.6	427	222	2	0.02	81.42
DO7	43.22	2.70	129.24	0.79	163.5	299	299	2	0.02	131.94

4.5. Organic Matter Type

In order a rock to carry a property of being a source rock, it should absolutely contain enough organic material and the organic matter types should be proper for petroleum or gas generation. For this reason, organic matter types are defined with geochemical data. Besides organic petrographic analysis, Hydrogen Index (HI), Oxygen Index (OI) and Tmax analysis' results are used to determine organic types of the materials with evaluating HI-OI and HI-Tmax diagrams of the samples. With pyrolysis analysis, kerogen types and maturation level are determined. Hydrocarbon rock potential data are obtained from kerogen type data, received from Rock-Eval pyrolysis, and organic matter types as well as their results. According to HI and OI data, organic material points out three types of Kerogens which may carry petroleum generation potentials, classified as Type I, II and III (Tissot and Welte, 1984).

Mineral matter content, as seen on these samples, which are rich in clays and carbonates, affects pyrolysis results (Peters, 1986; Langford and Blanc-Valleron, 1990). Majority of the samples are scattered in Type II-III (terrestrial and marine) and Type III (terrestrial and residual organic material) regions, as Hydrogen Index-Oxygen Index and HI-Tmax graphics are considered. Petroleum generation potential of these samples seems to be limited but little amount of gas generation potential may be discussed.

Hydrogen index values of Hazro coals vary between 31 - 343 mg HC/g TOC and oxygen index values between 32 - 85 mg CO_2/g TOC. Production Index (PI): S_1 / (S_1+S_2) value especially should be higher than 0.05 %, then, interpretation becomes important. Hazro samples exhibit an average of 0.02 % value (Figure 7).

Some high oxygen index values (>50 mg CO_2/g TOC) have probably developed due to mineral matrices and mineral decomposition during pyrolysis. If mineral matter content of the studied samples is especially rich in clay and carbonates, the results of pyrolysis process may, then, be affected (Peters, 1986; Langford and Blanc-Valleron, 1990). In order to determine factors effecting pyrolysis data more, maceral composition, which are debated very much in comparisons, were taken into consideration. For example, though there is a negative relation between liptinite content and hydrogen index, hydrogen index relation becomes positive when liptinites are added to huminite ratios (Figure 9 and 10).

In addition, there is a negative relation between mineral matter content and hydrogen index, TOC, Pc, Rc, values, the correlation coefficient (Pearson Coefficient) is very low, therefore, was not shown on the graphics. In the Hydrogen Index-Oxygen Index and HI-T_{max} graphics, majority of the samples are distributed in Type II-III (Figure 9).

This definition is also supported with palynologic determinations from the Kerogen preparations, which indicates coaly-woody materials' dominance. Coaly organic matters of the samples seem to be of 78 - 87 %, woody 6 – 12 %, herbaceous 4-7 % and 5-9 % of algae amorphous organic matter (Figure 8). It is thought that amorphous organic materials probably

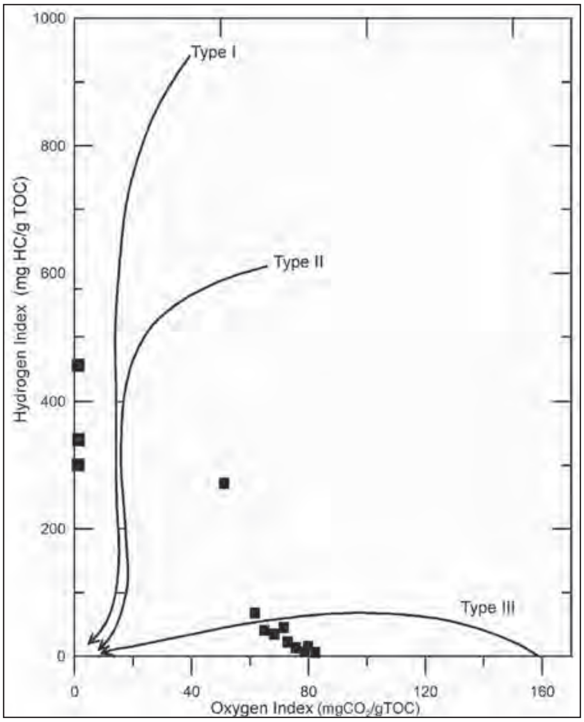

Figure 9- Hydrogen Index- Oxygen Index diagrams of the studied samples (Tissot and Welte, 1984).

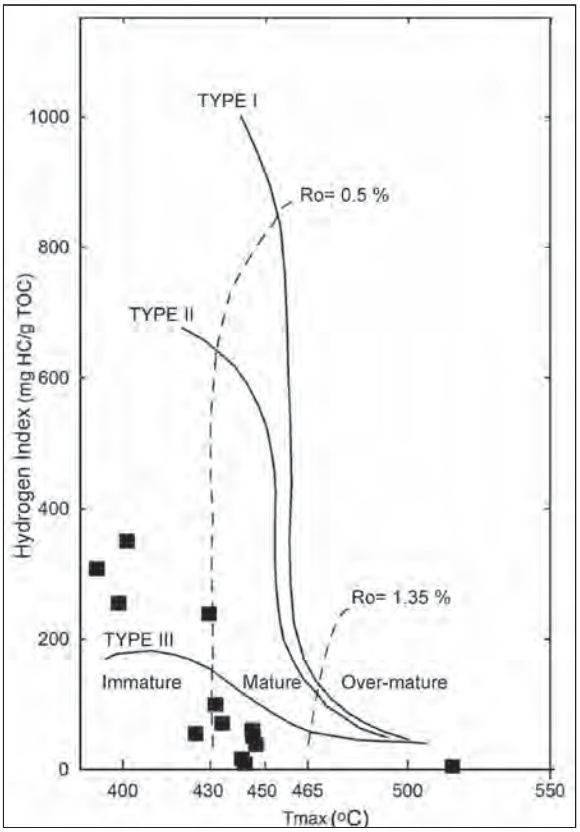

Figure 10- Classification of Kerogene types by Hydrogen Index-Tmax diagrams (Mukhopadyay et al., 1995).

formed during transportation of the terrestrial sourced materials, with alteration as well as disintegration of the materials.

Low detection value of low carbon numbered n-alkenes, especially of n-C_6 and n-C_{17}, additionally not having of organic compounds above C_{32} in gas chromatograms, point out terrestrial originated organic materials. In biomarker analysis of the Hazro samples, high molecular abundant (C_{20}+) compounds on n-alkenes are predominant and predominance of odd numbered n-alkenes of C_{27}-C_{28} as well as C_{29} steranes against to C_{27} - C_{28}, and abundance of C_{29} αααR isomers indicate organic matters derived from terrestrial materials.

4.6. Organic Maturation

Organics within sediments are affected with increasing heat, resulted from increase of burial depth and produce hydrocarbons as a result of various chemical reactions. In order hydrocarbons to generate, organic maturity and the required heat conditions should be attained to disintegrate kerogen. Organic analysis methods are classified as optic and chemical. The most commonly used method to obtain Tmax value as a result of pyrolysis. Tmax value which reveals maturity of the source rock, increase with dept increase (Espitalié et al., 1977).

But faulting, folding, disconformities, geothermal gradient like factors, migrated petroleum, quality of the sample, organic matter amount, mineral matrix within the rock and mistakes during analysis may exhibit differences in obtaining exact Tmax values (Peters, 1986; Arfaouni et al., 2007).

Tmax (^oC) value is an organic geochemical parameter to define heat maturity value and T_{max} (^oC) values for Hazro samples vary between 299-537^oC, and the average value is 418^oC (Table 7). These values point out that the maturity of the organic rich parts of the coals stand in immature-pre mature zone. From the kerogen samples, light yellow, light brown organic matter alteration color, light yellow- colorless spores, the reflection values all support the Tmax values. In the HI-T_{max} graphic, majority of the samples are scattered in pre mature-immature zone (Figure 7). PI values of these samples are >0.15 and refer to an immature source rock. Huminite (vitrinite) reflection values vary between 0.458 and 1.141 % which refer to matured material.

Since high ash content affects this comparison, huminite reflection and calorific values of the coal samples with less than 15% ash content were compared. Although both data individually indicate immature level, the reason for different huminite reflection (R_{max}) value and the parameters in Figure 7 is tectonic activity of the region to affect the values and produce organic matters with different properties during coalification.

Besides, low bitumen/TOC ratio as well as sterane and triterpane (biomarker) in the gas chromatographies also refer to an immature zone (Tissot and Welte, 1984). Another maturity parameter is generated from the C_{29} regular steranes, which are 5α(H), 14β(H), 17β(H) C_{29} sterane and 5α(H), 14α(H), 17α(H) C_{29} sterane (αββ/ (αββ+ααα)) ratio. Ts/Tm ratio is 0.52–0.58.

4.7. Hydrocarbon Generation Potential

Hydrocarbon generation potential is also evaluated with Potential Yield (PY: S1+S2), generally complies with TOC results. Interpretation of Hydrocarbon generation potential of the samples with different techniques and graphics as well as their comparison will prevent mistakes to be made. The source richness diagram (HI-TOC) (Jackson et al., 1985) was used to determine the source especially of the coal (Figure 11). For hydrocarbon generation, the required heat should especially be attained to a necessary temperature to disintegrate kerogens and to provide organic maturity. Maturity was evaluated with considering Tmax and PI values (Figure 10).

S_1 values of the samples seem to be very low and vary between 1.24–6.88 mg HC/g rock. S2 values change between 18.31 – 172.04 mg HC/g rock (Figure 7). When S_2 value is lower than 4.0 mg HC/g rock, weak source rock, but in the case of higher than 4.0, hydrocarbon mother rock potential is considered (Hunt, 1967 and 1995; Peters et al., 2004; Erik, et al., 2008). In this case, S_2 values of the samples refer good or very good mother rock potential (Figure 7). Though the coal samples present pretty good rock potential values, the organically rich carbonaceous levels do not have rock potential at all.

The most crucial data for liquid hydrocarbon generation from especially coal originated materials is the presence of hydrogen containing organic material. To Hunt (1995), a higher TOC value than 200 mg HC/g is required for hydrocarbon generation from coals and terrestrial materials. High hydrogen index and the distribution of the samples in HI-T_{max} diagram imply that there were pythogenetic organic input and limited gas generation potential in the environment.

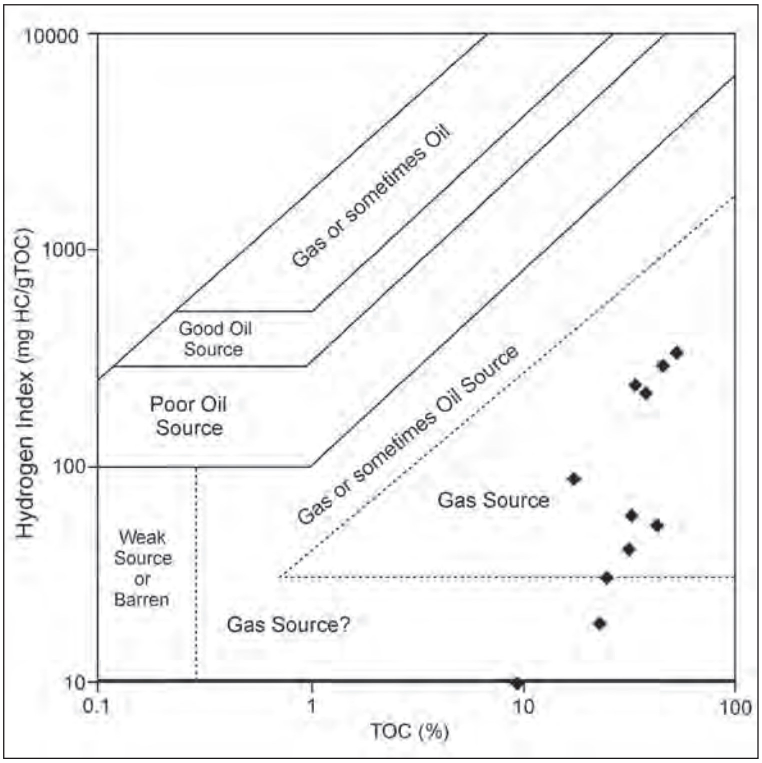

Figure 11- Hydrogen Index-TOC diagram of the Hazro Dadaş coal samples (developed from Jackson et al., 1985)

As in the studied samples, humic coals form from TYPE III kerogens and may have potential to generate gasses. Besides there is a gas generation capability potential of Diyarbakır-Hazro-Dadaş coals, their incomplete maturation has prevented it. Hydrocarbon generation index is also named as genetic potential or production index and show similar results in the same way of using (S1+S2), TOC values. Genetic potential values vary between 0.06 - 178.92 mg HC/g rock, and 19.30 mg HC/g rock as average (Figure 11). Some samples scatter in the weak generation potential area of the HI-TOC diagram and some samples indicate gas and little petroleum generation potential.

Table 8- Biomarker parameters derived from the m/z 217 and m/z 191 mass chromatograms.

			191			217			
Sample	^{13}**C**	**Standard Deviation**	**H/(H+M)**	**Ts/Tm**	C_{31} $\frac{22S}{22S+22R}$	C_{29} $\frac{20S}{20S+20R}$	C_{27} **%**	C_{28} **%**	C_{29} **%**
G4	-23.06	0.34	0.84	0.32	0.57	0.40	31	34	35
HDG	-22.86	0.02	0.71	0.06	0.58	0.46	20	44	36
D6	-21.96	0.09	0,59	0,19	0,59	0,42	24	42	34
DO7	-24.73	0.21	0.69	0.21	0.56	0,41	25	43	32

Table 9- Sterane peak determinations on m/z 217 mass chromatograms.

Peak Order	Components
1	C27 13β(H),17α(H)-DIASTERANE (20S)
2	C27 13β(H),17α(H)-DIASTERANE (20R)
3	C27 13β(H),17α(H)-DIASTERANE (20S)
4	C27 13β(H),17α(H)-DIASTERANE (20R)
5	C28 13β(H),17α(H)-DIASTERANE (20S)
6	C28 13β(H),17α(H)-DIASTERANE (20R)
7	C28 13β(H),17β(H)-DIASTERANE (20S)
8	C27 5α(H),14α(H),17α(H)-STERANE (20S)+C28 13α(H),17β(H)-DIASTERANE (20S)
9	C27 5α(H),14β(H),17β(H)-STERANE (20R)+C29 13β(H),17α(H)-DIASTERANE (20S)
10	C27 5α(H),14β(H),17β(H)-STERANE (20S)+C28 13α(H),17β(H)-DIASTERANE (20R)
11	C27 5α(H),14α(H),17α(H)-STERANE (20R)
12	C29 13β(H),17α(H)-DIASTERANE (20R)
13	C29 13α(H),17β(H)-DIASTERANE (20S)
14	C28 5α(H),14α(H)-17α(H)-STERANE (20S)
15	C28 5α(H),14β(H)-17β(H)-STERANE (20R)+ C29 13α(H),17β(H)-DIASTERANE (20R)
16	C28 5α(H),14β(H)-17β(H)-STERANE (20S)
17	C28 5α(H),14α(H),17α(H)-STERANE (20R)
18	C29 5α(H),14β(H),17α(H)-STERANE (20R)
19	C29 5α(H),14β(H),17β(H)-STERANE (20R)
20	C29 5α(H),14β(H),17β(H)-STERANE (20S)
21	C29 5α(H),14α(H),17α(H)-STERANE (20R)
22	C29 5α(H),14α(H),17α(H)-STERANE (20S)
23	C30 5α(H),14β(H)-17β(H)-STERANE (20R)
24	C30 5α(H),14β(H)-17β(H)-STERANE (20S)
25	C30 5α(H),14α(H),17α(H)-STERANE (20R)

Table 10- Triterpane peak determinations on m/z 191 mass chromatograms.

Peak Order	Components
1	C19 TRICYCLICTERPANE
2	C20 TRICYCLICTERPANE
3	C21 TRICYCLICTERPANE
4	C22 TRICYCLICTERPANE
5	C23 TRICYCLICTERPANE
6	C24 TRICYCLICTERPANE
7	C25 TRICYCLICTERPANE (22S+22R)
8	C24 TETRACYCLICHOPANE (SECO)
9	C26 TRICYCLICTERPANE 22 (S)
10	C26 TRICYCLICTERPANE 22 (R)
11	C28 TRICYCLICTERPANE
12	C29 TRICYCLICTERPANE
13	C27 18α(H)-22,29,30-TRISNORHOPANE (Ts)
14	C27 17α(H)-22,29,30-TRISNORHOPANE (Tm)
15	17α(H)-29,30-BISNORHOPANE
16	C30 TRICYCLICTERPANE
17	17α(H)-28,30-BISNORHOPANE
18	C29 17α(H),21β(H)-30-NORHOPANE
19	C29 Ts (18α(H)-30-NORHOPANE
20	C30 17α(H) DIAHOPANE
21	C29 17β(H),21α(H)-30 NORMORATENE
22	OLEANANE
23	C30 17α(H),21β(H)-HOPANE
24	C30 17β(H),21α(H)-MORETANE
25	C31 17α(H),21β(H)-30-HOMOHOPANE (22S)
26	C31 17α(H),21β(H)-30-HOMOHOPANE (22R)
27	GAMMACERANE
28	HOMOMORETANE
29	HOMOHOPANE
30	C32 17α(H),21β(H)-30,31-BISHOMOHOPANE (22R)
31	C33 17α(H),21β(H)-30,31,32-TRISHOMOHOPANE (22S)
32	C33 17α(H),21β(H)-30,31,32-TRISHOMOHOPANE (22R)
33	C34 17α(H),21β(H)-30,31,32,33-TETRAKISHOMOHOPANE (22S)
34	C34 17α(H),21β(H)-30,31,32,33-TETRAKISHOMOHOPANE (22R)
35	C35 17α(H),21β(H)-30,31,32,33,34-PENTAKISHOMOHOPANE (22S)
36	C35 17α(H),21β(H)-30,31,32,33,34-PENTAKISHOMOHOPANE (22R)

According to organic maturation data of the coals as well as organically rich levels, despite containing enough organic material, their maturation level prevents the generation.

4.8. Molecular Composition of the Coals

The leaching amount of the studied coals were low (between 14.69 and 92.40 ppm), the composition contains mostly resins and asphalthenes which are of low organic maturity. The distributions of steranes and triterpanes and their peak definitions were carried out on m/z 191 and m/z 217 chromatograms (Table 9 and 10).

n-alkenes are distributed in C_{20}/C_{32} (Table 11) interval (Figure 12a and b). In GC analysis low carbon numbered n-alkenes as n-C_{17}, n-C_{27}, n-C_{30} and n-C_3, as well as n-alkenes with CS2 and benzene were determined. Typical saturated hydrocarbon GC-MS data of the samples are shown on Figure 13a, b. c. The main biomarkers are C_{25} (22S+22R) tricyclicterpane, C_{24} tetracyclicterpane (seco), C_{26} 22R tricyclicterpane and C_{28} tricyclicterpanes. Presence of such triterpanoid compounds in the coals indicates their high terrestrial plant composition but the presence of gammacerane, their hypersaline depositional conditions. Relative abundance of long chained C_{27}-C_{31} alkenes with total n-alkenes indicate terrestrial plants (Moldowan et al., 1985), the short chained n-alkenes (<C_{20}) of their low ratio within the Hazro samples mostly present in algae and microorganisms. Predominantly medium and high molecular weighted n-alkenes (C_{21}-$_{25}$) are common in the samples, indicating the presence of terrestrial and limnic organic material together.

In m/z 217 mass chromatograms of the samples, C_{27}, C_{28}, C_{29} steranes and their 20S as well as 20R epimers (Table 8 and Figure 12b) were defined. The samples contain of C_{28} sterane and C_{28} predominantly (C_{29}>C_{27}>C_{28}) (Table 8). As algae were indicated to be the main sources of C_{27} sterolles, C_{29} sterolles form essentially from terrestrial vegetations (Moldowan et al., 1985 and Erik, at al., 2008).

C_{20}, C_{21}, C_{23}, C_{24}, C_{26}, C_{28}, C_{29} tricyclic terpanes were also determined in the samples. The abundance of C_{24} tetracyclic terpane within the leachate indicates terrestrial organic inputs (Peters and Moldowan, 1993). C_{23}/C_{24} ratio in the coals vary between 0.83-1.52 and sterane ratio between 1.32 - 1.48; C_{27}/$C_{29.}$

Especially, as in the coal samples, peat formation in terrestrial environments may be traced with C_{27} regular sterane relative abundance to C_{29} and C_{28} steranes. To Bray and Evans (1961), calculated CPI (C_{24}-C_{34}) value is equal to 1 and CPI (C_{16}-C_{26}) value is 2.00. At the m/z 191 mass fregmantograms, very low tricyclicterpane were traced in two samples (Figure 12a). In studied samples, there is not any more composition which has higher numbered carbon compound than $C_{32.}$ Sterane / hopane ratio is between 0.62 - 0.67. C_{29}/C_{30} hopane is used to differentiate carbonates and clastic lithologies (Waples and Machihara, 1991), and this ratio is between 0.62 - 0.67 for the samples (Table 8, 9 and 10).

There is a negative relation between diasterane/sterane ratio of R_o and T_{max} values, a positive relation between Tmax value and ββ/(ββ+αα) ratio, and a negative relation between R_{max} and C_{32} (22S/(22S+22R) ratios.

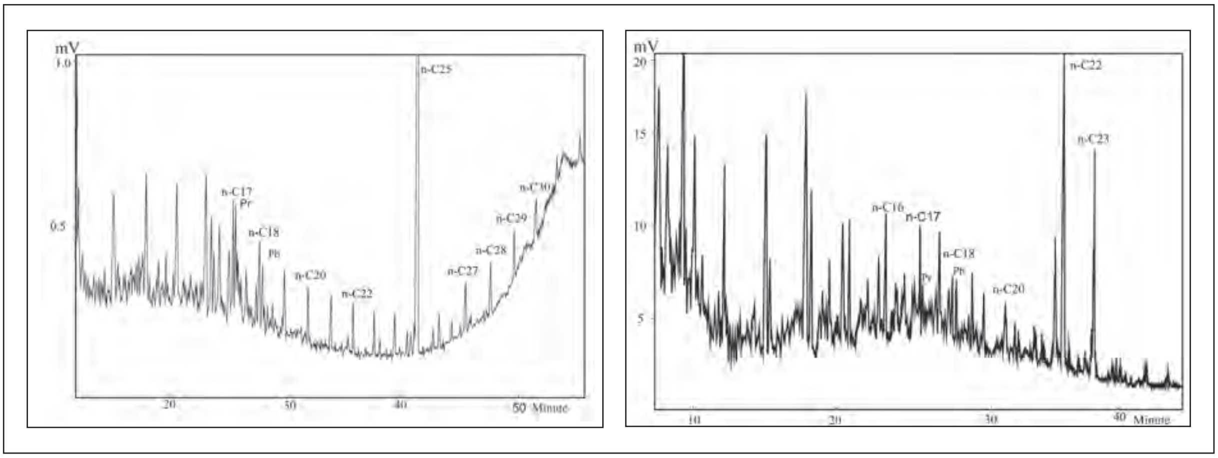

Figure 12a- GC diagram (important n-alkenes series' peaks are exhibited on them).
b- GC-MS Total Ion Current (TIC) diagram

Table 11- Gas chromatographic results (developed as in Bray and Evans, 1961) of the Hazro coal samples.

Sample	Pr/Ph	CPI	n-Alkenes Distribution	Explanations
G4	0.7	-	Mixture of nC12 - nC33	2 types of organics were found to have contribution in coal formation.
D6	1.5	1.0	nC13-nC33	„
HDG	2.2	1.2	nC13-nC33	„
DO7	3.5	1.2	nC13-nC33	„

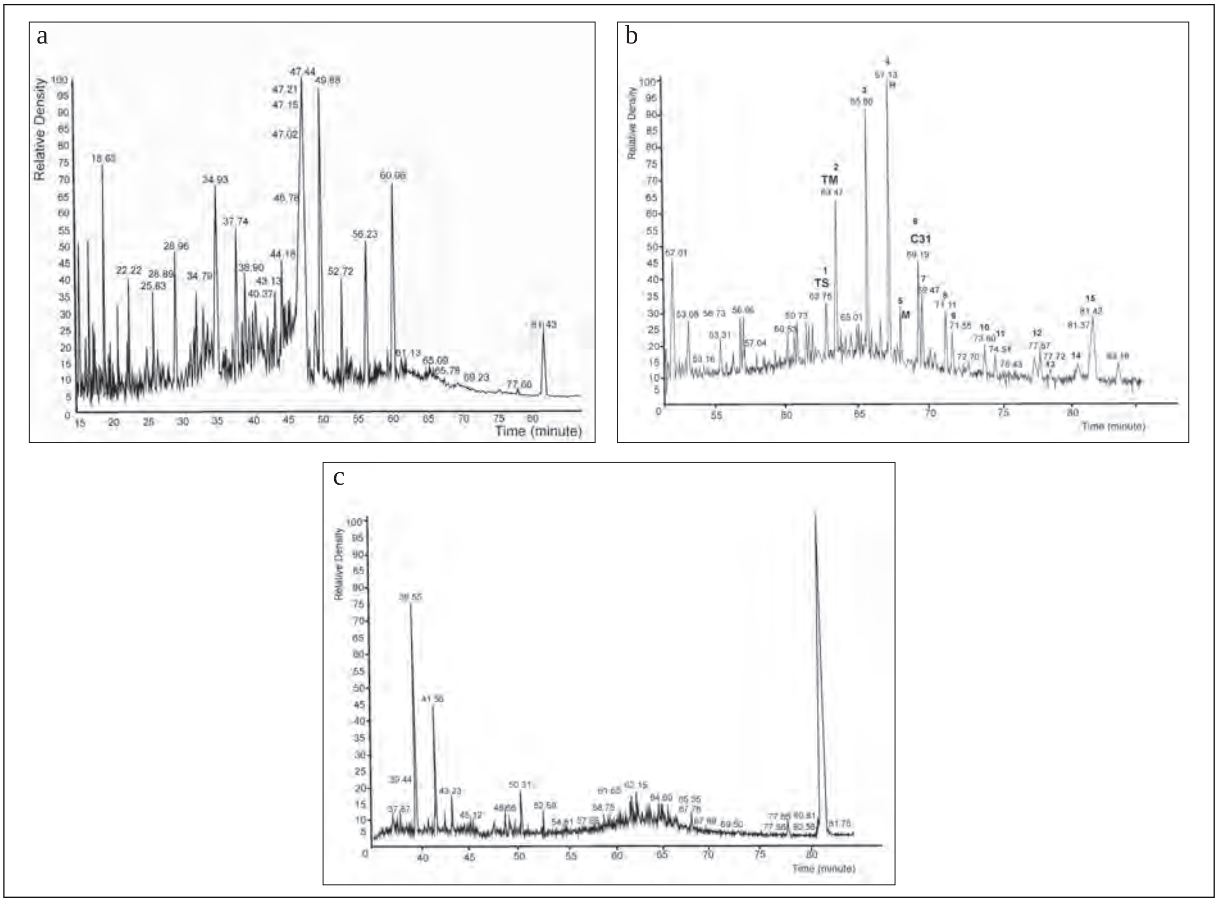

Figure 13- a. TIC GC-MS diagram of the sample G4.
b. GC-MS diagram for 191 of the sample G4
c. GC-MS diagram for 217 of the sample G4

4.9. Depositional Environment Properties

The coals were formed in suitable terrestrial and limnic conditions which the plant parts get decayed, mostly at high but oscillating water levels. This event may be explained predominantly with abundance of huminite (gelinite) macerals. Abundance of gelinite macerals reveals terrestrial moor conditions, but fusinites moor oxidations or fires taken places (Toprak, 1996; Altunsoy and Özçelik, 1993). Abundant densinite content of the coals indicate a possible effect of tectonic or dynamic activity of the region (Toprak, 2009). According to the reflection values (Rmax %) and paleo-thermal values (Boggs, 1987), the environment was probably undergone a burial thermal history which the temperature varied between 100-200 °C.

Biomarker analysis of the coals is essential to reveal paleo-environmental properties. For instance, 17 α (H)-Homohopane ratio is an indicator of paleo-climates (Waples and Machihara, 1991). As the ratio decrease, from C_{31} to C_{35} reflects clastic facies, high C_{31} hopane ratio indicates peat and coal presences. As evaluated in this manner, in the three samples, homohopanes are recorded and a gradual decrease of homohopane peak insensitive between C_{31}, and C_{35}, are typically observed for clastic lithology (Waples and Machihara, 1991). Gammacerane ratio, which is an indicator of salinity, indicates layering in water column of deposition of the coals and the samples to be of Late Proterozoic age (Waples and Machihara, 1991; Connan et al., 1986; Connan, 1993; Peters and Moldowan, 1993; Hunt 1995).

C_{25}/C_{26} tricyclicterpane ratio is higher than 1 and indicates terrestrial depositional environment conditions (Burwood et al., 1992; Hanson et al., 2000). Tricyclic terpanes are present in the whole samples. Comparative ratio of C_{25} tetracylic terpanes indicates terrestrial organic material content (Peters and Moldowan, 1993; Kvenvolden and Simoneit, 1990). αβ – moretane / αβ - hopane (moretane / hopane) ratio is between 0.55 - 0.58 and points out immature stage.

Framboidal pyrites were recorded from the whole coal veins vastly and reflects anaerobic environmental conditions. Pr/Ph and diasterane/sterane ratios remark the variations in redox and depositional conditions (Peters and Moldowan, 1993; Bechtel et al., 2005). Low Pr/Pn (Ten Haven et al., 1987) value as (changes between 0.5 and 2) as well as Pr/n C_{17} ratios to be < 0.5 indicate anoxic and hypersaline environment (Ten Haven et al., 1987). Low value or absence of C_{30} steranes points out limnic environment deposition (Peters and Moldowan, 1993).

With the light of these data, it can be said that the studied coals were deposited in a limnic moor environment which was occasionally affected by different sourced water inputs, and input of two different organic material types (Table 8 and 11).

5. Results

Organic geochemical, petrographic analysis and coal quality evaluation studies were conducted in the Hazro Permian aged organically rich and coaly series. To petrographic evaluation results, Hazro group coals are rich in huminite group macerals but rather poor in liptinite and inertinites. Gelinite is the most abundant huminite maceral of the coals. Pyrite content of the coals is considerably high, mostly in the form of framboids.

Huminite reflection values change between 0.458 and 1.141 % and correspond to a diagenesis stage of maturity. The reflection values of the coals which own a broad range refer that they were resulted from the effects of different tectonic developments as well as the covering units' thicknesses. In some areas, probably the tectonic effects were rather high but opposite in the other places. It is thought that Hazro coals were deposited in a limnic environment. The reflection values are much lower at the places where the associated minerals such as carbonate and clay minerals are abundant. Tmax values vary between 299 and 537 °C (average Tmax value is 418 °C).

These values indicate immature- premature organic stage. n-alkenes ratios are high due to resin and asphalthene content and the maturity is low as well. On HI-Tmax and hydrogen index-oxygen index diagrams, TYPE II-III and TYPE III organic material seem to be much more abundant. The parameters obtained from organic geochemical analysis and coal petrography as well as coal quality values match with each other. Petrographic evaluation of the studied coals refers the coal ranks as Sub-Bituminous B/C – Bituminous coalification ranks. Moretane/hopane and C_{32} homohopane isomerization ratios comply with the other maturity parameters. As petrographic data, coal quality parameters also are compatible with Hazro coalification rank and indicate alkali as well as reduction environments. The pristane/phytane ratio is low than 1 and refers anoxic conditions.

In general, there is a good correlation between optical and geochemical data. The whole parameters indicate low lithostatic pressure effect and low maturity level. High ash content and low coalification rank of Hazro coals limit the utilization potential of them. According to the organic material types and amount, the coals carry no generation potential due to low maturity level, although they seem to exhibit some gas generation potentials.

Acknowledgement

This study was realized by means of DÜAPK–03-MF–85 project. The authors are thankful to Prof. Dr. M. Namık Yalçın (İstanbul University), Velat Alabaş, Kıvılcım Önen, Veysel Yalçındağ (Dicle University), Merve Fakılı (Cumhuriyet University), Reyhan Kara Gülbay (KTÜ) and the operator of Hazro Dadaş coal deposit, Faysal Kahraman, for their contributions.

Received: 15.03.2013
Accepted: 31.05.2013
Published: December 2013

References

Ağralı, B,, Akyol, E. 1967. Hazro kömürlerinin palinolojik incelenmesi ve Permo-Karbonifer'deki gölsel horizonların yaşı hakkında düşünceler: *Maden Tetkik ve Arama Dergisi*, c. 68, 1-26.

Altunsoy, M., Özçelik, O. 1993. Organik Fasiyesler, Jeoloji Müh. Dergisi, 43, 34-39.

Arfaouni, A., Montacer, M., Kamoun, F., Rigane, A. 2007. Comparative study between Rock-Eval pyrolysis and bio-markers parameters: a case study of Ypresian source rocks in central-northern Tunisia: *Marine and Petroleum Geology*, 24, 566-578.

ASTM. 1983. Annual book of ASTM standards. Gaseous Fuels; Coal and Coke (D-388-82, D-2798-79, D-3172-73, D-2799-72, D-3174-82, D-3175-82): 1916 Race Street, Philadelphia, PA 19103, 05.05, 520p.

Bechtel, A., Saschsenhofer, R. F., Zdravkov, A., Kostova, I., Gratzer, R. 2005. Influence of floral assemblage, facies and diagenesis on petrography and organic geochemistry of the Eocene Bourgas coal and the Miocene Maritza East lignite (Bulgaria): *Organic Geochemistry*, 36, 1498–1522.

Boggs, S. Jr. 1987. Principles of Sedimentology and Stratigraphy. Merill Publishing Company: A Bell&Howell Company, 784p., Columbus Toronto London Melbourne.

Bozdoğan, N., Bayçelebi, O., Willink, R. 1987. Güneydoğu Anadolu Hazro bölgesinde (X. Bölge kuzeyi) Paleozoyik stratigrafisi ve petrol üretkenliği: *Türkiye 7. Petrol Kongresi, Jeoloji Bildirileri*, 117-130.

Bozkaya, Ö, Yalçın, H., Kozlu, H. 2009. Hazro (Diyarbakır) Bölgesi Paleozoyik-Alt Mesozoyik Yaşlı Sedimanter İstifin Mineralojisi, *Türkiye Petrol Jeologları Derneği Bülteni*, 21, 1, 53-81.

Bray, E. E., Evans, E. D. 1961. Distribution of n-paraffins as a clue for recognition of source beds: *Geochemical Cosmochimica Acta* 22, 2-15.

Burwood, R., Leplat, P., Mycke, B., Paulet, J. 1992. Rifted margin source rock deposition: a carbon isotope and biomarker study of a West African Lower Cretaceous "Lacustrine" Section": *Organic Geochemistry* 19, 41-52.

Connan, J. 1993. Molecular geochemistry in oil exploration Bordenave, M.L. (Ed.): Applied Petroleum Geochemistry, Editions Techniq, Paris, 175-204.

Connan, J., Bouroullec J., Dessort, Albrecht, P. 1986. The microbial input in carbonate-anhydrite facies of a sabkha paleo-environment from Guatemala: a molecular approach: *Organic Geochemistry* 10, 29-50.

Diessel, K. 1986. The correlation between coal facies and depositional environments. Advances in the Study of the Sydney Basin: *Proceedings of 20th Symposium*, the University of Newcastle, 19-22.

Durand, B., Nicaise, G. 1980. Procedures for kerogen isolation Durand, B. (Ed.), Kerogen-insoluble organic matter from sedimentary rocks): Editions Techniq, Paris, 35-53.

Durand, B., Paratte, M. 1983. Oil potential of coals: a geochemical approach Brooks, J. (Ed.). *Petroleum Geochemistry and Exploration of Europe*: Blackwell, Oxford, 255-265.

Erik. Y.N., Sancar, S., Toprak, S. 2008. Hafik Kömürlerinin (Sivas) organik jeokimyasal ve organik petrografik özellikleri, *Türkiye Petrol Jeologları Derneği Bülteni*, 20, 2, 9-33.

Espitalié, J., La Porte, J.L., Madéc, M., Marquis, F., Le Plat, P., Paulet, J., Boutefeu, A. 1977. Méthode rapide de caractérisation des roches méres de leur potentiel pétrolier et de leur degré D.Évolution: *Rev. L.Inst. Francais pétrole*, 32 (1), 23-42,

Espitalié, J., Deroo, G., Marquis, F. 1985. La pyrolyse Rock-Eval et ses applications (deuxiéme partie). *Revue Institut Francais du Pétrole*, 40, 755-784.

Flores, D. 2002. Organic facies and depositional palaeo-environment of lignites from Rio Maior Basin (Portugal): *International Journal of Coal Geology*, 48, 181-195.

Fowler, M. G., Gentzis, T., Goodarzi, F., Foscolos, A. E. 1991. The petroleum potential of some Tertiary lignites from northern Greece as determined using pyrolysis and organic petrological techniques: *Organic Geochemistry*, 17, 805-826.

Georgakopoulos, A., A., Valceva, S. 2000. Petrographic characteristics of Neogene Lignites from the Ptolemais and Servia basins, Northern Greece: *Energy Sources* 22, 587-602.

Gümüşsuyu, M. 1988. Diyarbakır Hazro Maden Kömürünün Jeolojisi ve Madenciliği, *Maden Tetkik ve Arama Genel Müdürlüğü, Rapor No*: 2745, 22

Günay, Y. 1998. Güneydoğu Anadolu'nun Jeolojisi, Stratigrafi: *Türkiye Petrolleri Anonim Ortaklığı Rapor No*: 3939, 227.

Hanson, A. D., Zhang, C., Moldowan, J. M., Liang, D. G., Zhang, B. M. 2000. Molecular organic geochemistry of the Tarim Basin, Northwest China: *Bulletin of the American Association of Petroleum Geologists* 84, 1109-1128.

Hubard, B. 1950. Coal as a possible petroleum source rock: *Bulletin of American Association of Petroleum Geologists* 34 (12), 2347-2359.

Hunt, J.M. 1967. The Origin Of Petroleum in Carbonate Rocks, Chilingar, G.V., Bissel, H.J., Farbridges R.W. (Ed.), Carbonate Rocks, *Elsevier*, New York, 225-251.

Hunt, J. M. 1995. Petroleum Geochemistry and Geology *W. H. Freeman and Company*, New York, 743.

International Committee for Coal and Organic Petrology (ICCP). 1998. The new vitrinite classification. *Fuel* 77, 349-358.

International Committee for Coal and Organic Petrology (ICCP). 2001. The new inertinite classification: Fuel 80, 459-471.

Iordanidis, A., Georgakopoulos, A. A. 2003. Pliocene lignites from Apofysis mine, Amynteo basin, Northwestern Greece: Petrographical characteristics and depositional environment: *International Journal of Coal Geology*, 54, 57-68.

İnan, S. 2007. Coalbed gas of biogenic origin in the Miocene Soma Basin (Western Turkey): 23rd *International Meeting on Organic Geochemistry*, International Conference Centre, September 9-14, Turkey.

Jackson, K. S., Hawkins, P. J., Bennett, A. J. R. 1985. Regional facies and geochemical evolution of Southern Denison Though: *Australian Petroleum Exploration Association Journal*, 20, 143-158.

Kalkreuth, W., Keuser, C., Fowler, M., Li, M., Mcintyre, D., Püttmann, W., Richardson, R. 1998. The petrology, organic geochemistry and palynology of Tertiary age Eureka Sound Group coals, Arctic Canada: *Organic Geochemistry* 29, 799-809.

Kavak, O. 2005. GAP Bölgesinin Kömür Potansiyeline Genel Bir Bakış *Doğu ve Güneydoğu Anadolu Maden Kaynaklarının Değerlendirilmesi Sempozyumu*, Diyarbakır, Türkiye, Bildiriler Kitabı, 81–86, 21–23 Nisan.

Kavak, O., Toprak, S. 2011. Gölbaşı Harmanlı (Adıyaman) Kömürlerinin Organik, Jeokimyasal ve Petrografik Özellikleri, *Jeoloji Mühendisliği Dergisi*, 35, 1, 43-78.

Kavak, O., S. Toprak, S. 2012. "Karlıova Halifan (Bingöl) Kömürlerinin Organik Jeokimyasal ve Petrografik Özellikleri", *Maden Tetkik ve Arama Dergisi*, 144, 23-50,

Kolcon, I., Sachsenhofer, R. F. 1999. Petrography, palynology and depositional environments of the early Miocene Oberdof lignite seam, (Styrian Basin, Austria): *International Journal of Coal Geology*, 4, 275-308.

Korkmaz, S., Kara Gülbay, R. 2007. Organic geochemical characteristics and depositional environments of the Jurassic coals in the Western Taurus of Southern Turkey: *International Journal of Coal Geology*, 70, 4, 292-304.

Kranendonk, O. 2004. Geo- and Biodynamic Evolution during Late Silurian/Early Devonian Time (Hazro Area, SE Turkey), Schriften des forschungszentrums Lülich Reihe Umwelt/Environment band/volume 49, p. 41.

Kvenvolden, K. A., Simoneit, B. R. T. 1990. Hydrothermal derived petroleum examples from Guaymas Basin, Gulf of California, and Escabana Trough, north-east Pacific Ocean: *American Association of Petroleum Geologists Bulletin*, 74, 223-237.

Langford, F. F., Blanc-Valleron, M. M. 1990. Interpreting Rock-Eval pyrolysis data using graphs of pyrolizable hydro-carbons vs. total organic carbon:. American *Association of Petroleum Geologists Bulletin* 74, 799-804.

Lebküchner, F. R. 1961. Kömür bakımından ümitli olan Hazro/Diyarbakır Antiklinali Sahasında Yapılan Detay Jeolojik Etütler ve Madencilik Çalışmaları Hakkında Rapor, *Maden Tetkik ve Arama Genel Müdürlüğü, Derleme Rapor No*. (H.Ö.) : 2944, 48. (unpublished), Ankara.

Lebküchner, R.F. 1969. Occurrences of the asphaltic substances in Southeastern Turkey and their genesis. *Bulletin of the Mineral Research and Exploration Institute of Turkey* 72-74.

Lebküchner, F. R. 1976. Güneydoğu Anadolu'daki Hazro Antiklinalinin Paleozoyik Çekirdeği Hakkında Ek Bilgiler, *Maden Tetkik ve Arama Genel Müdürlüğü Dergisi*, 86, 1-14.

Moldowan, M., Seifert, W. K., E. J. 1985. Gallegos, Relationship between petroleum composition and depositional environment of petroleum source rocks: *Association of Petroleum Geologists Bulletin* 69, 1255-1268.

MTA 2002. 1:500.000 ölçekli Türkiye Jeoloji Haritası, Erzurum ve Hatay paftaları.

Mukhopadhyay, P. K., Wade, J. A., Kruge, M. A. 1995. Organic facies and maturation of Jurassic/ Cretaceous rocks, and possible oil-source rock correlation based on pyrolysis of asphaltenes: Scotian Basin, Canada, Org. Geoch., 22, 1, 85-104.

Perinçek, D., Duran, O., Bozdoğan, N., Çoruh, T. 1991. Stratigraphy and paleo-geographical evolution of the autochthonous sedimentary rocks in the SE Turkey. *Ozan Sungurlu Symposium*, Ankara, Proceedings, 274-305.

Peters, K. E. 1986. Guidelines for evaluating petroleum source rock using programmed pyrolysis: *American Association of Petroleum Geologists Bulletin*, 70, 318-329

Peters K. E., Moldowan, J. M. 1993. The Biomarker Guide: Interpreting molecular fossils in petroleum and ancient sediments: *Prenctile-Hall*, Englewood Cliffs, NJ.

Peters, K. E., Walters, C.C., Moldowan, J.M. 2004. The Biomarker Guide Volume 2: Biomarkers and Isotopes in Petroleum Exploration and Earth History (second ed.): Cambridge, pp. 475-1155.

Stach, E., Mackowsky, M.Th., Teichmüller, M., Taylor, G. H., Chandra, D., Teichmüller, R. 1982. Stach's textbook of coal petrology: *Gebrüder Borntraeger*, Berlin, 535p.

Stolle, E., Yalçın, M.N., Kavak, O. 2011. "The Permian Kas Formation of SE Turkey-palynological correlation with strata from Saudi Arabia and Oman", *Geological Journal*, 46 (6), 561–573.

Teichmuller, M., Durand, B. 1983. Fluorescence microscopical rank studies on liptinites and vitrinites in peat and coals, and comparison with results of the Rock-Eval pyrolysis: *International Journal of Coal Geology*, 2, 197- 230.

Teichmüller, M., Littke, R., Taylor, G. H. 1998. The origin of organic matter in sedimentary rocks (In Taylor, G. H., Teicmüller, M., Davis, A., Diessel, C. F. K., Littke, R., Robert, P., (Eds): Organic petrology, Gebrüder Borntraeger, Berlin, 704.

Ten Haven, H. L., de Leeuw, J. W., Rullkotter, J., Sinninghe Damste, J. S. 1987. Restricted utility of the pristane/ phytane ratio as a paleo-environmental indicator: *Nature* 330, pp. 641- 643.

Tissot, B. P., Welte, D. H. 1984. Petroleum Formation and Occurrence: *Springer-Verlag*, Berlin, 699p.

Toprak, S. 1996. Alpagut - Dodurga (Osmancık - Çorum) bölgesi çevresindeki kömürlerin oluşum ortamları ve özelliklerinin belirlenmesi, Hacettepe Üniversitesi Fen Bilimleri Enstitüsü, Doktora tezi, Ankara.

Toprak, S. 2009. Petrographic properties of major coal seams in Turkey and their formation, *International Journal of Coal Geology*, 78, 263-275

Waples, D. W., Machihara, T. 1991. Biomarkers for geologists-a practical guide to the application of steranes and triterpanes in petroleum geology: *American Association of Petroleum Geologists Bulletin* 9, 91.

Wilkins, R. W. T., George, S. C. 2002. Coal as a source rock for oil: a review: *International Journal of Coal Geology*, 50, 317–361.

Yalçın, M. N., Schaefer, R. G., Mann, U. 2007. Methane generation from Miocene lacustrine coals and organic-rich sedimentary rocks containing different types of organic matter: *Fuel*, 86, 4, 504-511.

Yalçın, M.N., Kavak, O., Stolle, E. 2010. Gondwanan Permian coals of the Hazro area (Southeastern Turkey). *8th European Coal Congress (GEO DARMSTADT 2010)*, Darmstadt-Germany. Abstracts of Lectures and Posters, 619-620, 10-13 Oct.2010

Yılmaz, E., Duran, O. 1997. Güneydoğu Anadolu Bölgesi Otokton ve Allokton Birimler Stratigrafi Adlama Sözlüğü (Leksikonu): *Türkiye Petrolleri Anonim Ortaklığı*, Eğitim Yayınları, No.31, 460s.

Bulletin of MTA (2013) 147: 115-126

Bulletin of the
Mineral Research and Exploration

http://bulletin.mta.gov.tr

SLOPE INSTABILITY IN OPEN PITS AND AN EXAMPLE OF A RETROSPECTIVE ANALYSIS: AFŞİN-ELBİSTAN-KIŞLAKÖY OPEN PIT COAL DEPOSIT

İbrahim AKBULUT[*,a], İlker ÇAM[a], Tahsin AKSOY[a], Dinçer ÇAĞLAN[a] and Tolga ÖLMEZ[a]

[a] *General Directorate of Mineral Research and Exploration, Department of Feasibility Study, 06800 Ankara, Turkey*

Key words:
Block sliding, circular sliding, retrospective analysis, movement observation, landslide, failing model

ABSTRACT

The subject of this study is to study the instabilities that have developed in the permanent east and west slopes of the Kışlaköy open pit of the Elektrik Üretim A.Ş. Afşin-Elbistan Linyitleri İşletmesi and to work out the sliding mechanism causing it. In the Kışlaköy open pit to establish if mass movement is continuing and if so which direction it would move, amount of mass to be involved and the failing model. Six movement control observations stations were established along 3 lines in each of west and east slopes. No movement was observed in the west slopes. On the other hand up to 90 cm cumulative movement was observed at the at D24 and D18 observation station on the east slopes. Measurements taken showed that there were failings in the lignite horizon fitting to the 'block sliding model'. During the field study circular sliding model type failings were observed in the basal units. In the open pit in general before and after the sliding, plans were prepared of the instabilities to enable geometries could be worked out. By using these plans cross sections were prepared to show the geometry of the instabilities before it actually took place and retrospective analyses of the failing model have been carried out. Correlations have been made of the results of the retrospective analyses and resistance parameters obtained from the laboratories. It was concluded that during the movement of the mass, shear strength of the sliding planes were then represented by the shear resistance parameters. During the study it was found out that the black coloured clay band with high plasticity within the lignite horizon is one of the most crucial factors controlling slope stabilities.

1. Introduction

Kışlaköy lignite open pit is located within the township limits of Elbistan and Afşin, Kahramanmaraş (Figure 1).

The first geological studies carried out in the Afşin-Elbistan lignite area was conducted jointly by MTA and OTTO GOLD (German company) in 1966. Systematic drillings resulted with the discovery of lignite deposit in 1967 (Gürsoy et al 1981). Work continued and 578 million tons lignite reserves were discovered in the Kışlaköy section. A Total of 3.4 billion tons of lignite reserves have been discovered in the Afşin-Elbistan area (Yörükoğlu 1991).

Slope instability provides information of the conditions during failing. By carrying out retrospective analysis, basal zone's resistance strength, groundwater level and instability model could be studied. Conditions of failing during a slope's failing and formulating a suitable slide model is described as retrospective model (Duncan and Wright 2005)

A step base landslide developed on the east slope of the Kışlaköy open pit in 2005. Following this landslide a 1/2000 scale detailed geological map was prepared. Disturbed/Undisturbed samples were taken inside the pit, towards possible movements. Movement observation studies were conducted on the permanent steps. (Akbulut et al 2007).

* *Corresponding author: İ. AKBULUT, ibrahim.akbulut@mta.gov.tr*

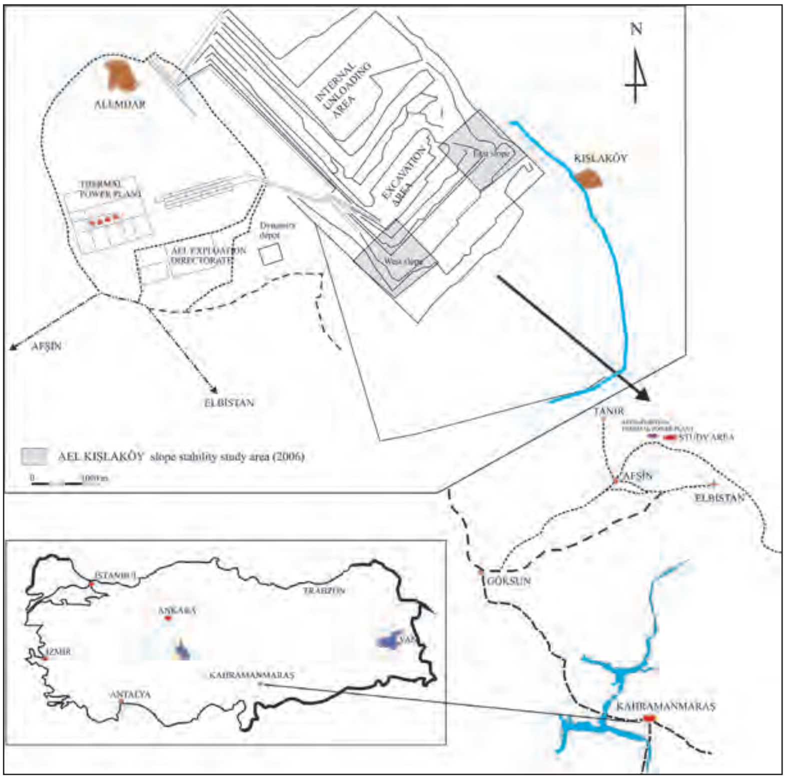

Figure 1- Location map of the study area

In 2005 in the western permanent slopes of the open pit, a step base land slide followed by a landslide within the lehim unit with undisturbed geometry occurred and a step base landslide developed in the eastern permanent slope. In 2006 and a big landslide developed involving the whole of the slope. Plans and sections of all these landslides were prepared and retrospective analyses have been carried out.

2. Geology

Pleistocene shallow water and Quaternary stream sediments are the lithological units present in the study area (Figures 2-3). Turquoise coloured clays form the base of the study area. As they form the base of the lignite horizon, they are also so called basement clay. The unit is greenish blue colour (turquoise colour) and has clay with carbonate concretion levels. Base clays display little-medium level plasticity. Lignite horizon concordantly overlies the base clay unit. The unit is black-light brown colour, has medium level hardness, formed of medium-thin beddings. The lignite horizon in places has black coloured 5-80 cm thick bituminous rich clay levels with high plasticity, in places it has green coloured small pebbly clay levels with medium-high level plasticity. It is transitional with the grey coloured gidya unit, so has numerous gidya alternations. Age of the unit is Pliocene-Pleistocene (Gürsoy et al 1981). Grey gidya unit is formed of brownish grey-dark grey coloured clay levels, displaying medium-thick beddings. Beige coloured gidya has light brown-beige colour and has clayey silt levels rich in gastropod fossils. Limestones form the upper most units of the units representing shallow water (lake) environments (Gürsoy et al 1981). Limestones are present in the western part of the pit. They are light grey-grey coloured, rich in fossils, tough-very tough, display medium-thick beddings and with jagged broken surfaces. Limestones are overlain with discordance by light green clays with medium plasticity.

The Quaternary lehim unit covers large part of the study area. It has reddish brown sandy clays with some pebbles in it. The unit is rich in carbonate concretions. In the carbonate rich parts 0.5-1.0 m thick limestons have developed. The youngest unit in the study area consists of silt-sands and pebbly units, in places it consists of loosely cemented, medium level rounded pebbles.

The faults in the study area developed in Pliocene and later along the eastern slopes at the basin's edge. They run in the NW-SE direction. As the study area is

Figure 2- Geological and engineering geological map of the west face of the Kışlaköy open pit (Akbulut et al 2007).

covered with the young sediments surface expressions of the faults were not observed.

In the Afşin-Elbistan basin the beddings of the sediments have horizontal, near horizontal attitudes. In and near to the edge of the basin, because due to faulting beddings of the sediments have 2 to 20 degrees dipping.

3. Instability Studies

Field studies were carried out to study the instabilities developed in the permanent steps and in the pit and to conduct retrospective analyses. During the field study numerous landslides in different units were detected. Following landslides five instabilities without any geometrical deformations were also detected. Out of these three landslide plans were prepared. As two of the landslides were small scale, so works were limited with field observations for them only (look figures 2-3). The landslides developed have been marked as H1 in the lehim unit, H2, H3 and H4 in the lignite unit and H5 in the gidya unit (Akbulut et al 2007).

3.1. H1 Landslide

In the western part of the pit numerous various scales step base landslides have developed. These landslides did not obstruct lignite productions. These landslides display spoon like shallow circular sliding planes. Only one of these landslides (H1) displays distinct pre and post landslide geometrical features (Figure 4). 1/250 scale plan and engineering geological map of the H1 landslide has been prepared. As it is seen in the figure 4, 1.5-2.0 m thick weakly cemented pebble bearing units are overlying the H1 landslide; this is why no instability has developed in this part. In parts where loosely cemented clay-silt and sand are the main rock units, there 13 m high and 15 m wide failings developed in the circular sliding model.

3.2. H2 Landslide

In August 2005, H2 landslide developed at step base in the eastern permanent slope of the pit. All of the landslides including the H2 developed in the lignite horizon in the block sliding model. Failings

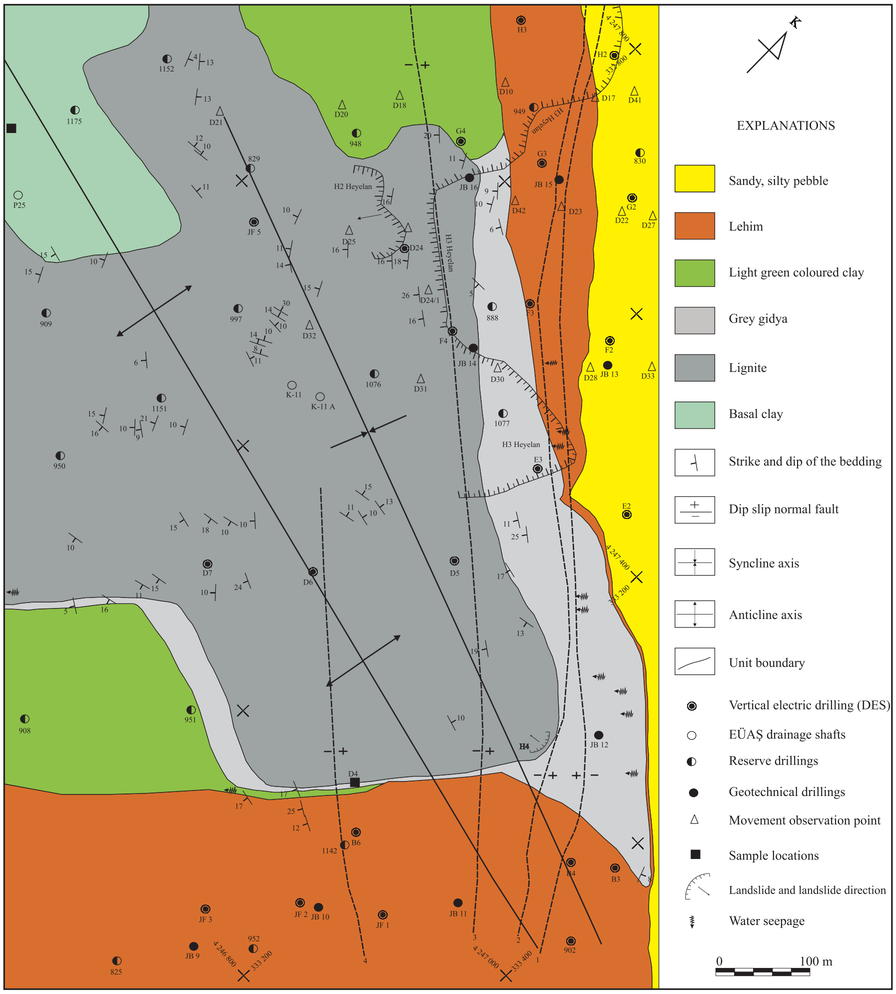

Figure 3- Geological and engineering geological map of the East face of the Kışlaköy open pit (Akbulut et al 2007).

Figure 4- Circular sliding (H1) developed in the lehim unit

developed in the lignite zone. The movement first started in the black clays which formed the first sliding plane, have low dip angle and have very low shearing resistance. Then the movement continued along the faults and discontinuity zones which formed the second sliding plane and movement developed in line with the block sliding model.

H2 landslide developed at step base and was 50 m wide, 25-33 m high (Figure 5). In the H2 landslide the black clay band in the lignite horizon formed the first sliding plane. A test trench cut just in front of the landslide showed that back face (II surface) was developed from the result of discontinuities in the lignite (Akbulut et al 2007).

3.3. H3 Landslide

H3 landslide developed on the 23/10/2006 in the eastern permanent slope of the pit covering all of the steps (Figure 6). This landslide has been marked as one of the biggest landslides developed in the pit to day. Although it affected all of the steps but still coal

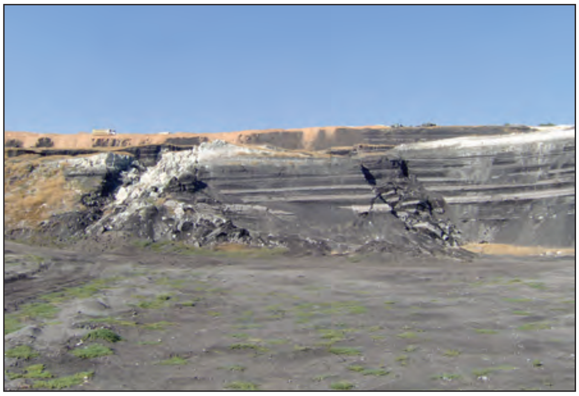

Figure 5- General view of the H2 landslide

production continued as usual. But all access roads to the overburden dump site were destroyed so access to the dump site was prevented. A new access road had to be built in front of the landslide.

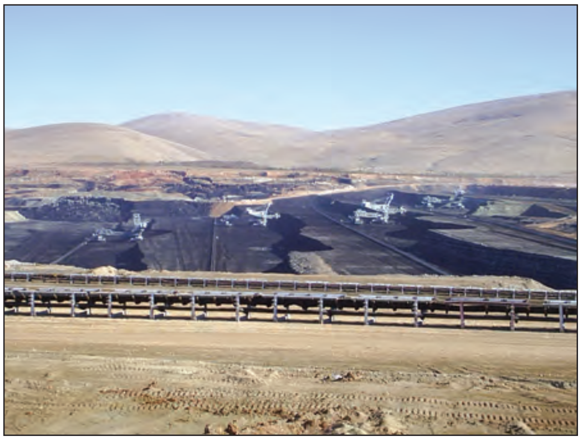

Figure 6- A large landslide (H3) developed in the permanent east slope

The H3 landslide developed at least in three stages. The movement started from the beginning of 800 m long 2nd step and in line with the block sliding model progressed towards inside the pit (1st stage). Number 3 fault crossing the 2nd step forms the back face of the landslide. Following the sliding a high, sharp cliff face developed in front of the 2nd step. This caused instability to the back part. As a result 2nd fault plane crossing the 1st step formed a sliding plane and another block sliding type landslide developed (2nd stage). 2nd stage landslide affected whole of east slopes, developed in the north and south of the slope. It covered 200 m and 400 m wide areas in the north and in the south respectively. Following the 1st stage landslide, in the middle part of the east slope there stayed a 200-300m wide unbroken section. Following the 2nd stage landslide, the sliding continued its movement backwards (3rd stage). In this part sliding in the basal units developed in the circular failing model (Figure 7)

Figure 7- Circular sliding developed at the most back part of the H3 landslide

3.4. H4 Landslide

H4 landslide developed in the eastern part of the pit at the corner where production steps and eastern permanent slopes meet. H4 landslide developed in the lignite horizon in the step base at very small scale. Nature of it fits to the block sliding model. H4 landslide neither effected coal production nor it affected the stability of the pit in general.

As all of the landslides in the lignite horizon developed in the block sliding model, it indicates that stability analyses should be made to fit to this model.

Figure 8-General view of the H4 landslide

3.5.H5 Landslide

H5 landslide developed in block sliding model in the gidya unit in the western part of the production steps. It developed only in one of the steps. Accumulated data indicates that stability analyses for the gidya unit should be made in accordance with block sliding model along with circular sliding model.

4. Movement Observation Studies

Movement observation studies have been carried out to estimate nature and speed of the movements which could cause instability in the east and west permanent slopes. For this purpose at the east and west permanent slopes, along total of 6 lines, 3 on each line, movement observation stations were set up. To this, numbered stakes were dug into the earth along right angle to the steps (parallel to the possible movement direction). By setting up the observation stations coordinate (X, Y, Z) changes of the stakes by using topographical survey instrument (Distomat LAICA 1102) meant to be periodically recorded. By taking systematic coordinate readings, movements along the coordinate axis have been made known. All of the changes have been evaluated together, amount of movements' and resultant vector at each station have been established.

Measurements' taken in the west slope of the pit indicated no movement.

Measurements' taken from D28 and D30 stations in the upper steps in the east slope of the pit showed 7-9 cm movement, on the other hand measurement from D24 station in the lower steps showed up to 90 cm movement. Resultant vector of the amount of movements at D24 as well as D18 stations has been found out to be parallel to the slide direction and has 69.7º and 61.7 º angles with the horizontal plane (Akbulut et al 2007). Observation station 32 is located at the lower most part of the line of which line up number is given above. At this station value of the resultant vector is 20 and makes 5 º angles with the horizontal plane. This shows that back sliding face (2nd surface) have higher then 60º angle and in the front parts (1st surface) it acquired near horizontal position. Following the landslide the fault which appeared on the surface is dipping towards the pit and has a dip angle varying 65º to 80º degrees. It was found out that in the lover levels of the east slope the dip angle of the lignite horizon as well as the black clay vary to 2º-6º degrees. Dip angle of the back face (2nd sliding surface) of the H3 landslide, dip angle of the fault measured in the field and the dip angle of the 1st sliding surface are in line with the dip angle of the black clay. It clearly shows that this landslide developed jointly (two separate joint surfaces) with the effect of discontinuity and the black clay (Figure 9).

Movement observation studies in conjunction with the field studies and observations of the landslides have been all in accord with each other. This indicates that landslides fit to the block sliding model.

5. Retrospective Analyses

Safety factor value (F) calculated in slope stability analyses is the indicator of the stability and is the ratio of resisting forces to the forces causing sliding. If this value is equal to 1 (F = 1) it shows that the slope in question is in sliding position (instable) and this is known as 'Limit Balance Condition'.

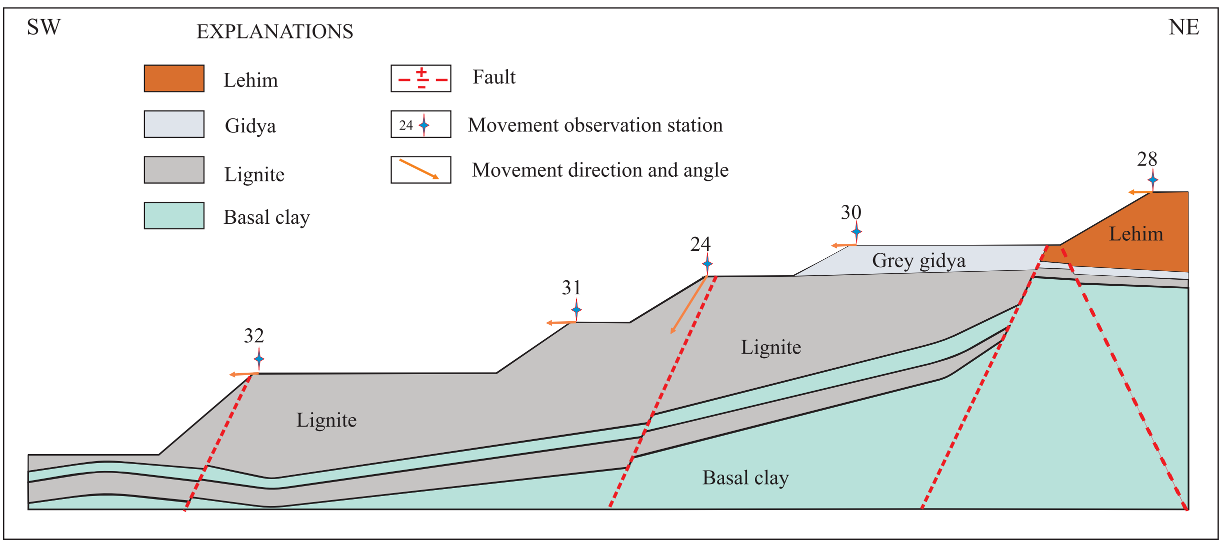

Figure 9- Cross section along movement observation stations showing movement vectors (Akbulut et al 2007)

According to these retrospective analyses carried out in the study area showed that during sliding which occurred in various parts of the Kışlaköy open pit, effective shearing resistance parameters should be made known. The value obtained to be correlated with the laboratory test results. Purpose of doing that is to calculate parameters to design permanent slopes.

Retrospective analyses have been carried out for H1, H2 and H3 instabilities. Field and movement observation studies were important to establish which sliding model to be adapted for the slope stability analyses. Result of these studies showed that H1 landslide fits to the circular sliding model, other landslides (H2 and H3) fit to the block sliding model.

Morgenstern-Price method (Mergensten and Price 1965) has been used in the retrospective analyses. This method takes forces into account between slices and at the same time uses moment and force balances in the calculations. This method with limited balance approach has been used for the stability analyses of the sliding surfaces. Geo Slope SLOPE/W 2004 (Geo-Slope 2004) computer program have been used in the calculations. This program takes into account the effects of seismic forces and ground water in the heterogeneous and homogeneous environments

5.1. Retrospective Analysis of the H1 Landslide

In the study area retrospective analysis has been carried out of the H1 landslide which developed in the lehim unit at the west permanent slopes in the uppermost step. First of all 1/250 scale plan (Figure 10) of the landslide was prepared, and then from this plan 5 cross sections were prepared (Figure 11). Limit balance position of each section was studied, different cohesion (c) value was chosen. Afterwards, depending upon the sliding geometry, friction angle (ϕ) suitable for F=1 condition was found, then "c-ϕ" diagrams were prepared for this instability (Figure 12).

Peak and residual shearing resistance parameters of the unit have been obtained from the laboratory tests carried out under consolidated drainage conditions. Obtained values are; maximum peak values c_p=48.7 kPa, ϕ_p=26.7º; minimum peak values c_p=19.7 kPa, ϕ_p= 16.1º; maximum residual values c_r=15.6 kPa and ϕ_r=10.3º. These values have been plotted on to the c-ϕ diagram and have been correlated with the retrospective analyses results (Akbulut et al 2007).

Figure 12 shows that resistance parameters obtained from the retrospective analyses are within the variation range of the shearing resistance parameters of the laboratory tests. Because of this for the analyses of the lehim unit shearing values obtained from the laboratory tests have been used.

5.2. Retrospective Analysis of the H2 and H3 Landslides

In 2005 H2 landslide developed in the lignite zone at the steps of the east permanent slopes and in 2006 H3 landslide (big landslide) developed in the same place. Both of the landslides developed in the block sliding model.

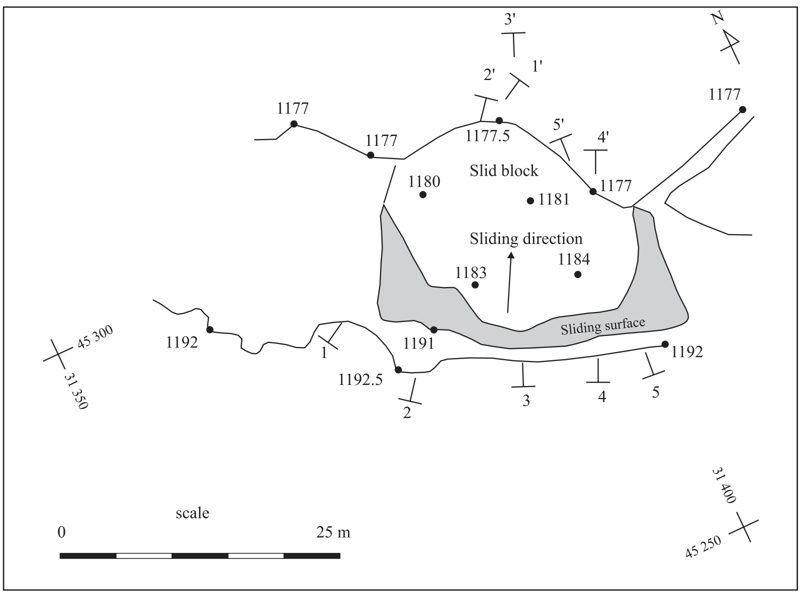

Figure 10- View of the H1 landslide (Akbulut et al 2007)

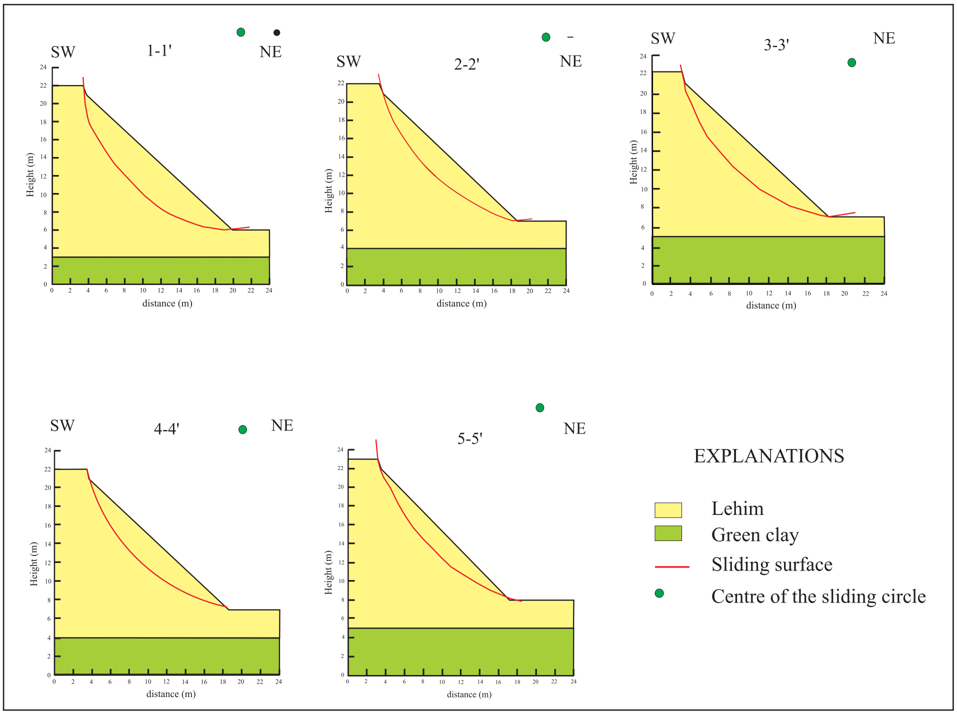

Figure 11- Cross sections of the H1 landslide (Akbulut et al 2007).

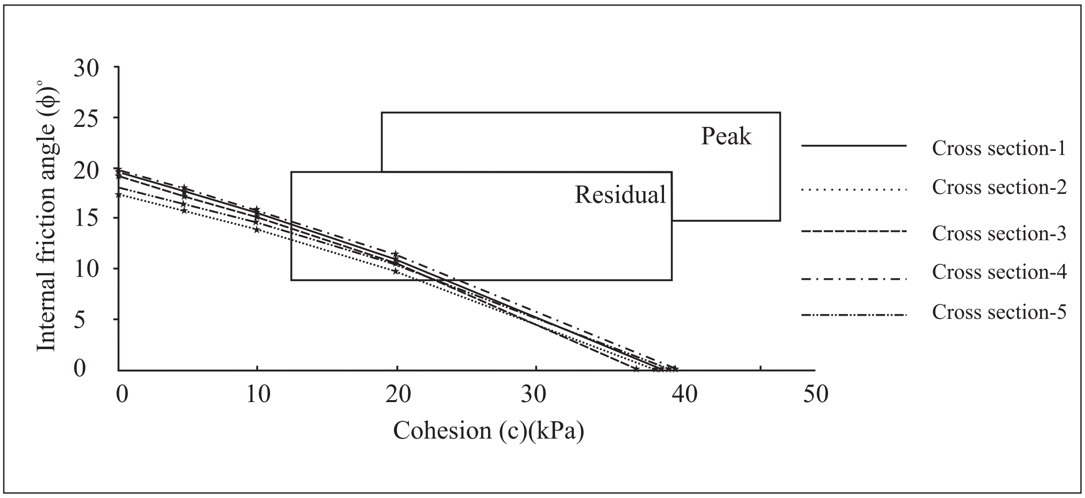

Figure 12- Comparison of retrospective analyses results and shearing resistance results of the H1 landslide (Akbulut et al 2007).

Black clays with very week resistance developed parallel to the bedding in the lignite horizon formed the first face of the block sliding; discontinuities formed the second face (back face).

In this sliding model movement initially starts in the first face at the bottom which has low shearing resistance, later on it breaks off from the weak zone in the lignite horizon (discontinuity or fault), moves forward and eventually dies out.

For the retrospective analyses 1/500 scale plan of the H2 and 1/2000 scale plan for the H3 landslides were prepared (Figures 13-14) and 5 cross sections were prepared from each plans (Figures 15-16). Resistance parameters (c=0 kPa, ϕ=29°) of the discontinuity face, forming the back face of the block sliding used for the retrospective analyses carried out on these sections have been taken from Akbulut et al 2007. Shearing resistance parameters of the black clay have been studied under the conditions; resistance

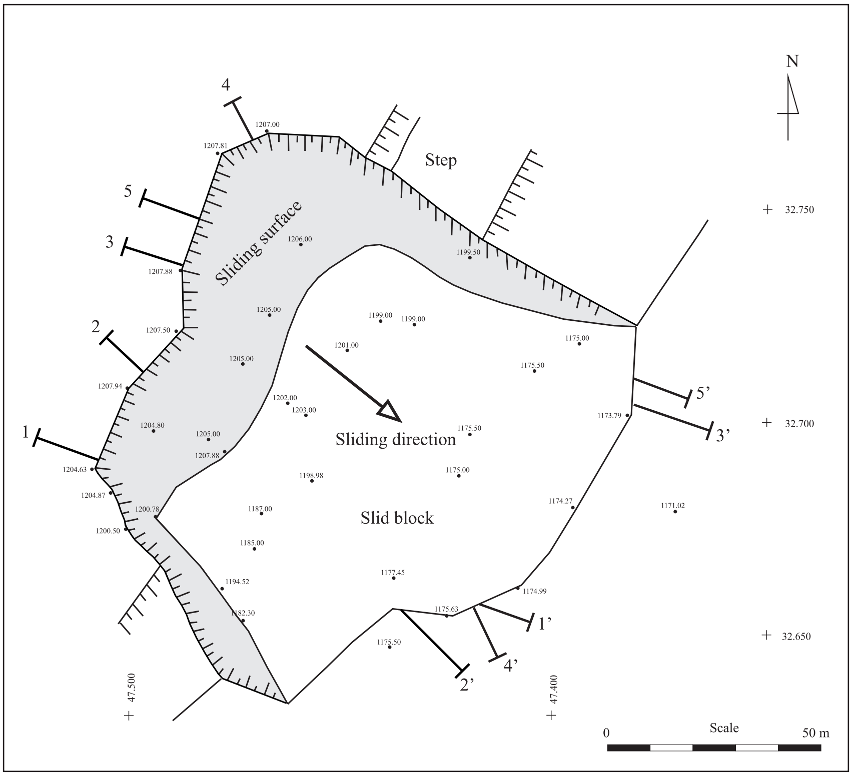

Figure 13- View of the H2 landslide (Akbulut et al 2007)

parameter values kept constant and F=1. Afterwards c-ϕ diagrams have been prepared separately for each section.

It is generally the preferred practice to study numerous failing diagrams jointly to establish weighted average of c and ϕ parameters effective during instability along the sliding surface for retrospective analyses (Sancio 1981, Tinoco and Salcedo 1981).

To be able to establish correctly the weighted average of effective c and ϕ parameters of the H2 and H3 landslides during sliding, retrospective analyses results of the relevant instabilities combined together and c-ϕ diagrams have been prepared (Figure 17).

Laboratory test results show following variations; maximum peak values: c_p=74.2 kPa, ϕ_p=18.4°; minimum peak values: c_p=24.7 kPa, ϕ_p=18.4°; maximum residual values: c_r=41.6 kPa, ϕ_r=11.4°; minimum residual values: c_r=9.8 kPa, ϕ_r=9.5° (Akbulut et al 2007).

Comparison of peak and residual shearing resistance parameters obtained from the laboratory tests with the retrospective analyses results shows that all of the 'c-ϕ' envelope are within the variation range of shearing resistance parameters (Look figure 17). Because of this, for the design analyses, use of laboratory test results of the residual shearing resistance parameters of the black clay would be preferred.

6. Results and Suggestions

Results of the geotechnical field studies, laboratory test and retrospective analyses carried out in the Kışlaköy open pit are here given below.

- During the course of movement observation practice no movement have been recorded in the west slopes. On the other hand in the east slopes at the D24 and D18 observation stations up to 90 cm cumulative movements were recorded before the big landslide.

- Movements' observation stations in the present slopes shows that movement vectors of the recorded movements indicated presence of block sliding instability.

- Following landslides in the geometrical characters still recognizable lignite horizon 3, gidya unit 1 and lehim unit 1, total of traces of 5 landslides have been identified. The landslide in the lehim unit

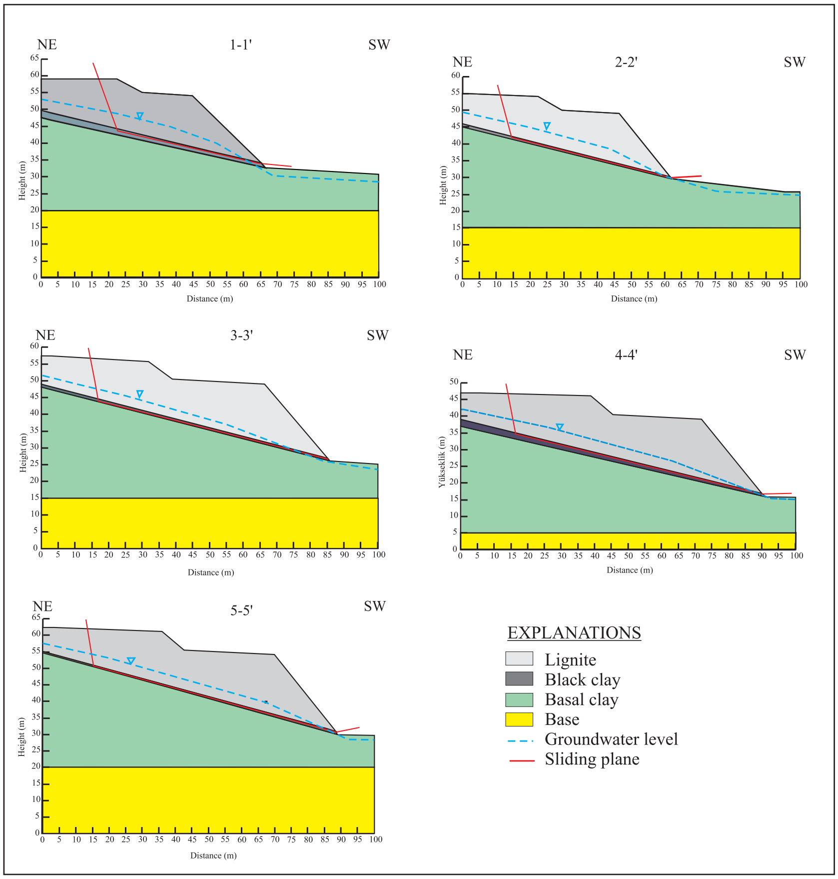

Figure 14- Geological cross sections of the H2 landslide (Akbulut et al 2007)

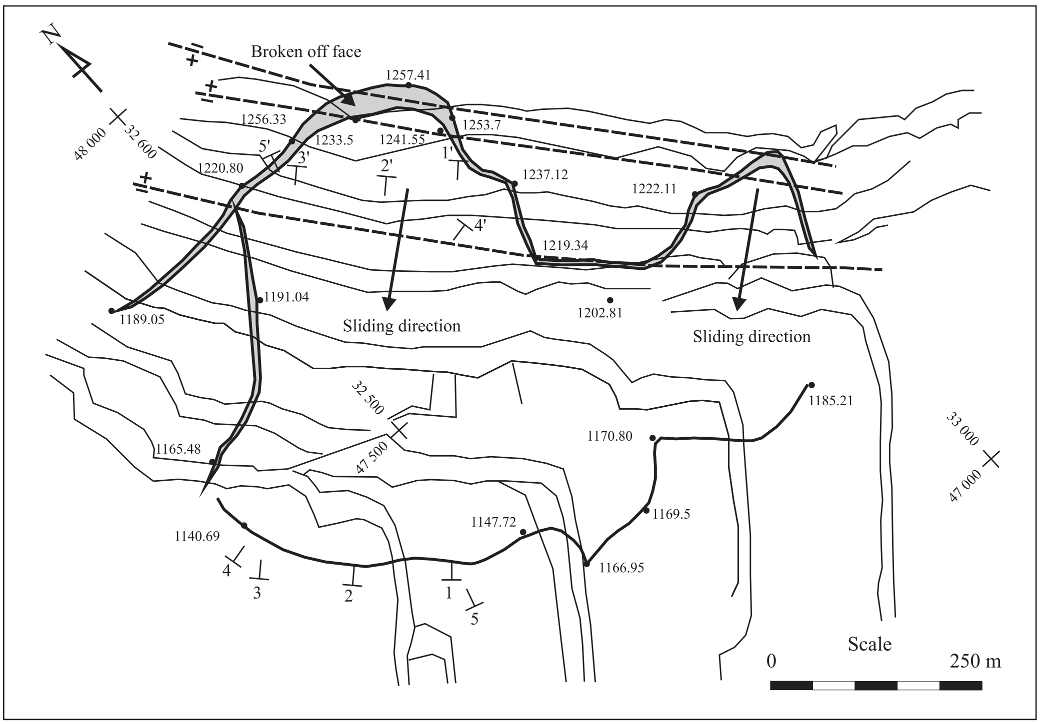

Figure 15- View of the H3 landslide (Akbulut et al 2007)

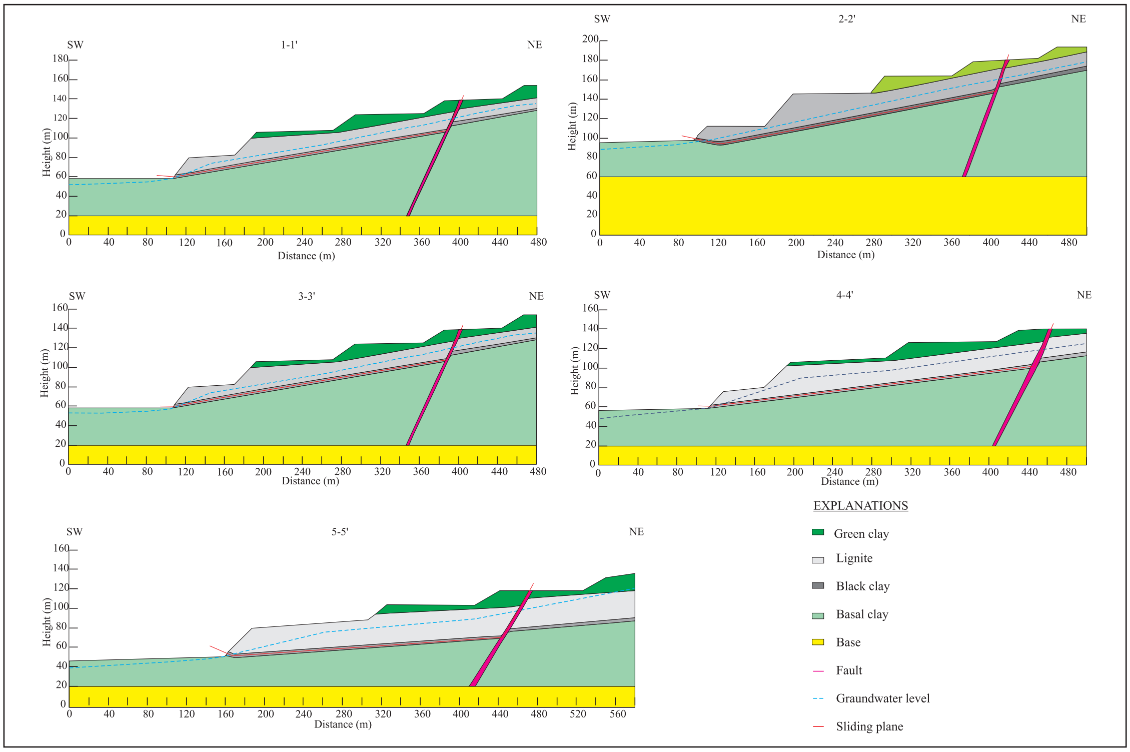

Figure 16- Geological cross sections of the H3 landslide (Akbulut et al 2007)

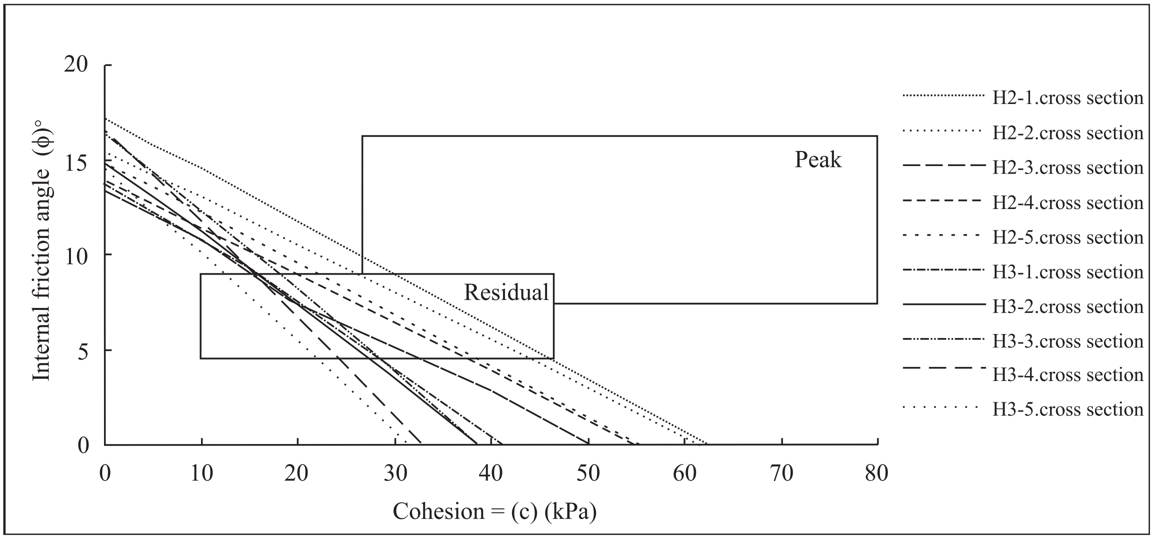

Figure 17- Comparison of the results of retrospective analyses results and laboratory test results of shearing resistance parameters of the H2 and H3 landslides (Akbulut et al 2007).

fits to the circular sliding model the others fit to block sliding model.

- In the block sliding type landslides in the lignite horizon, black clay bands in the lignite form the 1st surface, discontinuities and/or faults in the lignite horizon form the second surface.

- Studies showed that black coloured clay bands with high plasticity present in the lignite horizon have the most crucial part in controlling the slopes stability.

- When laboratory resistance parameter test results compared with the retrospective analyses results it shows that in the landslides during sliding shearing resistance of sliding surfaces is controlled by the shearing resistance parameters.

- It is suggested that shearing resistance parameters obtained from the laboratory tests should be used in slope designs.

- General slope analyses should be carried out in the block sliding model.

Received: 20.11.2012
Accepted: 11.07.2013
Published: December 2013

References

Akbulut, İ., Aksoy, T., Çağlan, D. ve Ölmez, T., 2007. Afşin-Elbistan Kıslaköy Açık Kömür İşletmesi Şev Stabilitesi Çalışması, *Maden Tetkik ve Arama Genel Müdürlüğü Report No*: 11194 (unpublished), Ankara.

Duncan, J.M. and Wright, S.G. 2005. Soil Strength and Slope Stability. J*ohn Wiley and Sons*, Inc., New York, NY, USA, 309 pp.

Gürsoy, E. Özcan, K., Yücel, A.R. 1981. K.Maraş Elbistan D1 Sektörü Kömür Yatağı Jeoloji Raporu. *Maden Tetkik ve Arama Genel Müdürlüğü Report No*: 7054, (unpublished), Ankara.

Koçak, S., Ulusay, R., Selçuk, Ş., İder, H. 1985.TKİ-AEL Kışlaköy Linyit İşletmesi Batı Şevi Stabilite Etüdü. *Maden Tetkik ve Arama Genel Müdürlüğü Report No*: 7717, (unpublished), Ankara.

Morgenstern, N.R., Price, V.E. 1965. The Analysis of The Stability of General Slip Surface. *Geotechnique*, 15, 79-93.

Sancio, R. T. 1981. The Use of Back Calculations To Obtain The Shear and Tensile Strength of Weathered Rocks. *Proc. Int. Symp. on Weak Rock*, Tokyo, V.2, 647-652.

Slope, W. 2004. Geo Studio 2004, Vers. 6.2, Geo-Slope International Ltd., Calgary, Canada.

Tinoco, F.H., Salcedo, D.A. 1981. Analysis of Slope Failures In Weathered Phylillite. *Proc. Int. Symp. on Weak Rock*, Tokyo, V.1,55-62.

Yörükoğlu, M. 1991. Afşin Elbistan Projesi ve TKİ Kurumu AELİ Müessesinde Madencilik Çalışmaları. *Madencilik* ,30, 3.

Bulletin of MTA (2013) 147: 127-151

Bulletin of the
Mineral Research and Exploration

http://bulletin.mta.gov.tr

NEW APPROACHES ON THE INVESTIGATION OF COVERED GEOTHERMAL FIELDS: EXPLORATION OF KÜTAHYA – ŞAPHANE – KARACADERBENT BURIED GEOTHERMAL FIELDS AND THEIR DEVELOPMENTS

Musa BURÇAK[a, *], Hüseyin DÜNYA[b] and Ömer HACISALİHOĞLU[c]

[a] *General Directorate of Mineral Research and Exploration (MTA), Department of Energy Raw Material Research and Exploration, 06800 Ankara, Turkey*

[b] *General Directorate of Mineral Research and Exploration (MTA), Regional Directorate of Aegean, İzmir*

[c] *General Directorate of Mineral Research and Exploration (MTA), Regional Directorate of Eastern Black Sea, Trabzon*

Keywords:
Şaphane, Karacaderbent, buried geothermal field, geophysics, conceptual model, well development.

ABSTRACT:

The basement in Şaphane region is constituted by Paleozoic gneiss, schist and marbles belonging to northern margin of the Menderes Massif. These basement rocks are overlain by Cretaceous aged Dağardı ophiolitic melange. All these rocks are discordantly covered by Neogene – Quaternary sedimentary and volcanic rocks deposited under lacustrine – continental environments.

The main purpose of this study is to explore buried geothermal system on a covered area using geological, geophysical and geochemical methods and to develop this system by drilling investigations. Geological, geophysical, geochemical and drilling investigations, well development and test studies were applied in this research. This study is a typical example for geothermal researches carried out in covered areas. Thus, a new approach was aimed to be brought out in such investigations. Especially; the profiling was applied, and geological structures and geochemical data were used for the selection of profiles at geophysical investigations instead of gridding which had typically been used for many years. The geothermal system was handled in regional scale rather than local scale with this study. As a result of research assessments, a drill location was selected on a totally covered area where there was no surface data around Şaphane Karacaderbent. At drilling number KŞÜ-3, a reservoir temperature of 181,2ºC were reached at a depth of 2500 m. From the well which its development and test studies had been completed at 10 psi at wellhead pressure (WHP), vapor + water production was obtained at a temperature of 114ºC and a flow rate of 25 l/s in case of artesian. As for the production tests carried out by compressor at 22 PSİ well head pressure (WHP), vapor + water was obtained at a temperature of 112ºC and a flow rate of 35 l/s. The fluid obtained from the well is suitable for the production of electricity and for heating of houses and greenhouses due to the production values revealed at the end of temperature and tests. When turbine rejection heat is taken as 75ºC, the apparent potential of electrical energy in the well is 21,3 MWt and owns a potential to heat 1300 houses or an area of 85000 m^2 for greenhouses.

1. Introduction:

The study area is located in the vicinity of Şaphane town, Kütahya City. Investigations were carried out in the license areas of number 7, 8, 9 and 10 of the General Directorate of Mineral Research and Exploration (MTA). Previous studies before exploration of the buried geothermal field around Şaphane, Karacaderbent, the selection of the target area, drilling studies of the well number KŞÜ-3 which was excavated at 2500 m, difficulties encountered during drilling, well development and test studies were explained in this article. Briefly saying; new approaches exhibited during exploration and the development of a covered field have been discussed in this article.

As a result of these studies, buried geothermal field at a temperature of 181,2ºC was explored within the boundaries of license number 7 in the vicinity of

* *Corresponding author: M. BURÇAK, mburcak65@gmail.com*

Şaphane, Karacaderbent. There is not any geothermal spring in the close vicinity of the field. Gediz – Abide geothermal springs are the closest sources that possess a source temperature of 70–76ºC and the KŞÜ-3 drilling explored in Karacaderbent is at a 8 km away from these springs (Figure 1). Several investigators have studied the structure and characteristics of the Menderes Massif in the study area. Schuiling (1958 – 1962) pointed out that gneisses were migmatitic and had been derived from sedimentary rocks that affected from alkaline rich melts. The author also stated that, gneisses were dome like structures, the degree of metamorphism was surrounded by schists decreasing in amount towards circumferences and schists were covered by marbles consisting of metamorphic bauxite appearances. Akdeniz and Konak (1979) specified that metamorphic rocks in the region belonged to northern margin of the Menderes Massif and were tectonically covered by Cretaceous Dağardı Melange. According to İzdar (1971), the massif possesses two different degrees of metamorphism. The first one has been completed by the Variscan Orogeny; the second one on the other hand has started by the Alpine Orogeny. The massif has a dome like structure and was probably made up of Precambrian rock core and of Paleozoic – Mesozoic schists. Burçak et al. (2004) carried out test and evaluation studies towards geothermal resource explorations and reservoir assessments for the central heating system of Gediz Municipality which hade been made under the name of İller Bank. Geological, geochemical and isotopic data have indicated that a buried geothermal system at a higher temperature could occur on the covered area, towards the north of Abide field. The drainage basin height was calculated as 1700 m and reached the top of Şaphane dağı (mountain) according to isotopic studies.

Geological, geochemical, magnetotelluric and resistivity studies were made on covered fields in the region between the years 2004 – 2006. Low resistivity masses observed at depths of 5-8 km in two dimensional MT models were interpreted as hot–solid or partly melted magmatic masses which their conductivities had increased due to heat (forming the heat source of the geothermal system) and these anomalies continued in two profiles at west (Burçak et al., 2007a and b). As a result of these studies, fluid at a temperature of 109ºC and a flow rate of 4 l/s was obtained from the well KŞÜ-1 at the depth of 1330 m around the vicinity of Üçbaş town. It was detected that, 800 m cover thickness was cut in the well KŞÜ-1 and the average geothermal gradient calculated for the cover in the well was detected as 0,78ºC/10 m. One of the profiles at west is the profile passing through Karacaderbent field where KŞÜ-3 drilling takes place.

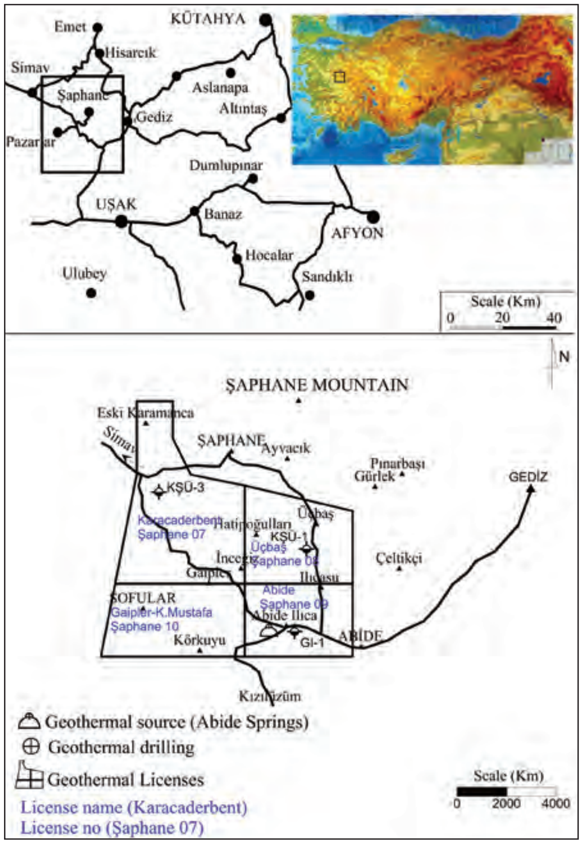

Figure 1- Location map of MTA Şaphane geothermal licenses in which Şaphane Karacaderbent geothermal field takes place.

Hydrothermal alteration samples at surface which influenced Neogene volcanic rocks were taken in the area and their XRD and XRF analyses were performed. An approach towards heat and chemical characteristics of paleo-fluids that caused alteration was also made in this study. Accordingly; it was asserted that two staged alteration had been effective at surface conditions. The first stage is at a temperature of 120–175ºC and weak acidic, and at the second stage is at a temperature of 100–120 ºC at basic pH condition (Burçak et al., 2007*b*).

2. Methods

Within the scope of investigations performed in and around the study area between the years 2003 – 2006, it was carried out 1/ 25 000 scale geological map, 45 hydrochemical and 10 isotopic analyses, magnetotelluric (MT) (at 42 locations) and resistivity studies (at 76 locations) along three profiles (Burçak et al., 2007a and b). Two drilling investigations were carried out at the depth 1330 m (drill no: KŞÜ-1, in 2006) and 2500 m (drill no: KŞÜ-3, between the years

2009 – 2010) at two locations determined at the end of these studies.

Geothermal well KŞÜ-1 was opened near Üçbaş town on the 1st profile and the fluid at a temperature of 109ºC (well bottom temperature) and a flow rate of 40 l/s was obtained at the depth of 1330 m. A cover thickness of 800 m was cut and the average geothermal gradient estimated was detected as 0,78ºC/10 m on well KŞÜ-1 (Burçak et al., 2007*b*). The second profile BB' has also been modeled but has yet been drilled. In this article; geological, chemical and physical conditions considered in selecting profiles, generated models on the third profile, well development and test studies belonging to drill KŞÜ-3 will be mentioned.

3. Geology

The basement rocks of the study area are constituted by Precambrian – Paleozoic gneiss and Upper Paleozoic–Mesozoic schist and carbonated rocks belonging to northern margin of the Menderes Massif. These are tectonically overlain by Upper Cretaceous Dağardı ophiolitic mélange. All these rock units are covered by Miocene–Pliocene sedimentary lacustrine and continental deposits and volcanic rocks of the same age. Quaternary alluvial deposits are the uppermost layers discordantly observed in the study area (Figures 2 and 3).

3.1. Gneiss

Gneisses forming the basement in the study area are widely represented by augen gneisses, granitic

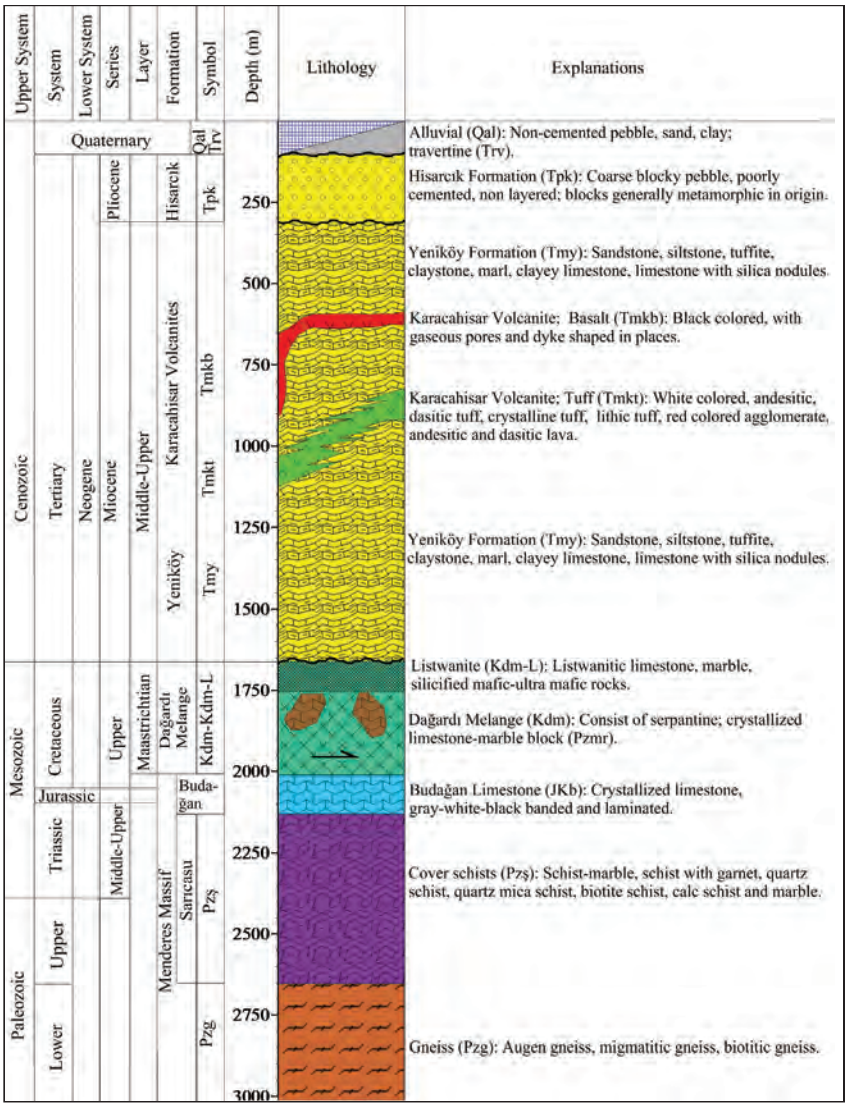

Figure 2- Stratigraphical columnar section of the study area and its surround.

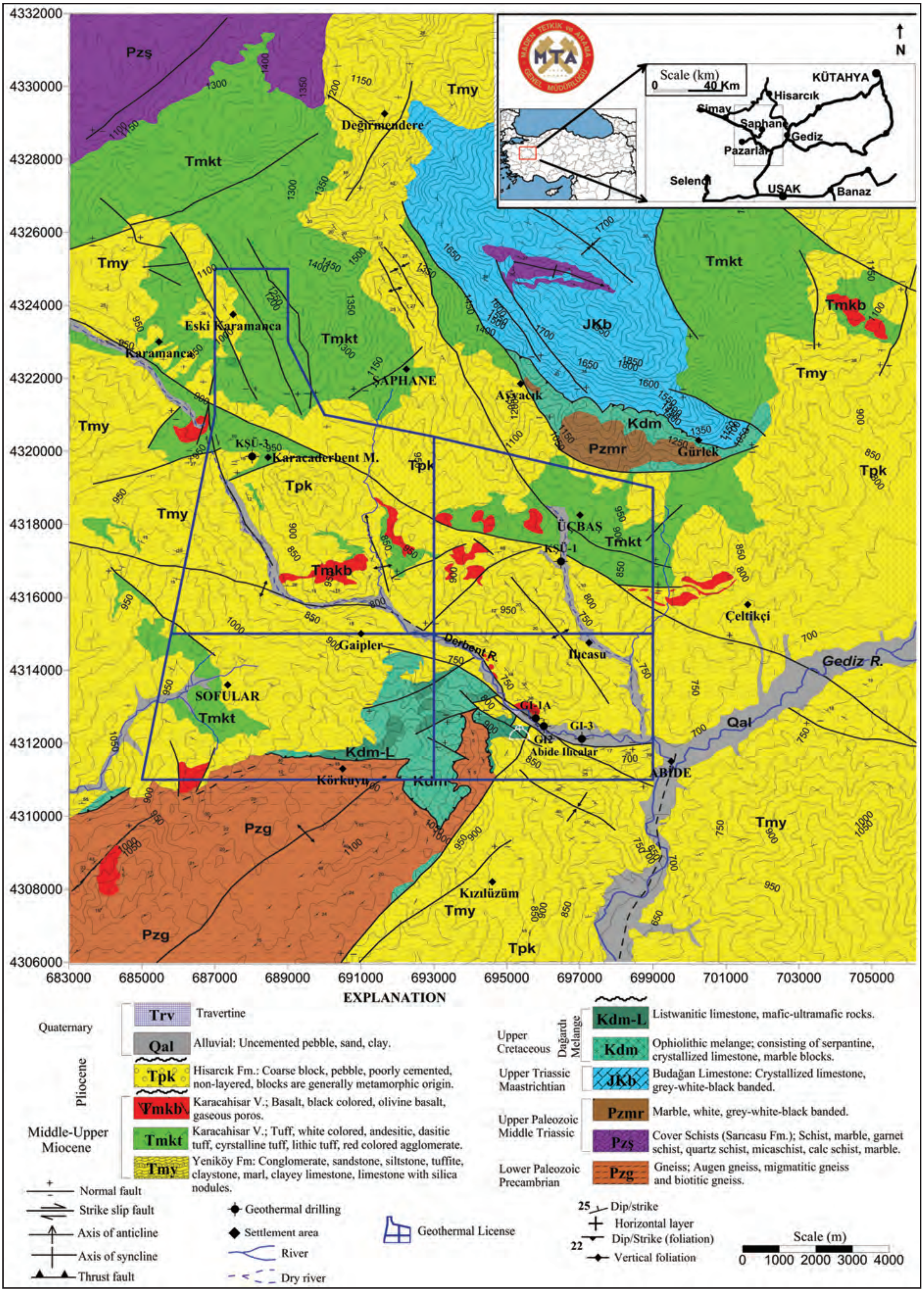

Figure 3- Geological map of the study area

gneisses and by biotitic gneisses. These are observed around Körkuyu village and in its vicinity in south of the study area (Figure 3). It also forms NE-SW trending and NE plunging anticlinal core. The approximate inclination of limbs of the anticline is 20° and the approximate plunge angle of the axis is 5-10° towards NE. The unit forms the basement in the area and its bottom cannot be observed.

Satır and Freidrichsen (1986) determined a probable age of 680 my. for the primary sedimentation of gneisses by using Rb/Sr method and Compton-Jeffcry and Nicolaysen composite diagram. Based on these data the primary formation age of gneisses was accepted as Lower Paleozoic – Precambrian. It was stated that the age of the unit was pre Hercynian (Lower Paleozoic – Precambrian) (Akdeniz and Konak, 1979).

3.2. Schist and Marble (Sarıcasu formation)

This unit crops out around Şaphane Mountain which is located at north of the study area and forms the upper layers of cover schists of the Menderes Massif. The unit was defined by Akdeniz and Konak (1979). The unit is formed by metamorphosed rock units mainly in greenschist facies. The main lithology of the unit is formed by muscovite quartz albite schist, muscovite chlorite calcite quartz schist, chlorite quartz schist, quartz albite sericite schist, talcschist, metaconglomerate, phyllites and quartz minerals consisting of both laterally and vertically transitional, lensoidal marble in variable sizes and metatuff and metadiabasic rock layers (Akdeniz and Konak, 1979). This unit crops out along WNW – ESE trending anticlinal axis in north of Asartepe on Şaphane Mountain in the study area and is made up of schists with variable mineral compositions of mica schist, quartz – mica schist, biotite schist consisting of banded marble and calc schist layers (Figures 2 and 3). One sample taken on this level was defined as muscovite chlorite quartz albite schist in petrographic analysis. The bottom of this unit does not crop out in the study area.

Triassic – Cretaceous aged crystallized limestones are observed as transitional on this unit. Akdeniz and Konak (1979) specified that there were not encountered any fossil for paleontological dating. Since the oldest age taken from Budağan limestones which transitionally overlies on top is Upper Triassic, the age of the unit was accepted as Upper Paleozoic – Middle Triassic based on stratigraphical relationship.

3.3. Budağan Limestone

The unit was first defined by Kaya (1972) and widely crops out on Şaphane Mountain and around Asartepe. Type section of the formation is at Budağan Mountain and in north of Eğrigöz (Figure 3). It is white, dark gray to blackish gray thick to medium layered and black, gray to white colored banded and laminated. It has dolomitic odor especially when black fragments are broken.

These are composed of thick layered gray-black and white banded, with dolomitic odor and recrystallized limestones. During the petrographical study of one sample it has been detected that these have been formed by microcrystalline calcite rarely consisting quartz and sericite. Budağan limestones have a thickness of 200 – 250 m (Figure 2). Schists of the Menderes Massive at the bottom conformably underlie marbles.

According to this fauna of which its paleontological description made on samples inside the unit, it has been detected that Budağan limestione is a continuous series deposited between Upper Triassic – Maastrichtian time (Akdeniz and Konak, 1979).

3.4. Dağardı Melange (Kdm)

The unit was first named by Akdeniz and Konak (1979) and Günay et al. (1986). Gün (1975) stated that the settlement age of allochthonous ultramafic rocks overlying metamorphites which form the basement in and around the study area was Upper Cretaceous. These are observed around Abide Hot Springs in south and around Körkuyu village and in south of Şaphane Mountain in the study area (Figure 3) and are formed by serpentinized mafic and ultramafic rocks, crystallized limestione and marble blocks.

3.5. Tertiary – Quaternary Deposits and Volcanic Rocks

Tertiary – Quaternary volcanic and sedimentary deposits which discordantly overlie basement rocks are largely exposed in the area. These units are represented by Yeniky Formation which deposited in Middle – Upper Miocene terrigenous – lacustrine environment and synchronous Karacahisar volcanics composed of agglomerate, tuff, dacite, andesite and basalt lavas and by Quaternary alluvials (Figure 3).

Yeniköy formation starts with 15 – 20 m thick basal conglomerate which are formed by well rounded, badly sorted and hardly silica cemented metamorphic rock (quartzite, gneiss, schist) pebbles. These are underlain by fine grained pebbles and sandstones. The succession ends with pebbly clay, sandstones, claystone, siltstone, plant bearing and fossiliferous shale, marl and by white clayey and siliceous limestones in upper layers. This depositional sequence is both vertically and laterally transitional with volcanics (Karacahisar volcanics) consisting of tuff, tuffite, agglomerate, dacite, andesite and basalt lavas. Total thickness of this volcano-sedimentary sequence reaches up to 2000 m.

Yeniköy formation was dated as Middle – Upper Miocene based on findings of spore and pollen it contains (Ercan et al., 1978).

These are unconformably overlain by Pliocene aged Hisarköy Formation and crops out at south and east of Karacaderbent. This unit consists of loose cemented block, pebble and sands, and has an approximate thickness of 250 m.

Quaternary alluvial deposits form the topmost layer of the sequence.

4. Hydrochemistry and Isotope Studies

Results of analyses belonging to water samples previously taken from the study area (Burçak et al., 2004; Burçak et al., 2007) and the water samples taken from the well KŞÜ-3 were assessed together (Burçak and Dünya, 2010).

4.1. Classification of Waters

Results of analyses of 45 samples were used in hydrochemical studies. Some physical and chemical characteristics of waters are given below (Tables 1 and 2). It is observed that all water samples accumulate in three groups in Piper diagram. First group waters are represented by cold and low temperature waters. These are Ca-Mg-HCO_3 composition enriched by carbonate and bicarbonate waters. Cations (Ca+Mg>Na+K) fall into 1st region, anions (HCO_3+CO > Cl+SO_4) fall into 3rd region and arrangement of anions and cations fall into 5th region (Figure 4).

Second group of waters are again represented by cold and low temperature waters enriched in Cl+SO_4. Anions and cations fall into 1st and 4th regions, respectively. The arrangement of anions and cations fall into 6th region.

Third group of waters are represented by high temperature Gediz Abide hot spring source and drill water and by hot waters samples of Şaphane hot water drills (KŞ-1 and KŞÜ-3). The composition of waters in this group is Na_2-SO_4, Na-Cl and their carbonate alkalinity is higher than their non-carbonate alkalinity. Cations (Na+K>Ca+Mg) and anions (Cl+SO_4>HCO_3+CO_3) fall in to 2nd and 4th regions. The arrangements of cations and anions fall into 7th region.

It was determined that cold waters were shallow circulating waters having the composition of Ca-Mg-HCO_3 when the Piper diagram was studied in terms of all waters. Samples shown by empty square symbol enriched by Na+K dissolve more Na+K than cold and low temperature waters. It differentiates from those waters indicating more deepened circulation and approaches hot waters. The source of Na+K here is considered as feldspars within basement rocks. SO_4 enrichment is observed in samples forming the 2nd group and in some samples of the 1st group. The mixture of water enriched in SO_4 into Derbent stream within the flow direction can be explained by Abide hot waters (Figure 4).

SO_4 enrichment in 2nd group of waters however, can be explained by gypsum fissures which they might have originated from vapors and gases that cause the formation of alunite deposits by a geothermal system which is considered to have occurred at depths.

High temperature waters fall into 7th region by being enriched in Na+K and SO_4+Cl. This situation indicates that these are more deeply circulating than cold and low temperature waters. It also shows that these might have been affected from deep origin vapors and gases (the origin of Cl-SO_4) and from basement rocks (gneiss, schist) (the origin of Na and K).

Starting from cold waters, it can be said that these waters show an evolution indicating a deep origin towards KŞÜ-3 sample from Gediz sources and KŞÜ-1 drill waters depending on Na+K amount they dissolve (Figure 4). According to this relationship, it was observed that the most evolved and deepest origin water was taken from KŞÜ-3 drill water.

Cold waters accumulate in three different groups in Schoeller Diagram.

Among cold waters in the 1st group, samples D-1, D-2, D-3, KÜ-6, KŞ-11, KŞ-12, KŞ-14, KŞ-53, KG-54, KŞ-77, KG-123, KG-124 are similar type of waters with their more or less a parallel ionic arrangement. The dominant cation in these waters is

Table 1- Results of chemical analyses of water samples (Burçak et al., 2007*a*, *b*; 2010).

Sample	Coordinates			Heat	EC		Na+K	Ca	Mg	Na+K	Ca	Mg	Cl	SO_4	HCO_3	Cl	SO_4	HCO_3+HCO_3
No	Y	X	Z	ºC	µS/cm	pH	Meq/l	Meq/l	Meq/l	% Meq	% Meq	% Meq	Meq/l	Meq/l	Meq/l	% Meq	% Meq	% Meq
GI-2	696008	4312470	719	93,10	3.160,00	7,6	35,52	2,76	1,44	89,43	6,95	3,63	3,44	24,00	13,00	8,51	59,35	32,15
GI-3	697044	4312113	719	78,00	3.410,00	7,3	34,23	3,00	3,57	83,90	7,35	8,75	3,33	23,49	19,01	7,27	51,25	41,48
GI-1A	695789	4312684	719	77,80	2.870,00	7,2	24,93	4,64	4,79	72,56	13,50	13,94	2,74	19,70	16,49	7,04	50,60	42,36
GD-6	695652	4312698	702	76,10	2.990,00	6,9	26,91	5,69	4,50	72,53	15,34	12,13	2,88	20,00	16,98	7,23	50,18	42,60
GD-4	694564	4312776	700	75,30	2.710,00	6,8	22,92	5,29	4,89	69,24	15,98	14,77	2,48	17,67	15,62	6,93	49,40	43,67
GD-7	695695	4312679	705	74,00	3.000,00	7	26,58	5,53	4,57	72,46	15,08	12,46	2,93	18,59	16,98	7,61	48,29	44,10
GD-5	695620	4312747	702	71,50	2.980,00	6,9	27,15	5,78	4,54	72,46	15,43	12,12	2,90	19,88	16,98	7,29	50,00	42,71
GD-2	695346	4312810	719	69,10	2.680,00	6,6	22,57	5,24	5,50	67,76	15,73	16,51	2,48	17,60	15,72	6,93	49,16	43,91
GD-1	695332	4312823	719	65,50	2.830,00	6,5	24,34	5,00	5,40	70,06	14,39	15,54	2,67	18,73	16,48	7,05	49,45	43,51
GD-3	695403	4312820	719	57,10	2.550,00	6,5	20,26	5,24	5,74	64,85	16,77	18,37	2,26	15,74	15,60	6,73	46,85	46,43
KŞÜ-1	696481	4316978	775	90,00	3.490,00	8,3	31,96	5,80	2,51	79,36	14,40	6,23	3,66	22,30	14,27	9,10	55,43	35,47
KŞÜ-3	688020	4319860	874	181,00	3.990,00	7,4	43,27	0,91	0,27	97,35	2,05	0,61	8,51	20,00	12,30	20,85	49,01	30,14
KŞ-20	697609	4323924	994	27,60	409,00	7,6	1,20	1,79	1,57	26,32	39,25	34,43	0,10	1,46	3,42	2,01	29,32	68,67
KG-125	693877	4312258	958	22,40	1.088,00	8,4	8,26	0,26	16,37	33,19	1,04	65,77	0,13	0,24	17,84	0,71	1,32	97,97
KŞ-88	689849	4309517	1014	22,00	418,00	7,3	1,79	2,70	0,57	35,38	53,36	11,26	0,73	0,45	3,52	15,53	9,57	74,89
KK-121	691280	4312586	1078	21,30	1.018,00	7,3	0,31	4,40	9,13	2,24	31,79	65,97	0,37	6,16	9,00	2,38	39,67	57,95
KÇ-103	695113	4306564	775	21,20	888,00	7,5	0,64	2,73	8,30	5,48	23,39	71,12	0,68	0,45	11,88	5,23	3,46	91,31
KÇ-127	701396	4315869	727	20,60	641,00	7,3	7,60	4,00	4,54	47,09	24,78	28,13	0,16	0,36	8,73	1,73	3,89	94,38
KK-119	691550	4313619	984	20,50	1.934,00	7,4	1,02	7,90	21,57	3,35	25,91	70,74	0,61	19,11	12,83	1,87	58,71	39,42
KŞ-118	691293	4314199	948	20,50	1.176,00	7,6	0,45	5,10	10,60	2,79	31,58	65,63	0,41	6,30	10,93	2,32	35,71	61,96

Table 2- Results of chemical analyses of water samples (Burçak et al., 2007*a*, *b*; Burçak and Dünya, 2010).

Sample	Coordinates			EC	Temp.		Na+K	Ca	Mg	Na+K	Ca	Mg	Cl	SO_4	HCO_3	Cl	SO_4	HCO_3+HCO_3
No	Y	X	Z	µS/Cm	ºC	pH	Meq/l	Meq/l	Meq/l	% Meq	% Meq	% Meq	Meq/l	Meq/l	Meq/l	% Meq	% Meq	% Meq
KG-126	693730	4313371	899	1.102,00	19,70	8,6	8,20	0,49	16,53	32,51	1,94	65,54	0,11	0,35	18,00	0,60	1,90	97,51
KG-129	699702	4319930	1112	410,00	19,20	7	0,20	4,90	2,18	2,75	67,31	29,95	0,27	0,27	8,00	3,16	3,16	93,68
KG-123	694817	4310710	826	616,00	18,80	7,6	0,35	1,80	5,18	4,77	24,56	70,67	0,54	0,63	6,10	7,43	8,67	83,91
D-2	693786	4314750	720	821,00	18,60	7,5	1,20	4,14	5,00	11,61	40,04	48,36	0,28	4,85	5,70	2,59	44,78	52,63
KŞ-53	688029	4304863	962	457,00	18,50	7,2	1,42	2,00	1,37	29,65	41,75	28,60	0,22	0,11	4,38	4,67	2,34	92,99
KG-54	694966	4309829	785	732,00	17,10	7,9	0,29	2,70	6,92	2,93	27,25	69,83	0,42	0,97	9,60	3,82	8,83	87,35
D-1	691776	4315732	748	883	17	7,5	1,68	1,84	6,13	17,4	19,1	63,5	0,24	2,56	6,94	2,5	26,1	71,4
KG-124	694295	4310540	906	666,00	16,50	7,5	0,21	1,50	6,80	2,47	17,63	79,91	0,26	0,35	8,74	2,78	3,74	93,48
D-3	695257	4313050	710	894,00	16,50	7,4	1,30	2,39	5,78	13,73	25,24	61,03	0,26	4,95	5,32	2,47	47,01	50,52
KŞ-16	694124	4319585	985	665,00	16,00	7,4	0,34	4,96	1,64	4,90	71,47	23,63	0,44	0,52	5,80	6,51	7,69	85,80
KG-122	691472	4312088	1123	561	15,4	7,1	0,39	5,47	1,84	5,1	71	23,9	0,68	1,27	6,56	8	14,9	77,1
KŞ-78	686073	4311960	925	908,00	15,40	7,1	0,38	5,83	5,56	3,23	49,53	47,24	0,17	4,30	8,60	1,30	32,90	65,80
KÜ-6	694559	4312116	908	812,00	15,00	7,8	0,55	2,89	7,23	5,15	27,09	67,76	0,58	0,81	10,35	4,94	6,90	88,16
KŞ-84	688544	4314402	983	848,00	15,00	7,2	0,62	5,28	3,94	6,30	53,66	40,04	0,10	2,89	8,17	0,90	25,90	73,21
KŞ-11	694379	4324156	1547	323,00	15,00	7,8	0,06	1,77	2,00	1,57	46,21	52,22	0,21	0,67	3,04	5,36	17,09	77,55
KŞ-77	687471	4310074	1008	332,00	14,50	6,8	4,28	1,82	2,00	52,84	22,47	24,69	0,34	0,73	3,43	7,56	16,22	76,22
KG-93	695845	4318262	892	911,00	14,30	7,3	1,93	3,27	2,67	24,52	41,55	33,93	2,00	0,52	5,88	23,81	6,19	70,00
KŞ-21	687642	4323794	991	89	14	5,9	0,28	0,59	0,12	28,3	59,6	12,1	0,09	0,54	0,38	8,9	53,5	37,6
KŞ-112	690367	4322563	1167	81,00	13,80	4,8	0,45	0,24	0,00	65,22	34,78	0,00	0,16	0,44	0,19	20,25	55,70	24,05
KG-92	697687	4317494	823	563,00	13,70	7,1	0,58	3,23	2,35	9,42	52,44	38,15	0,39	1,40	4,17	6,54	23,49	69,97
KG-91	697040	4314875	736	3.560,00	13,40	7,6	1,23	22,70	43,27	1,83	33,78	64,39	1,05	54,34	8,93	1,63	84,48	13,88
KŞ-110	695880	4325679	1807	266,00	9,30	7,6	0,00	2,03	1,42	0,00	58,84	41,16	0,00	0,22	3,60	0,00	5,66	94,34
KŞ-14	695004	4323505	1447	327,00	9,00	7,8	0,05	1,90	2,00	1,19	48,14	50,67	0,16	0,44	3,13	4,29	11,80	83,91
KŞ-107	698806	4326473	1430	686,00	7,20	7,2	0,26	4,49	2,67	3,50	60,51	35,98	0,18	3,25	5,80	1,95	35,21	62,84
KŞ-12	694766	4325469	1783	279,00	7,10	7,9	0,07	1,76	1,31	2,23	56,05	41,72	0,13	0,34	2,75	4,04	10,56	85,40

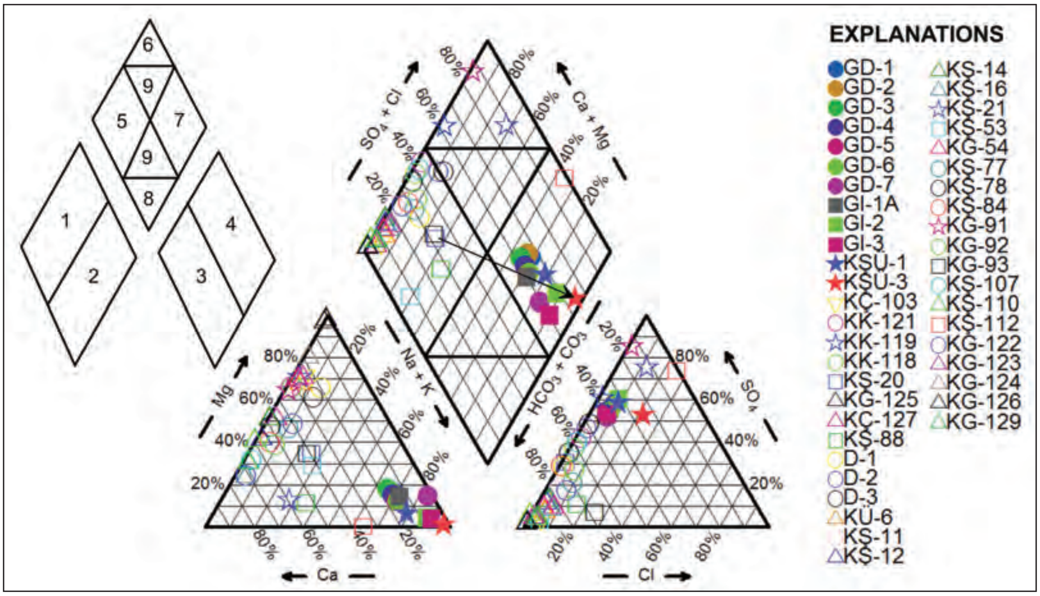

Figure 4- Piper diagram of water samples (direction of the arrow indicates the evolution of waters towards deep origin).

Mg (Mg>Ca>Na+K) and the dominant anion is HCO_3 with HCO_3>SO_4>Cl arrangement. Sulfate enrichment is observed only in samples D1, D2 and D3 taken from Derbent River. There is observed a sulfate enrichment in the direction of Derbent river towards Abide hot springs (from D1 towards D2 and D3) and this situation can be explained by the mixing of some sulfate rich wastes and/or by the mixing of Abide hot springs into the river (Figure 5).

In samples KG-110, KŞ-1, KŞ-78, KŞ-84, KG-92, KŞ-107 KG-129 which form the second group, dominant cations are Ca, Ca/Mg and the cation arrangement is Ca≥Mg>(Na+K). However, the dominant anion in these samples is HCO_3 and the type of arrangement is Ca-Mg-HCO_3 and Ca/Mg-HCO_3. These have closely parallel ionic concentration to each other and are waters with the same origin (Figure 5).

When first and second group of waters are considered in terms of their ionic arrangements, they can be regarded as waters fed from shallow depths.

However; samples KG-122 and KŞ-27 show a parallelism with respect to anion and cations except HCO_3+CO_3 though having a bit different concentration. Therefore; these can be accepted as a water type having the same origin. Enrichment in Na in sample KŞ-77 taken from fractures of gneisses and in sample KG-122 taken from Dağardı mélange located at the tectonical contact on gneiss could be originated from feldspars within the body of gneiss and these waters might be fed from a bit deeper levels compared to other waters.

Samples KŞ-126, KG-91, KG-93, KŞ-112 and KŞ-21 which form the third group possess water type originated from different sources (Figure 5). Besides; these waters do not much resemble to each other as well. Samples and their related anion and cation arrangements indicating the type of waters are as follows; KŞ-126: Mg>(Na+K)>Ca cation and HCO_3>SO_4>Cl anion arrangement, KG-91: Mg>Ca>(Na+K) cation and SO_4>HCO_3>Cl anion arrangement, KŞ-93: Ca>Mg>(Na+K) cation and HCO_3>Cl>SO_4 anion arrangements, KŞ-112: (Na+K)>Ca>Mg cation and SO_4>HCO_3>Cl anion arrangement, KŞ-21: Ca>Na+K>Mg cation and HCO_3>SO_4>Cl anion arrangement. These samples are different than 1st and 2nd group of cold waters with their ionic arrangements and more deeply charged waters (Figure 5).

Areas where these waters are observed indicate a much deeper charging with the increase of SiO_2 and Cl values (Figure 5). Among these samples; KŞ-93 possesses ionic concentration contours cutting through samples in other groups. KŞ-91 is the cold water sample having the highest ionic concentration. This sample shows enrichment in terms of Ca and SO_4 different than all other samples.

Among low temperature waters according to Schoeller diagram, samples of 103, 118, 119, 121 and 127 are the waters having the same type of origin.

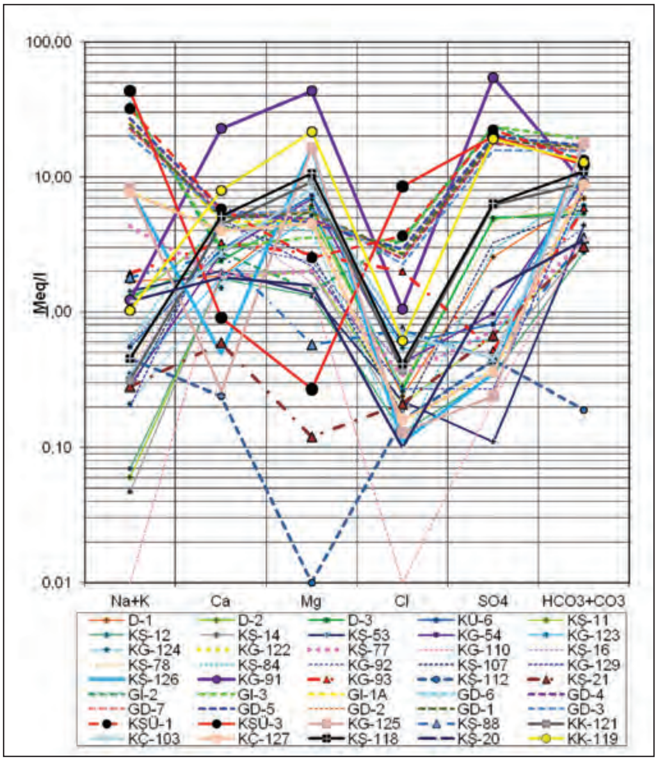

Figure 5- Semi logarithmic Schoeller diagram of water samples

They have the similar origin because of having parallel ionic arrangement with cold waters in the 2nd group though they possess a bit higher ionic concentration. Sample 125 differs from these samples but shows a similarity with sample 126. However; samples KŞ-21 and KŞ-88 have completely different origin than cold waters but have a closer origin in them (Figure 5).

It is seen in the Schoeller diagram that, hot water sample of KŞÜ-3 well is the sample enriched the most in Cl. Considering the temperature of this sample; it is the deep originated water. Also regarding the ionic distribution, the sample of KŞÜ-3 well shows more differences than other waters in terms of Cl content and becomes different passes through the contours of concentration. It can also be stated that, all other high temperature water samples have the similar origin (Figure 5).

It is also seen that, samples KŞ-20, KŞ-88 and KK-127 among low temperature waters show an approximate parallelism with high temperature waters but are similar waters in origin considering their low ionic arrangements. However; other low temperature samples do not show any resemblance with how waters (Figure 5).

4.2. Isotope Studies

Total of 22 Oxygene-18 (^{18}O), deuterium (D) analysis results were used in order to determine the origin and height of the drainage area in the study area (Burça et al, 2004).

All samples collected from the area lies between Mediterranean Aegean Meteoric line and Global Meteoric line in O18-D graph. (Burçak et al 2007*a*, 2007*b*). Samples accumulate in three groups according to O18-D analysis results. Waters in the 1st group are closely parallel to Mediterranean Aegean Meteoric water line and represent the waters of the margin zone which have high drainage area. There was observed enrichment in O18 and D in waters forming the 2nd group. This indicates that these waters have been subjected to vaporization during or after drainage. Hot waters forming the 3rd group (Abide region) show a rightward deviation from Meteoric line by being enriched in ^{18}O. The enrichment of ^{18}O depends on the reaction between water and rock. The water was enriched in ^{18}O due to silicates which it melts during its circulation within rock (Figure 6).

When deuterium values are plotted against topographic elevations of points where water samples taken from different heights, H: Height (m)

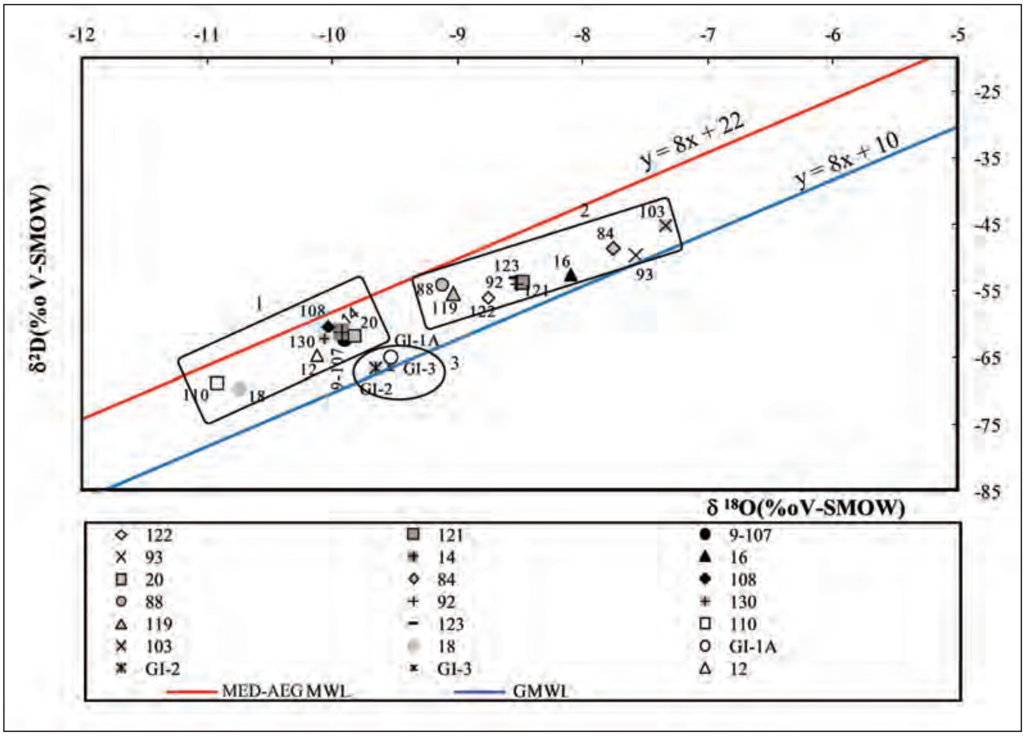

Figure 6- [18]OδD graph of waters collected from the study area (Burçak et al, 2007*a*).

"Deuterium = - 0.00168 (H) – 35.823" (1)

Line 1 was denoted as the height tendency line (Figure 7). When deuterium value of hot waters collected from Gediz Abide area are put into (1) in the equation above, the drainage height of these waters were calculated as 1.700 m (Burçak et al, 2007*a*). This height value corresponds to the top of Şaphane Mountain located at north within surficial drainage area (Burçak et al, 2007*a*).

5. Selecting The Target Area For Geothermal Investigation

The boundary of the catchment area on the field was detected by topographical data, isotopic and hydrochemical studies. Cl and SiO_2 distribution of water samples were gridded and their contour maps were prepared by Kricking method using Surfer10 software (Figures 8 and 9). In doing so, the Cl and

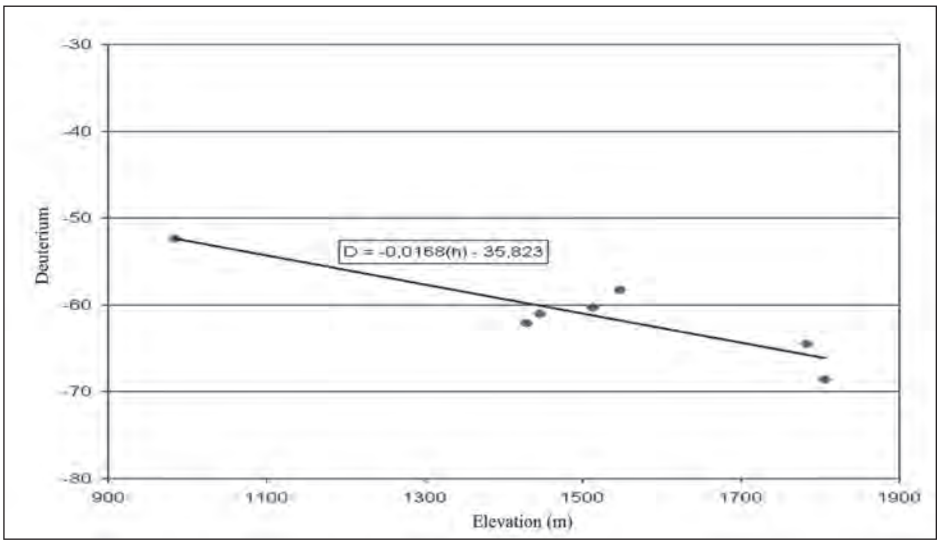

Figure 7- Deuterium vs. height graph of the study area (Burçak et al, 2007a).

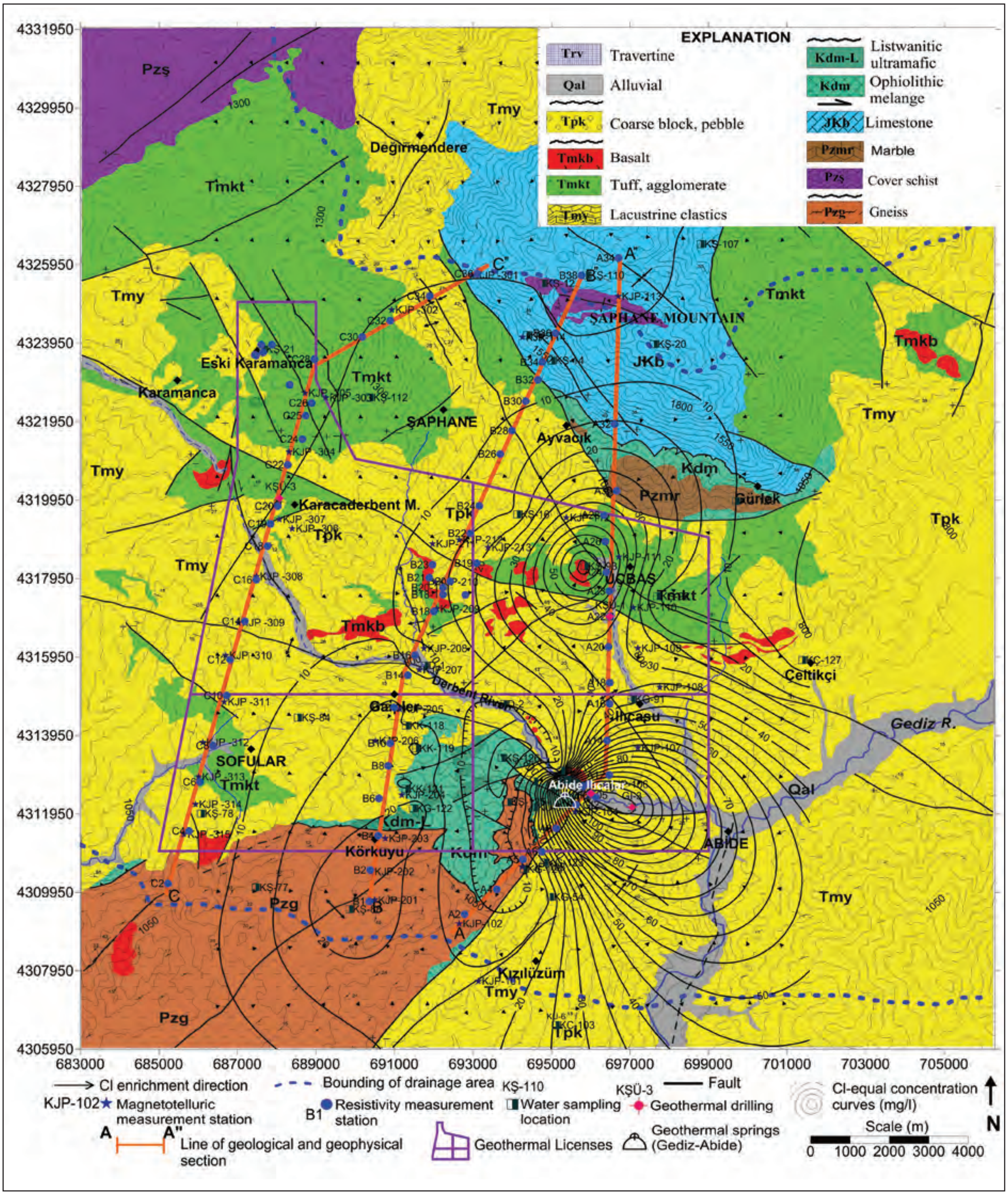

Figure 8- Map showing the geology of the study area and its surround, license areas, water sampling points, Cl equal concentration, boundary of the catchment area, generated geophysical profiles and the map of measurement points.

SiO_2 enrichments and the flow and drainage directions were revealed. There was detected SiO_2 enrichment in two regions and Cl enrichment in one region outside the Abide geothermal field which are observed on equal concentration maps of Cl and SiO_2 (Figures 8 and 9). It was observed that these fields corresponded with covered areas within graben (Figures 6 and 7) and Cl and SiO_2 enrichments in waters from Şaphane Dağı tops to the south. It was observed that this situation was compatible with boundaries

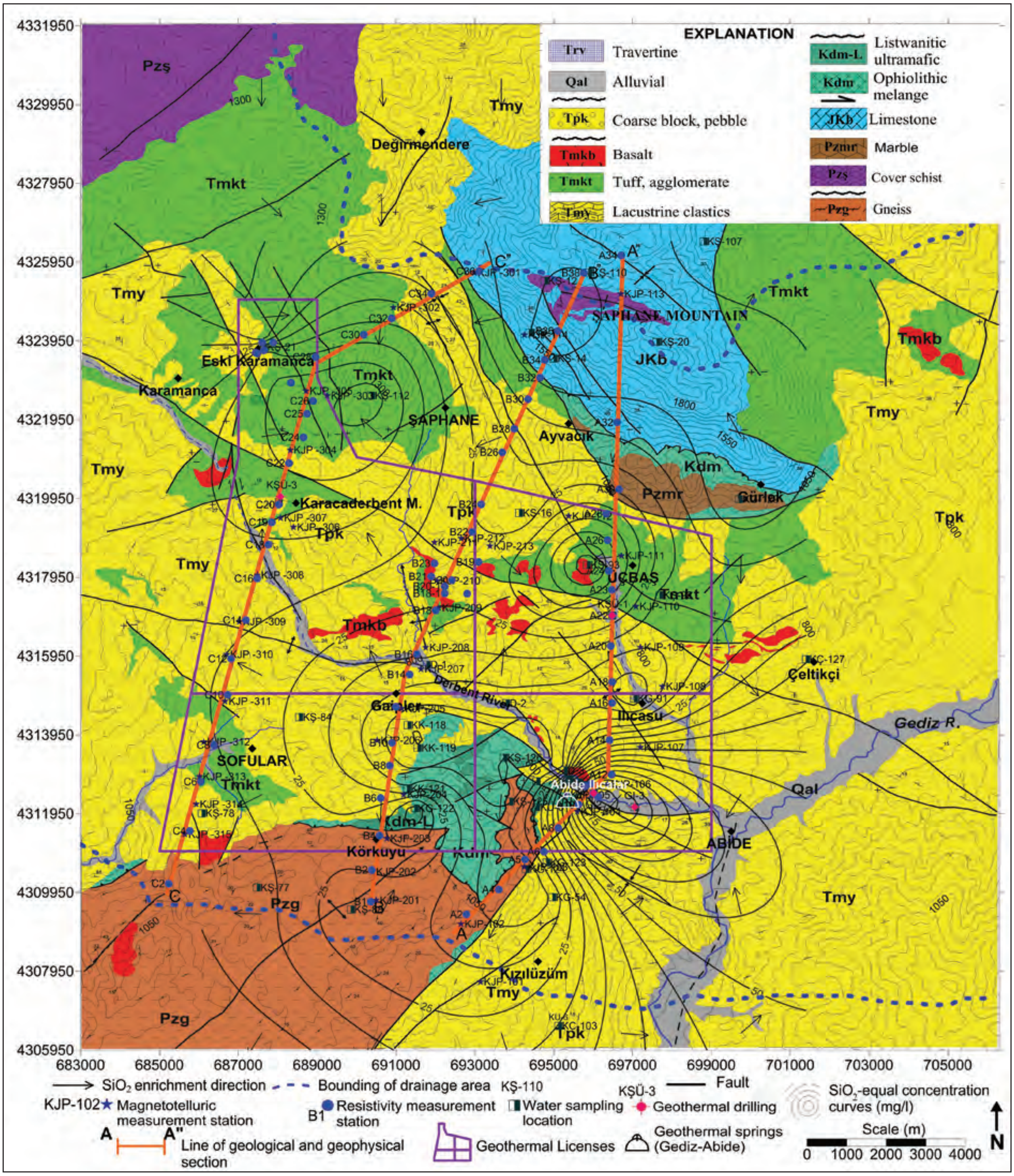

Figure 9- Map showing the geology of the study area and its surround, license areas, water sampling points, SiO2 equal concentration, boundary of the catchment area, generated geophysical profiles and the map of measurement points.

of the catchment area which had been drawn based on the geological structure and topography (Figures 8 and 9). Isotopic studies have also indicated that the boundary of the catchment area reached the tops of Şaphane Mount at north (Burçak et al., 2007). It was revealed in geological studies that the area had a graben structure covered by NW-SE directed, thick Miocene deposits and volcanic rocks. This graben deepens towards south starting from Şaphane Dağ and towards north starting from Derbent valley where available springs are present (Burçak et al., 2007). It was seen that the field was important in terms of geothermal activity and a buried geothermal system might have developed when geology, hydrochemistry, isotope and topographical data mentioned within this scope were assessed altogether. Suitable profiles for geophysical investigations (MT and resistivity) which will bring out the geological structure and the expected deep seated geothermal system were made in the area, considering that a buried geothermal system in the area could have developed. All geophysical investigations were applied in 20 km long, approximately directing in N-S three profiles (Figures 8 and 9).

6. Geophysical (Magnetotelluric and Resistivity) Investigations

Magnetotelluric and resistivity measurements were taken along three profiles in the selected target area (Figure 10). Within this scope, MT studies at 42 points and resistivity studies at 76 points were performed. Magnetotelluric estimations were modeled in two dimensions using WinGLink™ software. Low resistivity zones detected at the depth of 5–8 km by MT investigations were interpreted as the probable heat source. Resistivity measurements taken along the same profiles were assessed generating apparent resistivity sections and electrical structure sections as well. Profiles AA' and BB' will not be mentioned, only the studies carried out along the profile CC' which is 19 km long located at the westernmost part of the study area (Figures 5 and 6) will be explained here. The profile extends in directions at N20E in south and at N45E in north (east of Eski Karamanca). The reason of this break is because the profile was generated as vertical to fault delineation along the trend.

6.1. Magnetotelluric Studies

Total of 15 measurements was taken along the profile CC'. Resistivity change of the profile CC' in two dimensional MT section is observed both along profile and in vertical direction. Signal values belonging to measurement results in MT stations taken along the profile were back analyzed until 0,01 Hz (100 s) and two dimensional models are down to a depth of 1000 m (these generated models were presented in the form of sections).

When the profile was studied from north to south, it was seen that high resistivity units (257 – 150.000 ohm.m) measured at point KJP-301 to the north of the profile match with the basement rocks (Budağan limestones and schists) (Figures 8 and 9). It was

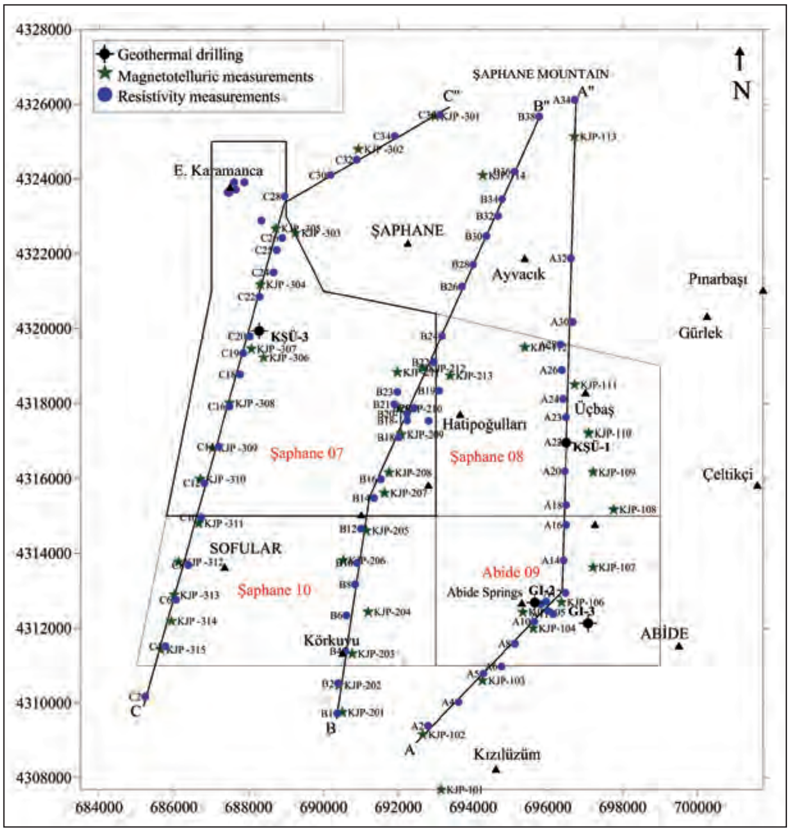

Figure 10- Location map of geophysical measurements.

observed that these high resistivity measurements at measurement points of KJP-302, KJP-303, KJP-305 and KJP 304 were at shallow depths (Figure 9). Faults forming the northern boundary of the graben are clearly observed around the measurement point KJP-304 along two dimensional MT model. However the faults forming the southern boundary are easily detected around the measurement point of KJP-313. Miocene deposit and volcanic tuffs are evident with low resistivity (<60 ohm.m). Although there is certain data about thickness of these units, it is considered that it might be around 1500–2000 m thick also taking geological data into account. Sections represented by high resistivity beneath this low resistivity section which is represented by sedimentary and volcanic rocks display basement rocks consisting of gneiss, schist, marble and limestone of the Menderes Massif and granitic rocks of which it is considered to have been at much deeper parts of the crust. The resistivity values with basement rocks increase up to 150.000 ohm.m at deeper parts of the crust (Figure 11).

There was observed two anomalies which divided very high resistant structure in a highly resistant crust along the profile CC' (A1 and A2). It is also considered that these profiles originated from deeper parts of the earth. These two masses which are independent from each other and distinct with low resistivity were interpreted as magmatic intrusions which have not yet lost their heat, as partly melt and/or as solid state at depths of 5000 – 6000 m (Burçak et al., 2005; 2007a, b and c). It is considered that these intrusions form the heat source of the geothermal system.

6.2. Resistivity Studies

The profile CC' starts from the south of Sofular village and extends until Şaphane Dağı through Eski Karamanca. It is in N-S direction and is 19 km long. There are 20 measurement locations along the profile (Figure 10).

When the apparent resistivity section is studied, low resistant, distinctive anomaly zones were detected at depths of 400 – 1500 m between the points of C18, C12, C14, C16 and C19, C20, C22. These zones were then correlated with cover type units (fine grained and impervious). Resistivity values increase towards northern part of the profile and reaches its maximum value around Şaphane Dağı where the basement rock crops out (Figure 12).

The section of electrical structure was extracted assessing the apparent resistivity. It is highly believed that among points of C6-8-10-12-14-16-18-20 in the section of electrical structure, the thickness of

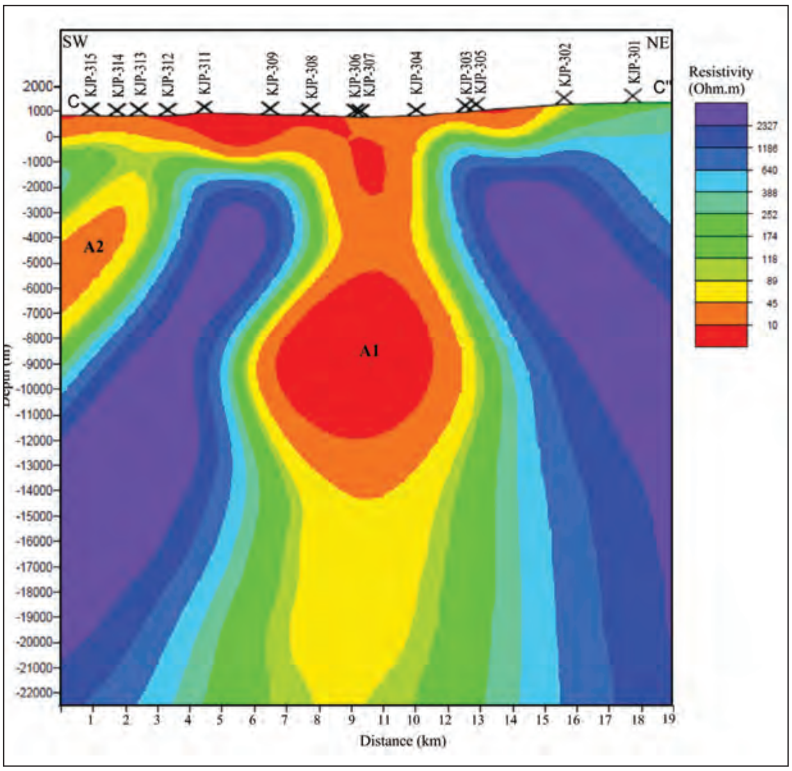

Figure 11- Two dimensional magnetotelluric model of the profile CC'.

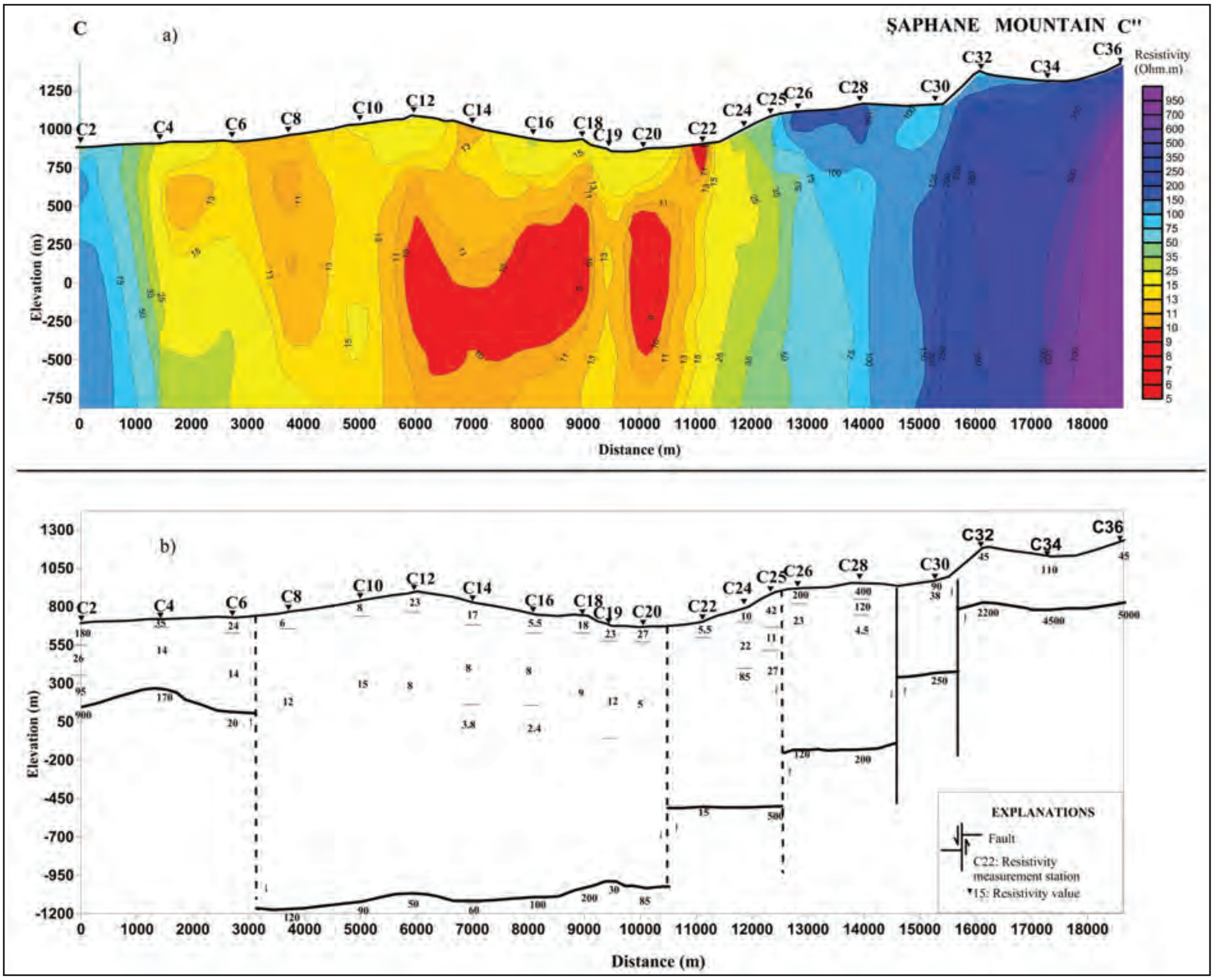

Figure 12- The apparent resistivity and structural section of the profile CC'.

fine grained units which starts from the surface is extremely thick. However; limestones taking place at the basement of these points (probably) are distinctive with high resistivity. The depth of the basement here was anticipated as 900 -1000 m (Figure 12b). The depth of electrical basement did not exactly match with the depth of geological basement. The resistive basement associated with depth at which the curve starts to incline in geological resistivity studies may not always correspond with basement rocks (mostly metamorphic). This is a case frequently encountered when fine grained units (such as; conglomerate, agglomerate, blocky conglomerate) at depths are close to the basal section of cover rock type units. Therefore, bearing geological data in mind and considering that the depth of base rocks is higher than 2000 m, the drilling depth was foreseen as 2500 ±250 m.

7. Drilling and Test Studies

Based on all this information, drilling investigations started in November 2009 at selected drilling location (KŞÜ-3) and completed in July 2010 at depth of 2500 m. The development and test studies in the well were applied after the well had been completed. In the exploratory geothermal well KŞÜ-3 which was run at 2500 m around Şaphane Karacaderbent, following units were cut starting from surface; tuff and claystone, sandstone, siltstone and conglomerate intercalating with tuffite belonging to Middle – Upper Miocene Yeniköy Formation between 0-2030 m; rocks such as serpentine and pyroxene belonging to Upper Cretaceous Dağardı Melange between 2030-2430 m. Upper Jurassic – Lower Cretaceous Budağan Limestones were penetrated at a depth of 2430 m, which are below the tectonical contact of Dağardı mélange then full mud loss occurred in the drilling (Burçak and Dünya, 2010). Drilling with mud loss was proceeded down to 2500 m then the well was completed and equipped at this depth (Figure 13).

The well was drilled by a 17½" diameter sized drill bit between 0-716,25 meters and was equipped with 13$^{3/8}$" diameter sized closed casing. Between 716,25–

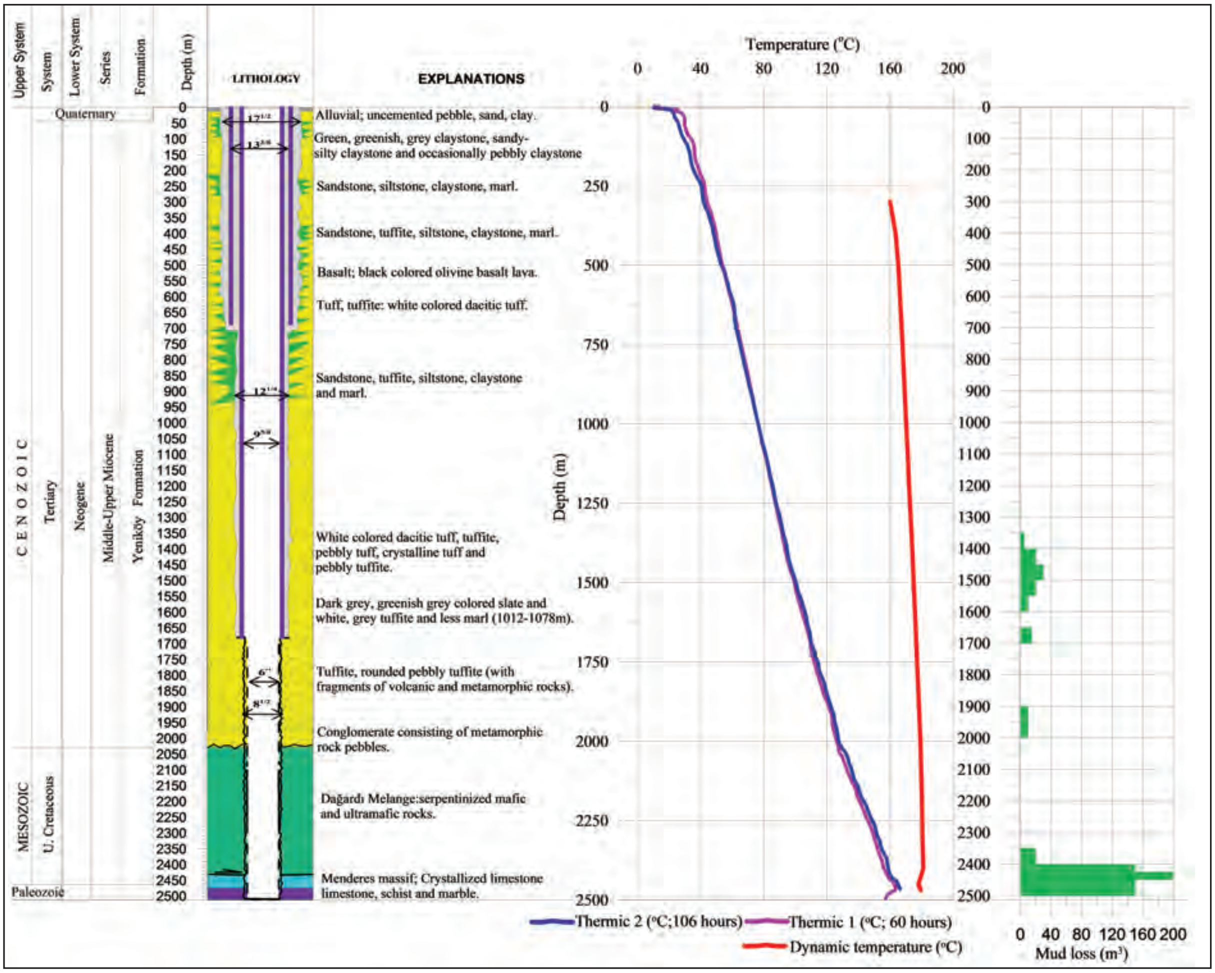

Figure 13- KŞÜ-3 geothermal drill, composite well log (lithology, thermal logs, dynamic temperature and mud losses).

1.685 m, a 12¼" diameter sized drill bit was used for drilling and between 0-1.1680 meters; the well was equipped by a $9^{5/8}$" diameter sized casing hole. A well bottom temperature of 166,5ºC was estimated at 2500 m in thermal log size waiting 100 hours on the wellhead.

During drilling operation, sometimes problems such as the sticking and compaction of the equipment at clayey layers were experienced within mantle rock Yeniköy formation between 1200 – 1400 m. During this investigation in layers of Dağardı mélange between the depths of 2030-2430 m, risk of compaction of equipment were experienced due to downfalls. These risks were tried to be solved by using condensed mud with barite and tap cement. The drilling has been completed in big difficulties. Passing into Budağan limestones which form the reservoir between 2430-2500 meters, mud condensed with barite at a density of 1,25 – 1,30 g/cm^3 was used in order to prevent the downfall of mélange in upper layers. During this injection, mud more than 500 m^3, cuts and cuts of the mélange that had fallen down from upper layers escaped into the reservoir. So, the reservoir was subjected extremely to physical contamination by mud and falling cuts. Long and endeavoring test and development studies were carried out in order to improve the well performance and remove the physical contamination that had occurred in the reservoir. In doing so; twice acidification and three times test studies were done before and during each acidification. Within this scope, static temperature, static pressure, water loss, multi flow rate injection, build up and fall off tests were performed. At the very end, investigations were completed performing production test studies.

7.1. Pre-acidification Production Development and Test Studies with Compressor

Following the wash in the equipped well, the production at a flow rate of 1-2 l/s and 35-40ºC temperature was obtained during production tests with compressor. During 10 days production with compressor, the flow rate has continuously increased and reached 8 l/s and the temperature increased to 90ºC.

Later on; following studies were proceeded such as; static temperature, static pressure, water loss test, multi flow rate injection, build up and fall off tests.

7.1.1. Pre-acidification Static Temperature and Static Pressure Tests

Static temperature test was started approximately after 5 days wait. Since the measurement device sat down on the fill at 2.475 m, the measurement was taken at 2.475 m. and the temperature was measured as 178,57ºC. According to static pressure measurements, the static level in the well was observed as 180 m. (Figure 14).

7.1.2. Pre-acidification Water Loss Test

Water loss measurements to determine reservoir levels were taken at a pump rate of 8,6 l/s and a well head pressure (WHP) of 670 psi (46 bar). Total of 160 tons freshwater was pumped into the well during the study. When the temperature graph was studied after water loss; it was detected that, cooling increased starting from the level of 2000 m. The level at which the maximum cooling was observed is between 2425 – 2450 meters and this level forms the main reservoir (Figure 15).

7.1.3. Multi Flow Rate Injection and fall-off Tests

The measurement was started lowering the pressure measurement apparatus down to 2450 m and measurements were taken at two different flow rates (5,06 l/s and 10 l/s). At minutes 145' and 225', total of 170 psi pressure drop was observed in the reservoir during multi flow rate injection test. Break and rupture (relief) was generated in the reservoir (Figure 16). The injection index was estimated as 0,2615 (ton/h) according to results of the first multi flow rate injection measurement (Figure 17). Pressure drop according to fall off measurements before the acidification have occurred at a long time period. This indicates that the reservoir is less permeable and there is a contamination (Figure 18).

7.2. Development Study with Acidification

At drilling stage; mud losses condensed with barite and fall offs occurred and cuts of the formation escaped into the reservoir. Therefore; acidification process was planned in order to remove the blockage in the reservoir. To do that; HCl and HF acid mixture was used as the reservoir consists of limestone and the cuts that escaped into the reservoir is formed by Fe-Mg silicates (such as; pyroxenite, dunite) which were silicified along fractures at places belonging to mélange. For this purpose; mixture of 30 tons of HCl at a concentration of 30% and 1,5 tons of HF at a concentration of 70% was used.

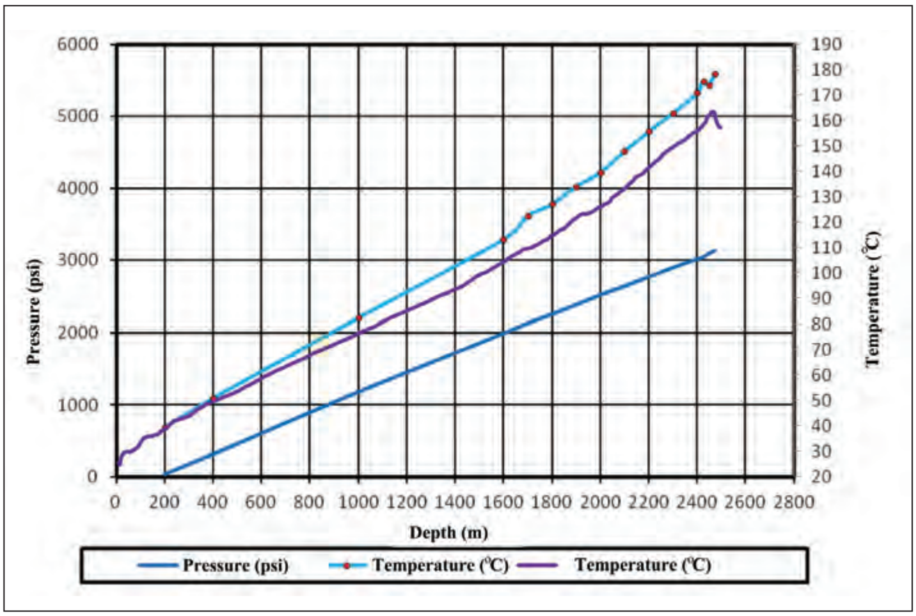

Figure 14- Pre-acidification graph of static temperature and pressure measurements.

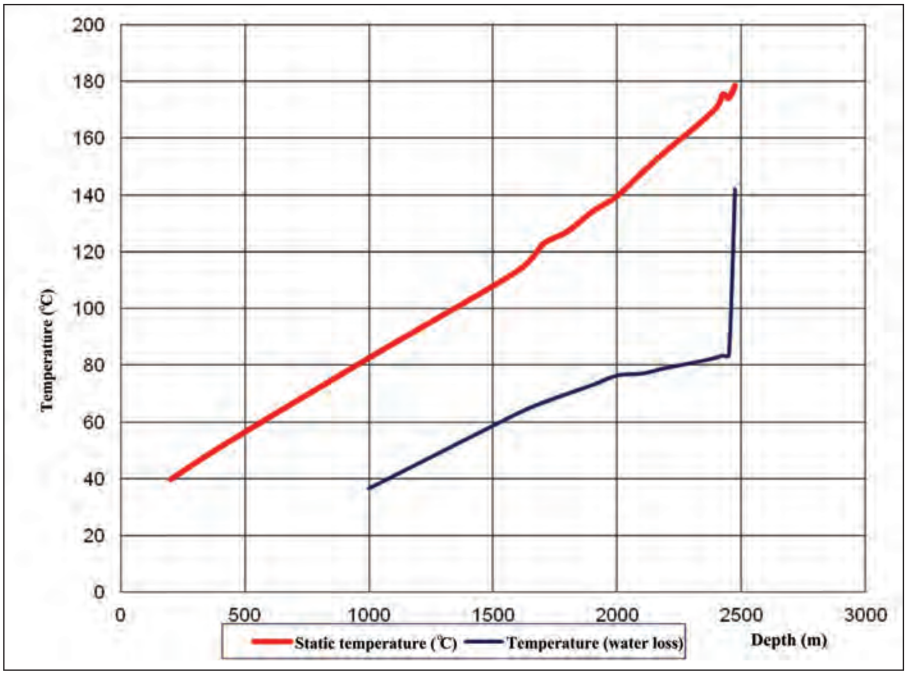

Figure 15- Graph of static temperature and water loss temperature measurements.

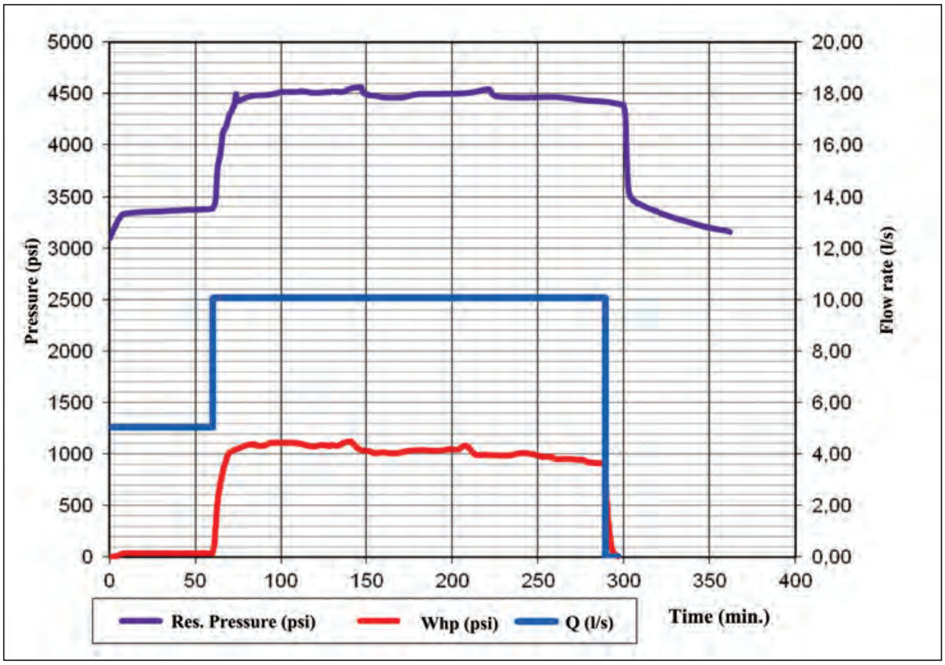

Figure 16- Pre-acidification graph of multi flow rate injection and pressure measurement.

For acidification, drill pipe (DP) at a diameter size of 3 ½” was set to a depth of 2.404 m. After acid cap and pump connections had been made, the acid pumping was started at 5:28 pm and completed at 6:15 pm. WHP (well head pressure) started to drop down 20 minutes after the acid pumping had started and 35 minutes later the pressure dropped down to 0 (Figure 19). Drill pipe was then pulled back and the operation was completed.

On 11th of June 2010 at 9:30 pm, production studies were started running compressor, lowering 3 ½’ diameter sized drill pipe to a depth of 360 m. Approximately 2 minutes later the flow started in the

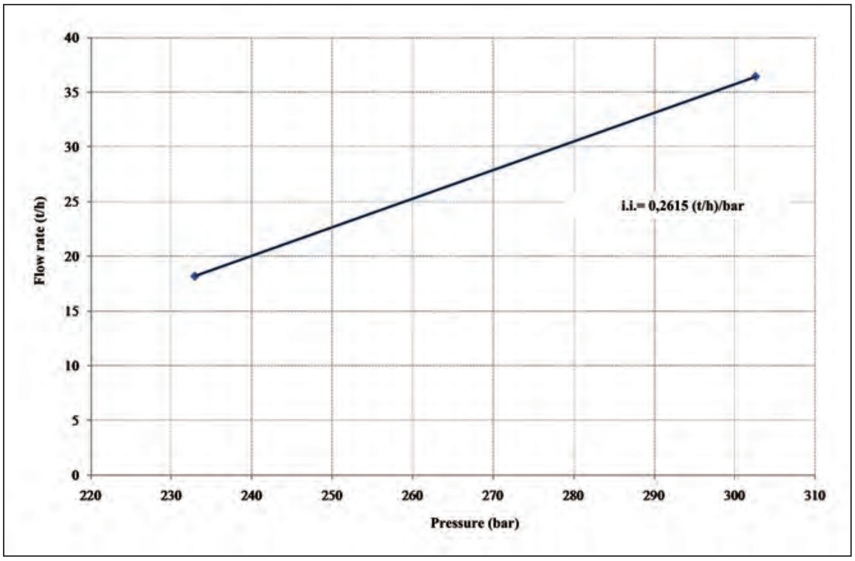

Figure 17- Graph of pre-acidification injection index.

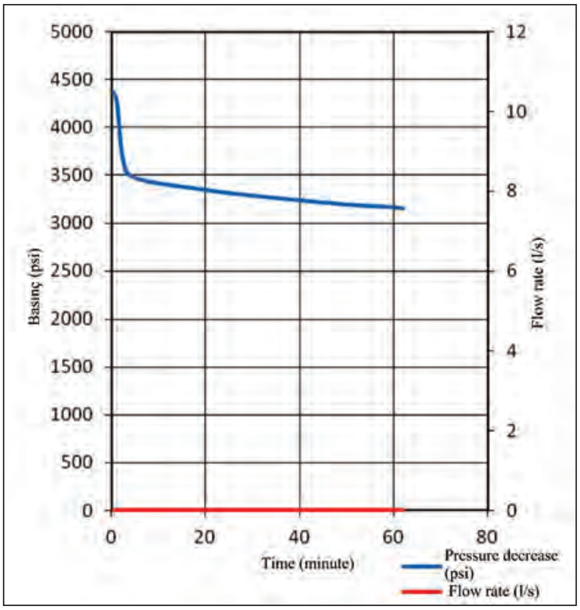

Figure 18- Graph of fall-off in the well belonging to pre-acidification.

well. During this stage, the area was environmentally secured. At 9:00 pm gases which occurred as a result of reaction started to smell out. Smell of sulfur was encountered at the production and controlled dilution was made. The fluid color was observed as blurry at the beginning but became clear around 11:30 pm. The continuity in the production was observed.

Production continued until 11:30 am, 12th June, 2010 at a WHP of 1,5 bar without shutting down the compressor. Compressor was stopped when the well head reached to a temperature of 101ºC. The well then started to production stage as artesian at a WHP of 1,1 bar. Fluid flowing out of the well was drained out under control and pH was estimated around 8-9 by multi conductivimeter.

7.3. Post-acidification Test and Production Studies

Some tests were repeated after acidification. Dynamic temperature, dynamic pressure, build up, multi flow rate injection, fall off and production test studies were performed.

The pollution which caused blockage in the well was mostly removed by acidification studies. After acidification, production stage in the well has started with artesian, and injectivity, productivity indices and production values of the well have significantly increased.

7.3.1. Post-acidification Dynamic Temperature and Pressure Measurements

Considering that the well reached its stable state, dynamic measurements began 24 hours later than the artesian production had started. While the production of the well was at a flow rate of 72 tons/h at 1 bar WHP, the dynamic temperature measurement was taken starting from a depth of 300 m to bottom (Figure 20). As there was 360 m long drill pipe inside the well, 300 m long measurements were taken within drill pipe. As the measurement device sat over the cut at a depth of 2.471 m, the measurement had to be completed pulling the device back to a depth of 2.470 m. The maximum dynamic temperature estimated inside the well is 181,2ºC at 2400 m depth.

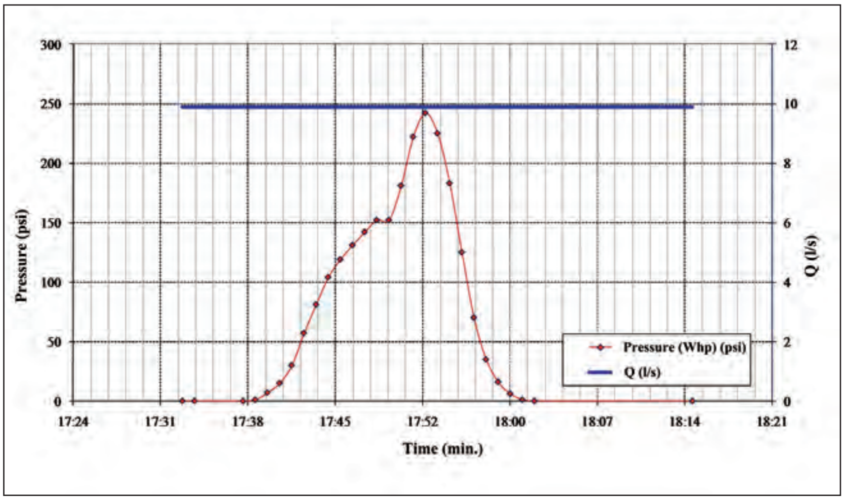

Figure 19- Well head pressure (WHP) change during acidification.

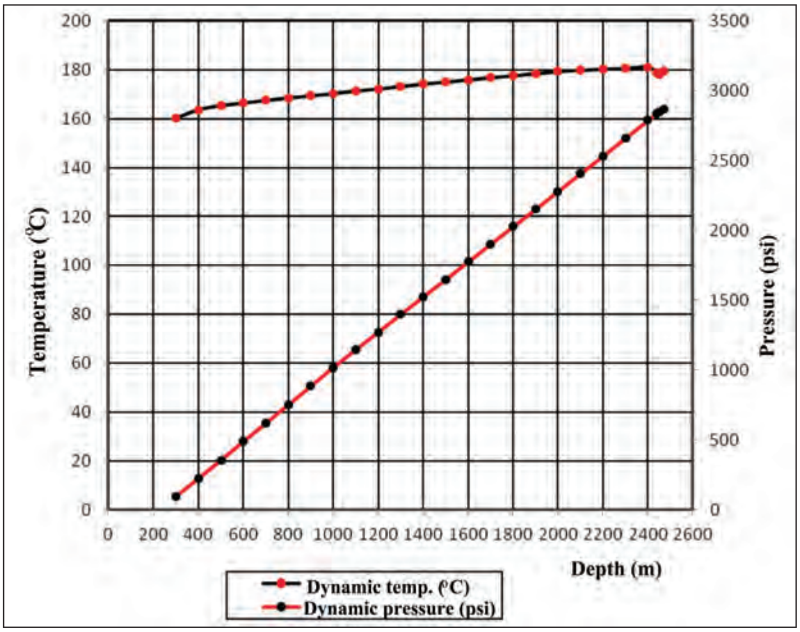

Figure 20: Graph of dynamic temperature and dynamic pressure measurements.

7.3.2. Post-acidification Build-up Measurements

The test was performed setting the measurement device to a depth of 2.450 m while the production of the well had been running at a flow rate of 72 tons/h and at a pressure of 1 bar WHP. According to the results of measurement the productivity index was calculated as; Pi: 4,303 (tons/h) (Figure 21).

7.3.3. Post-acidification Multi Flow Rate Injection and Fall off Tests

For stabilization, the well was completed after sufficient production had been made then measurement started after 18 hours wait. Injection studies at three different flow rates as; 9,8 – 19,11 and 28,18 l/s were carried out and pressure change with respect to time was estimated (starting at 2.270 m) (Figure 22). According to measurement results the injection index was calculated as 1.2093 (tons/h) bars. Significant improvements were supplied in the post-acidification injection index of the well. The pre-acidification injection index which was 0,2615 tons/h/bar then increased to 1,2093 tones/h/bar after acidification (Figure 23).

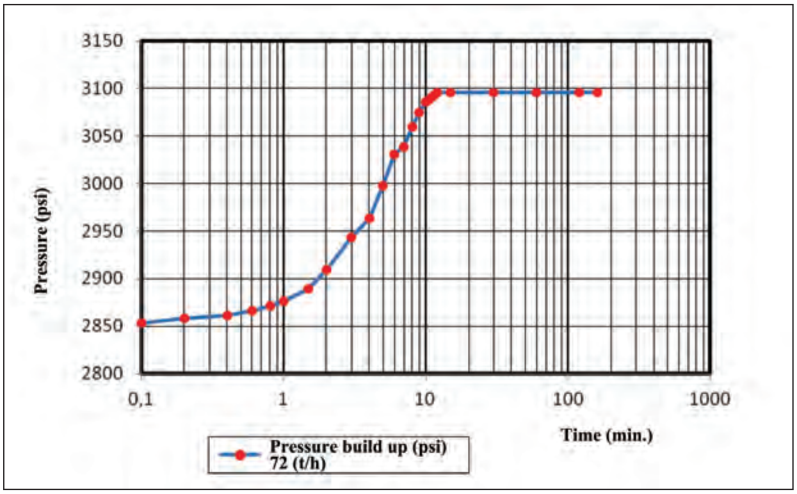

Figure 21: Graph of post-acidification build-up measurement.

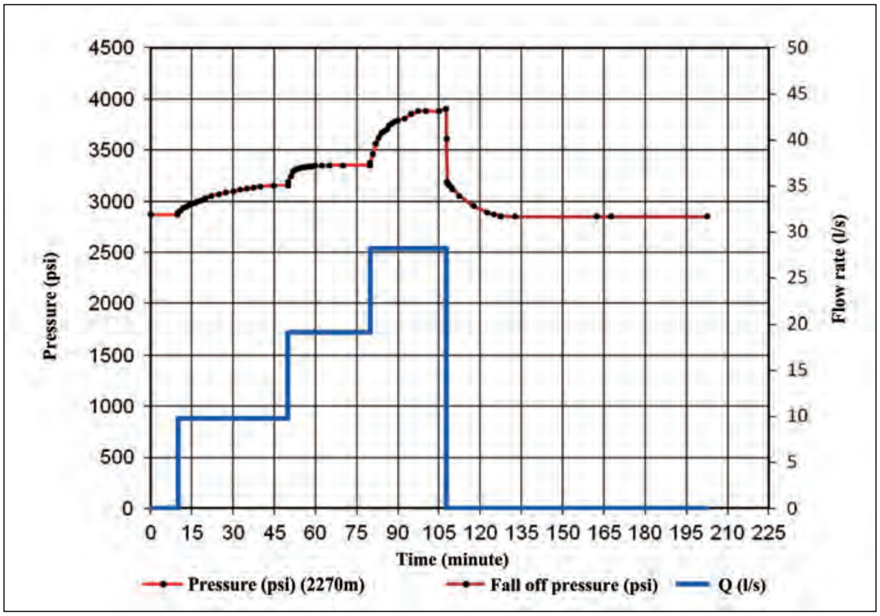

Figure 22- Graph of post-acidification multi flow rate injection fall off measurements.

7.3.4. Post-acidification Production Test Studies

Production test studies were performed in two different ways; by compressor and as artesian. On 18th of June, 2010 at 11:00 pm the air was pumped from inside 360 m long drill pipe with compressor then fluid began to flow out of the well. Production by compressor continued until 19th of June 2010, 11:00 pm. Total production flow rate of the well with compressor was estimated as 22 psi WHP and 35 l/s at spillway and the temperature inside the pipe at valve level was measured as 112ºC. The compressor was shut down at 11:00 pm and left artesian for production. Total production values of the well at different WHP pressures were measured after artesian production had continued a while (Figure 24). At a WHP of 10 psi and at a flow rate of 25 l/s, temperatures of 114ºC and 96ºC were measured inside the pipe at valve and on spillway levels, respectively. The vapor ratio was estimated as 16% during calculation using reservoir and spillway temperatures.

8. Building up the Conceptual Model

The model was built on the westernmost profile which is approximately 20 km long (profile C). Conceptual geothermal model of the field was made assessing all studies together (Figure 25). Members

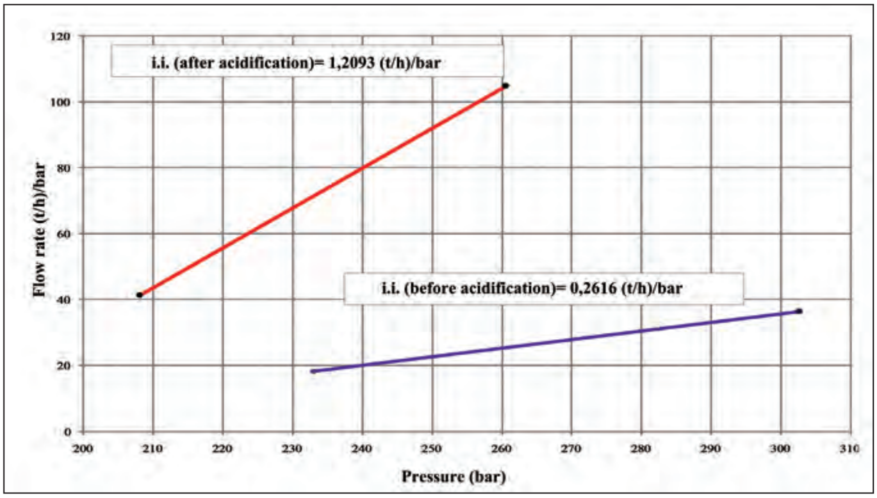

Figure 23- Pre and post-acidification injection indices estimated in KŞÜ-3 well.

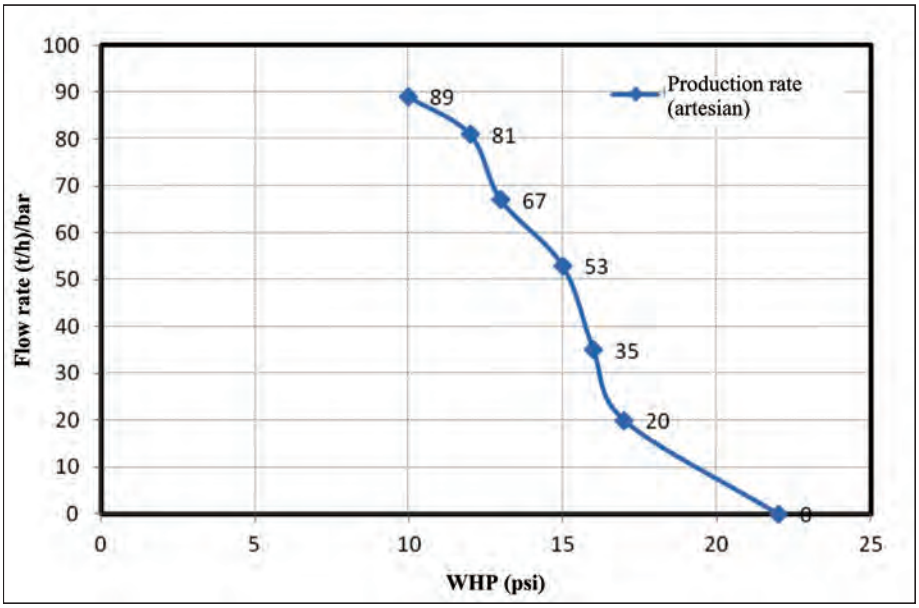

Figure 24- Production test graph in well KŞÜ-3.

of the geothermal system which are; heating source, reservoir rock, mantle rock, water source and drilling locations were plotted on this model. Geological, hydrochemical, isotopic geophysics (magnetotelluric and resistivity) and drilling data were used in generating the conceptual model.

First; data on surface geology was marked on the measured geological section and their depths on this section were determined according to resistivity measurements taken at each 500 m intervals along the profile. The equal resistivity section of the same profile which was generated by resistivity studies was projected on geological model and low resistant region shown in shaded area was interpreted as the mantle rock located on the reservoir (<11 ohm.m). Buried faults were detected from sudden changes at the depth of basement. Water source of the geothermal system was marked by hydrochemical and isotopic studies on the model. On the other hand, the heat source of the system was marked on the model considering intrusions distinctive by low resistivity, located at depths of 5 – 8 km within crust detected by MT analyses. The catchment area, thickness of the mantle rock, reservoir depth, location of the heat source and its depth and data revealing the geothermal system were shown on this model.

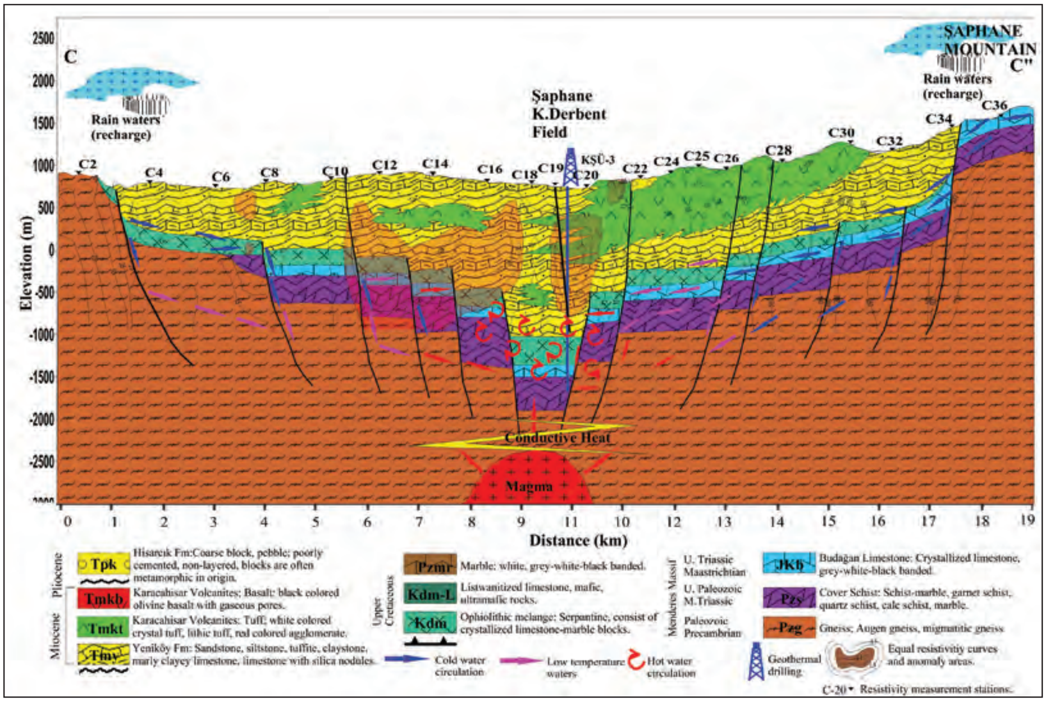

Figure 25- Conceptual geothermal model of the Şaphane-Karacaderbent field.

9. Results

In this study, it was aimed at bringing out a new point of view regarding the methods that will be applied in geothermal investigations carried out on covered areas. The importance of profiling method was pointed out in geophysical investigations especially for covered areas. It was also revealed that the use of geochemical data together with geological data would give more reliable results for selecting profile. In this scope, a new buried geothermal system was explored which is suitable for the electrical generation with a reservoir temperature of 181,2ºC at 2500 m depth in KŞÜ-3 geothermal drill around Şaphane, Karacaderbent. There is a cover thickness of 2430 m in the well and the average gradient was calculated as 0,557ºC/10 m within this cover between 0-2000 m. However, the gradient was calculated as 0,83ºC/10 m between 2000-2400 m. The increase in gradient within last 400 m above the reservoir is quite considerable.

During production studies carried out in the case of artesian, water and vapor were obtained at a WHP of 10 psi, temperature at 114ºC and a flow rate at 25 l/s. However, for the case of production tests made by compressor, water and vapor was acquired at a WHP of 22 psi, temperature at 112ºC and flow rate at 35 l/s. The water obtained (belonging to well KŞÜ-3) is a mineralized thermal water type bearing fluoride, sodium, sulfate, bicarbonate, chloride.

KŞÜ-3 drill is suitable for integrated use in terms of its heat (production of electrical energy, greenhouse and house heating). When the turbine rejection heat was taken as 75ºC, the electrical energy apparent potential was calculated as 2,2 MWe. The thermal potential of the well is 21,3 MWt which is equal to warm up 1300 houses or an area of 85000 m^2 for heating the greenhouse. The conceptual model of the field was revealed assessing all the results of analyses together. Heat source, thickness of mantle rock and reservoir propagation were shown on this model. It is believed to have been attained the target as a result of studies performed. In addition to suitable heating potential attained in the first drilling, a new buried field suitable for the production of geothermal electricity (electrical energy) with 181ºC was explored.

It will be suitable to use polymer mud instead of water based benthonite added drill mud. As condenser (as an alternative for development studies with acid), it will be good to utilize calcite which could be removed out of the reservoir which is dissolved with acid instead of nonreactive barite.

Received: 05.12.2012
Accepted: 12.07.2013
Published: December 2013

References

Akdeniz, N., Konak, N. 1979. Menderes Masifinin Simav dolayındaki kaya birimleri ve meta bazik, meta-ultramafik kayaların konumu. *Türkiye Jeoloji Kurumu Bülteni*, 22, 175-183.

Burçak, M., Gökmenoğlu, O., Aytekin A., Duman, O.,Yeltekin., K Erkan, B., Özmutaf, M., Özkan, H., Erdoğan, H. İ., Şahin, H. 2004. Gediz (Kütahya) belediyesi jeotermal merkezi ısıtma sistemi için jeotermal enerji aramaları ve rezervuar değerlendirmesine yönelik sonuç raporu. *Maden Tetkik ve Arama Genel Müdürlüğü Report No*: 10160, 153, (unpublished), Ankara.

Burçak, M., Sevim, F., Hacısalihoğlu, Ö. 2007*a*. Jeolojik, jeofiziksel ve jeokimyasal yöntemlerle yeni bir jeotermal sahanın keşfedilmesi, Üçbaş-Şaphane- Kütahya. *Maden Tetkik ve Arama Genel Müdürlüğü*, 135, 45-64.

Burçak, M. and Hacısalihoğlu, Kılıç, A.R. 2007*b*. Şaphane-Üçbaş-Karacaderbent sahaları jeotermal etüt (jeoloji-jeofizik) KŞÜ-1, KŞÜ-2 jeotermal sondajları kuyu bitirme raporu. *Maden Tetkik ve Arama Genel Müdürlüğü Report No*: 11516, 112p., (unpublished), Ankara.

Burçak, M., Dünya 2010. Kütahya-Şaphane-Karacaderbent sahası KŞÜ-3 jeotermal sondajı kuyu bitirme ve test raporu. *Maden Tetkik ve Arama Genel Müdürlüğü Report No*: 11503, 96p, (unpublished), Ankara.

Fournier, R.O. 1977. Chemical geothermometers and mixing models for geothermal systems. *Geothermics*, 5, 41-50.

İzdar, K. E. 1971. Introduction to geology and metamorphism of Menderes Massif of western Turkey. Campel A.S., (Ed.), Geology and history of Turkey, Petroleum Expl. Soc.. of Lib., Tripoli, 495-500.

Schuling, R.D. 1958. Menderes masifine ait bir gözlü gnays üzerinde zirkon etüdü. *Maden Tetkik ve Arama Dergisi*, 51, 38-42.

Schuling, R.D. 1962. Türkiye'nin güneybatısındaki Menderes migmatitik kompleksinin petrolojisi, yaşı ve yapısı hakkında. *Maden Tetkik ve Arama Dergisi*, 58, 71-85.

Bulletin of the
Mineral Research and Exploration

http://bulletin.mta.gov.tr

A NEW MEDIUM TO HIGH ENTHALPY GEOTHERMAL FIELD IN AEGEAN REGION (AKYAR) MENDERES – SEFERİHİSAR – İZMİR, WESTERN ANATOLIA, TURKEY

Metin BULUT[*,a]

[a] General Directorate of Mineral Research and Exploration, Regional Directorate of Aegean, Bornova, İzmir

Keywords:
Seferihisar, geothermal, hydrogeochemistry, drilling

ABSTRACT

This study was performed considering that low to medium enthalpy geothermal areas are important besides the geothermal fields with high temperature located in Western Anatolia for heating, thermal tourism and agricultural applications. It was also aimed at obtaining fluids at high temperature in areas which were observed at a temperature relatively lower than the surface temperature. The study area is located at a region between the towns of Menderes and Seferihisar to the south-southwest of Izmir. This is a multidisciplinary investigation which obtained fluids and studied the geothermal energy potential of the area. Field studies were finalized carrying out geological prospection and detailed geological prospection, hydrogeological, hydrogeochemical, geophysical and drilling studies which formed a potential for geothermal energy. As a result of these studies, the fluid with a flow rate of 104 tons per hour and a temperature of 141,18°C was obtained in the form of vapor + water with compressor machine. This fluid was obtained at a depth of 1215,50 m in the conducted exploratory drilling around Akyar Tepe. It was seen that the fluid obtained is sodium chloride type water and consists of a mixture of hot spring, surface water and marine water. This, which had been known as the low temperature field was introduced as a medium-high enthalpy geothermal system.

1. Introduction:

Due to the increase of environmental problems in the world because of fossil fuels, the use of renewable energy has become important in recent years as it had positive effects of natural environment. All countries in the world have begun to prefer renewable energy sources such as; environmentally friend biomass, solar, wind and geothermal energy to limit and control the environmental polluting emissions within the framework of Kyoto Protocol in order to reduce the greenhouse effect. The use of geothermal energy which is cheap and environmentally friend has a broad range of application areas such as; the generation of electricity, heating and cooling in urban areas, desiccation in food industry, thermal tourism, greenhouse cultivation and aquaculture farming. These areas steadily increase the importance of geothermal energy in the world.

As it is known; Turkey, especially the Western Anatolia Region, has a great potential in terms of geothermal energy resources. The study area lies in between Seferihisar and Menderes districts of İzmir City in the Western Anatolia. Seferihisar geothermal field has been known for years as a high temperature geothermal area and its temperature at source varies between 49–85ºC. Due to the hot water drillings run in this area, it was observed that temperatures in the well varied between 56–153ºC. The study area is 7 – 14 km away from the Seferihisar geothermal field in plan view. The temperature of available springs

* *Corresponding author: M. BULUT, metinbulut@mta.gov.tr*

ranges between 33–36,5ºC and these were assessed as low enthalpy areas with respect to their surface temperatures.

The investigation, development, management and the preservation of geothermal systems with low, medium and high enthalpy have a great significance in Turkey. For this purpose, the geological prospection, detailed geological and geophysical researches and hydrochemistry studies were performed in June - September 2009 within the framework of “İzmir Güneyi Jeotermal Enerji Aramaları Project” of the General Directorate of Mineral Research and Exploration. As a result of these studies, it was decided to perform a geothermal exploratory drilling around Akyar Tepe (Hill). This investigation was carried out in June – October 2011 at a depth of 1215,50 m. Drilling studies were performed by MR-6000 tower type drill machine. Cut samples were taken at each 2 meters during advance, studied under binocular microscope and their well lithologies were described. Geophysical well logs (thermal, sp, neutron, gamma ray, resistivity and density) had been taken before the well was cased and during the well completion. So, the well development and completion processes have been managed correlating with well lithology. At well completion, 7” diameter sized production boreholes were set into the well, and well bleaching and development processes were carried out. Reservoir parameters were determined by Amereda Test equipment. In-well tests were completed and the well was prepared for production.

Not only the exploration of hot springs but also the development and careful attention of continuous usage of these known and explored energy sources are of big importance. It should always be bared in mind that, if geothermal systems which are the sources of renewable energy are not well protected then these sources will not be productive as same as before and terminate in the near future. Therefore; re-injection studies and controls should be accelerated in geothermal fields. Besides; as thermal springs which are used balneologically are good to human health, the hydrogeochemical preservation of these sources are of great importance.

2. Regional Geology

The study area is located among Seferihisar, Menderes and Gümüldür towns, in south–southeastern parts of the İzmir City. The Cumaovası basin in which the study area lies is one of the basins belonging to Miocene – Quaternary period in western Anatolia. The basin is NE trending and has an approximate width of 5 -17 km and a length of 35 km, which has developed under the control of active strike-slip and normal faults (Uzel and Sözbilir, 2008). It has previously been named as Çubukludağ graben in previous studies (Eşder and Şimşek, 1975) (Figure 1).

Cover units of the Paleozoic Menderes massif form the basement of the study area, but this unit is exposed outside the study area along the İzmir – Gümüldür auto road. Cover units of the massif were passed over at a depth of 850 meters at the drilling. The Menderes Massif in regional scale consists of a core made up of gneissic, high grade metamorphic rocks and cover rocks made up of schist, phyllites, metaquartzite and of recrystallized limestone (Hetzel et al., 1995; Bozkurt and Park, 1994). Despite the age of the unit was determined as Paleozoic – Mesozoic in literature (Şengör et al., 1984; Dora et al., 1990; Güngör, 1998; Yılmaz et al., 2000; Güngör and Erdoğan, 2002), recent studies have indicated that this age reached even up to Eocene (Özer and Sözbilir, 2003). The unit is tectonically overlain by the rocks of İzmir – Ankara Zone (Başarır and Konuk, 1982; Erdoğan, 1990).

The rocks of the İzmir – Ankara Zone are the one of the paleotectonic units in western Anatolia. These are made up of flysch facies rocks consisting of highly deformed sandstone – shale matrix in which olistoidal limestone and serpentine blocks are present. The unit which was defined as İzmir Flysch has formerly been defined as “Bornova Complex” by Erdoğan (1990) and as “Bornova Flyschoidal Zone” by Okay and Siyako (1991). The age of the unit was given as Late Cretaceous – Paleocene according to these two investigations and is unconformably overlain by Neogene deposit (Figures 2 and 3).

Neogene aged units in the study area begin with Bahçecik Formation consisting of the alternation of Lower Miocene conglomerate, millstone, sandstone, lignite and limestone (Eşder, 1988). These units then continue with Middle Miocene aged Yeniköy Formation which is the alternation of red conglomerate, green sandstone, claystone at bottom then grading into clayey limestone towards upper layers (Eşder and Şimşek, 1975; Eşder, 1988, Genç et al., 2001) (Figures 2 and 3).

Volcanic rocks made up of tuff, rhyodacitic tuff, rhyolitic tuff, agglomerate, perlite, alkaline rhyolite, trachy andesite, rhyolite, hyalorhyolite, dacites and dacitic tuff known as the Cumaovası volcanites (Eşder and Şimşek, 1975; Özgenç, 1978; Kaya, 1979, 1981; Eşder, 1988; Genç et al., 2001) broadly crops out throughout the region (Figures 2 and 3). The

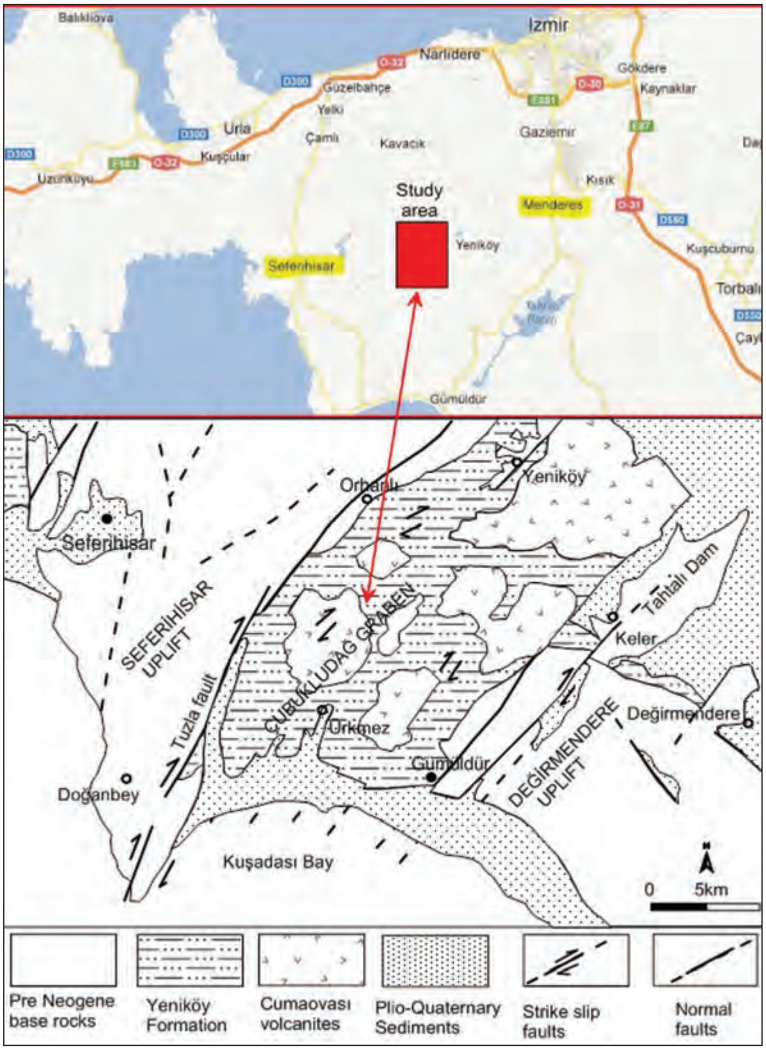

Figure 1- The location of the study area and generalized geological and tectonical maps of its surround (modified from Uzel and Sözbilir, 2008).

age of Cumaovası volcanites were dated as 12,5 my according to Sr, Rb, Sr isotopic ratios (Borsi et al., 1972) and aged as Upper Miocene according to their stratigraphical positions (Genç et al., 2001).

3. Tectonics

The neotectonism of the western Anatolia is represented by tensional tectonism (Şengör; 1979, 1980). Regionally; N-S trending tensional tectonism is a result of the neotectonism which is observed throughout Anatolia. It was stated that, both strike and normal slip active faults were in İzmir and in its close vicinity, and also within the study area located in Aegean region active tectonic belt. It was shown that, normal faults were in E-W direction and strike slip faults were right lateral N-S, NE-SW, NW-SE directions. There was observed intensive seismicity along these active faults in the region and was emphasized that these faults had produced many earthquakes both during historical and prehistorical times (Emre et al. 2005).

NE-SW directing, right lateral Tuzla Fault which is located at NW of the study area forms the most significant tectonical structure. This fault is 42 km long between Doğanbey – Gaziemir towns and exceeds 50 km when its submarine delineation is also considered (Figure 1). However; there are many geothermal activities that developed along this fault zone and are accepted as an active fault system.

4. Drilling Studies

NW-SE directing, oblique, right lateral slip fault that developed along Çamalan River in Akyar area

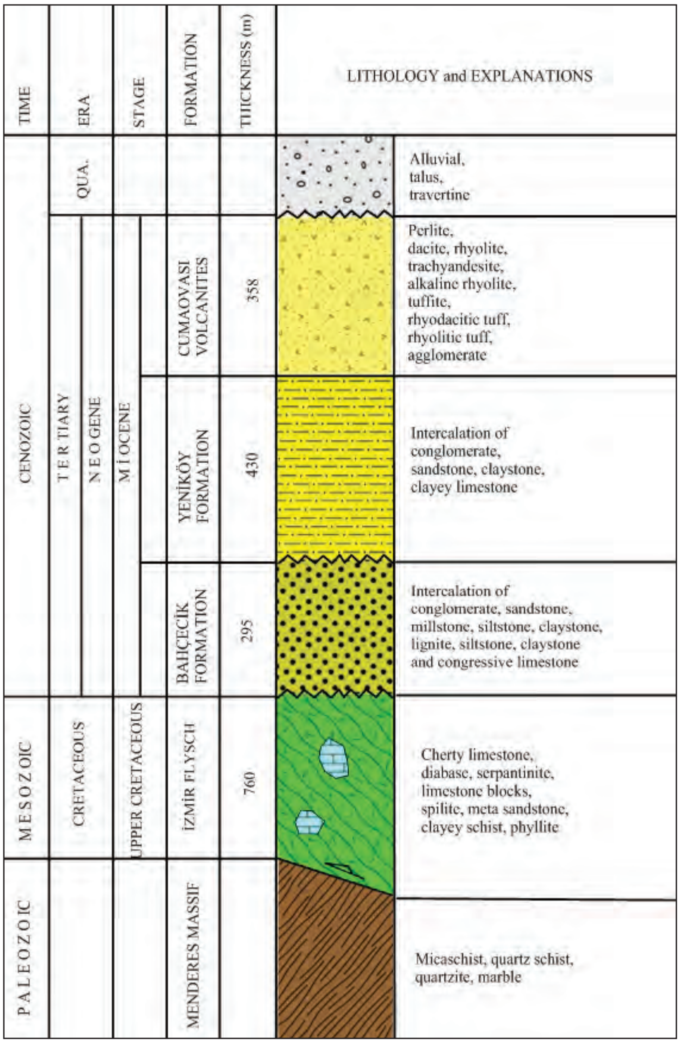

Figure 2- Generalized stratigraphical columnar section of the study area (modified from Eşder, 1988).

and shear faults cutting across this fault approximately in N-S directions indicate a geothermal activity. Geophysical investigations were carried out by deep electrical drilling in Akyar area in order to determine a probable drill location to obtain a fluid, (Bulut et al., 2013).

At the location in L17–c2 sheet around Akyar Tepe and Çamalan River (X: 4220830, Y: 499214), a geothermal energy exploratory drilling with a drill number of İSA-2011/10 (İzmir – Seferihisar – Akyar) was performed at a depth of 1215,50 meters, as a result of geological, geophysical and hydrogeochemical investigations carried out. Between 0,00 – 60,00 meters, altered tuff; between 60,00 – 440,00 meters, Yeniköy Formation (sedimentary rocks composed of conglomerate, sandstone and claystone alternation); between 440,00 – 840,00 meters, İzmir Flysch (rocks in flyschoidal facies composed of sandstone cemented with carbonate, clayey limestone, claystone alternation) and 840,00 – 1215,50 meters, Menderes metamorphites (alternation of mica schist, quartz schist, sericitic schist) were cut at the drilling (Figure 4). In drilling investigation, between 1175 – 1185 meters the fault zone were cut and mud circulation could not be resupplied. This zone is the full water loss zone and was determined as the main production zone. Geophysical logs were also taken inside the well and probable well development risks were also checked. As a result, the well was completed at a depth of 1215,50 meters. Core sample was taken at the well bottom making an extra 1,80 meters advance and this sample was detected as mica schist – quartz schist. Casing with a diameter size of 9 5/8” were lowered to a depth of 595,00 meters inside the well and its outer side was cemented. Later on; 7 “ diameter sized,

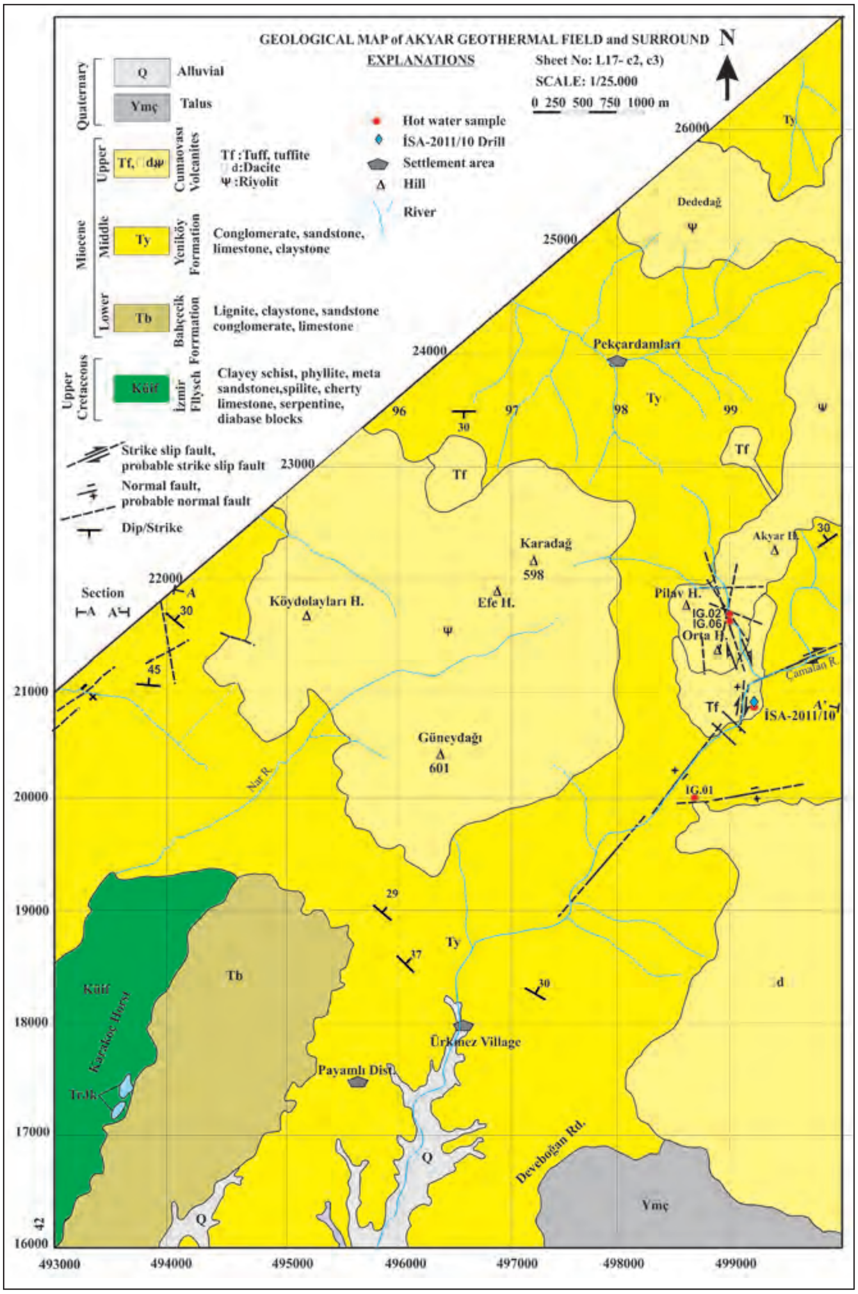

Figure 3- Geological map of the study area (modified from Eşder and Şimşek, 1975; Eşder, 1988).

closed, filtered production wells were placed down to 1215,50 meters (Figure 4).

Static temperature, static pressure, water-loss and injectivity tests were performed by Amerada test equipment in order to determine in-well reservoir parameters in İSA-2011/10 Akyar geothermal exploratory drilling and besides; production test investigations were carried out. It was detected that the main production in the well was at a depth of 1.176 meters and the temperature at this point was measured as 124,04ºC. The temperature at the well bottom was also estimated as 129,28ºC and as 141,18ºC at the depth of 850 meters. The approximate temperature inside the well was measured above 130ºC. The temperature of the fluid production made by compressor on the well (vapor + water) was estimated as 115ºC by digital thermometer in the horizontal production pipe. The fluid temperature and flow rate estimated inside the weir box are 84ºC and

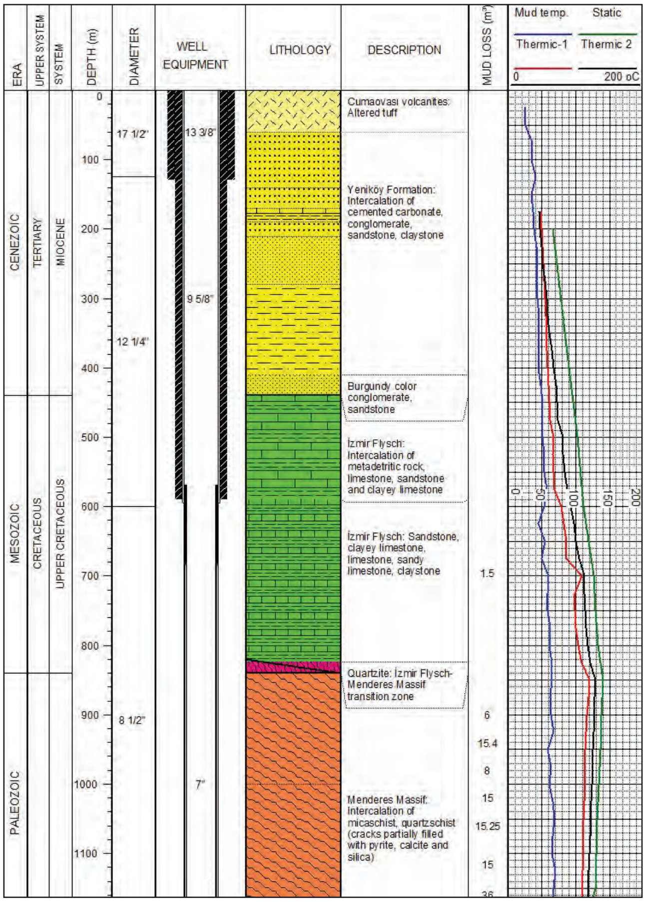

Figure 4- Lithology of the geothermal exploratory drill (from Bulut et al., 2013).

104 tons/h, respectively (Figure 5). Static water level inside the well starting from the level of rotary height was detected as 125,00 meters (Bulut et al., 2013).

Stratigraphically; the Middle Miocene aged sedimentary rocks forming the Yeniköy formation within conglomerate, sandstone, claystone and clayey limestone facies and the Upper Miocene aged volcanic rocks preferably consisting of rhyolite, rhyodacite, dacitic lava and tuffs and agglomerates which unconformably overlie pre Neogene rocks are in the character of cover rocks (Cumaovası volcanites). Fracture zones within metamorphic units belonging to Paleozoic aged Menderes Massif, fractured, fissured mica schist and quartz schists, tectonic fractures and limestone layers within İzmir Flysch are considered as reservoir rocks in the study area (Figure 6). According to hydrochemical data, the geothermal system fed both by surface and marine waters. Waters entering the system in this manner are heated under the effect of high geothermal gradient that is formed by the crustal thinning and mantle uplift which developed due to graben tectonism in Western Anatolia.

Figure 5- Fluid production in İSA-211/10 geothermal drill.

5. Hydrogeochemical Studies

Looking at the field in terms of geothermal resources, it is seen that the study area is located between the Balçova geothermal field at north and the Seferihisar geothermal field at southwest. There are four low enthalpy springs in the study area as; Ilık Pınar 1 (İG.1), Ilık Pınar 2 (İG.3) and Akyar Pınar (İG.2 and İG6) of which their temperatures are in between 33-36,5ºC. Ilık Pınar springs (İG.1 and İG.3) discharge at a low flow rate (0,5 – 1 l/s), Akyar Pınarı springs (İG.2 and İG.6) discharge as in leaks. Chemical analyses of these hot waters were carried out by the sampling of cold waters (İG-4, İG-5, İG-7, İG-8) and drilling waters (İG-9 and İSA-10) (Figure 7 and Table 1).

In order to assert hot-cold water relationships, the chemical analyses of hot water, cold water and drilling water samples discharging in the form of spring and leakage were performed in MTA hydrogeochemistry laboratories (Table 2).

Among these samples, the cation-anion order of İG-01, İG-02, İG-03, İG-04, İG-08, İG-09 samples are as; rCa+rMg>rNa+rK, $rHCO_3$+rCO_3 >rCl+rSO_4 and are classified as carbonate, bicarbonate type waters. However, the cation-anion order of samples İG-05, İG-06, İG-07, İG-10 are in the form of rNa+rK>rCa+rMg, $rHCO_3$+CO_3>Cl+SO_4 and are classified as sodium and bicarbonate type waters (Table 3).

The cation order of the sample taken from the drill İSA-10 is rNa+rK>rCa+rMg. However; the anion order contrary to other waters is rCl+rSO_4>$rHCO_3$+CO_3 and in are sodium, chloride type waters (Table 3). This situation is interpreted as the drill water was mixed with marine water.

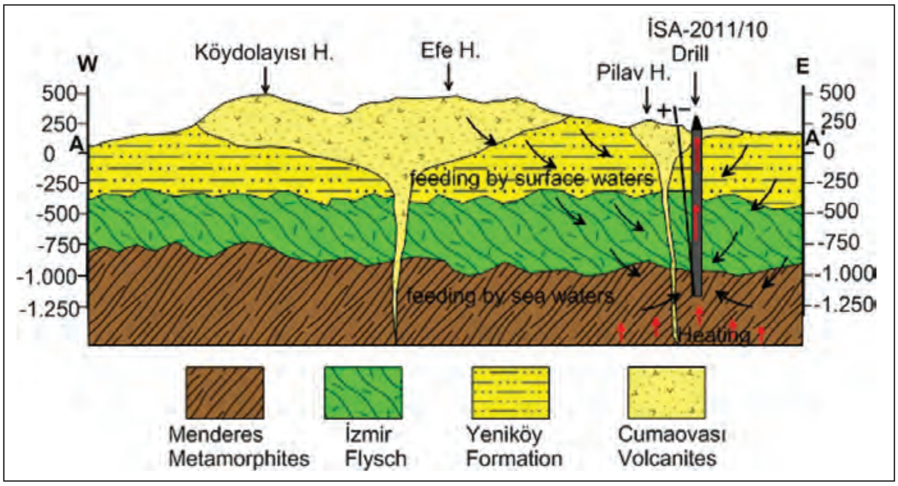

Figure 6- Tectonic model forming the geothermal system.

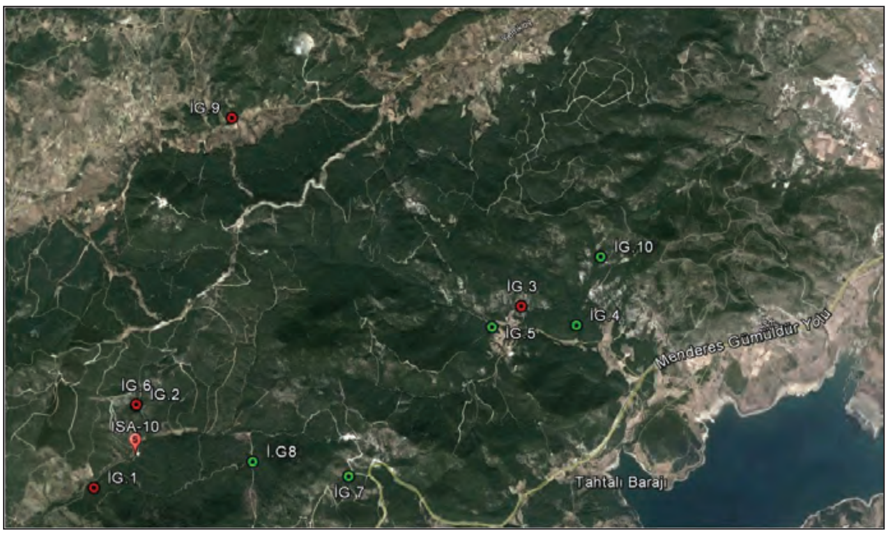

Figure 7- Water sample locations.

Table 1- Water sample coordinates.

Order No	Sample No	Date of sampling	Locality Name	Sampling location				
				Province	District	Village	Sheet No	Coordinate
1	İG-01	8/25/2009	Ilıkpınar	İzmir	Seferihisar	Ürkmez	L17-c2	X: 4220100 Y: 0498650
2	İG-02	8/25/2009	Akyar 1	İzmir	Seferihisar	Ürkmez	L17-c2	X: 4221740 Y: 0498995
3	İG-03	8/25/2009	Ilıkpınar	İzmir	Menderes	Deliömer	L18-d1	X: 4225225 Y: 0505300
4	İG-04	8/26/2009	Suluçay	İzmir	Menderes	Deliömer	L18-d1	X: 4225148 Y: 0506360
5	İG-05	8/26/2009	Bağtepe Pn.	İzmir	Menderes	Deliömer	L18-d1	X: 4224724 Y: 0504881
6	İG-06	8/27/2009	Akyar 2	İzmir	Seferihisar	Ürkmez	L17-c2	X: 4221725 Y: 0498995
7	İG-07	8/31/2009	Çakmak T.	İzmir	Menderes	Deliömer	L18-d1	X: 4221500 Y: 0503075
8	İG-08	9/1/2009	Kovuklu T.	İzmir	Menderes	Deliömer	L18-d1	X: 4221300 Y: 0501325
9	İG-09	9/2/2009	Kuyucak S.	İzmir	Seferihisar	Kuyucak	L17-c2	X: 4227187 Y: 0499335
10	İG-10	9/3/2009	Ali Molla Pn.	İzmir	Menderes	Deliömer	L18-d1	X: 4226457 Y: 0506467
11	İSA-10	10/4/2011	Akyar Drill MTA	İzmir	Seferihisar	Ürkmez	L17-c2	X: 4220830 Y: 0499214

Table 2- Results of water sample analysis.

Sample No	Locality Name	Date of sampling	Temp.	pH	EC	Na^+	K^+	Ca^{++}	Mg^{++}	Cl^-	HCO_3^-	SO_4^{--}	SiO_2	Water type
			°C		mS/cm	(mg/l)	(mg/l)	(mg/l)	(mg/l)	(mg/l)	(mg/l)	(mg/l)	(mg/l)	
İG-1	Ilıkpınar	25.08.2009	36,0	6,9	284	25,4	8,05	26,7	2,59	16,6	113	32,5	81,5	$Ca-HCO_3$
İG-2	Akyar 1	25.08.2009	33,0	7,1	449	23,3	8,16	62,1	6,85	24,6	255	3,3	62,7	$Ca-HCO_3$
İG-3	Ilıkpınar	25.08.2009	33,0	7,0	379	27,9	10,3	47,2	2,3	22,2	201	15,3	83,8	$Ca-HCO_3$
İG-4	Suluçay	26.08.2009	17,6	6,9	546	7,34	1,0	112	2,22	15,7	343	13,5	9,1	$Ca-HCO_3$
İG-5	Bağtepe Pn.	26.08.2009	22,5	6,9	127	18,7	4,81	5,0	1,0	12,8	53	3,3	77,1	$Na-HCO_3$
İG-6	Akyar 2	27.08.2009	36,5	6,8	326	33,0	15,6	25,6	2,28	26,2	160	36,5	72,9	$Na-HCO_3$
İG-7	Çakmak T.	31.08.2009	22,5	6,4	116	16,2	4,1	5,2	1,0	14,5	41,4	4,3	61,5	$Na-HCO_3$
İG-8	Kovuklu T.	01.09.2009	22,0	7,8	366	28,0	6,2	51	1,0	18,4	213	7,2	71,8	$Ca-HCO_3$
İG-9	Kuyucak S.	02.09.2009	41,0	7,1	800	39,8	4,62	78,9	40,5	26,6	450	66,6	29,5	$Ca-HCO_3$
İG-10	Ali Molla Pn.	03.09.2009	20,0	6,5	181	21,5	5,54	14,3	1,1	14,2	88,8	4,4	91,3	$Na-HCO_3$
İSA-10	Akyar S.	04.10.2011	84,0	8,5	5.690	1.154	158	9,2	7,8	1.697	272	203	153	Na-Cl
Sea water		Somay, 2006	x	8,3	58.800	12.720	398,8	476,0	48,1	17.800	156,2	2920,7	x	Na-Cl
Balçova-9		MTA,1993	122	9,0	1.500	440	31	8	4	223	467	169	109	$Na-HCO_3$
Doğanbey		MTA,1995	78	6,8	12.370	2750	254	235	100	4941	689	375	93	Na-Cl

The percentages of major element analysis values of waters were calculated in terms of milliequivalent based on the classification of Association of International Hydrogeologists (AIH). Samples which have percentages more than 20% were categorized according to the highest anion and cation percentages and by means of ternary diagrams at the same time (Table 3 and Figure 8). When looking at their positions in the diagram it was seen that there was not a distinct accumulation and both hot and cold water samples had similar chemical characteristics. High sodium and chloride content in drill water İSA-10 indicates that this water is affected from marine water.

According to this diagram, it was concluded that the drilling water showed similarity with marine water and Seferihisar geothermal waters but had no relation with Balçova geothermal field located at north.

Schoeller semi logarithmic diagram is a frequently used diagram in hydrogeology in order to easily display ions as cumulative in one diagram and to compare waters from similar and different origins at the same time. According to this diagram, waters with similar origin, aquifer and drainage areas give similar peaks. It is observed that hot and cold water

Table 3- Estimated meq/l and % values of water chemistry samples.

Sample No	Na^+	K^+	Ca^{++}	Mg^{++}	Cl^-	HCO_3^-	SO_4^{--}	Water type
	(meq/l); %	(meq/l); %	(meq/l); %	(meq/l); %	(meq/l); %	(meq/l); %	(meq/l); %	
İG-01	1,105; %19	0,206; %4	1,332; %23	0,213; %3	0,468; %8	1,852; %32	0,677; %11	Ca-HCO_3
İG-02	1,013; %10	0,209; %2	3,099; %32	0,564; %6	0,694; %7	4,180; %42	0,069- %1	Ca-HCO_3
İG-03	1,214; %15	0,263; %3	2,355; %29	0,189; %2	0,626; %7	3,200; %40	0,319; %4	Ca-HCO_3
İG-04	0,319; %3	0,025; %0	5,589; %45	0,183; %1	0,443; %4	5,622; %45	0,281; %2	Ca-HCO_3
İG-05	0,813; %31	0,123; %5	0,250; %10	0,082; %3	0,361; %14	0,874; %34	0,069; %3	Na-HCO_3
İG-06	1,435; %21	0,399; %6	1,277; %19	0,188; %3	0,739; %11	2,623; %38	0,135; %2	Na-HCO_3
İG-07	0,705; %30	0,105; %5	0,259; %11	0,082; %4	0,409; %17	0,679; %29	0,090; %4	Na-HCO_3
İG-08	1,218; %15	0,159; %2	2,545; %31	0,082; %1	0,519; %6	3,491; %43	0,150; %2	Ca-HCO_3
İG-09	1,731; %9	0,118; %1	3,937; %21	3,337; %18	0,750; %4	3,376; %40	1,387; %7	Ca-HCO_3
İG-10	0,935; %25	0,142; %4	0,714; %19	0,090; %2	0,401; %10	1,456; %38	0,092; %2	Na-HCO_3
İSA-10	50,196; %44	4,041; %4	0,489; %1	0,642; %1	47,866; %42	4,227; %4	4,458; %4	Na-Cl
Sea water	5533; %47	10,2; %1	23,7; %2	3,95; <%1	502,1; %44	2,5; <%1	60,8; %5	Na-Cl
Balçova-9	19,13; %46	0,79; %2	0,39; %1	0,32; %1	6,29; 15	7,65; %20	3,5; %9	Na-HCO_3
Doğanbey	119; %40	6,49; %2	11,7; %4	8,2; %3	139; %46	11,29; %4	7,8; %3	Na-Cl

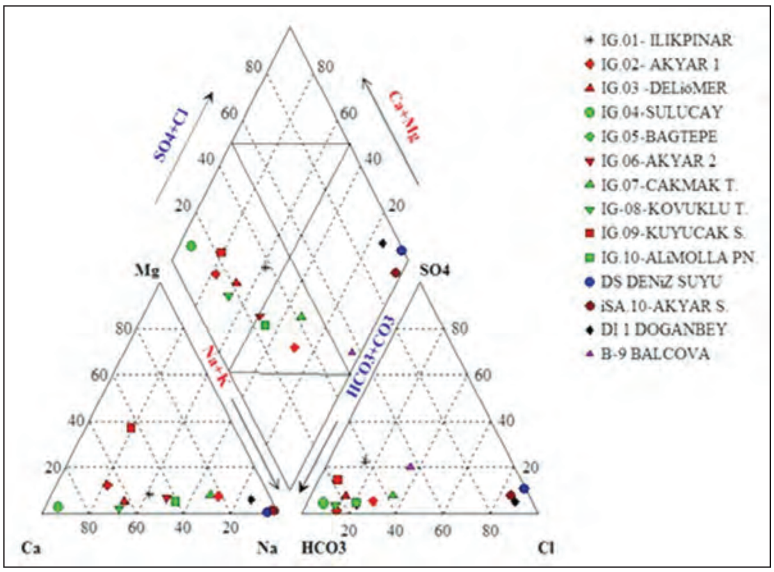

Figure 8- Piper diagram of water samples.

samples taken from the study area give similar peaks (Figure 9). It can be stated that surface waters filter out beneath the surface through fractures and fissures then come up to the surface followed by heating. However, it is probable to say that drill waters are fed by marine waters in addition to surface waters.

Cl-SO_4-HCO_3 ternary diagram is used in order to determine whether waters are deep or shallow circulating. Samples taken are HCO_3/Cl>4 and all these samples plot out at HCO_3 corner showing that these are shallow circulating waters and were subjected to an effect of mixing process at the same time when assessed in this diagram (Figure 10). According to this diagram, it is seen that water sample belonging to Akyar drill (İSA-10) takes place in the category of saturated water. This water is admixed with marine water and is in saturated water category because of its high chloride content.

6. Saturation Indexes

It is an important issue to predict chemical precipitations that might occur along pipes and pumps during the production and usage of hot waters through drilling wells. The precipitation of calcite and dolomite minerals namely the "coating" can be considered as the first precipitation type. The solubility of calcite and dolomite in waters increases with respect to the amount of CO_2 gas in water. The results of mineral

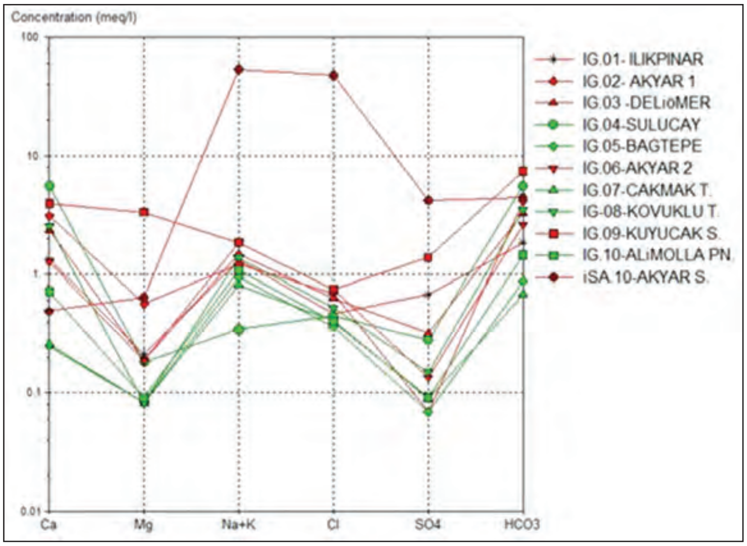

Figure 9- Schoeller diagram of water samples.

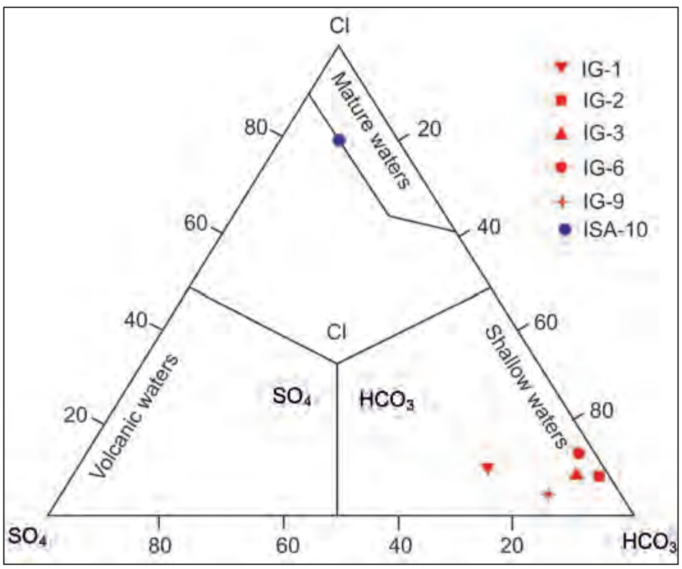

Figure 10- Cl-SO_4-HCO_3 diagram of water samples.

saturation index calculated by thermodynamic methods are interpreted as shown below;

If;

SI (log Q/K) = 0; then water is in equilibrium with mineral.

SI (log Q/K) > 0; then water is saturated with the related mineral.

SI (log Q/K) < 0; then water is not saturated with the related mineral.

For this reason, the saturation of water samples of which their chemical analysis were carried out against calcite, dolomite and some other minerals were calculated and shown graphically (Table 4 and Figure 11). It was observed that, hot and cold water samples except the drilling water number İSA-10 were not saturated mainly with minerals such as; anhydrate, aragonite, calcite, dolomite and gypsum and water could easily dissolve these minerals. It was also detected that these samples were saturated with minerals such as; chalcedony and quartz, and these minerals could precipitate in water. It was determined that, drilling water number İSA-10 was not saturated for anhydrate, chalcedony and gypsum, and hot water could dissolve these minerals. However; it was also seen that this drilling water was saturated for aragonite, dolomite and quartz minerals and these minerals could easily dissolve out in water.

7. Geothermometer Applications

It is significant to predict the temperature of reservoir rock before the application of deep drillings in geothermal systems. For this purpose, chemical geothermometer applications are used. There are

Table 4- Saturation indexes of water samples for some minerals.

Sample No	T (°C)	Anhydrite	Aragonite	Calcite	Chalcedony	Dolomite	Gypsum	Quartz
İG-01	36,0	-2,52	-1,02	-0,88	0,56	-2,33	-2,36	0,96
İG-02	33,0	-3,27	-0,18	-0,14	0,48	-0,6	-3,08	0,88
İG-03	33,0	-2,67	-0,48	-0,34	0,61	-1,57	-2,49	1,01
İG-04	17,6	-2,51	-0,25	-0,1	-0,18	-1,65	-2,27	0,27
İG-05	22,5	-4,18	-2,19	-2,05	0,69	-4,48	-3,95	1,12
İG-06	36,5	-3,24	-0,97	-0,84	0,51	-2,66	-3,07	0,9
İG-07	22,7	-4,04	-2,78	-2,63	0,59	-5,66	-3,81	1,02
İG-08	22,0	-3,01	0,21	0,36	0,66	-0,68	-2,78	1,1
İG-09	41,0	-1,98	0,19	0,32	0,06	0,84	-1,85	0,45
İG-10	20,0	-3,65	-1,98	-1,83	0,79	-4,49	-3,42	1,24
İSA-10	84,0	-1,24	1,01	1,09	-0,17	1,17	-2,27	0,05

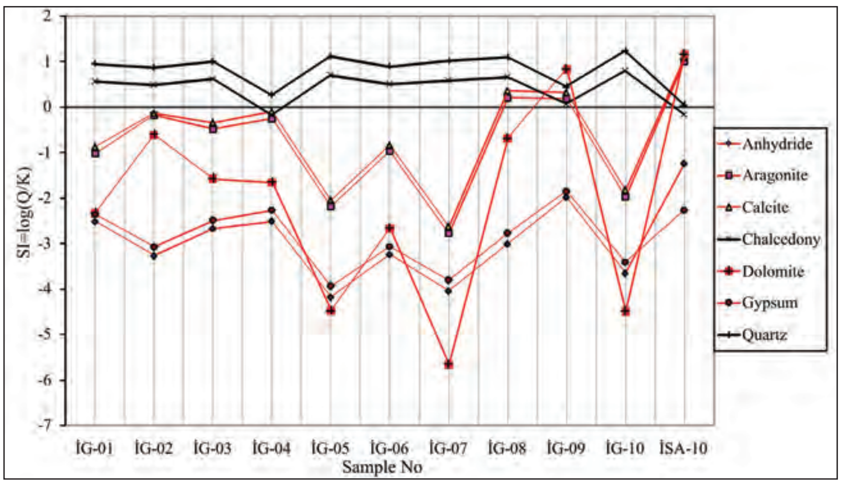

Figure 11- Saturation diagram of water samples for some minerals.

several formula developed on this issue. One of them is Na-K-Mg (Giggenbach, 1988) ternary diagram. It is used to determine reservoir rock temperatures according to cation geothermometers of hot waters and to study mineral equilibrium relationships between the water and rock. The curve separating immature waters from partly mature waters is where the maturity index equals to 2 (MI=2,0) and is formed by connecting points that have equal chemical features. Samples taken from the investigation area have MI<2 and waters fall into immature water category (water – rock equilibrium not provided). In this case, results of reservoir rock temperature calculated according to cation geothermometers are suspicious. The drilling water takes place in which the rock-water equilibrium is partly balanced. It is also necessary to consider reservoir rock temperatures calculated by cation geothermometers in future studies (Figure 12).

It was seen that reservoir rock temperatures calculated by silica geothermometers could vary between 48 and 127ºC. It was understood that the temperature of reservoir rock could even increase up to 162ºC according to silica geothermometers which were applied to the sample taken from the drilling (Table 5).

8. Results and Discussion

The Akyar geothermal field which has geographically very irregular topography has been thought as an area which has a lower temperature compared to its surround. This field can be assessed as a medium to high enthalpy geothermal system based on geological, geophysical, hydrogeochemical results and drilling investigations within the scope of Geothermal Energy Explorations of the General Directorate of MTA. The maximum temperature and flow rate of the fluid (vapor + water) inside the well were obtained as 141,8ºC and 104 tons/h, respectively. The fluid is sodium chloride type water and the system is fed by the mixture of surface and marine water. Investigations made so far are the beginning stage to determine the potential of a geothermal system and these should be improved more. The electrical conductivity values of hot and cold water samples taken from the study area vary between 116-800 µs/cm, and dominant cation and anion in waters are Na, Ca and HCO_3, respectively. According to AIH classification, both hot and cold water springs fall into mineral poor water types as; sodium, bicarbonated and calcium. The electrical conductivity value of Akyar İSA-10 drill water sample is 5,690 µs/cm, and the dominant cation and anion are; Na and Cl, respectively. It falls into hot and mineralized water region with sodium and chloride. pH value for this drilled water is 8,5. However; pH values of hot and cold springs vary between 6,9-7,8. This situation indicates a probable mixing of the drilled water with marine water.

Based on previous studies made so far in the region, the general lithostratigraphic succession and tectonical characteristics of the area were investigated. Accordingly; the well lithology and geophysical measurements carried out inside the İSA-

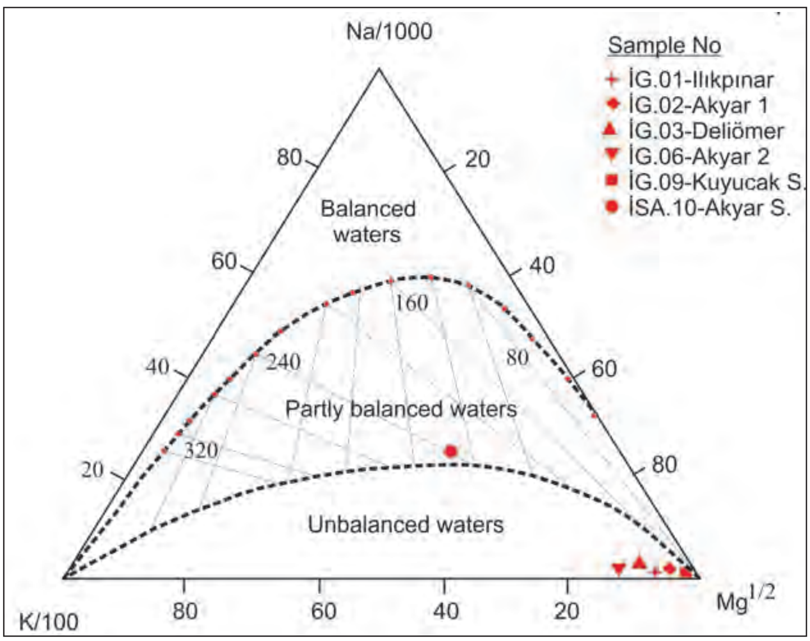

Figure 12- Giggenbach diagram of hot water samples.

Table 5- Reservoir rock temperatures calculated in hot water samples.

Sample No	İG-01	İG-02	İG-03	İG-06	İG-09	İSA-10
Measured temperature (°C)	36	33	33	36	41	84
Thermometer	Calculated temperature					
Amorphous silica[a]	x	x	x	x	x	x
Crystobalite alpha[a]	75	62	77	70	x	112
Crystobalite beta[a]	x	x	x	x	x	x
Chalcedony[a]	98	84	100	92	48	139
Quartz[a]	126	113	127	120	79	162
Quartz (vapor loss)[a]	123	112	125	118	83	154
K/Mg [b]	x	40	x	x	65	x
Na/K[c]	375	399	413	485	202	224
Na/K[d]	358	379	391	451	204	224
Na/K[e]	379	395	404	448	252	270
Na/K[f]	341	355	362	400	230	245
Na-K-Ca[f]	208	204	213	240	152	247
Na-K-Ca-Mg corrected[f]	135	120	175	165	x	152
x ; Temperatures calculated are below the outlet temperatures.						
[a]; Fournier and Potter 1977, [b]; Giggenbach at al., 1988, [c];Fournier and Truesdell, 1973						
[d];Truesdell 1976, [e];Fournier and Potter 1979, [f]; Fournier 1979						

2011/10 geothermal exploratory drill were correlated. As a result, the thickness of the İzmir Flysch which was tectonically deposited over Menderes Massif was estimated as 400 m. This unit is unconformably overlain by the Middle Miocene aged Yeniköy formation and the thickness of this sedimentary unit is 380 m.

Stratigraphically; the Middle Miocene aged sedimentary rocks forming the Yeniköy formation within conglomerate, sandstone, claystone and clayey limestone facies and the Upper Miocene aged volcanic rocks consisting of rhyolite, rhyodacite, dacitic lava and tuffs, and agglomerates which unconformably overlie pre Neogene rocks are in the character of mantle rocks (Cumaovasi volcanites). Fracture zones within metamorphic units belonging to Paleozoic aged Menderes Massif and fractured, fissured mica schist and quartz schists, and tectonic fractures and limestone layers within İzmir Flysch are considered as reservoir rocks in the study area (Figure 6). According to hydrochemistry, the geothermal system is fed by both from surface and marine waters. Waters entering the system in this manner are heated under the effect of high geothermal gradient that is formed by the crustal thinning and mantle elevation due to graben tectonism in Western Anatolia.

The Seferihisar Geothermal Field which is located at the southwest of the area (Cumali hot springs, Tuzla Field, Karakoç hot spring, Doğanbey springs) has been a significant well known geothermal field for years. Geological, geophysical and drilling investigations in these areas have been performed for many years and temperatures inside the well were detected up to 153ºC. The well temperature of the Balçova geothermal field which is located at the north of the study area was detected around 142ºC as a result of geological, geophysical and drilling investigations carried out. The study area which lies in between these two geothermal fields is located within Çubukludağ Graben. As a result of geological, geophysical and geothermal drilling investigations performed, 104 tons/h flow rate and 141,8ºC maximum in-well static temperature were measured and these values indicate that the field is a prominent area.

Acknowledgement

This study was made within geothermal projects of the General Directorate of Mineral Research and Exploration (MTA) 2009-33-13-04.2 prospection and 2011-33-13-04.1 drilling). The author thanks to all staffs of MTA who have participated in field studies.

Received: 22.12.2012
Accepted: 20.06.2013
Published: December 2013

References

Başarır, E., Konuk, Y.T. 1982. Gümüldür yöresinin kristalin temeli ve allokton birimleri. *Türkiye Jeoloji Kurumu Bülteni* 24, 1–6.

Bozkurt, E., Park, R.G. 1994. Southern Menderes Massif: an incipient metamorphic core complex in western Anatolia, Turkey. *Journal of Geological Society* 151, 213-216.

Borsi, S., Ferrara, G., Innocenti, F., Mazzuoli, R. 1972. Geochronology and Petrology of Recent Volcanics in the Eastern Aegean sea (West Anatolia and Leovos Island). *Bulletin of Volcanology* 36, 473–496.

Bulut, M., Büyükboyacı, Ü., Dünya H. 2013. Akyar-Ilıkpınar (Seferihisar-Menderes-İzmir) ruhsat sahalarının jeotermal etüt (Jeoloji-Jeofizik) ve Akyar İSA-2011/10 jeotermal arama sondajı kuyu bitirme raporu. *Maden Tetkik Arama Genel Müdürlüğü*,109, (unpublished) Ankara.

Dora, O., Kun, N., Candan, O. 1990. Metamorphic history and geotectonic evolution of the Menderes massif. *International Earth Sciences Congress on Aegean Regions*, İzmir-Turkey, Proceedings, 102–115.

Emre Ö., Özalp S., Doğan A., Özaksoy V., Yıldırım C., Göktaş F. 2005. İzmir yakın çevresinin diri fayları ve deprem potansiyelleri. *Maden Tetkik Arama Genel Müdürlüğü Rapor No*: 10754, 80, (unpublished) Ankara.

Erdoğan, B. 1990. İzmir-Ankara Zonu'nun, İzmir ile Seferihisar Arasındaki Bölgede Stratigrafik Özellikleri ve Tektonik Evrimi. *Türkiye Petrol Jeologları Dergisi Bülteni* 2/1, 1–20.

Eşder, T. 1988. Gümüldür-Cumaovası (İzmir) alanının jeolojisi ve jeotermal enerji olanaklarının araştırılması. PhD Thesis, İstanbul Üniversitesi. Fen Bilimleri Enstitüsü, Jeoloji Mühendisliği Bölümü Anabilim Dalı, 401 p. (unpublished).

Eşder, T, Şimşek, Ş. 1975. İzmir (Seferihisar) alanı, Çubukludağ grabeni ile dolaylarının jeolojisi ve jeotermal olanakları. *Maden Tetkik ve Arama Enstitüsü Raporu*, 190, (unpublished), İzmir.

Fournier, R. O. 1977. Chemical geothermometers and mixing models for geothermal system. Geohthermics, 5, 41-50.

Fournier, R. O. 1979. A revised equation for the Na/K geothermometer. *Geothermal Res. Council Trans.*, 3, 221-224.

Fournier, R. O., Truesdell, A.H. 1973. An Empirical Na-K-Ca Geothermometer for Natural Waters. *Geochimica et Cosmochimica Acta*, 37, 1255-1275.

Fournier, R. O., Potter, R. W. 1979. Magnesium correction to the Na-K-Ca chemical geothermometer. *Geochimica et Cosmochimica Acta*, 43, 1543-1550.

Genç, S.C., Altunkaynak, Ş., Karacık, Z., Yılmaz, Y. 2001. The Çubukludağ graben, Karaburun peninsula: it's tectonic significance in the Neogene geological evolution of the western Anatolia. *Geodinamica Acta* 14, 45–55.

Giggenbach, W. F. 1988. Geothermal solute equilibria. Derivation of Na-K-Mg-Ca geoindicators. *Geochimica et Cosmochimica Acta*, 52, 2749-2765.

Güngör, T. 1998. Stratigraphy and Tectonic Evolution of the Menderes Massif in the Söke-Selçuk Region. Doktora Tezi, Dokuz Eylül University.

Güngör, T., Erdoğan, B. 2002. Tectonic significance of mafic volcanic rocks in a Mesozoic sequence of the Menderes Massif, West Turkey. *International Journal of Earth Science* 91, 386–397.

Hetzel, R., Ring, U., Akal, C., Troesch, M. 1995. Miocene NNE-directed extensional unroofing in the Menderes Massif, southwestern Turkey. *Journal of Geological Society* 152, 639–654.

Kaya, O. 1979. Ortadoğu Ege çöküntüsünün Neojen stratigrafisi ve tektoniği. *Türkiye Jeoloji Kurumu Bülteni* 7/22, 35–58.

Kaya, O. 1981. Miocene reference section for the coastal parts of West Anatolia. *Newsletters on Stratigraphy* 10, 164–191 pp.

MTA, 2005. Türkiye Jeotermal Kaynakları Envanteri, Ankara.

Okay, A.İ., Siyako, M. 1991. The New Position of the İzmir-Ankara Neo-Tethyan Suture Between İzmir and Balıkesir. *Proceedings of the Ozan Sungurlu Symposium*, Ankara, 333–355.

Özer, S., Sözbilir, H. 2003. Presence and tectonic significance of Cretaceous rudist species in the so-called Permo-Carboniferous Göktepe Formation, central Menderes Massif, western Turkey. *International Journal of Earth Sciences* 92, 397–404.

Özgenç, İ. 1978. Cumaovası (İzmir) asit volkanitlerde saptanan iki ekstrüzyon aşaması arasındaki göreceli yaş ilişkisi. *Türkiye Jeoloji Kurumu Bülteni*, 21/1, 31–34.

Somay, M. 2006. Hydrogeology of Küçük Menderes River coastal wetland. Dokuz Eylül Üniversitesi Fen Bilimleri Enstitüsü Doktora Tezi, 222. (unpublished).

Şengör, A.M.C. 1979. The North Anatolian Transform Fault: its age, offset and tectonic significance. *Journal of the Geological Society of London*, 136, 269–282.

Şengör, A.M.C. 1980. Türkiye'nin neotektoniğinin esasları, *Türkiye Jeoloji Kurumu yayını*, 40.

Şengör, A.M.C., Satır, M., Akkök, R. 1984. The timing of tectonic events in the Menderes Massif, western Turkey: implication for tectonic evolution and evidence for Pan-African basement in Turkey. *Tectonics* 3, 693–707.

Truesdell, A.H. 1976. Summary of section III geochemical techniques in exploration. Proceedings of second United Nations Symposium on the development and use of geothermal resources. 1975, San Francisco, 1, 53-89 pp.

Uzel, B., Sözbilir, H. 2008. A First record of strike-slip basin in western Anatolia and its tectonic implication: The Cumaovası basin as an example. *Turkish Journal of Earth Sciences* 17, 559–591.

Yılmaz, Y., Genç, S.C., Gürer, O.F., Bozcu M., Yılmaz K., Karacık Z., Altunkaynak Ş., Elmas A. 2000. When did the western Anatolian grabens begin to develop Bozkurt E., Winchester J.A., Piper J.D.A. (Eds.), Tectonics and magmatism in Turkey and the surrounding area, *Geological Society of London*, Special Publication 173, 353–384.

Bulletin of MTA (2013) 147: 169-177

Bulletin of the
Mineral Research and Exploration

http://bulletin.mta.gov.tr

THE AIRBORNE MAGNETIC SIGNATURE OF GÖKOVA GULF

Uğur AKIN[a,*] and Ahmet ÜÇER[a]

[a] *General Directorate of Mineral Research and Exploration (MTA), Department of Geophysical Research, 06800, Ankara, Turkey*

Key words:
Gökova gulf, Datça, Bodrum, Magnetic, Gradient, Tensor, FTG

ABSTRACT

Gökova gulf situated in the Aegian extension zone in Turkey has been considered very interesting for numerous research workers. Gökova gulf is located in the N-S regional extentional tectonic regime. N-S extension of western Anatolia initiated development of E-W extended grabens here. The bay extends 100 km E-W and 25 km N-S directions. Datça peninsula is in the south, Bodrum peninsula is located in the north of the Gökova gulf.

In recent years ‘Full Tensor Gradiometer Potential Field’ methods (FTG) has found a practice area in between the gravimetric and magnetic methods. In the past as it was in the gravimetric methods vertical component of the magnetic field measurments used to be recorded. In recent years total field (x, y, z components) measurments have become more applicable. This method has been applied to the airborne magnetic field data. Total magnetic data components of the airborne survey have been calculated and FTG method has been used. Gökova gulf is seismicly very active. There is a magnetic anomaly recorded in the Gökova gulf. To be able to bring a new outlook to the geology of the bay, the magnetic anomaly has been analysed by using ‘Full Tensor Magnetic Gradiometer’ (FTG) method. At first T_x, T_y, T_z magnetic field components of the airborne anomaly have been calculated. To the calculated components T_{xx}, T_{xy}, T_{xz}, T_{yy}, T_{yz}, T_{zz} derivatives have been applied to have an impression of the geological feature causing the anomaly. The anomaly in the bay indicated that ultramafic rocks, ophiolitic melange in the Datça peninsula continue under the sea to the Gökova gulf. Data indicate that northern boundary of the peridotites continues up to about 9 km to the northern coast of the bay. The method is considered to be useful to help mapping of the geological features with different magnetic sensitivities.

1. Introduction

Airborne magnetic data collected during 1978-1989 have been used in this work to study the geological feature causing a magnetic signature under the sea in the Gökova gulf in the south western Turkey. Airborne magnetic anomalies of the ultrabasic rocks, Upper Cretaceous ophiolite melánge present in the area assisted to the understanding of the airborne magnetic signature in the bay. Using the magnetic data extension of the geological units, position and geometry have been studied. Data of the total magnetic field tensors (T_x, T_y, T_z) have been calculated.

In recent years with the technological developments correct and reliable measurement techniques have been developed in potential methods. In recent years full tensor gradiometer measurements on moving platforms became applicable in gravimetric methods.

Traditional total magnetic field studies for mineral and oil explorations have been compared with the

* *Corresponding author: U. AKIN, ugurakin11@gmail.com*

magnetic gradient tensor studies of recent years. Many workers claimed that latter method is more advantages (Christensen and Rajagopalan, 2000; Schmidt and Clark, 2000; Heath et al 2003).

Murphy (2004) associated FTG method with the underground geology. In this association horizontal components (T_{xx}, T_{xz}, T_{xy}, T_{yy} ve T_{xz}) provides information in geological boundaries, vertical component (T_{zz}) provides information on depths of geological features.

Bracken and Brown (2005) using proto type tensor magnetic gradiometer carried out a successful study on buried explosive materials. The result map they prepared showed that the anomalies well coincided on the target object.

Because of the scalar measurements it took some time, new generation potential field studies to be accepted as such. FitzGerald et al (2006) in his studies used randomly selected complex appearing data group so helped developing the method.

Murphy (2007), Murphy and Brewster (2007), Murphy and Dickinson (2010) worked with gravity gradient tensor data. They joined all/or certain tensor components together. Purpose of their study was using new tensor models (presentations) to collect data towards understanding extension and orientation of underground geological structures.

FTG is one of the methods applicable to the ground, sea and airborne gravimetric and magnetic studies. Wan et al (2008) used this method to study hydrocarbons in sea, salt domes and complex geological structures.

Rompel (2009) used full tensor magnetic gradiometer method in more then 20 studies during the course of 3 years. He used the method to study some dikes with weak magnetic signals or no magnetism at all.

Mataragio et al (2011) to explore iron oxide minerals in particular, they carried out magnetic method together with airborne full tensor gradiometer method covering 600 km^2 areas in Brazil. By studying positive high amplitude anomalies over the iron ore deposit they worked out lithology and structure of the study area, suggested ground survey for possible new iron ore targets.

2. Regional Geology

Study area is located in the southwest Turkey. Gökova gulf is surrounded by Bodrum peninsula in the north, Datça peninsula in the south and Greek Kos island in the west (Figure 1). The region is under extensional tectonic regime and seismically active, so it continues to be one of the most interesting areas in Turkey. As a result of extensional tectonic activities numbers of grabens such as Büyük Menderes, Gediz, Burdur grabens developed. The Gökova gulf is located in one of this E-W oriented graben.

One of the most noticeable E-W oriented depressions in western Turkey is the Gökova graben

Figure 1- General position of the study area (red circle), (http://www.hgk.msb.gov.tr).

filled up by Aegean Sea. Gökova gulf has developed under the control of E-W oriented normal faults. Offsets of the faults gradually increase from north towards south reaching up to 1 km dislocation on the southern border fault (Görür et al 1995).

In south western Turkey geologically, allocthon masses known as Likya Nappes are located in between the Menders Massif and Beydağları autochthon and were thrusted on to the Beydağları autochthon in Early Langien (Figure 2). Likya nappes are consisted of different rock units developed in different various settings and have thrusted on to each other. Likya nappes have been separated into 5 main tectonic units. They are Tavas nappe, Bodrum nappe, Domuzdağı nappe, Gülbahar nappe and Marmaris nappe. Marmaris ophiolite nappe in general overlies the Bodrum nappe. Tectonic slices of the Marmaris nappe can be seen under the Bodrum nappe and even under the Tavas nappe. Marmaris ophiolite nappe consists of ultrabasic and basic rocks, ophiolite melange and Kızılcadağ melange and olistostrome (Şenel 2007)

Gökova gulf is in the Denizli sheet in the 1/500.000 scale geological map of Turkey. Akın and Duru (2006) carried out heat flow potential study of Turkey. They calculated the heat flow of the study area as 86 mW/m^2. This value is much higher than Turkey's average. Akın and Çiftçi (2011) analysed gravimetric, magnetic and geological data of the region. They showed that gravimetric and magnetic discontinuities run along NE-SW (30^o-60^o) directions, geological discontinuities also have equal affect on NW-SE and NE-SW directions.

3. Geophysics Applications

Mineral Research and Exploration General Directorate (MTA) carried out airborne magnetic surveys in 1978-1989 periods to study general geological settings, tectonic positions and mineral resources of Turkey. During these 11 years period flights covered 460000 km at 610 m altitude. At the end regional airborne magnetic map of Turkey was prepared (Ateş et al 1999, Aydın et al 2005). Flight lines were 1-5 km spaced. IGRF magnetic corrections have been applied to the measurements. During the airborne survey topography and geology of the country were taken into consideration.

Before FTG studies carried out, total airborne magnetic field measurements for the Gökova gulf were reduction to the pole during data processing (Figure 3).

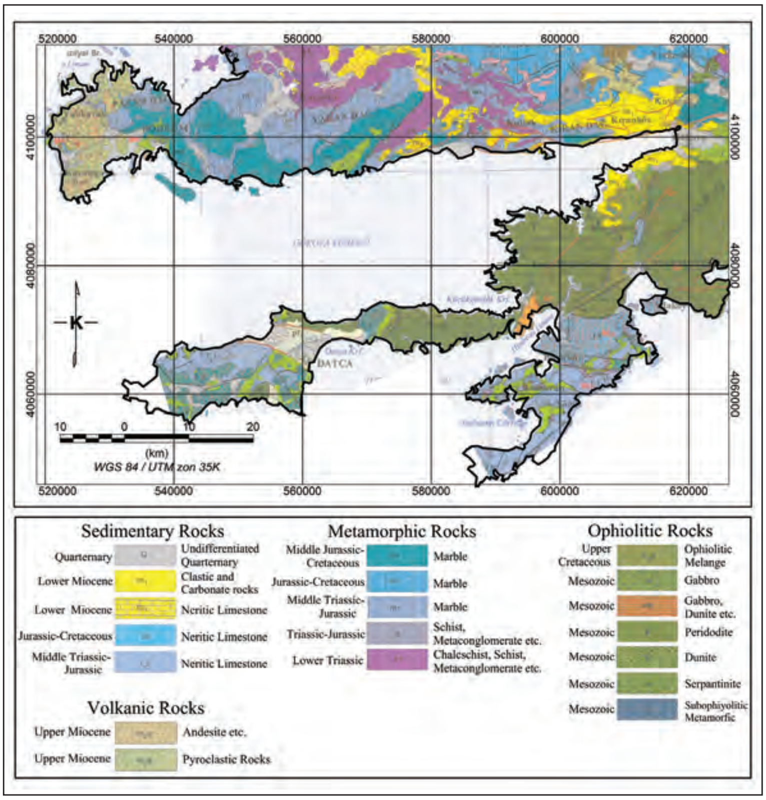

Figure 2- Geological map of the area (MTA, 2002).

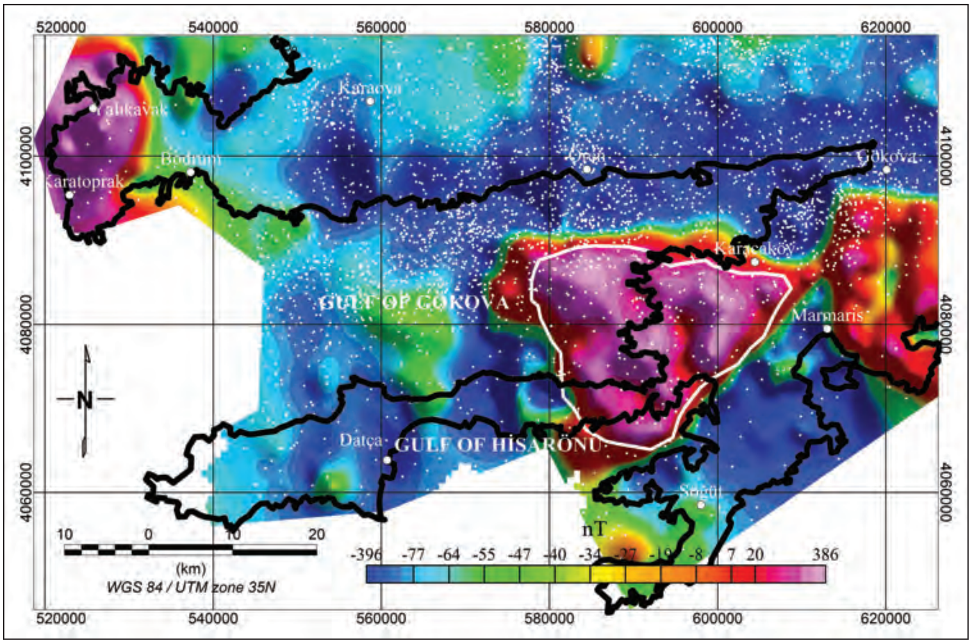

Figure 3- Reduction to the pole=RTP and earthquake epicentre map marked with white spots. Earthquakes with magnitudes greater than 3 took place since 1919. Earthquake data have been obtained from the Boğaziçi University, Kandilli Observatory, Earthquake Research Centre

In the RTP map there are 3 distinct anomalies. First anomaly is located in the NW on the Upper Miocene andesites and pyroclastics in Yalıkavak. The western part of the anomaly is not closed as it is outside Turkey's boundary and has not been flown. Second anomaly (patchy) is in the east of Marmaris and is on the Mesozoic peridotites. The third anomaly which is the subject of this work has 25 km long wave lengths along EW and NS directions (Figure 3). Almost half of the anomaly is on the land on the Mesozoic peridotites. On these peridotites high susceptibility values have been measured in between $8x10^{-3}$ ile $16x10^{-3}$ SI.

Gökova gulf is covered with up to 2.5 km thick Miocene-Pliocene sediments (Kurt et al 1999).

In recent years the region started displaying high seismicity. In Gökova gulf, in the study area 3497 earthquakes have been recorded since 1919. Epicentres of the earthquakes with magnitudes higher than 3 is calculated to be 14.8 km deep. 178 of these earthquakes coincides with the ophiolites. Again the anomalies with higher than 3 magnitude have 32.5 km epicentre depth.

Study area is about 4968 km^2, the ophiolite anomaly is 471 km^2 area, this is about 10% of the study area, 5% of the earthquakes are on this ophiolite anomaly (Figure 3).

The other interesting thing is 88% of the earthquakes took place in the last 10 years. This shows that in recent years seismicity in the area increased considerably.

Reduction to the pole magnetic data's field components along *x, y, z* directions have been calculated with the return path (T_x, T_y ve T_z). Tensors position in a fixed coordinate system along *x, y, z* is presented (Figure 4).

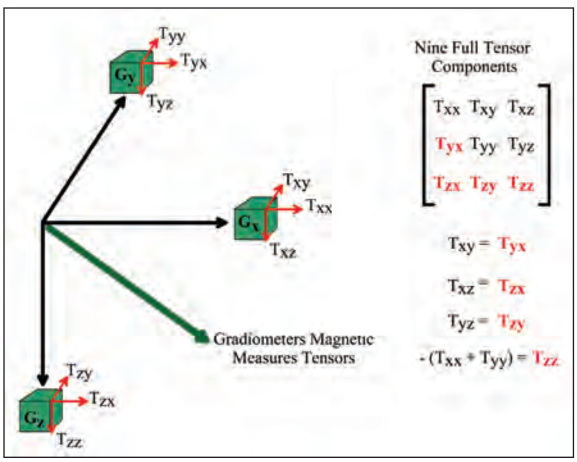

Figure 4- Tensor presentation.

• T_{zz} tensor location of the target mass,

• T_{xx} and T_{yy} tensors bordering north/south and east/west end of the target mass,

• T_{xz} and T_{yz} tensors along with defining central axis's of the target mass, definition of faults from heights and sharp drops,

• T_{xy} brings out anomalies near to the centre of the mass (Figure 4),

T_{xx} tensor divided the anomaly into parts as negative and positive. This anomaly at the same time borders the ophiolite in the east and west sides (Figure 5).

T_{xy} tensor divides the anomaly along SW-NE; division strength along NW-SE is not very definite (Figure 6).

Grey line marks the boundary of the ophiolite anomaly. T_{xz} tensor divides the ophiolite anomaly into two from the central axis along east/west direction (Figure 7).

T_{yy} tensor divides the anomaly into two as negative and positive parts. This anomaly also borders the ophiplite in the north and south. But T_{yy} division is not as clear as T_{xx} tensor's (Figure 8).

T_{yz} tensor, grey line marks the ophiolite anomaly's boundary. This anomaly is divides into 2 as north and south (Figure 9).

T_{zz} tensor clearly marks the ophiolite boundary, marked with grey line (Figure 10)

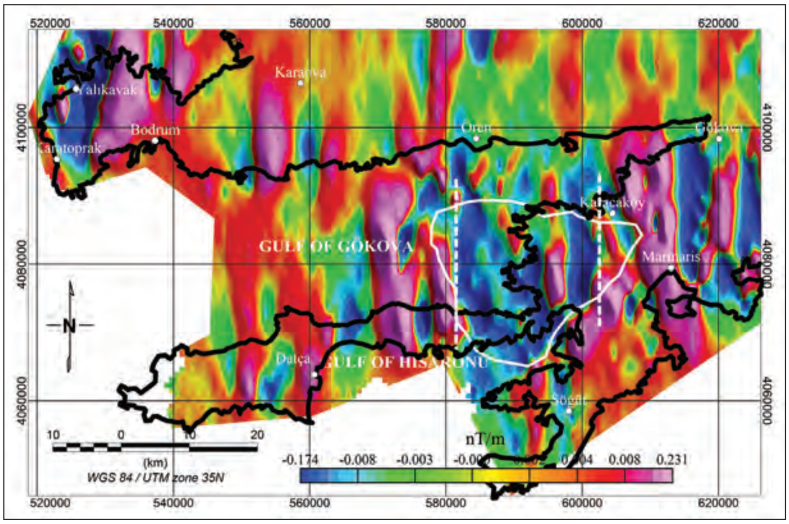

Figure 5- FTG T_{xx} map

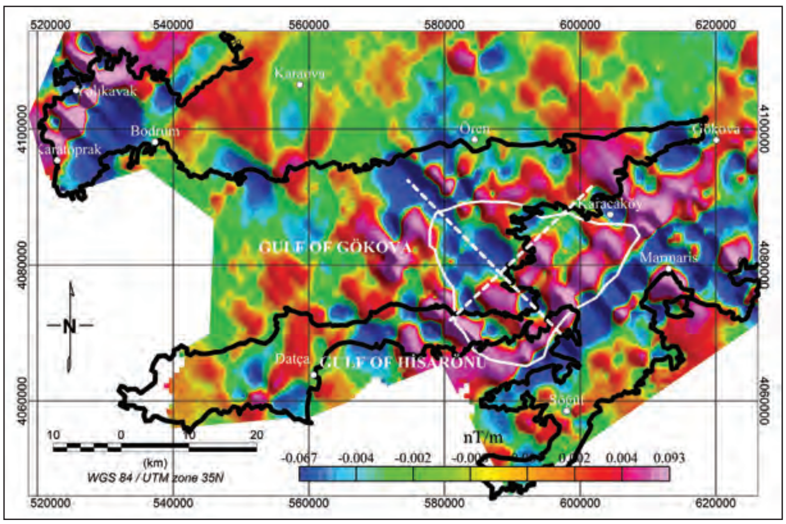

Figure 6- FTG T_{xy} map.

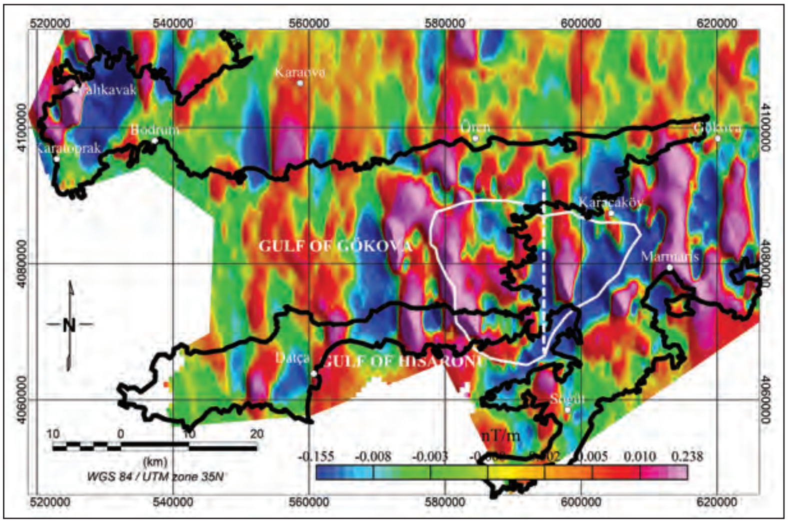

Figure 7- FTG T_{xz} map.

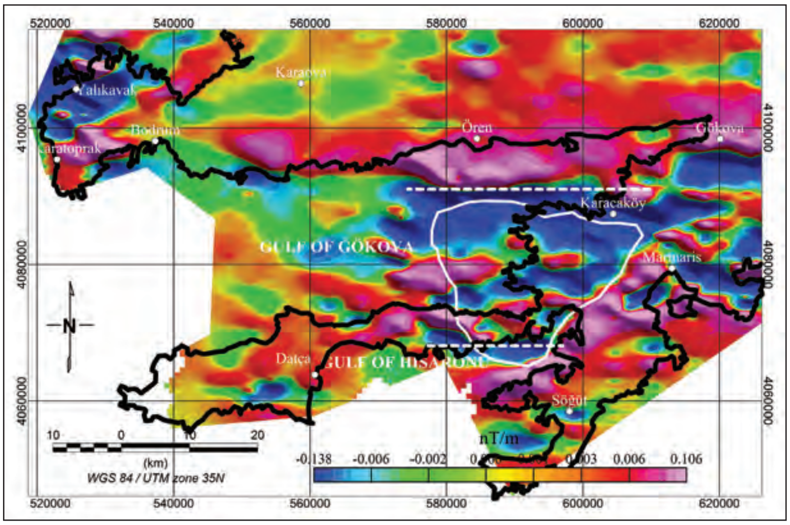

Figure 8- FTG T_{yy} map.

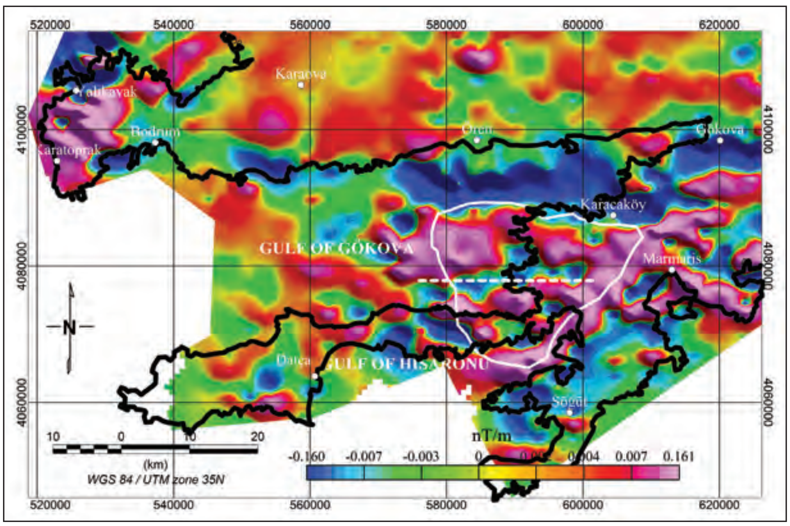

Figure 9- FTG T_{yz} map.

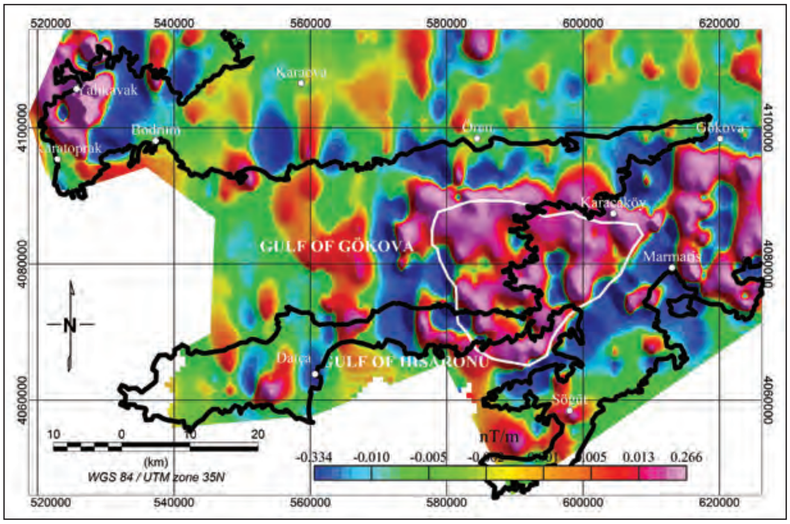

Figure 10- FTG T_{zz} map.

Rotational constant 1(R_1) and rotational constant 2 (R_2) were defined for the first time by Pedersen and Rasmussen (1990). In this study these constants have been calculated. To calculate R_1 and R_2 rotational constants T_{xx} T_{xy} T_{xz} T_{yy} T_{yz} ve T_{zz} maps (Figures 5, 6, 7, 8, 9, 10) have been used.

$$R\_1= ((T_{xx}T_{yy}+T_{yy}T_{zz}+T_{xx}T_{zz})-(T_{xy}^{\ 2}T_{yz}^{\ 2}+T_{zx}^{\ 2}))^{1/2}$$

$$R\_2= ((T_{xx}(T_{yy}T_{zz}-T_{yz}^{\ 2})+T_{xy}(T_{yz}T_{xz} - T_{xy}T_{zz})+T_{xz}(T_{xy}T_{yz}-T_{xz}T_{yy}))^{1/3}$$

R_1 rotational, made shape and borders of the small intrusions more distinct. Three small intrusions have been recognized within the circle defining main body of ophiolite unit (Figure 11).

In Figure 12, R_2 has been calculated. R_2 rotational brought out shapes of very small structures. In Figure 12 presence of ophiolite mass has been made more distinct.

By using data in Figure 12 shallow structures on the main structure with short wave lengths have been made more distinct with the calculation of 1st degree derivative (Figure 13). Main body is within the ophiolite boundary. 1st vertical derivative of the R_2 rotation has separated shallow small structures from deep main target mass.

4. Conclusions

There is an airborne magnetic anomaly in the Gökova bay. Meaning of this anomaly has been

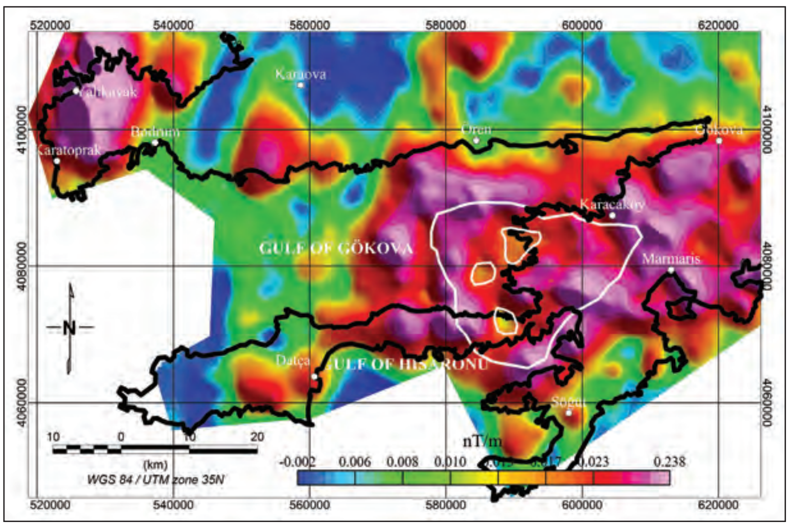

Figure 11- R_1 Rotational map.

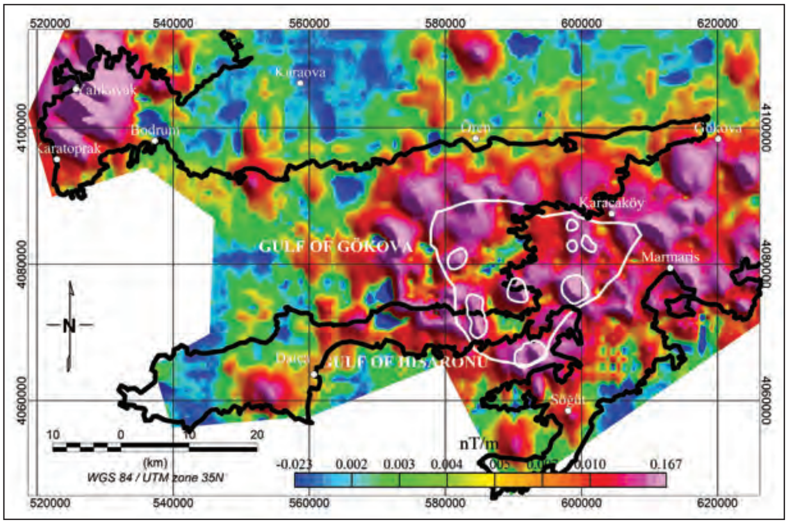

Figure 12- R_2 Rotational map.

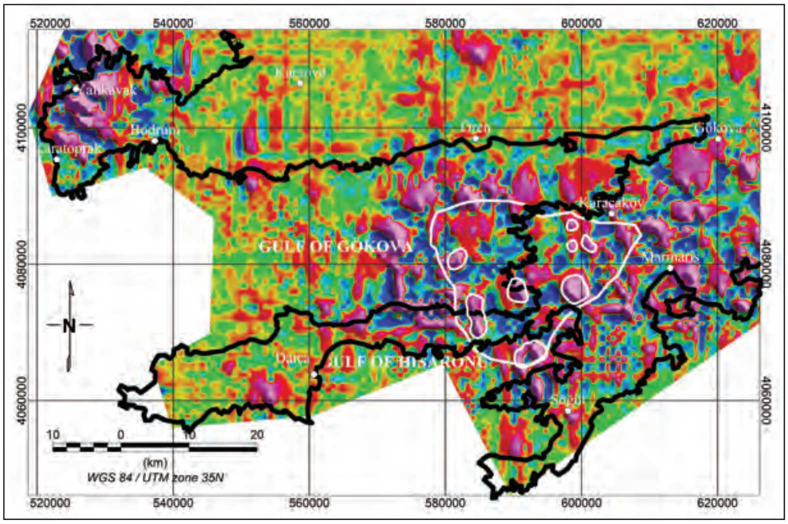

Figure 13- 1st vertical derivative map of the R_2 rotation

analysed in this work. Total airborne magnetic anomaly has been studied by applying FTG method. The anomaly represents continuation of the Marmaris ophiolite nappe in the gulf.

There are two distinct anomalies in the RTP map in Figure 3. The anomaly in the west (the one in the gulf) closes in itself. The anomaly in the east is extending beyond Turkey's frontier, so meaning of it has not been analysed.

We carried out some power spectrum studies (unpublished study), according to the findings of this study, in the study area there is about 2 km thick sediments lying on the top. Under this sedimentary unit Marmaris ophiolite nappe with 5-6 km thickness is located.

Magnetic field components (T_x, T_y, T_z) have been calculated. Following conversions, in the components' (T_{xx}, T_{xy}, T_{xz}, T_{yy}, T_{yz} ve T_{zz}) maps strong negative and positive contrasts have become noticeable. With the FTG method amplitudes and sharpness of the anomalies have become important. Prepared FTG maps showed that covered geological structure in the Gökova gulf caused the subject anomaly.

In western Turkey numbers of grabens developed as a result of N-S extensions in western Turkey. In the Gökova gulf, like in many others, extension developed. It is 100 km long along EW and 25 km long along NS directions.

In recent years seismic activities in the Gökova gulf increased considerably. It is understood that many of these seismic activities, recognizable as magnetic anomalies which have developed along the borders of the ophiolite unit. With the FTG method borders of ophiolite units and tectonic belts have been identified. Earthquake epicentres are mainly located along the borders of the ophiolite units and beyond. There is not any tectonic activity in the ophiolite itself. It is pointed out that as earthquakes occur in the ophiolite border zones and in the parts beyond it, so these parts are tectonically active zones.

Acknowledgment

Authors would like to thank to Ünal Dikmen, Halil İbrahim Yusufoğlu and Bülent Kaypak for their contributions.

Received: 11.12.2012
Accepted: 08.05.2013
Published: December 2013

References

Akın, U., Duru M. 2006. Türkiye Isı Akısı Haritası (manyetik verilerden) raporu, *Maden Tetkik ve Arama Genel Müdürlüğü Rapor No*: 10840 (unpublished), Ankara.

Akın, U., Çiftçi, Y. 2011. Türkiye'nin Yapısal Süreksizlikleri: Jeolojik-Jeofizik Gravite ve Manyetik Analiz. *Maden Tetkik ve Arama Genel Müdürlüğü Monografi Serisi* No:6, 155 sf. MTA

Ateş, A. 1999. Possibility of deep gabbroic rocks, east of Tuz Lake, central Turkey, interpreted from aeromagnetic data. *Journal of Balkan Geophysical Society*, 2,15–29.

Aydın, İ., Karat, H.İ., Koçak, A. 2005. Curie-point depth map of Turkey. Geophys. *Journal International* 162, 633-640.

Bracken, E.B., Brown P.J. 2005. Reducing Tensor Magnetic Gradiometer Data for Unexploded Ordnance Detection. Scientific Investigations Report 2005-5046 U.S. Geological Survey.

Christensen, A., Rajagopalan, S. 2000. The magnetic vector and gradient tensor in mineral and oil exploration: *Preview*, 84, 77.

FitzGerald, D., Argast, D., Paterson, R., Holstein, H. 2010. Full tensor magnetic gradiometry processing and interpretation developments Part A. Adding new value to Electromagnetic, Gravity and Magnetic Methods for Exploration. *EGM 2010 International Workshop*, Capri, Italy.

Görür, N., Sengör, A. M. C., Sakinü, M., Akkök, R., Yiğitbaş, E., Oktay, F.Y., Barka, A., Sarica, N., Ecevitoğlu, B., Demirbağ, E., Ersoy, Ş., Algan, O., Güneysu, C., Aykol, A. 1995. Rift formation in the Gökova region, southwest Anatolia: implications for the opening of the Aegean Sea. *Geological Magazine*, 132, 06, 637-650.

Heath, P., Heinson, G., Greenhalgh, S. 2003. Some comments on potential field tensor data: *Exploration Geophysics*, 34, 57–62.

Kurt, H., Demirbağ, E., Kuşçu, İ. 1999. Investigation of the submarine active tectonism in the Gulf of Gökova, southwest Anatolia–southeast Aegean Sea, by multi-channel seismic reflection data. *Tectonophysics* 305, 477-496.

Mataragio, J., Jorgensen, G., Carlos, D.U, Braga, M. 2011. State of the Art Techniques for Iron Oxide Exploration. *Twelfth International Congress of the Brazilian Geophysical Society*. August 15-18.

MTA, 2002. 1/500.000 Scoile Geological Map of Turkey, General Directorate of Mineral Research and Exploration of Turkey, Ankara

Murphy, C.A. 2004. The Air-FTG airborne gravity gradiometer system. Lane R.J.L., (Ed.), Airborne Gravity 2004 – *ASEG-PESA Airborne Gravity Workshop: Geoscience Australian Record* 2004/18, 7-14.

Murphy, C.A. 2007. Interpreting FTG Gravity data using horizontal Tensor components: *EGM 2007 International Workshop* - Innovation in EM, Grav and Mag methods: new Perspective for Exploration.

Murphy, C.A., Brewster, J. 2007. Target delineation using Full Tensor Gravity Gradiometry data. *ASEG, Perth*, Australia, Extended Abstracts.

Murphy, C.A., Dickinson, J. L. 2010.Geological Mapping and Targeting using Invariant Tensor analysis on Full Tensor Gravity data. *EGM 2010 International Workshop* Adding new value to Electromagnetic, Gravity and Magnetic Methods for Exploration Capri, Italy, April 11-14.

Pedersen, L.B., Rasmussen, T.M. 1990. The gradient tensor of potential field anomalies: some implications on data collection and data processing of maps. *Geophysics*, 55, 1558-1566.

Rompel, A.K.K. 2009. Geological Apllications for FTMG. *11th SAGA Biennial Technical Meeting and Exhibition* Swaziland 16-18 September, pages 39-42.

Schmidt, P.W., Clark, D.A. 2000. Advantages of measuring the magnetic gradient tensor: *Preview*, 85, 26–30.

Şenel, M. 2007. Likya Naplarının Özellikleri ve Evrimi, *Menderes Masifi Kolokyumu*, 51-55s., İzmir.

Wan, L., Zhdanov, M.S. 2008. Focusing inversion of marine full-tensor gradiometry data in offshore geophysical exploration. *SEG Las Vegas 2008* Annual Meeting.

Bulletin of MTA (2013) 147: 179-183

Bulletin of the
Mineral Research and Exploration

http://bulletin.mta.gov.tr

BRIEF NOTE ON NEW DATA RELATED TO THE CHRONOSTRATIGRAPHIC LOCATION OF CUMAOVASI VOLCANICS

Fikret GÖKTAŞ[a]

[a] *General Directorate of Mineral Research and Exploration, Regional Directorate of Aggean, Bornova, İzmir, Turkey*

This study was made in order to contribute for reviewing Neogene stratigraphy proposed in previous studies (Figure 2a, b, c, d) based on new K/Ar ages obtained from acidic volcanics in Çubukludağ section (Figure 1a, b) of the Akhisar Depression (Kaya, 1979).

Starting with Early Miocene extension, the infill of Çubukludağ half graben under the control of İzmir fault proposed by Kaya et al. (2007) (ancestor of Tuzla fault proposed by Emre et al., 2005) Is formed by deposits of Bahçecik, Yeniköy and Tahtalı formations from bottom to top and of Cumaovası volcanics (Figure 2e). The lower part of Bahçecik formation symbolizing the Early Miocene deposition does not crop out over the area, because Tuzla fault has generated a depression. The observable part of the sedimentary deposit is formed by lacustrine and fluvial deposits consisting of lignite layers at bottom and by the overlying crimson-maroon lacustrine fan delta deposits with distinctive contacts which reflect a probable unconformity. Algal limestone interlayers symbolizing temporal lacustrine deposit take place within fan delta. Yeniköy formation which unconformably overlies Bahçecik formation and evolves from alluvial environment into lacustrine environment, and Tahtalı formation (Göktaş, 2013) which is formed from bottom to top by alluvial, fluvial and lacustrine deposits reflect Middle Miocene sedimentation (Figure 2e). At the main explosion phase of phreatomagmatic Cumaovası volcanism which began in lacustrine environment and where Yeniköy formation was deposited in, the western side of the basin was enclosed with the emplacement of multi layered ignimbrites following the base surge deposition. Then, Tahtalı formation was deposited to the east of the volcanic axis trending in NE-SW direction. Upper Miocene alluvial fan delta deposits overlying Cumaovası volcanics with angular unconformity forms the youngest Neogene infillings of the study area.

1. Cumaovası Volcanics

Cumaovası volcanics contribute to lacustrine suspension deposition which forms the upper section of Yeniköy formation with felsic ash fall interlayers and mainly show a lateral relationship with Tahtalı formation. These volcanics reflect calc alkaline rhyolitic volcanism which have become active in late Middle Miocene and consist of pyroclastics at bottom and lavas in the form of domal flows at top (Figure 1 and 2e).

Akartuna (1962) is the first investigator who mentioned about the presence of rhyolitic volcanics in Çubukludağ basin. Previous studies have begun with Zucci (1970) then continued with Innocenti and Mazzuoli (1972), Borsi et al. (1972) ("Izmir-Lebedos rhyolites"). The products of rhyolitic volcanism have been called as "Cumaovası volcanics" since Eşder and Şimşek (1975) (Eşder and Şimşek, 1976; Özgenç, 1975, 1978; Eşder, 1988; Genç et al., 2001; Wipp, 2006; Uzel and Sözbilir, 2008; Karacık and Genç, 2009, 2011,2012; Karacık, 2011; Karacık et al., 2011).

Ignimbrites flowing into the lake where Yeniköy formation had been deposited and the outer zones of rhyolitic lavas were subjected to strong devitrification

* *Corresponding author: F. GÖKTAŞ, fikretgoktas50@gmail.com*

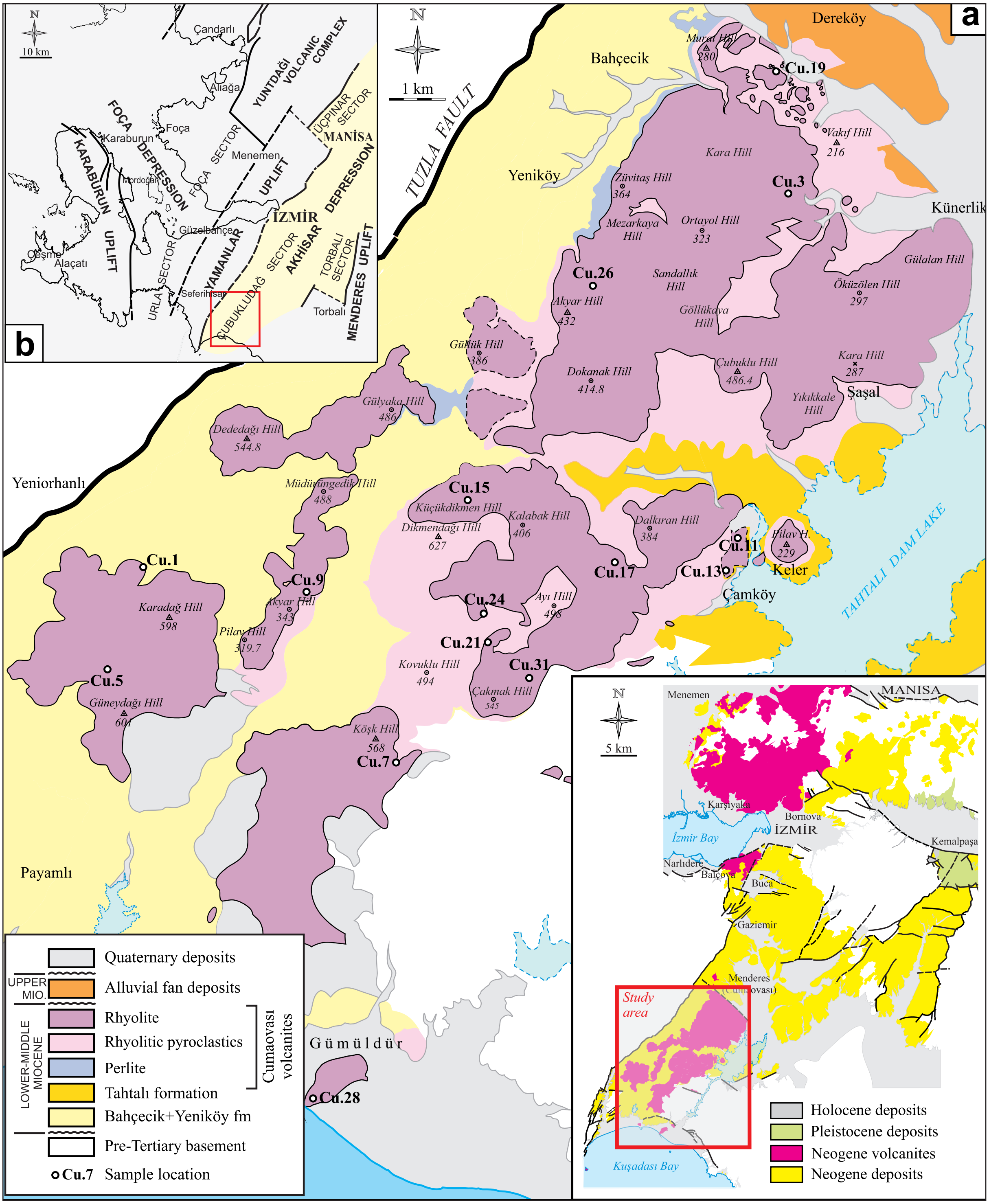

Figure 1- Simplified geological map of Çubukludağ basin (a) and its geographical location in "Akhisar Depression" (Kaya (1979) (b).

and became perlitised (Figure 1). Laterally continuous perlitisation observed especially on basal sections of lavas reflects the entrance of domal flows into the water. Lavas are generally blocky decomposed, bluish dark gray, pink, crimson, maroon and pale yellowish gray, flow laminated or massive, and spatially cooling columns have been developed. Vapor phase products are also common and gas spaces filled with opal and chalcedony, lithophyses and spherulites formed on the outer zones of lava masses are frequently

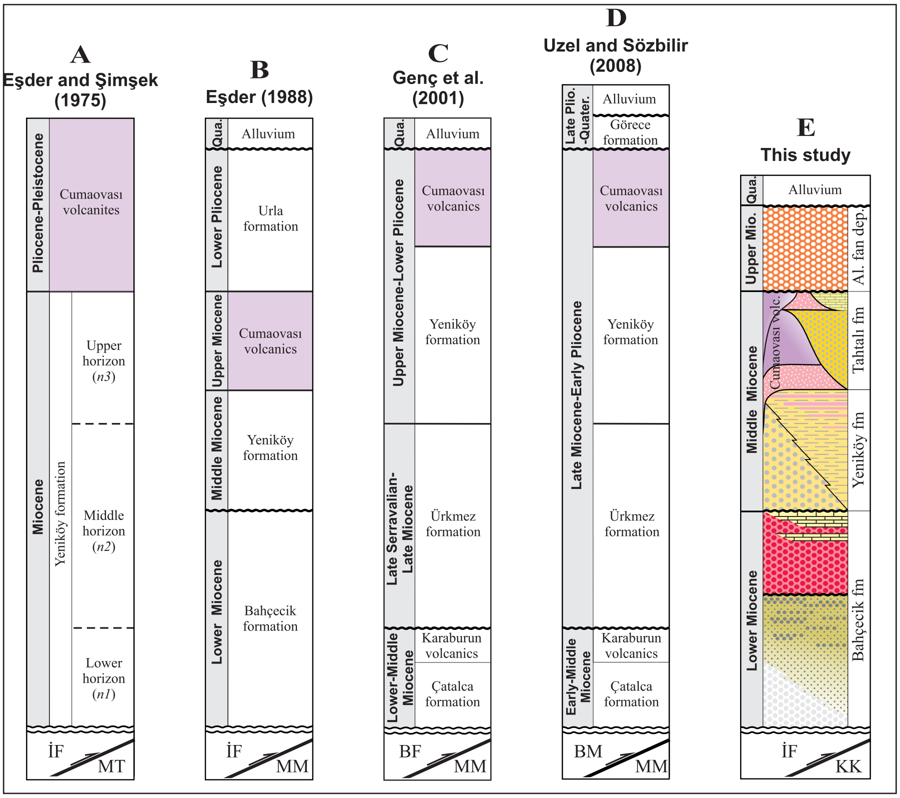

Figure 2- Stratigraphical models proposed for Çubukludağ basin infilling. BM: Bornova melange, BF: Bornova Flysch, İF: İzmir Flysch, KK: Cycladic Complex (Candan et al., 2011), MM: Menderes Massif, MT: Metamorphic Basement.

encountered. Wipp (2006) has determined garnet crystals (almandine – spessartine) that have grown up to 1,5 cm mostly in lithophye and seldom in compact lavas.

Total of 15 chemical and 5 radiometric samples were taken from rhyolitic lavas which were less affected from hydrothermal alteration and devitrification in order to perform analysis. XRF and K/Ar analyses of samples were performed in ACME (Canada) laboratories.

1.1. Major Element Geochemistry

Results of the major element analysis of samples taken from rhyolitic lavas and the location map of the study area are given in table 1 and figure 1, respectively.

All high siliceous lava samples called "rhyolite" in total alkaline-silica diagram of Le Bas et al. (1986) plot on the sub alkaline region and are calc alkaline in

Table 1- The result of major element analysis of Çubukludağ rhyolites. Samples of which radiometric analyses were carried out are shown in yellow color.

Sample	SiO_2	Al_2O_3	Fe_2O_3	MgO	CaO	Na_2O	K_2O	TiO_2	P_2O_5	MnO	Cr_2O_3	LOI	Total
CU 1	79.39	11.40	0.75	0.11	0.19	1.20	4.83	0.09	0.03	<0.01	<0.002	2.0	99.98
CU 3	77.48	11.49	1.35	0.06	0.39	2.94	4.36	0.05	0.03	0.02	0.003	1.8	99.98
CU 5	79.63	10.84	0.35	0.07	0.23	2.34	5.08	0.02	0.03	<0.01	<0.002	1.4	99.96
CU 7	71.00	15.51	0.70	0.22	1.02	2.95	6.79	0.30	0.06	<0.01	<0.002	1.3	99.85
CU 9	75.61	12.46	1.44	0.15	0.50	2.28	5.20	0.08	0.03	0.01	<0.002	2.2	99.97
CU 11	75.31	12.47	1.16	0.14	0.42	2.95	4.77	0.04	0.01	<0.01	0.006	2.7	99.98
CU 13	75.84	12.29	1.00	0.12	0.42	2.75	4.68	0.05	0.02	<0.01	<0.002	2.8	99.98
CU 15	77.21	12.59	1.02	0.06	0.25	3.09	4.62	0.06	0.02	0.03	<0.002	1.0	99.99
CU 17	76.84	12.49	1.18	0.02	0.37	3.51	4.56	0.04	0.02	0.02	0.002	0.9	99.98
CU 19	78.91	10.83	1.08	0.04	0.44	3.10	4.16	0.05	0.01	0.04	<0.002	1.3	100.00
CU 21	76.91	12.51	1.10	0.09	0.36	3.31	4.70	0.07	0.02	0.03	<0.002	0.9	99.98
CU 24	76.23	12.85	1.42	0.03	0.40	3.28	4.81	0.06	0.02	0.03	<0.002	0.9	99.97
CU 26	79.03	10.82	1.14	0.16	0.42	3.24	4.13	0.03	0.02	0.08	0.003	0.9	99.98
CU 28	76.63	12.56	0.60	0.03	0.15	1.14	7.83	0.14	0.03	<0.01	<0.002	0.8	99.93
CU 31	77.45	12.15	1.19	0.05	0.35	2.94	4.55	0.05	0.02	0.02	<0.002	1.2	99.98

character (Figure 3a). Samples which were assessed in K_2O vs SiO_2 diagram of Le Maitre et al. (1989) accumulate in High-K rhyolitic area (Figure 3b).

1.2. Geochronology

K/Ar age (12,5±3,5 Ma) which Borsi et al. (1972) have obtained from rhyolites has been used as the only data for a long time in previous studies related with Cumaovası volcanics though it has a high margin of error. According to the generalized stratigraphies of Genç et al. (2001) and Uzel and Sözbilir (2008) Cumaovası volcanics are located above Upper Miocene-Lower Pliocene “Yeniköy formation” in accordance with the proposal of Akartuna (1962) (Figure 2c, d). K/Ar ages indicating late Early Miocene of Karacık and Genç (2009) vary between 17,2 – 17,9 Ma.

However, in this study K/Ar ages varying between 13,0 – 13,8 Ma were obtained (Table 2). Layers of felsic ash fall taken by Sözbilir et al. (2011) in “Kocaçay basin” (Torbalı sector of Akhisar depression: Figure 1b) which have an Ar^{40}/Ar^{39} age of 13.8±0.1 Ma were associated with Cumaovası rhyolitic volcanism (Göktaş, 2012). The difference in geochronological data of this study with Karacık and Genç (2009) might support two staged volcanism argued by Özgenç (1978).

Acknowledgement

This study consists of one part of the project called “Çeşme, Urla, Cumaovası, Kemalpaşa-Torbalı Çöküntülerindeki Neojen ve Kuvaterner Havzalarının Stratigrafisi ve Paleocoğrafik Evrimi Projesi” (Stratigraphy of Neogene and Quaternary Basins and Paleogeographical Evolution in Çeşme, Urla, Cumaovası, Kemalpaşa-Torbalı Depressions) conducted by the coordinatorship of the Department of Geological Researches, MTA (General Directorate of Mineral Research and Exploration).

Received: 09.05.2013

Accepted: 26.09.2013

Published: December 2013

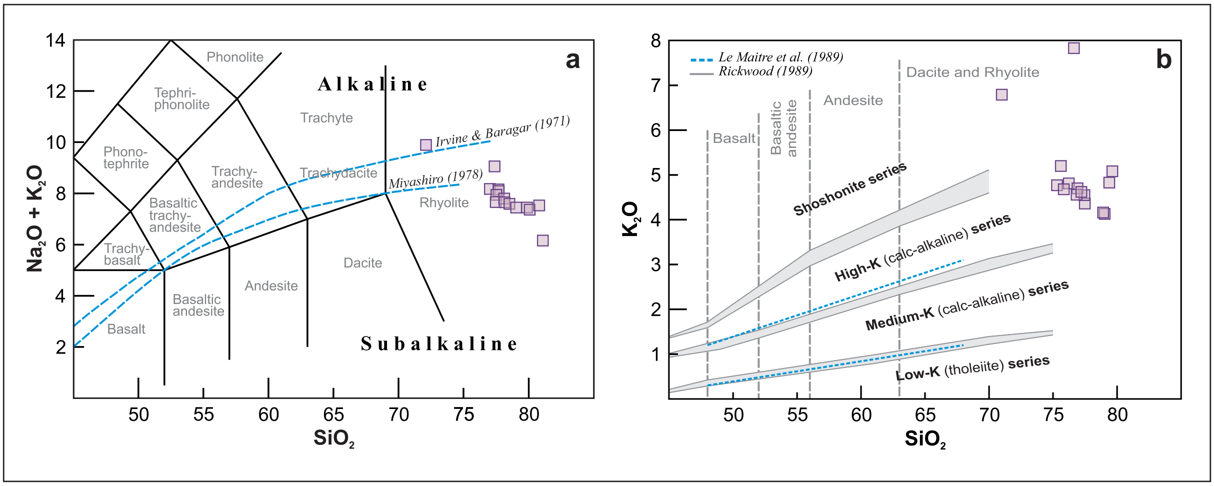

Figure 3- Evaluation of Karaburun volkanites in a) TAS (Le Bas et al., 1986) and b) K_2O vs SiO_2 (Le Maitre et al., 1989) diagrams.

Table 2- The result of radiometric analyses obtained from Cumaovası rhyolites.

Sample	Material	(%)K	$^{40}Ar_{rad}$ (nl/g)	(%) $^{40}Ar_{air}$	Age (My)
CU 3	K-spar	3.28	1.729	68.7	13.8 ± 0.4
CU 5	K-spar	4.52	2.337	86.9	13.5 ± 0.4
CU 7	K-spar	3.98	1.978	69.5	13.0 ± 0.4
CU 15	K-spar	7.23	3.787	14.0	13.7 ± 0.4
CU 24	%15 Q, %85 plj	2.57	1.345	92.8	13.7 ± 0.5

References

Akartuna, M. 1962. İzmir-Torbalı-Seferihisar-Urla bölgesinin jeolojisi hakkında. *Maden Tetkik ve Arama Dergisi*, 59, 1-18.

Borsi, J., Ferrara, G., Innocenti, F., Mazzuoli, R. 1972. Geochronology and petrology of recent volcanics in the eastern Aegean Sea (West Anatolia and Lesbos Island). *Bulletin of Volcanology*, 36, 473–496.

Emre, Ö., Özalp, S., Doğan, A., Özaksoy, V., Yıldırım, C., Göktaş, F. 2005. İzmir yakın çevresinin diri fayları ve deprem potansiyelleri. *Maden Tetkik ve Arama Genel Müdürlüğü Rapor No*: 10754 (unpublished), Ankara.

Eşder, T., Şimşek, Ş. 1975. İzmir Seferihisar alanı Çubukludağ grabeni ile dolaylarının jeolojisi ve jeotermal olanakları. *Maden Tetkik ve Arama Genel Direktörlüğü Rapor No*: 5842, (unpublished), Ankara.

Eşder, T., Şimşek, Ş. 1976. Geology of İzmir-Seferihisar geothermal area. *Second United Nations Symposium on the Development and Use of Geothermal Resources*, San Francisco, California, USA, 20-29 May 1975, Proceedings 1, 349-361.

Eşder, T. 1988. Gümüldür-Cumaovası (İzmir) alanının jeolojisi ve jeotermal enerji olanaklarının araştırılması. Doktora Tezi, 401, (unpublished).

Genç, C. Ş., Altunkaynak, Ş., Karacık, Z., Yazman, M., Yılmaz, Y. 2001. The Çubukludağ graben, South of İzmir: its tectonic significance in the Neogene geological evolution of the western Anatolia. *Geodinamica Acta*, 14, 45-55.

Göktaş, F. 2012. Kemalpaşa-Torbalı (İzmir) havzası ile yakın çevresindeki Neojen-Kuvaterner tortullaşması ve magmatizmasının jeolojik etüdü. *Maden Tetkik ve Arama Genel Müdürlüğü Rapor No*: 11575 (unpublished), Ankara.

Göktaş, F. 2013. Çubukludağ (Menderes-İzmir) havzasındaki Neojen tortullaşması ve volkanizmasının jeolojik etüdü. *Maden Tetkik ve Arama Genel Müdürlüğü Raporu*.

Innocenti, F., Mazzuoli, R. 1972. Petrology of İzmir-Karaburun volcanic area (West Turkey). *Bulletin of Volcanology*, 36, 83-104.

Irvine, N., Baragar, W.R.A. 1971. A guide to chemical classification of the common volcanic rocks. *Canadian Journal of Earth Sciences*, 8, 523–548.

Karacık, Z., Genç, Ş. C. 2009. Cumaovası (İzmir-Menderes) volkaniklerinin volkanik stratigrafisi, petrolojisi ve Batı Anadolu genç magmatizması içindeki yeri ve anlamı. TÜBİTAK Proje No: 107Y014, 96 s.

Karacık, Z., Genç, Ş. C. 2011. Volcano-stratigraphy of the extension-related silicic volcanism in the Çubukludag graben, western Turkey: implications for generation of thephretomagmatic eruptions triggered by dome emplacement. *Geophysical Research*, Abstracts, 13.

Karacık, Z., Genç, Ş. C., Esenli, F., Göller, G. 2011. The Gümüldür fire opal: mode of Occurrence and Mineralogical Aspects. *Turkish Journal of Earth Sciences*, 20, 99–114.

Karacık, Z. 2011. Cumaovası ve Karaburun yöreleri Alt-Orta Miyosen yaslı asidik volkanizmasının petrolojik evrimi, petrojenezi ve yasıt (?) bazik volkanizma ile kökensel iliskilerinin araştırılması. TÜBİTAK Proje No: 110Y161, 34 s.

Karacık, Z., Genç, Ş. C. 2012. Petrology of the Miocene volcanism at around the Karaburun Peninsula and Çubukludağ graben (Western Anatolia, Turkey): Geochemical and radiochronological data for its regional implications. *International Earth Sciences Colloquium on the Aegean Region (IESCA)*, 1-5 Ekim 2012, İzmir, Abstracts, 25.

Kaya, O. 1979. Ortadoğu Ege çöküntüsünün (Neojen) stratigrafisi ve tektoniği; *Türkiye Jeoloji Kurumu Bülteni*, 22/1, 35-58.

Kaya, O., Ünay, E., Göktaş, F., Saraç, G. 2007. Early Miocene stratigraphy of Central West Anatolia, Turkey: implications for the tectonic evolution of the Eastern Aegean area. *Geological Journal*, 42, 85-109.

Le Maitre, R. W. 1989. A Classification of Igneous Rocks and Glossary of Terms. *Blackwell Scientific Publications*, Oxford, 208 s.

Le Bas, M. J., Le Maitre, R. W., Streckeisen, A., Zanettin, B. 1986, A chemical classification of volcanic rocks based on total alkali-silica diagram. *Journal of Petrology*, 27, 745-750.

Özgenç, İ. 1975. İzmir-Cumaovası bölgesi perlit yataklarının jeolojisi. *TÜBİTAK V. Bilim Kongresi*, Bildiriler, 261-272.

Özgenç, İ. 1978. Cumaovası (İzmir) asit volkanitlerinde saptanan iki ekstrüzyon aşaması arasındaki göreli yaş ilişkisi. *Türkiye Jeoloji Kurumu Bülteni*, 21, 31-34.

Rickwood, P. C. 1989. Boundary lines within petrologic diagrams which use oxides of major and minor elements. *Lithos*, 22, 247-263.

Sözbilir, H., Sarı, B., Uzel, B., Sümer, Ö., Akkiraz, S. 2011. Tectonic implications of transtensional supradetachment basin development in an extension parallel transfer zone: the Kocaçay Basin, western Anatolia, Turkey. *Basin Research*, 23, 4, 423-448.

Uzel, B., Sözbilir, H. 2008. A first record of a strike-slip basin in Western Anatolia and its tectonic implication: The Cumaovası basin. *Turkish Journal of Earth Sciences*, 17, 559-591.

Wipp, Ç. L., 2006, İzmir-Cumaovası-Görece köyü civarı volkanitleri ve Menderes Masifi metamorfitleri içindeki bazı granatların mineralojik-petrografik ve jeokimyasal incelenmesi ve olası arkeogemolojik bağlantıları. Doktora Tezi, Hacettepe Üniversitesi, 138 (unpublished).

Zucchi, F. 1970. Batı Türkiye Perlit yatakları (İzmir-Manisa bölgesi). *Maden Tetkik ve Arama Genel Direktörlüğü Rapor No*: 4704 (unpublished), Ankara.

ACKNOWLEDGEMENT

In the editorial process of the MTA Bulletins of 2013, each contribution was reviewed by at least two specialists in order to secure an international standart of the volumes. We would like to thank the following respectable group of referees who assisted us by consenting to provide with thorough and constructive review.

Ali İhsan KARAYİĞİT
Ali UÇURUM
Ali YILMAZ
Aral OKAY
Atike NAZİK
Baki VAROL
Burhan SADIKLAR
Bülent ORUÇ
Candan GÖKÇEOĞLU
Cemal GÖNCÜOĞLU
Cemal TUNOĞLU
Ercüment SİREL
Erdinç YİĞİTBAŞ
Funda AKGÜN
Fuzuli YAĞMURLU
Güner ÜNALAN
Halim MUTLU
Harun SÖNMEZ
İbrahim AYDIN
Kenan KILIÇ
Lütfü SÜZEN
Mehmet ALTINSOY
Mehmet EKMEKÇİ
Muharrem SATIR
Muhittin GÖRMÜŞ
Mustafa AFŞİN
Mustafa ERGÜN
Nazire ÖZGEN
Necati TÜYSÜZ
Nilgün GÜLEÇ
Nizamettin KAZANCI
Okan TÜYSÜZ
Orhan TATAR
Osman PARLAK
Peter W. SKKELTON
Pınar ŞEN
Reşat ULUSAY
Sacit ÖZER
Selahattin KADİR
Selami TOPRAK
Şakir ŞİMŞEK
Şevket ŞEN
Tamer TOPAL
Tolga YALÇIN
Tuncay TAYMAZ
Ünal DİKMEN
Y. Kaan KADIOĞLU
Yurdal GENÇ
Yavuz BEDİ
Yener EYÜPOĞLU
Zafer AKÇIĞ

BULLETIN OF THE MINERAL RESEARCH AND EXPLORATION NOTES TO THE AUTHORS

1. Aims

The main aims of the journal are

- To contribute to the providing of scientific communication on geosciences in Turkey and the international community.
- To announce and share the researches in all fields of geoscience studies in Turkey with geoscientists worldwide.
- To announce the scientific researches and practices on geoscience surveys carried out by the General Directorate of Mineral Research and Exploration (MTA) to the public.
- To use the journal as an effective media for international publication exchange by keeping the journal in high quality, scope and format.
- To contribute to the development of Turkish language as a scientific language

2. Scope

At least one of the following qualifications is required for publishing the papers in the *Bulletin of Mineral Research and Exploration*.

2.1. Research Articles

2.1.1. Original Scientific Researches

- This type of articles covers original scientific research and its results related to all aspects of disciplines in geoscience.

2.1.2. Development Researches

- The studies using new approaches and methods to solve any problems related to geosciences and/or the researches using new approaches and methods to solve any problems related to the science of engineering performed in the General Directorate of Mineral Research and Exploration.

2.1.3. Review articles

- This type of papers includes comphrehensive scholarly review articles that summarize and critically assess previous geoscience reseach with a new perspective and it also reveals a new approach.

2.2. Discussion/Reply

- This type of article is intended for discussions of papers that have already been published in the latest issue of the *Bulletin*.
- The discussion/reply type articles that criticize all or a part of a recently published article, are published in the following first issue, if it is submitted within six months after the distribution of the *Bulletin*.
- The discussions are sent to the corresponding author of the original paper to get their reply, before publication. So that, the discussion and reply articles can be published at the same time, if they can be replied within the prescribed period. Otherwise, the discussion is published alone. Re-criticising of the replies is not allowed. The authors should keep the rules of scientific ethics and discussions in their discussion/reply papers. The papers in this category should not exceed four printed pages of the journal including figures and tables etc. The format of the papers should be compatible with the "Spelling Rules" of the *Bulletin*.

2.3. Short Notes

- Short notes publishing in the *Bulletin* covers short, brief and concisely written research reports for papers including data obtained from ongoing and/or completed scientific researches and practices related to geoscience and new and/or preliminary factual findings from Turkey and worldwide.
- The short notes will follow a streamlined schedule and will normally published in the following first or second issue shortly after submission of the paper to the *Bulletin*. To meet this schedule, authors should be required to make revisions with minimal delay.
- This type of articles should not exceed four printed pages of the journal including figures, tables and an abstract.

3. Submission and Reviewing of Manuscripts

Manuscript to be submitted for publishing in the Journal must be written clearly and concisely in Turkish and/or English and it should be prepared in the *Bulletin of Mineral Research and Exploration* style guidelines. All submissions should be made online at the **http://bulletin.mta.gov.tr** website.

The authors, having no facility for online submission can submit their manuscript by post-mail to the address given below. They should submit four copies of their manuscript including one original hard copy, and CD. The files belonging to manuscript should be clearly and separately named as “Text”, “Figures” and “Tables” at the CD.

Address:
Maden Tetkik ve Arama Genel Müdürlüğü
Redaksiyon Kurulu Başkanlığı
Üniversiteler Mah. Dumlupınar Bulvarı, No: 139
06800 Çankaya-Ankara

- The manuscript submitted for reviews has not been partially or completely published previously; that it is not under consideration for publication elsewhere in any language; its publication has been approved by all co-authors.

- The rejected manuscripts are not returned back to author(s) whereas a letter of statement indicating the reason of rejection is sent to the corresponding author.

- Submitted manuscripts must follow the *Bulletin* style and format guidelines. Otherwise, the manuscript which does not follow the journals' style and format guidelines, is given back to corresponding author without any reviewing.

- Every manuscript which passes initial Editorial treatise is reviewed by at least two independent reviewers selected by the Editors. Reviewers' reports are carefully considered by the Editors before making decisions concerning publication, major or minor revision or rejection.

- The manuscript that need to be corrected with the advices of reviewer(s) is sent back to corresponding author(s) to assess and make the required corrections suggested by reviewer(s) and editors. Authors should prepare a letter of well-reasoned statement explaining which corrections are considered or not.

- The Executive editor (Editorial Board) will inform the corresponding author when the manuscript is approved for publication. Final version of text, tables and figures prepared in the *Bulletin of Mineral Research and Exploration* style and format guidelines, will need to be sent online and the corresponding author should upload all of the manuscript files following the instructions given on the screen. In the absence of online submission conditions, the corresponding author should send four copies of the final version of the manuscript including one original hard copy, and CD by post-mail. The files belonging to manuscript should be clearly and separately named as “Text”, “Figures” and “Tables” at the CD.

- To be published in the *Bulletin of Mineral Research and Exploration,* the printed lenght of the manuscript should not exceed 30 printed pages of the journal including an abstract, figures and tables. The publication of longer manuscripts will be evaluated by Editorial Board if it can be published or not.

4. Publication Language and Periods

- *The Bulletin of Mineral Research and Exploration* is published at least two times per year, each issue is published both in Turkish and English. Thus, manuscripts are accepted in Turkish or English. The spelling and punctuation guidelines of Turkish Language Instution are preferred for the Turkish issue. However, technical terms related to geology are used in accordance with the decision of the Editorial Board.

5. Spelling Draft

Manuscripts should be written in word format in A4 (29.7 x 21 cm) size and double-spaced with font size Times New Roman 10-point, margins of 25 mm at the sides, top and bottom of each page. Authors should study carefully a recent issue of the *Bulletin of Mineral Research and Exploration* to ensure that their manuscript correspond in format and style.

- The formulas requiring the use of special characters and symbols must be submitted on computer.

- Initial letters of the words in sub-titles must be capital. The first degree titles in the manuscript must be numbered and left-aligned, 10 point bold Times New Roman must be used. The second degree titles must be numbered and left-aligned, they must be written with 10 point normal Times New Roman. The third degree titles must be numbered and left-aligned, they must be written with 10 point italic Times New Roman. The fourth degree titles must be left-aligned without having any number; 10 point italic Times New Roman must be used. The text must continue placing a colon after the title without paragraph returns (See:Sample article: http://bulletin.mta.gov.tr).

- Line spacing must be left after paragraphs within text.

- Paragraphs must begin with 0.5 mm indent.

- The manuscript must include the below sections respectively;
  - – Title Page
  - – Abstract

– Key Words
– Introduction
– Body
– Discussion
– Conclusion
– Acknowledgements
– References

5.1. Title Page

The title page should include:

A short, concise and informative title

The name(s) of the author(s)

The affiliation(s) and address(es) of the author(s)

The e-mail address, telephone and fax numbers of the corresponding author

The title must be short, specific and informative and written with capital letters font size Times New Roman 10-point bold. The last name (family name) and first name of each author should be given clearly. The authors' affiliation addresses (where the actual work was done) are presented below the names and all affiliations with a lower-case superscript letter is indicated immediately after the author's name and in front of the appropriate address. Provide the full postal address of each affiliation, including the country name and, if available, the e-mail address of each author.

The author who will handle correspondance at all stages of refereeing and publication, also post-publication are to be addressed (the corresponding author) should be indicated and the telephone, FAX and e-mail address given.

Please provide a running title of not more than 50 characters for both Turkish and English issue.

5.3. Abstract

- The article must be preceded by an abstract, which must be written on a seperate page as one paragraph, preferably. Please provide an abstract of 150 to 200 words. The abstract should not contain any undefined or non-standard abbreviations and the abstract should state briefly the overall purpose of the research, the principle results and major conclusions. Please omit references, criticisms, drawings and diagrams.
- Addressing other sections and illustrations of the text or other writings must be avoided.
- The abstract must be written with 10-point normal Times New Roman and single-spaced lines.
- "Abstract" must not be given for the writings that will be located in "Short Notes" section.
- English abstract must be under the title of "Abstract".

5.4. Key Words

Immediately after the abstract, please provide up to 5 key words and with each word seperated by comma. These key words will be used for indexing purposes.

5.5. Introduction

- The introdution section should state the objectives of the work, research methods, location of the study area and provide an adequate and brief background, avoiding a detailed literature survey.
- Non-standard or un-common classifications or abbreviations should be avoided but if essential, they must be defined at their first mention and used consistently thereafter.
- When needed reminder information for facilitating the understanding of the text, this section can also be used (for example, statistical data, bringing out the formulas, experiment or application methods, and others).

5.6. Body

- In this chapter, there must be data, findings and opinions that are intended to convey the reader about the subject. The body section forms the main part of the article.
- The data used the other sections such as "Abstract", "Discussions", and "Results" is caused by this section.
- While processing subject, care must be taken not to go beyond the objective highlighted in "Introduction" section. The knowledge which do not contribute to the realization of the purpose of the article or are useless for conclusion must not be included.
- All the data used and opinions put forward in this section must prove the findings obtained from the studies or they must be based on a reference by citation.
- Guidance and methods to be followed in processing subjects vary according to the characteristics of the subjects dealt with. Various phased topic titles can be used in this section as many as necessary.

5.7. Discussions

- This section should explore the significance of the results of the work, not repeat them. This must be written as a seperate section from the results.

5.8. Conclusions

- The main conclusion of the study provided by data and findings of the research should be stated concisely and concretely in this section.
- **T**he subjects that are not mentioned sufficiently and/or unprocessed in the body section must not be included in this section.
- The conclusions can be given in the form of substances in order to emphasize the results of the research and be understandable expression.

5.9. Acknowledgements

Acknowledgement of people, grants, funds, etc should be placed in a seperate section before the reference list. While specifying contributions, the attitude diverted the original purpose of this section away is not recommended. Acknowledgments must be made according to the following examples.

- This study was carried out under the..........................project.
- I/we would like to thank to ……… for contributing the development of this article with his/her critiques.
- Academic and / or authority names are written for the contributions made because of ordinary task requirement.

For example:

- "Prof. Dr. İ. Enver Altınlı has led the studies".
- "The opinions and warnings of Dr. Ercüment Sirel are considered in determining the limits of İlerdiyen layer."

- The contributions made out of ordinary task requirement:

For example:

– "I would like to thank to Professor Dr. Melih Tokay who gives the opportunity to benefit from unpublished field notes"; "I would like to thank to State Hydraulic Work 5. Zone Preliminary-Plan Chief Engineer Ethem Göğer." Academic and /or task-occupational titles are indicated for this kind of contributions.

- The contributions which are made because of ordinary task requirement but do not necessitate responsibility of the contributor must be specified.

For example:

- Such sentences as "I would like to thank to our General Manager, Head of Department or Mr. /Mrs. President ……………who has provided me the opportunity to research"must be used.

5.10. References

- All references cited in the text are to be present in the reference list.
- The authors must be sure about the accuracy of the references. Publication names must be written in full.
- Reference list must be written in Times New Roman, 9-point type face.
- The reference list must be alphabetized by the last names of the first author of each work.
- If an author's more than one work is mentioned, ranking must be made with respect to publication year from old to new.
- In the case that an author's more than one work in the same year is cited, lower-case alphabet letters must be used right after publication year (for example; Saklar, 2011*a, b*).
- If the same author has a publication with more than one co-author, firstly the ones having single author are ranked in chronological order, then the ones having multiple authors are ranked in chronological order.
- In the following examples, the information related to works cited is regulated in accordance with different document/work types, considering punctuation marks as well.
- If the document (periodic) is located in a periodical publication (if an article), the information about the document must be given in the following order: surnames of the author/authors, initial letters of author's/ authors' first names. Year of publication. Name of the document. Name of the publication where the document is published (in italics), volume and/ or the issue number, numbers of the first and last pages of the document.

For example:

- Pamir, H.N. 1953. Türkiye'de kurulacak bir hidrojeoloji enstitüsü hakkında rapor. *Türkiye Jeoloji Bülteni* 4, 1, 63-68.

- Barnes, F., Kaya, O. 1963. İstanbul bölgesinde bulunan Karbonifer'in genel stratigrafisi. *Maden Tetkik ve Arama Dergisi* 61,1-9.

- Robertson, A.H.F. 2002. Overview of the genesis and emplacement of Mesozoic ophiolites in the Eastern Mediterranean Tethyan region. *Lithos* 65, 1-67.

• If more than one document by the same authors is cited, firstly the ones having single name must be placed in chronological order, then the ones having two names must be listed in accordance with chronological order and second author's surname, finally the ones having multiple names must be listed in accordance with chronological order and third author's surname.

• If the document is a book, these are specified respectively: surnames of the author/authors, initial letters of author's/authors' first names. Year of publication. Name of the book (initial letters are capital). Name of the organization which has published the book (in italics), name of the publication wherethe document is published, volume and/ or the issue number, total pages of the book.

For example

- Meric, E. 1983. Foraminiferler. *Maden Tetkik ve Arama Genel Müdürlüğü Eğitim Serisi* 23, 280p.

- Einsele, G. 1992. Sedimentary Basins. *Springer-Verlag*, p 628.

• If the document is published in a book containing the writings of various authors, the usual sequence is followed for the documents in a periodic publication. Then the editor's surname andinitial letters of their name /names are written. "Ed." which is an abbreviation of the editor word is written in parentheses. Name of the book containing the document (initial letters are capital). Name of the organization which has published the book (*in italics*). Place of publication, volume number (issue number, if any) of the publication where the document is published, numbers of the first and last page of the document.

For example:

- Göncüoğlu, M.C., Turhan, N., Şentürk, K., Özcan, A., Uysal, Ş., Yalınız, K. 2000. A geotraverse across northwestern Turkey. Bozkurt, E., Winchester, J.A., Piper, J.D.A. (Ed.). Tectonics and Magmatism in Turkey and the Surrounding Area. *Geological Society of London* Special Publication 173, 139-162.

- Anderson, L. 1967. Latest information from seismic observations. Gaskell, T.F. (Ed.). The Earth's Mantle. Academic Press. London, 335-420.

• If name of a book where various authors' writings have been collected is specified, those must be indicated respectively: book'seditor/editors' surname/surnames, and initial letters of their name/names. "Ed." which is an abbreviation of the editor word must be written in parentheses. Year of Publication. Name of the book (initial letters are capital). Name of the organization which has published the book (*in italics*), total pages of the book.

For example:

- Gaskel, T.F.(Ed.)1967. The Earth's Mantle. *Academic Press*, 520p.

• If the document is an abstract published in a Proceedings Book of a scientific activity such as conference/symposium/workshop …etc. , information about the document must be given in the following order: surnames of the author/authors, initial letters of author's/authors' first names. Year of publication. Title of the abstract. Name (in italics), date and place of the meeting where the Proceedings Book is published, numbers of the first and last pages of the abstract in the Proceedings Book.

For example:

- Yılmaz, Y. 2001. Some striking features of the Anatolian geology. *4. International Turkish Geology Symposiums,* 24-28 September 2001, London, 13-14.

- Öztunalı, Ö., Yeniyol, M. 1980. Yunak (Konya) yöresi kayaçlarının petrojenezi. *Türkiye Jeoloji Kurumu 34. Bilim Teknik Kurultayı*, 1980, Ankara, 36

• If the document is unpublished documents as report, lecture notes, and so on., information about the document must be given by writing the word "unpublished" in parentheses to the end of information about the document after it is specifiedin accordance with usual order which is implemented for a document included in a periodic publication.

For example:

- Özdemir, C. Biçen, C. 1971. Erzincan ili, İliç ilçesi ve civarı demir etütleri raporu. *General Directorate of Mineral Research and Exploration Report No: 4461*, 21 p. Ankara (unpublished).

– Akyol, E. 1978. Palinoloji ders notları. *EÜ Fen Fakültesi Yerbilimleri Bölümü*, 45 p., İzmir (unpublished).

- The followings must be specified for the notes of unpublished courses, seminars, and so on: name of the document and course organizer. Place of the meeting. Name of the book, corresponding page numbers.

For example:

– Walker, G. R. Mutti, E. 1973.Turbidite facies and facies associations. Pacific Section Society for Sedimentary Geology Short Course. Annaheim. Turbitides and Deep Water Sedimantation, 119-157.

- If the document is a thesis, the following are written: surname of the author, initial letter of the author's first name. Year of Publication. Name of the thesis. Thesis type, the university where it is given, the total number of pages, the city and "unpublished" word in parentheses.

For example:

– Seymen, İ. 1982. Kaman dolayında Kırşehir Masifi'nin jeolojisi. Doçentlik Tezi, İTÜ Maden Fakültesi, 145 s.İstanbul (unpublished).

- Anonymous works must be regulated according to publishing organization.

For example:

– MTA. 1964. 1/500.000 ölçekli Türkiye Jeoloji Haritası, İstanbul Paftası. Maden Tetkik ve Arama Genel Müdürlüğü, Ankara.

- The date, after the name of the author, is not given for on-printing documents; "in press" and / or "on review" words in parenthesis must be written. The name of the article and the source of publication must be specified, volume and page number must not be given.

For example:

– Ishihara, S. The granitoid and mineralization. Economic Geology 75th Anniversary (in press).

- Organization name, web address, date of access on web address must be indicated for the information downloaded from the Internet. Turkish sources must be given directly in Turkish and they must be written with Turkish characters.

For example:

– ERD (Earthquake Research Department of Turkey). **http://www.afad.gov.tr**. March 3, 2013.

- While specifying work cited, the original language must be used; translation of the title of the article must not be done.

6. Illustrations

- All drawings, photographs, plates and tables of the article are called "illustration".
- Illustrations must be used when using them is inevitable or they facilitate the understanding of the subject.
- While selecting and arranging the illustrations' form and dimensions, page size and layout of the *Bulletin* must be considered, unnecessary loss of space must be prevented as much as possible.
- The pictures must have high quality, high resolution suitable for printing.
- The number of illustrations must be proportional to the size of the text.
- All illustrations must be sent as separate files independent from the text.
- While describing illustrations in the text, abbreviations must be avoided and descriptions must be numbered in the order they are mentioned in the text.
- Photographs and plates must be given as computer files containing EPS, TIFF, or JPEG files in 600 dpi and higher resolutions (1200 dpi is preferred) so that all details can be seen in the stage of examination of writing.

6.1. Figures

- Drawings and photos together but not the plate in the text can be evaluated as "Figure" and they must be numbered in the order they are mentioned in the text.
- The figures published in the *Bulletin of Mineral Research and Exploration* must be prepared in computing environment considering the dimensions of single-column width 7.4 cm or double-column width 15.8 cm. Figure area together with the writing at the bottom should not exceed a maximum 15.8x21.

- Figures must not be prepared in unnecessary details or care must be taken not to use a lot of space for information transfer.
- Figures must be arranged to be printed in black-and-white or colored. The figure explanations being justified in two margins must be as follows: Figure 1 -Sandıklı Town (Afyon); a) Geological map of thesouth-west, b) general columnar section of the study area (Seymen 1981), c) major neotectonic structures in Turkey (modified from Koçyiğit 1994).
- Drawings must be drawn by well-known computer programs painstakingly, neatly and cleanly.
- Using fine lines which can disappear when figures shrinks must be avoided. Symbols or letters used in all drawings must be Times New Roman and not be less than 2 mm in size when shrink.
- All the standardized icons used in the drawings must be explained preferably in the drawing or with figure caption if they are very long.
- Linear scale must be used for all drawings. Author's name, figure description, figure number must not be included into the drawing.
- Photos must have the quality and quantity that will reflect the objectives of the subject.

6.2. Plates

- Plates must be used when needed a combination of more than one photo and the publication on a special quality paper.
- Plate sizes must be equal to the size of available magazine pagespace.
- Figure numbers and linear scale must be written under each of the shapes located on the Plate.
- The original plates must be added to the final copy which will be submitted if the article is accepted.
- Figures and plates must be independently numbered. Figures must be numbered with Latin numerals and plates with Roman numerals (e.g., Figure1, Plate I).
- There must be no description text on Figures.

6.3.Tables

- Tables must be numbered consecutively in accordance with their appearence in the text.
- All tables must be prepared preferably in word format in Times New Roman fonts.
- Tables together with table top writing must not exceed 15x8 cm size.
- The table explanations being justified in two margins must be as follows:
- Table 1- Hydrogeochemical analysis results of geothermal waters in the study area.

7. Nomenclature and Abbreviations

- Non-standard and uncommon nomenclature abbreviations should be avoided in the text. But if essential, they must be described as below: In cases where unusual nomenclatures and unstandardized abbreviations are considered to be compulsory, the followed way and method must be described.
- Full stop must not be placed between the initials of words for standardized abbreviations (MER, SHW, etc.).
- Geographical directions must be abbreviated in English language as follows: N, S, E, W, NE …etc.
- The first time used abbreviations in the text are presented in parenthesis, the parenthesis is not used for subsequent uses.
- The metric system must be used as units of measure.
- Figure, plate, and table names in the article must not be abbreviated. For example, "as shown in generalized stratigraphic cross-section of the region (Figure 1…………."

7.1. Stratigraphic Terminology

Stratigraphic classifications and nomenclatures must be appropriate with the rules of International Commision on Stratigraphy and/or Turkey Stratigraphy Committee. The formation names which has been accepted by International Commision on Stratigraphy and/or Turkey Stratigraphy Committee should be used in the manuscript.

7.2. Paleontologic Terminology

Fossil names in phrases must be stated according to the following examples:

- For the use authentic fossil names:
- e.g. Calcareous sandstone with *Nummulites*
- When the authentic fossil name is not used.
- e.g. nummulitic Limestone
- Other examples of use;

  e.g. The type and species of Alveolina/ Alveolina type and species

- Taxonomic ranks must be made according to following examples:

Super family: Alveolina Ehrenberg, 1939 Family: Borelidae Schmarda, 1871 Type genus: *Borelis* de Montfort, 1808 Type species: *Borelis melenoides de Montfort, 1808*; *Nautilus melo* Fitchel and Moll, 1789	*Not reference, Not stated in the Reference section*
Borelis vonderschmitti (Schweighauser, 1951) (Plate, Figure, Figure in Body Text)	*Schweighauser, 1951 not reference*
1951 *Neoalveolina vonderschmitti* Schweighauser, page 468, figure 1-4	*Cited Scweighauser (1951), stated in the Reference section.*
1974 *Borelis vonderschmitti* (Schweighauser), Hottinger, page, 67, plate 98, figure 1.7	*Cited Hottinger (1974), stated in the Reference section.*

- The names of the fossils should be stated according to the rules mentioned below:
  - For the first use of the fossil names, the type, spieces and the author names must be fully indicated

  Alveolina aragoensis Hottinger

  Alveolina cf. Aragoensis Hottinger

  - When a species is mentioned for the second time in the text:

  A.aragoensis

  A.cf.aragoensis

  A.aff.aragoensis

  - It is accepted as citiation if stated as *Alveolina aragoensis* Hottinger (1966)
- The statment of plates and figures (especially for articles of paleontology):
  - for statment of the species mentioned in the body text

Borelis vonderschmitti (Schweighauser, 1951).

(plate, figure, figure in the body text).

- When citing from other articles

  1951 Neoalveolina vonderschmitti Schweighauser, page 468, figure 1-4, figure in body text

  1974 *Borelis vonderschmitti* (Schweighauser), Hottinger, page 67, plate 98, figure 1-7

- For the citiation in the text
- (Schweighauser, 1951, page, plate, figure, figure in the body text) (Hottinger, 1974, page, plate, figure 67, plate 98, figure 1-7, figure in the bodytext.)

8. Citations

All the citiations in the body text must be indicated by the last name of the author(s) and the year of publication, respectively. The citations in the text must be given in following formats.

- For publications written by single author:
  - It is known that fold axial plain of Devonian and Carboniferious aged units around Istanbul is NS oriented (Ketin, 1953, 1956; Altınlı, 1999).
  - Altınlı (1972, 1976) defined the general characteristics of Bilecik sandstone
- For publications written by two authors:
  - The upper parts of the unit contain Ilerdian fossils (Sirel and Gündüz, 1976; Keskin and Turhan, 1987, 1989).
- For publications written by three or more authors:

According to Caner et al. (1975) Alıcı formation reflects the fluvial conditions.

The unit disappears wedging out in the East direction (Tokay et al., 1984).

- If reference is not directly obtained but can be found in another reference, cross-reference should be given as follows:

– It is known that Lebling has mentioned the existance of Lias around Çakraz (Lebling, 1932: from Charles, 1933).

10. Reprints

The author(s) will receive 5 free reprints and two hard copies of the related issues

11. Copyright and Conditions of Publication

- It is a condition of publication that work submitted for publication must be original, previously unpublished in whole or in part.
- It is a condition of publication that the authors who send their publications to the *Bulletin of Mineral Research and Exploration* hereby accept the conditions of publication of the Bulletin in advance.
- All copyright of the accepted manuscripts belong to MTA. The author or corresponding author on behalf of all authors (for papers with multiple authors) must sign and give the agreement under the terms indicated by the Regulations of Executive Publication Committee. Upon acceptance of an article, MTA can pay royalty to the authors upon their request according to the terms under the "Regulations of Executive Publication Committe" and the "Regulations of Royalty Payment of Public Office and Institutions"

All the information and forms about the *Bulletin of Mineral Research and Explorations* can be obtained from http://bulletin.mta.gov.tr